

Reversible and Mechanism-Based
Irreversible Inhibitor Studies on
Human Steroid Sulfatase
and
Protein Tyrosine Phosphatase 1B

by

F. Vanessa Ahmed

A thesis

presented to the University of Waterloo

in fulfilment of the

thesis requirement for the degree of

Doctor of Philosophy

in

Chemistry

Waterloo, Ontario, Canada, 2009

© F. Vanessa Ahmed 2009

Author's Declaration

I hereby declare that I am the sole author of this thesis. This is a true copy of the thesis, including any required final revisions, as accepted by my examiners.

I understand that my thesis may be made electronically available to the public.

Abstract

The development of reversible and irreversible inhibitors of steroid sulfatase (STS) and protein tyrosine phosphatase 1B (PTP1B) is reported herein. STS belongs to the aryl sulfatase family of enzymes that have roles in diverse processes such as hormone regulation, cellular degradation, bone and cartilage development, intracellular communication, and signalling pathways. STS catalyzes the desulfation of sulfated steroids which are the storage forms of many steroids such as the female hormone estrone. Its crucial role in the regulation of estrogen levels has made it a therapeutic target for the treatment of estrogen-dependent cancers. Estrone sulfate derivatives bearing 2- and 4-mono- and difluoromethyl substitutions were examined as quinone methide-generating suicide inhibitors of STS with the goal of developing these small molecules as activity-based probes for proteomic profiling of sulfatases. Kinetic studies suggest that inhibition by the monofluoro derivatives is a result of a quinone methide intermediate that reacts with active-site nucleophiles. However, the main inhibition pathway of the 4-difluoromethyl derivative involved an unexpected process in which initially formed quinone methide diffuses from the active site and decomposes to an aldehyde in solution which then acts as a potent, almost irreversible STS inhibitor. This is the first example where this class of inactivator functions by in situ generation of an aldehyde. 6- and 8-mono- and difluoromethyl coumarin derivatives were also examined as quinone methide-generating suicide inhibitors of STS. The 6-monofluoromethyl derivative acted as a classic suicide inhibitor. The partition ratio of this compound was found to be very large indicating that this class of compounds is not likely suitable as an activity-based probe for proteomic profiling of sulfatases. Boronic acids derived from steroid and coumarin

platforms were also examined as STS inhibitors with the goal of improving our understanding of substrate binding specificity of STS. Inhibition constants in the high nanomolar to low micromolar range were observed for the steroidal derivatives. The coumarin derivatives were poor inhibitors. These results suggest that the boronic acid moiety must be attached to a platform very closely resembling a natural substrate in order for it to impart a beneficial effect on binding affinity compared to its phenolic analog. The mode of inhibition observed was reversible and kinetic properties corresponding to the mechanism for slow-binding inhibitors were not observed.

PTP1B catalyzes the dephosphorylation of phosphotyrosine residues in the insulin receptor kinase and is a key enzyme in the down regulation of insulin signaling. Inhibitors of PTP1B are considered to have potential as therapeutics for treating type II diabetes mellitus. The difluoromethylenesulfonic (DFMS) acid group, one of the best monoanionic phosphotyrosine mimics reported in the literature, was examined as a phosphotyrosine (pTyr) mimic in a non-peptidyl platform for PTP1B inhibition. The DFMS-bearing inhibitor was found to be an approximately 1000-fold poorer inhibitor than its phosphorus analogue. It was also found that the fluorines in the DFMS inhibitor contributed little to inhibitory potency. In addition, [sulfonamido(difluoromethyl)]-phenylalanine (F₂Smp) was examined as a neutral pTyr mimic in commonly used hexapeptide and tripeptide platforms. F₂Smp was found to be a poor pTyr mimic. These inhibition studies also revealed that the tripeptide platform is not suitable for assessing pTyr mimics for PTP1B inhibition.

Taken together, the kinetic data on the inhibition of STS and PTP1B provide valuable information relevant for future design of inhibitors of these two therapeutic targets.

Acknowledgements

I would foremost like to thank my dedicated supervisor, Dr. Scott D. Taylor for his guidance in overseeing my development from an undergraduate to a graduate researcher. I am grateful for his support, mentorship and encouragement during my doctoral research, which has been a fulfilling, rewarding journey and a true privilege.

I extend sincere appreciation to the members of my advisory committee for their advice, constructive criticism and helpful discussions throughout the stages of my graduate research. I thank Drs. Guy Guillemette, Elizabeth Meiering, and Richard Manderville for their support and insight.

I am indebted to my coworkers in the lab who made instrumental contributions to my project, in particular Yong Liu, Bryan Hill and Munawar Hussain, who synthesized many of the compounds integral toward my study of steroid sulfatase and protein tyrosine phosphatase 1B. I also thank them and other members in the lab for their support and contributions to my professional development, particularly, Jason Trinh, Cassandra Silvestro, Dustin Little, Andrea Dupont, Laura Ingram, Latifeh Navidpour, Farzad Mirzai, Mehdi Ispahany and Jennifer Lapierre.

Table of Contents

List of Tables	xi
List of Figures	xii
List of Abbreviations	xviii

CHAPTER 1 – STEROID SULFATASE: STRUCTURE, FUNCTION AND INHIBITOR DEVELOPMENT

	Page
1.1 Introduction	1
1.1.1 The sulfatase family of enzymes	2
1.1.2 Formylglycine	4
1.2 Steroid sulfatase	10
1.2.1 STS expression and location	10
1.2.2 STS and hormone-dependent breast cancer	12
1.2.3 STS action in prostate cancer	16
1.2.4 STS and skin	17
1.2.5 STS and neurofunction	17
1.2.7 Sulfatase deficiencies	18
1.2.8 Crystal structure of STS	21
1.2.9 Comparison of tertiary structures of sulfatases	26
1.2.10 Comparison of active site structures of sulfatases	28
1.2.11 Catalytic mechanism of sulfatases	30
1.3 STS inhibitor development	34
1.3.1 Reversible inhibitors	34
1.3.2 Irreversible inhibitors	40
1.4 Research Objectives	48

CHAPTER 2 – PURIFICATION OF STEROID SULFATASE

2.1 Introduction	50
2.2 Results and Discussion	57
2.2.1 Study of the effect of neutralization of pH of STS after immunoaffinity purification	60
2.2.2 Evaluation of kinetic properties and comparison to literature	63
2.3 Conclusions	70
2.4 Experimental	71
2.4.1 Materials	71
2.4.2 Methods	71
2.4.2.1 Activity Assay	71
2.4.2.2 Homogenization and Chromatography	72
2.4.2.4 Protein concentration determination	74
2.4.2.5 Determining kinetic properties	75
2.4.2.6 Determining pH-rate profile	75

CHAPTER 3 – QUINONE METHIDE-GENERATING ACTIVE SITE-DIRECTED MECHANISM-BASED IRREVEVERSIBLE INHIBITORS OF STEROID SULFATASE

3.1	Introduction	76
3.1.1	Mechanism-based enzyme inhibitors	77
3.1.2	Quinone methide-generating suicide inhibitors	80
3.1.3	Objectives	83
3.2	Results and Discussion	84
3.2.1	General criteria for SIs	84
3.2.2	Evaluation of time- and concentration-dependence of compounds 3.10 and 3.11	85
3.2.3	Active site protection and trapping experiments for compounds 3.10 and 3.11	88
3.2.4	Irreversibility of inhibition of STS by compounds 3.10 and 3.11 .	92
3.2.5	Evaluation of time- and concentration-dependence for compound 3.9 .	93
3.2.6	Evaluation of time- and concentration-dependence, effect of exogenous nucleophiles and active site protection for compound 3.12	96
3.2.7	Monitoring reaction products and intermediates produced by incubation of compound 3.12 and STS by HPLC	100
3.2.8	Examination of 4-FE1 as a time- and concentration dependent inhibitor of STS	101
3.2.9	Specificity of inhibition of STS by formylated steroids	102
3.2.10	2- and 4-Hydroxymethylestrone as STS inhibitors	108
3.2.11	Screening of coumarin derivatives 3.13-3.16 as time-dependent STS inhibitors	112
3.2.12	Kinetic studies with compound 3.14	113
3.2.13	Determination of the partition coefficient of 3.14	115
3.2.14	Potential for quinone methide-generating SIs as activity-based proteomic profiling probes	118
3.3	Conclusions and Future Work	121
3.4	Experimental	124
3.4.1	General	124
3.4.2	Preliminary screening of compounds 3.13-3.16	125
3.4.3	General procedure for the determination of time and concentration-dependent inhibition of STS	125
3.4.4	Lineweaver-Burk analysis of compound 3.9	126
3.4.5	Time and concentration-dependent inhibition of STS in the presence of estrone-3- <i>O</i> -phosphate (E1P) (protection experiments)	126
3.4.6	Time and concentration-dependent inhibition of STS in the presence of β -mercaptoethanol (β -ME) (trapping experiments)	127
3.4.7	Dialysis experiments	128
3.4.8	Effect of NaBH ₄ on STS activity	129
3.4.9	Generation of standard curve for coumarin 3.28	129

3.4.10	Determination of partition coefficient for compound 3.14	130
3.4.11	Monitoring the reactions of compounds 3.9-3.12 with STS by HPLC	131

CHAPTER 4 – BORONIC ACIDS AS INHIBITORS OF STEROID SULFATASE

4.1	Introduction	133
4.1.1	Boronic acids as enzyme inhibitors	133
4.1.2	Objectives	136
4.2	Results and Discussion	138
4.3	Conclusions and Future Work	146
4.4	Experimental	148
4.4.1	General	148
4.4.2	Determination of K_i and αK_i values for compounds 4.1, 4.6, 4.7 and 4.10	148
4.4.3	Determination of IC_{50} values for compounds 4.8, 4.9, and 4.10	149

CHAPTER 5 – AN ASSESSMENT OF THE SULFONIC ACID AND SULPHONAMIDE GROUPS AS PHOSPHOTYROSINE MIMICS FOR PTP1B INHIBITION

5.1	Introduction: Protein Tyrosine Phosphatases	151
5.1.1	PTP1B as a drug target for diabetes and obesity	154
5.1.2	The PTP1B protein: catalytic and regulatory domains	156
5.1.3	Catalytic mechanism and structure of PTP1B	158
5.1.4	PTP1B reversible oxidation	162
5.1.5	PTP1B Inhibitor Development	163
5.1.5.1	<i>Phosphotyrosine mimics</i>	164
5.1.5.2	<i>Bidentate ligands</i>	171
5.1.6	Objectives	176
5.2	Results and Discussion	179
5.2.1	Inhibition studies with compounds 5.26-5.29	179
5.2.2	Inhibition studies with compounds 5.32-5.35, 5.42, 5.43	185
5.3	Conclusions	188
5.4	Experimental	190
5.4.1	Materials	190
5.4.1	Purification of PTP1B	190
5.4.3	Kinetic Assays	191
5.4.2	IC_{50} and K_i determinations of compounds 5.7, 5.26 to 5.29	192
5.4.3	IC_{50} Determinations for compounds 5.32 to 5.35, and 5.42 and 5.43	193
5.4.4	Assay for Time-Dependent Inhibition with Inhibitor 5.42	194
5.4.5	Assay for Irreversible Inhibition with Inhibitor 5.42	194
	REFERENCES	196

APPENDICES

APPENDIX A- PRELIMINARY KINETIC STUDIES WITH COMPOUNDS 3.24, 3.25 AND 3.32-3.34	224
A.1 General procedure for IC ₅₀ determinations of compounds 3.24, 3.25, 3.33 and 3.34	224
A.2 Preliminary studies on the time- and concentration-dependent inhibition of STS with compound 3.32	225
APPENDIX B – SUPPLEMENTARY FIGURES FOR COMPOUNDS 4.6, 4.7, 4.10, 4.11	227
APPENDIX C – SUPPLEMENTARY FIGURES FOR COMPOUNDS 5.26, 5.27, 5.28, 5.29, 5.34, AND 5.42	235
APPENDIX D — PERMISSION TO REPRODUCE FIGURES 1.7 TO 1.13 OBTAINED BY PERSONAL COMMUNICATION WITH A COLLABORATOR	239
APPENDIX E — PERMISSION TO REPRODUCE COPYRIGHT MATERIAL IN CHAPTER 3 IN ASSOCIATION WITH THIS THESIS	240
APPENDIX F — PERMISSION TO REPRODUCE COPYRIGHT MATERIAL IN CHAPTER 4 IN ASSOCIATION WITH THIS THESIS	241
APPENDIX G — PERMISSION TO REPRODUCE COPYRIGHT MATERIAL IN CHAPTER 4 IN ASSOCIATION WITH THIS THESIS	242

List of Tables

	Page
CHAPTER 1 – STEROID SULFATASE: STRUCTURE, FUNCTION AND INHIBITOR DEVELOPMENT	
Table 1.1 Human sulfatases: their substrates and cellular locations	4
Table 1.2 STS inhibitors as estrone-3- <i>O</i> -sulfate analogs	36
CHAPTER 2 – PURIFICATION OF STEROID SULFATASE	
Table 2.1 Comparison of Specific Activities of three methods to neutralize STS after immununoaffinity purification.	63
Table 2.2 Molecular mass for placental STS reported by SDS-PAGE in literature	66
Table 2.3 Comparison of literature K_m values for 4-MUS substrate	69
CHAPTER 4 – BORONIC ACIDS AS INHIBITORS OF STEROID SULFATASE	
Table 4.1 K_i or IC_{50} values for compounds 4.1 , 4.6-4.10 and E1	137
CHAPTER 5 – AN ASSESSMENT OF THE SULFONIC ACID AND SULPHONAMIDE GROUPS AS PHOSPHOTYROSINE MIMICS FOR PTP1B INHIBITION	
Table 5.1 Inhibition of PTP1B with compounds 5.7 and 5.26-5.29	180
Table 5.2 Inhibition of PTP1B with peptides 5.32-5.35 , 5.42 , 5.43 , and 5.11	185

List of Figures

	Page
CHAPTER 1 – STEROID SULFATASE: STRUCTURE, FUNCTION AND INHIBITOR DEVELOPMENT	
Figure 1.1	6
<p>(A) Reactions catalyzed by the formylglycine generating enzyme (FGE) in eukaryotes and some prokaryotes and AtsB in prokaryotes to convert the first cysteine in the pentapeptide consensus sequence (C/S-X-P/A-X-R) to a formylglycine (FGly)</p> <p>(B) Signature sequence of sulfatases</p>	
Figure 1.2	8
A proposed mechanism for formylglycine generation in eukaryotes by FGE	
Figure 1.3	9
The formylglycine generating sequence can be introduced recombinantly into a gene of interest	
Figure 1.4	14
Origins of estrogenic steroids in breast tumours	
Figure 1.5	15
Reaction catalyzed by estrone sulfotransferase (SULT1E1)	
Figure 1.6	16
Biosynthetic pathway for the production of the androgens testosterone and dihydrotestosterone from DHEAS	
Figure 1.7	20
X-LI point mutation sites depicted as amino acids in the wild-type enzyme (Ser341, Trp372, His444, Cys446 and Gln560).	
Figure 1.8	22
Stereographic ribbon diagram of tertiary and secondary structure of STS	
Figure 1.9	24
Active site residues coordinated to the Ca ²⁺ ion. The formylglycine (FGly) is sulfated as depicted by the red oxygen and yellow sulfur atoms	
Figure 1.10	25
STS active site lies at protein-lipid interface	
Figure 1.11	27
Comparison of the overall folds of human STS and ARSA	
Figure 1.12	28
Comparison of the tertiary structures of four sulfatases	
Figure 1.13	29
Active site residues of sulfatases share a highly similar spatial arrangement	
Figure 1.14	31
Proposed catalytic mechanism for sulfatases based on ARSB crystal structure evidence	
Figure 1.15	32
Proposed catalytic mechanism for sulfatases based on ARSA crystal structure evidence	
Figure 1.16	34
Proposed mechanism for sulfatases, including STS	
Figure 1.17	35
Small inorganic inhibitors of STS	
Figure 1.18	38
17 α -substituted estradiol derivative, 1.14 and 1.15 , and non-hydrolyzable estrone-3- <i>O</i> -sulfate derivatives 1.16-1.18	
Figure 1.19	39
STS inhibitors discovered by library screening	
Figure 1.20	40
Estrone-3- <i>O</i> -sulfamate (EMATE)	
Figure 1.21	41
Addition of aryl sulfamate to aldehyde FGly residue as proposed by Woo and coworkers	
Figure 1.22	42
Proposed inactivation of STS by aryl sulfamate when FGly hydrate initiates attack on aryl sulfamate	
Figure 1.23	44
Elimination mechanism of the sulfamate moiety from aryl sulfamate resulting in multiple sulfamoylated amino acid residues	

Figure 1.24	<i>N,N</i> -dimethyl-substituted EMATE, 1.26	45
Figure 1.25	The general structure of coumarin, 1.27 , and its numbering scheme	47
Figure 1.26	Dual aromatase and steroid sulfatase inhibitors, 1.32 and 1.33	48
CHAPTER 2 – PURIFICATION OF STEROID SULFATASE		
Figure 2.1	Structure of Triton X-100 detergent	55
Figure 2.2	4-methylumbelliferyl sulfate (4-MUS) fluorogenic assay of STS and aryl sulfatases (ARs)	58
Figure 2.3	Elution profile of STS activity by DEAE chromatography	59
Figure 2.4	Elution profile of STS activity by anti-STS immunoaffinity chromatography	60
Figure 2.5	Comparison of Specific Activities of three methods to neutralize STS after immunoaffinity purification	65
Figure 2.6	pH profile of STS activity in terms of k_{cat} measured with 4-methylumbelliferyl sulfate (4-MUS, 2.2) as substrate	67
Figure 2.7	pH profile of K_m values of 4-methylumbelliferyl sulfate (4-MUS, 2.2) for STS as a function of pH	68
Figure 2.8	pH profile of STS activity in terms of k_{cat}/K_m measured with 4-methylumbelliferyl sulfate (4-MUS, 2.2) as substrate	68
CHAPTER 3 – QUINONE METHIDE-GENERATING ACTIVE SITE-DIRECTED MECHANISM-BASED IRREVERSIBLE INHIBITORS OF STEROID SULFATASE		
Figure 3.1	General reaction scheme for mechanism-based inactivators	77
Figure 3.2.	General scheme for activity-based proteomic profiling	78
Figure 3.3	Compound 3.1 as a quinone-methide generating SI of a glycosidase	80
Figure 3.4	Examples of some quinone methide-generating SIs of glycosidases and phosphatases	82
Figure 3.5	Proposed quinone methide-generating inhibitors	83
Figure 3.6	Proposed mechanism for the inactivation of STS by compound 3.10	84
Figure 3.7	Time- and concentration-dependent inhibition of STS with inhibitor 3.10 over 20 minutes (A) and 5 minutes (B). Inset in B : Kitz-Wilson plot	87
Figure 3.8	Time- and concentration-dependent inhibition of STS with inhibitor 3.11 over 20 minutes (A) and 5 minutes (B)	88
Figure 3.9	Inactivation of STS in the presence of E1P and compound 3.10 (A) and compound 3.11 (B)	90
Figure 3.10	Inactivation of STS in the presence of β -ME and compound 3.10 (A) and compound 3.11 (B)	92
Figure 3.11	RP-HPLC analysis of the reaction of compound 3.9 with STS	94
Figure 3.12	Possible products of reaction of 3.9 with STS	95
Figure 3.13	Lineweaver-Burk plot for compound 3.9 Inset A : replot of slopes of Lineweaver-Burk plot versus concentration of 3.9 Inset B : replot of y-intercept of Lineweaver-Burk plot versus concentration	96

	of 3.9	
Figure 3.14	Time- and concentration-dependent inhibition of STS with inhibitor 3.12	97
Figure 3.15	Inactivation of STS in the presence of inhibitor 3.12 and β -ME	97
Figure 3.16	Inactivation of STS with inhibitor 3.12 in the presence of E1P	97
Figure 3.17	RP-HPLC analysis of the reaction of inhibitor 3.12 with STS	99
Figure 3.18	Potential modes of inhibition by compound 3.12 and its breakdown product, 4-formylestrone (4-FE1)	100
Figure 3.19	Time- and concentration-dependence of STS by 4-FE1 over 60 minutes (A), and 30 minutes (B). Inset in B : Kitz-Wilson plot	103
Figure 3.20	Inactivation of STS in the presence of E1P and 4-FE1. See § 3.4.5 for details	104
Figure 3.21	Inactivation of STS in the presence of β -ME and compound 4-FE1	104
Figure 3.22	Estra-1,3,5(10)-triene-17-one-3-carbaldehyde (3.22)	105
Figure 3.23	A comparison of time-dependent inhibition of STS by formylated estrones	105
Figure 3.24	Schiff's base formation between a residue on STS and 4-FE1	106
Figure 3.25	Active site of STS	106
Figure 3.26	1-hydroxy-2-naphthaldehyde 6-phosphate (HNA-P, 3.23), a time-dependent inhibitor of fructose-1,6-bisphosphate aldolase	107
Figure 3.27	2-Hydroxymethyl estrone (3.24), and 4-hydroxymethyl estrone, (3.25), are potential products of hydrolysis of compounds 3.10 and 3.11 , respectively	109
Figure 3.28	RP-HPLC analysis of the reaction of compound 3.10 with STS	110
Figure 3.29	RP-HPLC analysis of the reaction of compound 3.11 with STS	112
Figure 3.30	Time- and concentration-dependent inhibition of STS by 3.14 .	114
Figure 3.31	(A) Inactivation of STS in the presence of 3.14 and E1P (B) Inactivation of STS in the presence of 3.14 and β -ME	115
Figure 3.32	Potential hydrolysis products of 3.14	116
Figure 3.33	Relative fluorescence of 50 μ M coumarins 3.28 and 3.14 versus λ_{em} in 0.1 M tris, pH 7.0, 5% DMSO, 0.01% Triton X-100. (λ_{ex} = 360 nm).	118
Figure 3.34	Change in fluorescence with time during the reaction of STS with 500 μ M 3.14 in 0.1 M tris, pH 7.0, 0.1 % Triton X-100	118
Figure 3.35	Proposed mechanism for the irreversible inhibition of STS by compound 3.29	119
Figure 3.36	The structure of an activity-based probe for steroid sulfatase proposed by Lu and coworkers	121
Figure 3.37	Structures of compounds 3.31-3.34	123
CHAPTER 4 – BORONIC ACIDS AS INHIBITORS OF STEROID SULFATASE		
Figure 4.1	Examples of potent 17 α -benzyl estradiol inhibitors of STS reported by Poirier and coworkers	134
Figure 4.2	Proposed mechanism of inhibition of serine protease enzymes by boronic acids	135

Figure 4.3	Structure of Bortizomid	135
Figure 4.4	Proposed mechanism of inhibition of STS by boronic acids	137
Figure 4.5	Proposed boronic acid inhibitors of STS, 4.6-4.9	137
Figure 4.6	Lineweaver-Burk plot for boronic acid 4.6 at pH 7.0	139
Figure 4.7	Lineweaver-Burk plot for E1 at pH 7.0	140
Figure 4.8	Lineweaver-Burk plot for boronic acid 4.6 at pH 8.8	141
Figure 4.9	Lineweaver-Burk plot for boronic acid 4.7 at pH 7.0	142
Figure 4.10	Lineweaver-Burk plot for 4.1 at pH 7.0	143
Figure 4.11	Lineweaver-Burk analysis for 4.10 at pH 7.0	145
Figure 4.12	Structures of compounds 4.11 and 4.12	146

CHAPTER 5 – AN ASSESSMENT OF THE SULFONIC ACID AND SULPHONAMIDE GROUPS AS PHOSPHOTYROSINE MIMICS FOR PTP1B INHIBITION

Figure 5.1	(A) Protein phosphorylation is regulated by the dual action of protein tyrosine kinases (PTKs) and protein tyrosine phosphatases (PTPs) (B) General reaction scheme for the PTP reaction that catalyzes phosphate ester hydrolysis via a covalent phosphocysteine intermediate	153
Figure 5.2	The role of PTP1B in insulin and leptin signalling	157
Figure 5.3	Phosphotyrosine and its position in a hexapeptide portion of the epidermal growth factor receptor (EFG)	158
Figure 5.4	Ribbon diagram of the PTP1B tertiary structure	160
Figure 5.5	Proposed catalytic mechanism and transition state of PTP reaction	162
Figure 5.6	bis-(<i>para</i> -phosphophenyl) methane (BPPM)	163
Figure 5.7	(A) Schematic illustration of interrelationship of redox states of PTP1B. (B) Proposed mechanism for generating the sulphenylamide bond	164
Figure 5.8	Non-hydrolyzable phosphate mimics	167
Figure 5.9	Sulfotyrosine (sTyr) mimics of phosphotyrosine (pTyr)	168
Figure 5.10	Non-hydrolyzable phosphate mimic, difluorosulfonomethylphenylalanine (F ₂ Smp)	169
Figure 5.11	Carboxylic acid-containing phosphate mimics	170
Figure 5.12	Tripeptide display platform examined by Lee and coworkers	172
Figure 5.13	Bidentate ligands developed as inhibitors of PTP1B	174
Figure 5.14	Isothiazolidinone-based inhibitors of PTP1B	175
Figure 5.15	Structure of proposed sulfonate and difluorosulfonate inhibitors	176
Figure 5.16	Phosphotyrosine mimics	177
Figure 5.17	Proposed inhibitors of PTP1B	178
Figure 5.18	Lineweaver-Burk plot for the inhibition of PTP1B with inhibitor 5.26	180
Figure 5.19	Structure of peptide 5.37	181
Figure 5.20	Lineweaver-Burk plot for the inhibition of PTP1B with inhibitor 5.29	183
Figure 5.21	Examples of monoanionic inhibitors of PTP1B recently reported in literature	184

Figure 5.22	Tripeptide inhibitor 5.44 of YopH and PTP1B and a hydrophobic inhibitor 5.45 of PTP1B	188
Figure 5.23	Fluorogenic assay for PTP1B	192

APPENDIX A - PRELIMINARY KINETIC STUDIES WITH COMPOUNDS 3.24, 3.25 AND 3.32-3.34

Figure A.1	IC ₅₀ plot for compound 3.24 . Inhibitor concentrations range from 11-400 μ M. IC ₅₀ = 218 \pm 12 μ M.	225
Figure A.2	IC ₅₀ plot for compound 3.25 . Inhibitor concentrations range from 15-400 μ M. IC ₅₀ = 158 \pm 17 μ M.	225
Figure A.3	IC ₅₀ plot for compound 3.33 . Inhibitor concentrations range from 2-1000 μ M. IC ₅₀ = 62 \pm 7 nM.	225
Figure A.4	IC ₅₀ plot for compound 3.33 . Inhibitor concentrations range from 22-400 μ M. IC ₅₀ = 215 \pm 8 μ M.	226
Figure A.5	Time- and concentration-dependent inhibition of STS with inhibitor 3.32 over 30 minutes.	226

APPENDIX B – SUPPLEMENTARY FIGURES FOR COMPOUNDS 4.6, 4.7, 4.10, 4.11

Figure B.1	Replot of the data from Figure 4.6 to determine the K_i of inhibitor 4.6 at pH 7.0	227
Figure B.2	Lineweaver-Burk plot of inhibitor 4.6 at pH 7.5	227
Figure B.3	Replot of the data from Figure B.2 to determine the K_i of inhibitor 4.6 at pH 7.5	227
Figure B.4	Lineweaver-Burk plot of inhibitor 4.6 at pH 8.0	228
Figure B.5	Replot of the data from Figure B.4 to determine the K_i of inhibitor 4.6 at pH 8.0	228
Figure B.6	Lineweaver-Burk plot of inhibitor 4.6 at pH 8.5.	228
Figure B.7	Replot of the data from Figure B.6 to determine the K_i of inhibitor 4.6 at pH 8.5	229
Figure B.8	Replot of the data from Figure 4.8 to determine the K_i of inhibitor 4.6 at pH 8.8	229
Figure B.9	Replot of the data from Figure 4.9 to determine the K_i of inhibitor 4.7 at pH 7.0	229
Figure B.10	Replot of the data from Figure 4.9 to determine the αK_i of inhibitor 4.7 at pH 7.0	230
Figure B.11	Replot of the data from Figure 4.7 to determine the K_i of inhibitor estrone (E1) at pH 7.0	230
Figure B.12	Replot of the data from Figure 4.7 to determine the αK_i of inhibitor estrone (E1) at pH 7.0	230
Figure B.13	Replot of the data from Figure 4.10 to determine the K_i of inhibitor 4.1 at pH 7.0	231
Figure B.14	Replot of the data from Figure 4.10 to determine the αK_i of inhibitor 4.1 at pH 7.0	231
Figure B.15	Replot of the data from Figure 4.11 to determine the K_i of	231

	inhibitor 4.10 at pH 7.0	
Figure B.16	Replot of the data from Figure 4.11 to determine the αK_i of inhibitor 4.10 at pH 7.0	232
Figure B.17	IC ₅₀ plot for inhibitor 4.8 at pH 7.0	232
Figure B.18	IC ₅₀ plot for inhibitor 4.9 at pH 7.0	232
 APPENDIX C – SUPPLEMENTARY FIGURES FOR COMPOUNDS 5.26, 5.27, 5.28, 5.29, 5.34, AND 5.42		233
Figure C.1	Replot of the data from Figure 5.19 to determine the K_i of inhibitor 5.26	233
Figure C.2	Lineweaver-Burk plot of compound 5.27	233
Figure C.3	Replot of the data from Figure C.2 to determine the K_i of inhibitor 5.27	234
Figure C.4	Lineweaver-Burk plot of compound 5.28	234
Figure C.5	Replot of the data from Figure C.4 to determine the K_i of inhibitor 5.28	235
Figure C.6	Replot of the data from Figure 5.21 to determine the K_i of inhibitor 5.29	235
Figure C.7	IC ₅₀ of compound 5.42 using 3 nM PTP1B	236
Figure C.8	IC ₅₀ of compound 5.42 using 1.5 nM PTP1B	236
Figure C.9	IC ₅₀ of compound 5.42 using 6.0 nM PTP1B	237
Figure C.10	IC ₅₀ of compound 5.34	237
Figure C.11	IC ₅₀ of compound 5.35	238
Figure C.12	IC ₅₀ of compound 5.43	238

List of Abbreviations

Abbreviation	Full name
ABP	Activity-based probe
Adiol	Andro-5-ene-3 β ,17 β -diol
Adione	Androstenedione
ADP	Adenosine diphosphate
AH	Addition-Hydrolysis
ARS	Arylsulfatase
ARSA	Arylsulfatase A
ARSB	Arylsulfatase B
ARSC	Arylsulfatase C, also called Steroid Sulfatase (STS), Estrone Sulfatase (ES)
AP	Alkaline phosphatase
ATP	Adenosine triphosphate
β -ME	β -mercaptoethanol
BPPM	bis-(<i>para</i> -phosphophenyl) methane
BSA	Bovine serum albumin
3 β -HSD	3 β -hydroxysteroid dehydrogenase isomerase
17 β -HSD	17 β -hydroxysteroid dehydrogenase
CA II	Carbonic anhydrase II
CCK	Cholecystokinin
CD45	Cluster for differentiation 45
cDNA	Complementary deoxyribonucleic acid
CHO	Chinese hamster ovary cells
CMC	Critical micelle concentration
667-COUMATE	667 4-methyl coumarin sulphamate
COUMATE	4-methyl coumarin sulphamate
Da	Dalton
DASI	Dual aromatase and STS inhibitor
DEAE	Diethylaminoethyl cellulose
DFMP	α,α -difluoromethylenephosphonic acid
DHEA	Dehydroepiandrosterone
DHEAS	Dehydroepiandrosterone Sulfate
DHEA-STC	Dehydroepiandrosterone Sulfatase
DiFMUS	Difluoro-4-methyl-umbelliferyl sulfate
DiFMUP	Difluoro-4-methyl-umbelliferyl phosphate
DFMP	Difluoromethylene phosphonate
DMSO	Dimethylsulfoxide
DNA	Deoxyribonucleic acid
DSPs	Dual-specificity phosphatases
DTT	Dithiothreitol
EE	Ethinyl estradiol
293-EBNA	human embryonic kidney cells expressing Epstein Barr virus nuclear antigen-1
E.C.	Enzyme Commission

E-I	Enzyme-Inhibitor complex
E1	Estrone
ECM	Extracellular matrix
EGFR	Epidermal growth factor
EMATE	Estrone-3- <i>O</i> -sulphamate
E1-3-MTP	Estrone Methylthiophosphonate
E1S	Estrone-3- <i>O</i> -sulfate
E1P	Estrone-3- <i>O</i> -phosphate
E2	Estradiol
ER	Estrogen receptor
ER+	Estrogen receptor-positive
ER-	Estrogen receptor-negative
ESI	Electrospray ionization
4-DFME	4-difluoromethyl estrone
4-FE	4-Formylestrone
FGE	Formylglycine generating enzyme
FGly	Formylglycine
FGS	Formylglycine Sulfate
FOMT	fluoro- <i>O</i> -malonyl tyrosine
F ₂ Pmp	α,α -difluoromethylenephosphonic acid
GABA _A	γ -aminobutyric acid _A
GSH	Glutathione
HEK	Human embryonic kidney cells
HEPES	N-2-Hydroxyethylpiperazine-N'-2-ethanesulfonic acid
HPLC	High pressure liquid chromatography
IL-6	Interleukin 6
IPTG	Isopropyl- β -D-thiogalactopyranoside
IR	Insulin receptor
IRS	Insulin receptor substrates
JAK2	Janus kinase 2
kb	kilobase
kDa	Kilodalton
LC-MS	Liquid chromatography mass spectrometry
LMW	Low molecular weight
LNCaP	Prostate cancer cell line
MALDI	Matrix-assisted laser/desorption ionization
MBI	Mechanism-based inhibitors
MCF-7	Human breast cancer cell line
MLD	Metachromatic Leukodystrophy
MS	Mass spectrometry
MSD	Multiple Sulfatase Deficiency
4-MUS	4-Methylumbelliferyl Sulfate
4-MU	4-Methylumbelliferone
NCBI	National Centre for Biotechnology Information
NMR	Nuclear magnetic resonance
NRPTP	Non-receptor protein tyrosine phosphatase

mRNA	Messenger ribonucleic acid
ObR	Leptin receptor
OMT	<i>O</i> -malonyl tyrosine
PAPS	3'-phosphoadenosine-5'-phosphosulfate
PARS	<i>Pseudomonas aeruginosa</i> aryl sulfatase
PDB	Protein Data Bank
<i>p</i> -NCS	Para-nitrocatechol sulfate
pI	Isoelectric point
PMP	Phosphonomethyl phenylalanine
PRL	Phosphatase of regenerating liver
PTEN	Phosphatase and tesarin homolog
PTK	Protein tyrosine kinase
PTP	Protein tyrosine phosphatase
PTP1B	Protein tyrosine phosphatase 1B
pTyr	Phosphotyrosine
RBC	Red blood cell
RER	Rough Endoplasmic Reticulum
RFU(s)	Relative Fluorescence Unit(s)
rmsd	Root mean square deviation
RP-HPLC	Reverse Phase High Performance Liquid Chromatography
RPTP	Receptor protein tyrosine phosphatase
S	Svedberg
SD-1	Subdomain 1
SD-2	Subdomain 2
SDM	Site-directed mutagenesis
SDS PAGE	Sodium Dodecyl Sulfate Polyacrylamide Gel Electrophoresis
SI	Suicide inhibitor
SPPS	Solid phase peptide synthesis
STS	Steroid Sulfatase
SULT1E1	Estrone sulfotransferase (E.C. 2.8.2.4)
sTyr	Sulfotyrosine
sumf1	Sulfatase modifying factor 1 gene
TE	Transesterification-elimination
Th cell	T helper cell
TNF α	Tumour necrosis factor alpha
X-LI	X-linked ichthyosis

Chapter 1 – Steroid Sulfatase: Structure, Function and Inhibitor Development[†]

1.1 Introduction

1.1.1 The sulfatase family of enzymes

The sulfatase family is a class of enzymes that were discovered in eukaryotes and prokaryotes sporadically during the 20th century without receiving much research focus. It was originally thought that the role of these enzymes was limited to the degradation of organic sulfates in soil in prokaryotes or to render mammalian metabolites soluble for excretion in eukaryotes. The sulfatases began to receive more careful attention in the 1960s due to the discovery that they were responsible for human lysosomal storage disorders when deficiencies in certain sulfatases occurred. Sulfatases are now understood to have roles in diverse processes such as hormone regulation, cellular degradation, bone and cartilage development, intracellular communication, and signalling pathways (Hanson et al., 2004). As listed in **Table 1.1** there are currently seventeen members identified in the human sulfatase family (Obaya, et al., 2006; Sardiello et al., 2005) whose function is to catalyze the hydrolysis of sulfate monoester bonds (RO-SO₃⁻) from various physiological substrates such as hydrophobic steroid sulfates, water-soluble mono- and disaccharide sulfates, and amphiphilic carbohydrate

[†] Figures 1.7 to 1.13 in this chapter were provided courtesy of a collaborator, Dr. Debashis Ghosh of the Hauptman-Woodward Medical Research Institute and Roswell Park Cancer Institute, Buffalo, N.Y, and are reproduced herein with his express written consent as noted in Appendix E.

sulfates from glycosaminoglycans, proteoglycans, glycolipids. The reason many members of the class are named *aryl sulfatases* (ARSs) is because their ability to hydrolyze the sulfate ester bond from non-natural aryl substrates, such as *p*-nitrocatechol sulfate (*p*-NCS) (Roy, 1971), was discovered before their physiological substrates were known. Six members of the family reside in lysosomes, are soluble, and function at acidic pH in the degradative pathways of glycosaminoglycans and sulfolipids. Five other members are associated with organelle membranes where they function at neutral pH. Before being targeted to these cellular locations, sulfatases are extensively glycosylated in the secretory pathway (Stein et al., 1989). Two cell-surface carbohydrate sulfatases that reside in the extracellular matrix (ECM) have also been identified, hSulf1 and hSulf2 (Morimoto-Tomita et al., 2002). These sulfatases remove 6-*O*-sulfate *endo*-groups on glucosamine in heparan sulfate with the effect of fine-tuning the sulfation pattern of this glycosaminoglycan. Thus, the hSulf1 and hSulf2 sulfatases may have a role in the development and the pathogenesis of pancreatic cancer (Uchimura et al., 2006; Li et al., 2005). Four new human sulfatase genes, encoding aryl sulfatases ARSH, ARSI, ARSJ, and ARSK, have recently been identified and while their substrates and subcellular locations are still unknown, their expression is restricted mainly to embryonic tissues and cancer cell lines (Sardiella et al., 2005; Obaya, 2006).

The sulfatase class is highly conserved in sequence and structurally across members. For example, there is a 20-60% sequence homology over the entire protein length and particular homology is attributed to the N-terminal region where sulfatase consensus motifs are present (Ghosh, 2007). The level of homology has led to a theory that all sulfatases arise from a common genetic ancestor (Peters et al., 1990; Meroni et

al., 1996; Parenti et al., 1997). One of the most distinctive features of the sulfatase class is the presence of a post-translationally installed 2-amino-3-oxopropanoic acid, or α -formylglycine (FGly), residue that is established as a result of a post-translational modification that is unique in nature, as discussed in detail in § 1.1.2 and **Figure 1.1A**. Until recently, the sulfatase enzyme family was the only known example to carry a post-translationally installed FGly residue. A recent report structurally and kinetically characterized a phosphonate monoester hydrolase/phosphodiesterase derived from *Rhizobium leguminosarum* that bears a FGly post-translational modification (Jonas et al., 2008). This is the first example of a non-sulfatase to carry an active site FGly residue and to use it as a nucleophile in the catalytic manner of sulfatases. In addition the *R. leguminosarum* phosphonate monohydrolase possesses a close structural homology to the α/β core seen in sulfatases, although their sequences have diverged considerably. These findings support a theory that sulfatases belong to the alkaline phosphatase superfamily (O'Brien and Herschlag, 1998).

Table 1.1. Human sulfatases: their substrates and cellular locations

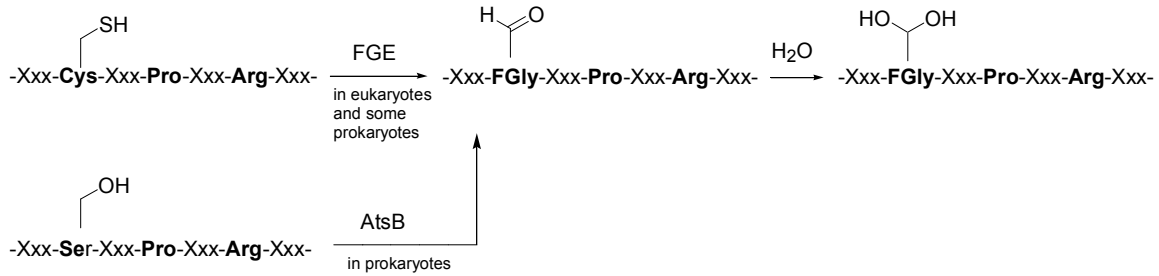
Sulfatase Name	Abbreviation	Location	Natural Substrate	Reference
Aryl sulfatase A	ARSA	Lysosome	Cerebroside sulfate	Stein et al., 1989
Aryl sulfatase B	ARSB	Lysosome	Dermatan sulfate	Peters et al., 1990; Anson et al., 1992
Steroid Sulfatase	STS, ARSC	ER	Steroid sulfates	Stein et al., 1989
Aryl sulfatase D	ARSD	ER	Unknown	Franco et al., 1995
Aryl sulfatase E	ARSE	Golgi apparatus	Unknown	Franco et al., 1995
Aryl sulfatase F	ARSF	ER	Unknown	Puca et al., 1990
Aryl sulfatase G	ARSG	ER	Unknown	Ferante et al., 2002
Aryl sulfatase H	ARSH	Unknown	Unknown	Sardiello et al., 2005; Obaya, 2006
Aryl sulfatase I	ARSI	Unknown	Unknown	Sardiello et al., 2005; Obaya, 2006
Aryl sulfatase J	ARSJ	Unknown	Unknown	Sardiello et al., 2005; Obaya, 2006
Aryl sulfatase K	ARSK	Unknown	Unknown	Sardiello et al., 2005; Obaya, 2006
Galactosamine (<i>N</i> -acetyl)-6-sulfatase	GALNS	Lysosome	Keratin sulfate, Chondroitin sulfate	Tomatsu et al., 1991
Glucosamine (<i>N</i> -acetyl)-6-sulfatase	G6S	Lysosome	Heparan sulfate	Scott et al., 1995
<i>N</i> -sulfoglucosamine sulfohydroloase	SGSH	Lysosome	Keratan sulfate	Freeman and Hopwood, 1991
Iduronate-2-sulfatase	IDS	Lysosome	Heparan sulfate	Bielicki et al., 1993
Endo sulfatase 1	Sulf 1	ECM	Heparan sulfate	Morimoto-Tomita et al., 2002
Endo sulfatase 2	Sulf 2	ECM	Heparan sulfate	Morimoto-Tomita et al., 2002

1.1.2 Formylglycine

All FGly-containing sulfatases in eukaryotes have a signature pentapeptide motif ¹, (Cys/Ser)-Xxx-(Pro/Ala)-Xxx-Arg, responsible for directing the post-translational modification of FGly at the site of the first cysteine residue, as shown in the partial alignment in **Figure 1.1B**. In prokaryotes this modification occurs at the site of the first serine residue and is catalyzed by an Fe-S cluster enzyme termed AtsB (Szameit et al., 1999). Biochemical data provides evidence that FGly is essential for catalysis in sulfatases (Dierks et al., 1997, Miech et al., 1998, Selmer et al., 1996). In

¹ According to the Prosite website (<http://us.expasy.org/prosite>), the N-glycosylation sulfatase signature sequence accession number is PS00523.

humans the essential FGly modification is underscored by serious pathological consequence, *multiple sulfatase deficiency* (MSD, Dierks et al., 2003), a lysosomal storage disorder that occurs due to a dysfunction in the enzyme responsible for catalyzing the installation of FGly. Multiple sulfatase deficiency is a rare autosomal recessive disease and is further discussed in § 1.2.7. Symptoms are severe and include ataxia, progressive loss of motor abilities, speech, vision and hearing, organomegaly and eventually death. The enzyme responsible for catalyzing the FGly modification was recently isolated, cloned and sequenced and is termed *formylglycine-generating enzyme* (FGE) and is encoded for by the sulfatase modifying factor 1 (*sumf1*) gene (Cosma et al., 2003; Dierks et al., 2003). Mutations to the gene coding for FGE lead to an inactive enzyme and this causes an absence or an incompletely modified Cys → FGly modification in all human sulfatases.

A**B**

	1	2	3	4	5	6	7	8	9	10	11	12	ExPASy Accession Number*
ARSA	C	T	P	S	R	A	A	L	L	T	G	R	P15289
ARSB	C	T	P	S	R	S	Q	L	L	T	G	R	NP_000037
STS	C	T	P	S	R	A	A	F	M	T	G	R	P08842
PARS	C	S	P	T	R	S	M	L	L	T	G	T	P51691

Figure 1.1. (A) Reactions catalyzed by the formylglycine generating enzyme (FGE) in eukaryotes and some prokaryotes and AtsB in prokaryotes to convert the first cysteine in the pentapeptide consensus sequence (C/S-X-P/A-X-R) to a formylglycine (FGly). (B) Signature sequence of sulfatases. A partial alignment of sulfatase genes from ARSA, ARSB, STS and PARS shows homology of the sulfatase signature sequence. This sequence is essential for directing the formylglycine generating enzyme to convert the first amino acid residue of the sequence to FGly.

FGE is located in the endoplasmic reticulum and mediates the modification during, or shortly after translocation of newly translated, unfolded target sulfatase to the membrane of the endoplasmic reticulum (Dierks *et al.*, 1997). Once the target sulfatase has folded, the cysteine residue is buried in a deep cleft and becomes inaccessible to FGE (Boltes *et al.*, 2001; Lukatela *et al.*, 1998).

The mechanism for modification of Cys → FGly is a multi-step redox process that requires calcium, molecular oxygen, and a reducing agent to generate FGly via a

* Please see the website: <http://us.expasy.org/prosite> operated by the [Swiss Institute of Bioinformatics](http://www.sib.ac.ch).

cysteine sulfenic acid intermediate (Fey et al., 2001; Dierks et al., 2005). Notably, the process does not employ any cofactors or any redox-active metal ions and molecular oxygen serves as the terminal electron acceptor. This redox process has been emulated in vitro using model peptides as substrates and dithiothreitol as a reducing agent (Dierks et al., 2003; Preusser-Kunze et al., 2005). The FGE redox process is unusual because many redox enzymes use metals in Fe-S- or Mo-Fe-clusters, or Ni²⁺ or Cu²⁺ to exchange electrons during catalysis. Alternatively, redox enzymes employ nucleotide or protein cofactor such as NAD(P)⁺, or FAD. The three-dimensional crystal structures of human FGE was elucidated in six different redox environments to provide structure-based evidence for a mechanism (Dierks et al., 2005). These structures reveal that the substrate-binding cleft bears a redox-active cysteine pair (Cys336 and Cys341) that is prone to oxidation to a disulfide bond in the presence of molecular oxygen. A mechanism has been proposed where a mixed disulfide forms between the target sulfatase substrate and Cys341 of FGE as shown in step (A) of **Figure 1.2**, while the other FGE cysteine residue, Cys336 is oxidized to a sulfenic acid (SOH) as shown in step (B). In the next step (C), transfer of the hydroxyl group from Cys336 to the substrate sulfatase cysteine residue occurs and the FGE disulfide Cys336/Cys341 pair is regenerated (D). An attack by a catalytic base occurs at C β of the substrate cysteine sulfenic acid to eliminate H₂O and generate the thioaldehyde intermediate (E), which is hydrolyzed to formylglycine (F), and can undergo further hydrolysis to form a formylglycine hydrate (H). In addition to crystal structure evidence for FGE under various oxidation states, this mechanism has been further supported by evidence

obtained by X-ray crystal structures² of FGE in complex with model peptides (Roeser et al., 2006). The model peptides, CTPSR and LCTPSRA, were based on the pentapeptide FGE-directing amino acid sequence of arylsulfatase A (ARSA). The X-ray crystal structure obtained of a complex between an expressed FGE mutant Cys341Ser and CTPSR demonstrate direct evidence of a disulfide bond between Cys336 of the mutant ARSA and the cysteine residue of the pentapeptide (Roeser et al., 2006).

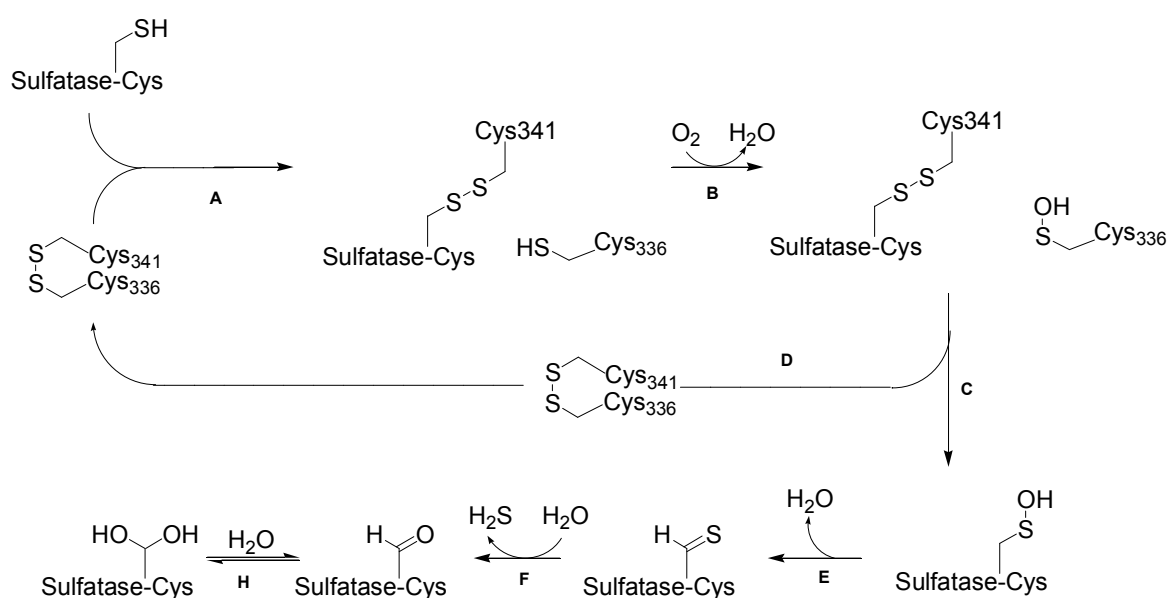


Figure 1.2. A proposed mechanism for formylglycine generation in eukaryotes by FGE.

Through genetic evaluation of patients with MSD to date, a total of 18 missense mutations have been found to occur to FGE over 17 different residues. By mapping the locations of these mutations on the three-dimensional X-ray crystal structure of FGE it becomes clear that they have serious effects on residues involved in structural stability,

² Protein Data Bank ID numbers: 2ajj, 2aik

substrate binding, and catalysis (Dierks et al., 2005). Thus, there is a molecular basis for MSD.

It is interesting to note that a strategy has been reported recently where the pentapeptide sequence, CXPXR, responsible for directing modification of Cys → FGly can be inserted into a gene of interest to produce a recombinant protein for expression in *E. coli* (Carrico et al., 2007). As illustrated in **Figure 1.3** prokaryotes such as *E. coli* have the ability to convert the cysteine residue in the pentapeptide sequence CXPXR to FGly via FGE. This sulfatase motif can serve as an FGly-directing modification for the site-specific introduction of an aldehyde tag which can be chemoselectively modified with an aminoxy- or hydrazide-functionalized reagent. The protein can then be labeled with a fluorescent dye in this manner.

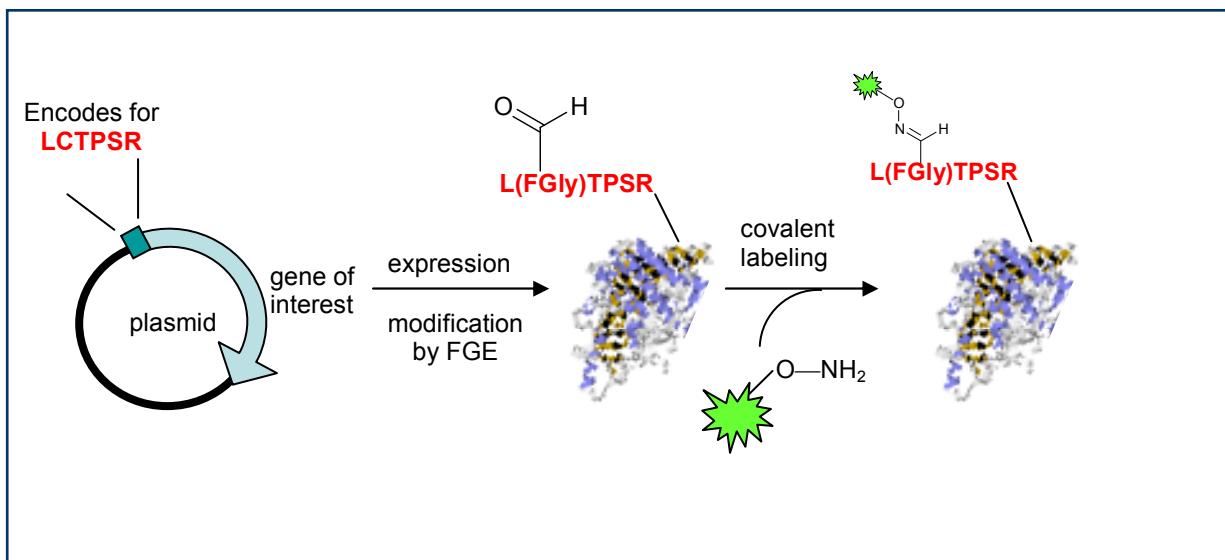


Figure 1.3. The formylglycine generating sequence can be introduced recombinantly into a gene of interest and *E. coli* formylglycine-generating enzyme (FGE) can be exploited to generate an aldehyde tag at this site. The aldehyde serves as a handle to which a fluorescent dye can be attached (Adapted from Carrico et al., 2007).

1.2 Steroid sulfatase

1.2.1 STS expression and location

Much of the work in this thesis is concerned with the development of inhibitors of an enzyme known as steroid sulfatase (STS). Human steroid sulfatase (E.C. 3.1.6.2) is an enzyme responsible for modulating the levels of steroid hormones. It is an integral membrane protein localized in the rough endoplasmic reticulum (Stein et al., 1989), lumen-oriented, and catalyzes the hydrolysis of sulfur ester bonds from diverse 3-*O*-sulfated steroids such as cholesterol sulfate, pregnelone sulfate, dehydroepiandrosterone sulfate and estrone sulfate. It was long thought that sulfated steroids merely represented a means to excrete these steroids, however, it is now well established that STS serves to convert these inactive precursors to their active, desulfated counterparts that feed into pathways for steroid-based signaling (Noel et al., 1981). STS is ubiquitously expressed in mammalian tissues (Warren and French, 1965). STS activity is detected in tissues ubiquitously in small quantities (Dooley *et al.*, 2000; Martel *et al.*, 1994). It is most richly expressed in placenta, and is also prevalent in testis, ovary, adrenal glands, fallopian tubes, prostate, skin, brain, fetal lung, viscera, endometrium, peripheral blood lymphocytes, aorta, kidney and bone (Miki *et al.*, 2002).

STS contains four possible *N*-linked glycosylation sites as a result of post-translation modifications (Stein et al., 1989; Yen et al., 1987). The site of post-translational modification is dictated by a consensus sequence³ Asn-Xaa-Ser/Thr. However, despite the consensus sequence the four possible glycosylation sites are not always glycosylated. Digestion studies performed with endoglycosidase H shows that

³ According to the Prosite website (<http://us.expasy.org/prosite>), the N-glycosylation sulfatase signature sequence is PS00149.

at least two sites, Asn47 and Asn259, of the four potential sites are glycosylated. The exact functional significance of these glycosylations with regard to modulating STS activity was not shown until recently when mutation studies were reported (Stengel et al., 2008). When the mutations N47Q and N259Q were made, the STS activity was significantly reduced, while STS mutants bearing N333Q, N459Q and N54Q had activity comparable to the wild type enzyme.

The STS gene lies on the distal short arm of the X-chromosome and has been cloned, sequenced and characterized (Yen *et al.*, 1988)⁴. The 146-kb gene is comprised of 10 exons, with introns ranging from 102 bp up to 35 kb in size. The cDNA for STS has also been cloned and sequenced (Yen *et al.*, 1987; Stein et al., 1989)⁵. It encodes a 583-amino acid protein with a short signal peptide of 21-23 amino acids and the four *N*-glycosylation motifs. Its apparent size is 63.5 kDa including the signal peptide that is cleaved during translocation to the endoplasmic reticulum in addition to the processing of the *N*-oligosaccharide chains, leaving a 61 kDa protein. However, there is disparity in the literature regarding the molecular size of STS purified from human placenta due to the presence of various *N*-linked glycosylations (Stein et al., 1989; Yen et al., 1987). There is no current agreement in the literature regarding molecular regulation of STS transcription. There was evidence that both cytokines TNF α and IL-6 up-regulate STS activity in MCF-7 breast cancer cells (Purohit *et al.*, 1997). However, this was refuted by evidence that the change in activity was effected post-translationally and not due to a change in gene transcription (Newman *et al.*, 2000). Nevertheless, there is strong evidence that upregulation of STS activity is a factor in hormone-dependent cancers

⁴ GenBank accession no. M23945

⁵ GenBank accession no. M16505 and J04964

such as breast cancer (Miyoshi et al., 2003; Suzuki et al., 2003). For this reason the enzyme has become a target for design of small molecule therapeutics.

1.2.2 STS and hormone-dependent breast cancer

The levels of sulfated estrogens are regulated through the actions of steroid sulfatase and sulfotransferase. Sulfated steroids are unable to bind to steroid hormone receptors and are biologically inactive until hydrolysis of their sulfate ester bond is catalyzed by steroid sulfatase. Circulating plasma concentrations of the sulfated steroids, estrone-3-*O*-sulfate (E1S), and dehydroepiandrosterone sulfate (DHEAS), are significantly higher than those of their non-sulfated counterparts, estrone (E1), and dehydroepiandrosterone (DHEA) (Noel et al., 1981). In addition, the half-life of E1S and DHEAS in plasma is about 10-12 hours, which is considerably longer than the 30-40 minute half-life of E1 and DHEA (Ruder et al., 1972). For these reasons, the role of sulfated steroids is seen a storage reservoir that acts as a source of biologically active steroid hormones when activated by STS.

Research directed toward STS has intensified in the last 15 years due to its role in estrogen receptor-positive (ER+) hormone-dependent breast and endometrial cancer. These types of endocrine-dependent cancers occur most frequently in post-menopausal women which is paradoxical as ovarian production of estrogen has stopped. Instead of local production of estrogens in tumours, the growth of the tumour is stimulated by estrogen produced by enzymes in peripheral tissues. For example, androstenedione is produced in the adrenal cortex and converted to E1 by the enzyme complex aromatase (James et al., 1987; Reed et al., 1989) (**Figure 1.4**). Subsequently, estrone is converted to E1S via estrone sulfotransferase (SULT1E1, E.C. 2.8.2.4) using 3'-

phosphoadenosine-5'-phosphosulfate (PAPS) as a cofactor as illustrated in **Figure 1.5** (Williams et al., 2008). The E1S produced in this fashion now acts as an estrogen reservoir in tissue and in plasma (Hobkirk, 1993; Reed and Purohit, 1993; Reed et al., 1994). There is agreement that estrogen formed in breast tumours is produced largely by the action of STS and not through that of aromatase (Santner et al., 1984; Masamura et al., 1996).

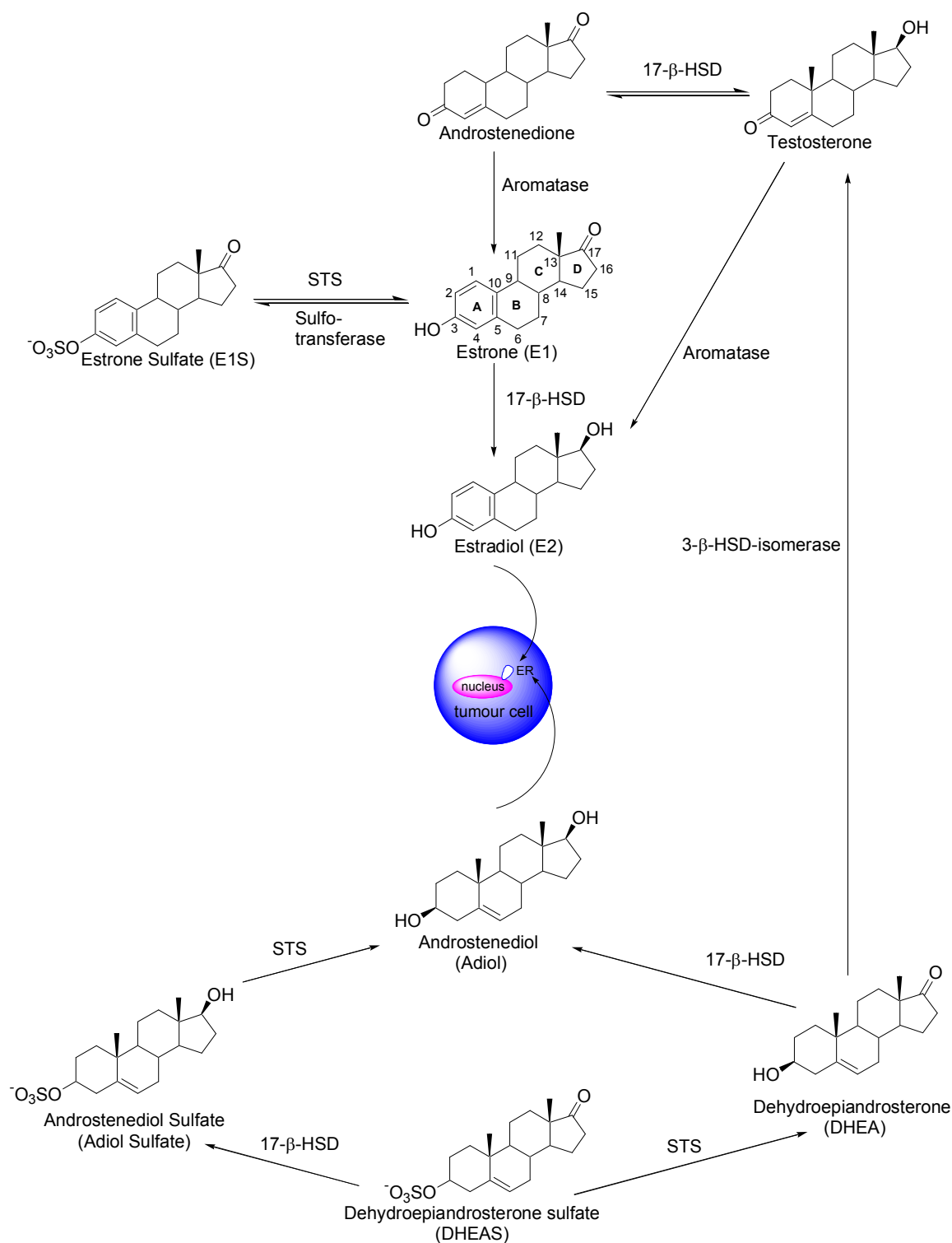


Figure 1.4. Origins of estrogenic steroids in breast tumours. The aromatase route forms estradiol which stimulates tumour cells. However, estradiol is also formed via STS. Additional stimulation of tumour growth occurs via Androstenediol production. Abbreviations: 17-β-HSD, 17-β-hydroxysteroid dehydrogenase; 3-β-HSD-isomerase, 3-β-hydroxysteroid dehydrogenase; ER, estrogen receptor.

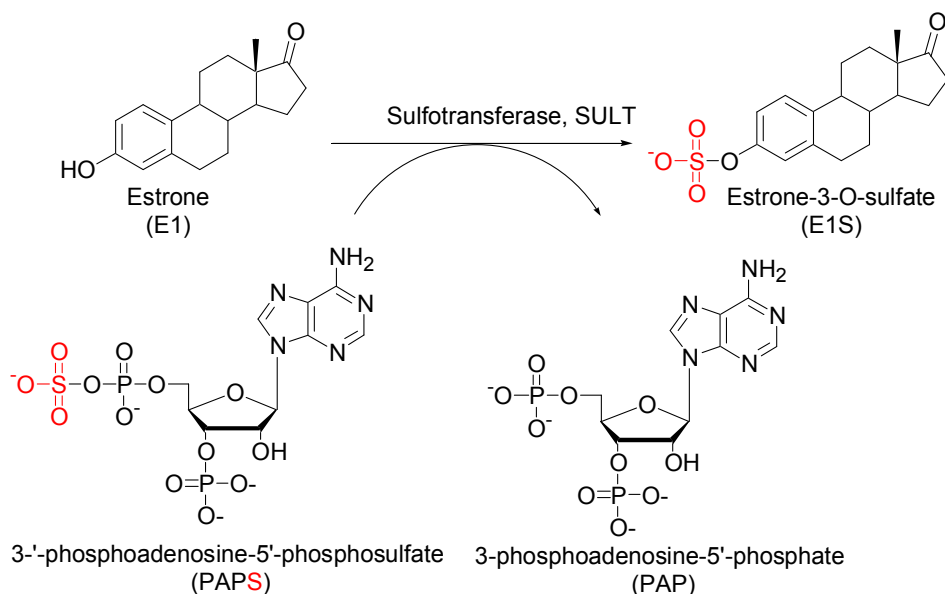


Figure 1.5. Reaction catalyzed by estrone sulfotransferase (SULT1E1).

Many aromatase inhibitors for treating ER+ breast cancer have been developed but have shown limited efficacy. In a stage III clinical trial of a potent aromatase inhibitor designed to block the production of estrone, only 11% of patients treated showed any response measured by the study's endpoints (Jonas et al., 1996). This major study highlights the inadequacy of blocking estrogen biosynthesis through inhibition of aromatase alone. This is because the reservoir of E1S is a source of estrogen when activated by STS, and estrogen stimulates tumour growth despite inhibition of its synthesis by aromatase. The other factor is that inhibition of aromatase does not prevent production of an androgen named 5-androstenediol (Adiol) that is able to bind to the estrogen receptor and stimulate growth of tumour cells (Poulin and Labrie, 1986). As E1S represents a storage reservoir of E1, so too does the sulfated form of Adiol. Evidently, 90% of Adiol in post-menopausal women originates from DHEAS, whose desulfation is also catalyzed by STS (Poortman et al., 1980). Thus, the strategy to curtail stimulation of ER+ tumour cells should include blocking the production of both

estrogen and Andiol. In addition to blocking aromatase activity, steroid sulfatase activity must also be blocked.

1.2.3 STS action in prostate cancer

DHEAS is an androgen produced primarily by the adrenal cortex, and can be converted to testosterone and dihydrotestosterone in prostate tissue as shown in **Figure 1.6** (Harper *et al.*, 1974, Boivin *et al.*, 2000). These two steroids stimulate prostate tumour growth (Labrie *et al.*, 1996). STS activity has been detected in prostatic gland where it serves as a major peripheral source of active androgen production (Farnsworth., 1973). In addition, STS activity has been demonstrated in a prostatic cancer cell line, LNCaP (Selcer *et al.*, 2002). When LNCaP cells were treated with a potent STS inhibitor, STS activity was almost completely blocked. This example demonstrates a potential application of STS inhibitors as therapeutics for prostate cancer treatment.

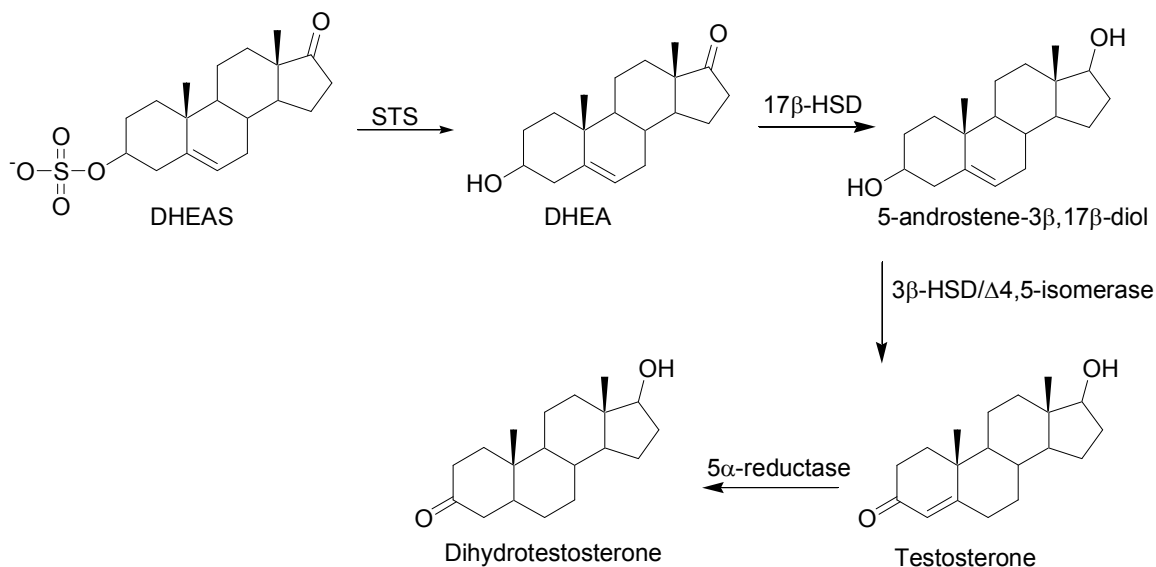


Figure 1.6. Biosynthetic pathway for the production of the androgens testosterone and dihydrotestosterone from DHEAS (3 β -HSD/ Δ 4,5 isomerase is 3 β -hydroxysteroid dehydrogenase/ Δ -4,5 isomerase) (Adapted from Boivin *et al.*, 2000).

1.2.4 STS and skin

STS is also active in the epidermis where it plays a role in local androgen production. A deficiency of STS is the cause of X-linked ichthosis (X-LI) and is further discussed in § 1.2.7. Individuals with X-LI experience scaling of the skin and a thickened *stratum corneum* (Hernandez-Martin *et al.*, 1999). Lipids form an important part of the *stratum* structure, and their absence make desquamation, or skin flaking, more difficult, leading to scaling. Without STS activity in the epidermis cholesterol sulfate accumulates as indicated by its higher than normal concentration in affected individuals compared to normal ones. Development of STS inhibitors for treatment of other diseases may cause a side effect of reduced STS activity in the skin. Treatment of X-LI is achieved through topical application of cholesterol cream and keratolytics such as ammonium lactate.

STS activity also plays a role in hair follicles by mediating conversion of DHEAS to 5 α -dihydrotestosterone, which activates the androgen receptor in hair follicles (Hoffman *et al.*, 2001). Individuals with androgenetic alopecia show elevated levels of DHEAS (Pitts *et al.*, 1987). It is proposed that there is a correlation between STS deficiency and androgenetic alopecia. It has also been proposed that increased STS activity is correlated with *acne vulgaris* according to studies examining STS immunoreactivity in affected skin (Chen *et al.*, 2002).

1.2.5 STS and neurofunction

In the brain, DHEAS and DHEA are suggested to act as a neurosteroid (Majewska *et al.*, 1995; Baulieu and Robel, 1996). It is thought that DHEAS acts as a γ -aminobutyric acid_A (GABA_A) receptor antagonist, increasing neuronal excitability

(Park-Chung *et al.*, 1999). Conversely, DHEA acts as a GABA_A receptor agonist (Park-Chung *et al.*, 1999). Studies in rodents indicated that DHEAS and DHEA are formed in the brain, in addition to their production in the adrenal cortex. However, a recent study on human temporal lobe biopsy samples showed that DHEA and DHEAS are not formed *de novo* in the brain due to lack of activity and mRNA expression of the enzymes essential for DHEA(S) synthesis (Steckelbroek *et al.*, 2004). Rather, DHEA production in the brain is likely due to STS conversion of DHEAS, as suggested by high levels of mRNA and strong activity of this enzyme. It is hypothesized that DHEAS originates from peripheral sources and is transported across the blood-brain barrier (Kriz *et al.*, 2008). Other studies of the role of STS activity in the brain have shown that certain STS inhibitors enhanced learning and spatial memory in rats (Li *et al.*, 1996; Le Roy *et al.*, 1999).

1.2.6 STS and the immune system

There are reports that DHEA modulates regulation of T-helper (Th) cell maturation into Th1- but not Th2-type profile (Daynes *et al.*, 1990; Rook *et al.*, 1994). DHEA has the ability to prevent release of cytokines from Th2 cells *in vitro*, while DHEAS does not. STS is present in macrophages and because it mediates conversion of DHEAS to DHEA, it has a significant effect in regulating part of the immune response (Daynes *et al.*, 1993).

1.2.7 Sulfatase deficiencies

The physiological significance of the sulfatases is underscored by the breadth of diseases that result from their deficiency (Bilabio and Shapiro, 1995). For example, point mutations to the arylsulfatase A (ARSA) gene cause a catalytic deficiency

resulting in a severe disorder of metabolic metabolism termed metachromatic leukodystrophy (MLD) (Kolodny et al., 1997). The onset of this disorder may occur at any age and is caused by accumulation of cerebroside sulfates in the white matter of the central and peripheral nervous system with dire neurological outcome.

Deficiency in arylsulfatase B (ARSB) is caused by genetic point mutations and results in a rare autosomal inherited disorder Maroteaux-Lamy syndrome. It is a mucopolysaccharidosis characterized by accumulation of mucopolysaccharides in the skeletal and nervous system, clouded cornea and increased urinary excretion of dermatan sulfates (Evers et al., 1996). ARSB deficiency may also have a role in cystic fibrosis, a condition characterized by excessive accumulation of secretions, including the sulfated glycosaminoglycans, chondroitin sulfate and dermatan sulfate (Tobacman et al., 2003). There are efforts to treat sulfatase deficiencies in humans with functional recombinant enzymes. For example, *galsulfatase* is a recombinant form of human ARSB and has been approved in the United States for the treatment of mucopolysaccharidosis (Hopwood et al., 2006).

Deficiency in STS due to a gene deletion and point mutations results in a condition called X-linked ichthyosis (XL-I) (Alperin and Shapiro, 1997). This inborn error in metabolism is due to a complete deletion of the 146-kb STS gene and its substantial flanking regions. Alternatively, XL-I can also result from point mutations within the STS gene, leading to a translation of a catalytically inactive STS protein (Alperin and Shapiro, 1997). Specifically, seven point mutations of the STS gene have been reported, all of which are located near the C-terminal domain (Alperin and Shapiro, 1997; Hernandez-Martin et al., 1999; Sugawara et al., 2000). Six of these point

mutations produce amino acid substitutions and one premature termination of translation of the full length protein. The six amino acid substitutions are Ser34Leu, Trp372Arg, Trp372Pro, His444Arg, Cys446Tyr and Gln560Pro. The seventh mutation which consists of a 19-base pair insertion at nucleotide 1477 at the splice junction of exon 8 and intron 8, produces a shift in the open reading frame and termination of protein translation at residue 427. The six substitution mutations have been mapped them onto the three-dimensional structure of STS in **Figure 1.7** (Ghosh, 2004). The locations of these mutations occur near catalytically active amino acids or the enzyme's membrane-associating motifs and most likely destabilize the active site architecture to a point where the enzyme is inactivated. Multiple sulfatase deficiency is manifested by large dark scales on the skin and by increased *stratum corneum* thickness (Williams et al., 1981). Because cholesterol sulfate is one of the substrates of STS, there is a 5-fold increased concentration of this substance in the *stratum corneum* of individuals affected by XL-I compared to that of normal individuals.

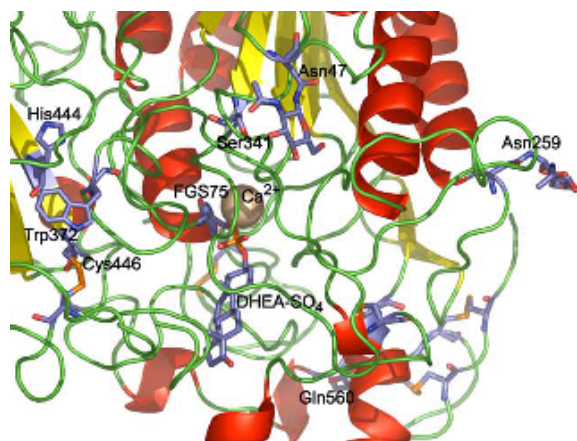


Figure 1.7. X-LI point mutation sites depicted as amino acids in the wild-type enzyme (Ser341, Trp372, His444, Cys446 and Gln560). Also shown are the catalytic residue, formylglycine 75 (FGly75), the bivalent cation Ca²⁺ and a modeled DHEA-sulfate are shown. The two potential glycosylation sites (Asn47 and Asn259) in this region are also shown, each with an *N*-acetyl glucosamine. (Obtained courtesy of Dr. D. Ghosh through personal communication.)

1.2.8 Crystal structure of STS

The X-ray crystal structures of four sulfatases have been published. There are structures for three human enzymes, arylsulfatase A (ARSA, Lukatela et al., 1998), arylsulfatase B (ARSB, Bond et al., 1997), and human placental steroid sulfatase (STS, Hernandez-Guzman et al., 2003). There is one structure for a bacterial sulfatase, *Pseudomonas aeruginosa* arylsulfatase (PARS, Boltes et al., 2001). There are also two more unpublished sulfatase crystal structures currently held in the Protein Data Bank (PDB), those for *Bacteroides fragilis*⁶ and *Bacteroides thetaiotomicron*⁷. An overlay of active site of human ARSs and PARS reveal a highly conserved architecture (Ghosh, 2007).

The crystal structure of human steroid sulfatase purified from placental microsomes was resolved to a 2.6 Å (Hernandez-Guzman *et al.*, 2003). As shown in **Figure 1.8**, the tertiary structure features two domains: a globular (55Å × 60Å × 70Å), polar domain and two antiparallel hydrophobic α-helices that protrude from the globular domain imparting to the structure an overall “mushroom-like” appearance. The 40-Å long α-helices putatively span the membrane of the endoplasmic reticulum (ER) and anchor the protein to the lumen side.

The polar domain’s tertiary structure is comprised of two sub-domains with an α/β sandwich fold. The first subdomain (SD1) winds around an 11-stranded mixed β-sheet surrounded by 13 α-helices and helical turns that contain the catalytic core. The second subdomain (SD2) consists of 110 C-terminal residues that wind around a 4-

⁶ Protein Data Bank ID number: 2qzu

⁷ Protein Data Bank ID number: 3b5q

stranded antiparallel β -sheet and resides against turn and loop regions of the β -sheet in SD1. The two putative anti-parallel helices, $\alpha 8$ and $\alpha 9$, stem from one side of the polar domain. There are loop regions in STS that have proposed membrane association, for example between $\alpha 4$ and $\alpha 5$, and between $\beta 9$ and $\alpha 13$.

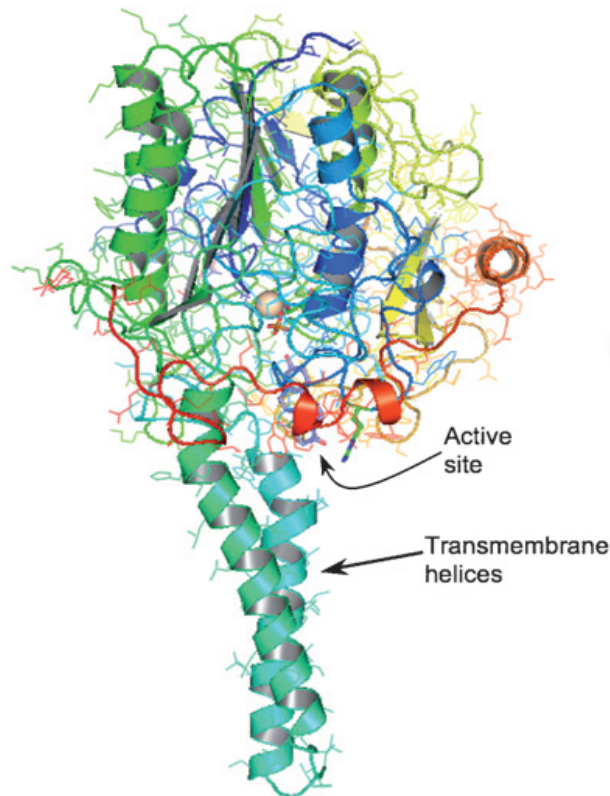


Figure 1.8. Stereographic ribbon diagram of tertiary and secondary structure of STS. (Obtained courtesy of Dr. D. Ghosh through personal communication.)

The 40-Å long hydrophobic helices, 8 and 9, putatively span the membrane of the ER and anchor the protein to the lumen side. STS has 12 cysteine residues and 6 disulfide bonds, all distributed in the globular polar domain. Of functional significance is a disulfide bond termed a “zipper-lock” between Cys170-Cys242 near the lipid-protein interface that is proposed to stabilize the putative antiparallel α -helices. Because all cysteine residues forming disulfide bonds are located exclusively in the globular

polar domain, this suggests that the entire portion faces the lumen side of the ER, and not the reducing environment of the cytosol. Further suggestion for the role of the antiparallel helices is the location of two residues, Lys183 and Arg184, near helices 8 and 9. The presence of two charged amino acids near a transmembrane helix has been previously observed (de Planque et al., 1999).

The active site is buried deep in the polar globular portion of the enzyme in subdomain 1, which is proposed to lie close to the luminal side of the membrane, suggesting that this architecture may play a role in catalysis. As described in § 1.1.2, a key cysteine in sulfatases is post-translationally modified to a formylglycine (FGly) residue. The FGly residue is covalently linked to a sulfate ester in the X-ray crystal structure. A large spherical electron density at the center of the catalytic site near the FGS residue is assigned as a divalent cation, Ca^{2+} , required for catalytic activity (Stevens et al., 1975). The divalent metal ion was interpreted to be a Ca^{2+} as it was in the crystal structures of ARSB and PARS. The crystal structure of ARSA depicted a Mg^{2+} ion, as did the structure of the Cys69Ala ARSA mutant complexed with *p*-nitrocatechol sulfate substrate.

Catalytically important residues (please see § 1.2.11 for a discussion of the mechanism) are depicted in the crystal structure as shown in **Figure 1.9**. The oxygen atoms of the side chains of Asp35, Asp36, Asp342, Gln343 and FGly75 are within contact distance (2.1 Å to 2.8 Å) to the Ca^{2+} ion to stabilize its charge. Lys134, Lys368 and Arg79 are in proximity (2.7 Å to 3.1 Å) to contact the sulfate oxygen atoms of the sulfated FGly residue. There are also two oxygen atoms of the sulfate FGly that are within coordination distance (2.7 Å) to the Ca^{2+} atom. The crystal structure also depicts

other contacts of residues important for catalysis (please see § 1.2.11). The imidazole ring of His136 is within H-bond distance (2.6 Å) of the oxygen atoms of one of the hydroxyl groups of the formylglycine hydrate, while the ϵ -nitrogen of His290 is a 2.6-Å distance away from a sulfate oxygen of the sulfated FGly. Finally, the His346 side chain is linked to side chains of Lys368 and Thr291 by a bridging water molecule.

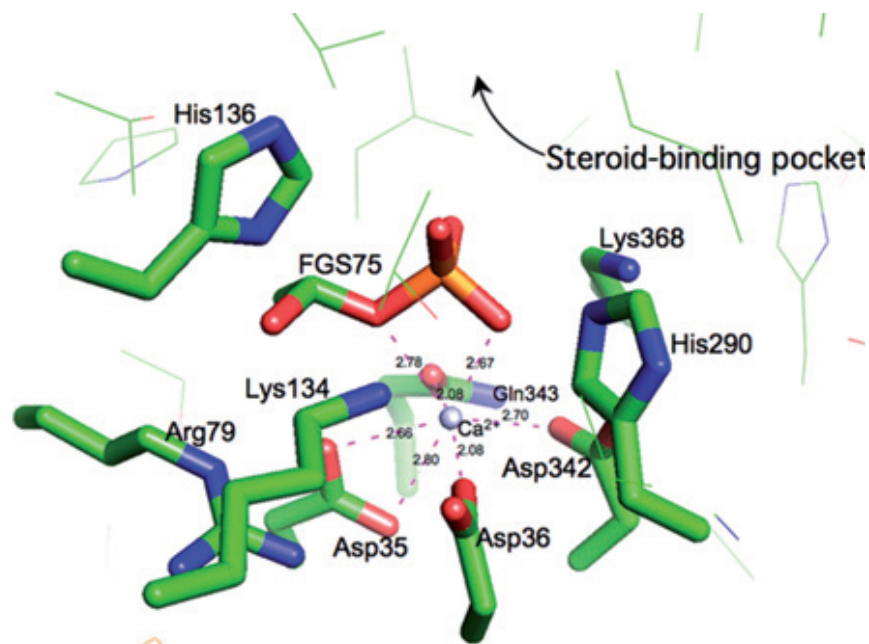


Figure 1.9. Active site residues coordinated to the Ca^{2+} ion. The formylglycine (FGly) is sulfated as depicted by the red oxygen and yellow sulfur atoms. Active site residues His290, Gln 343, Lys134, Asp342, Asp35 and Asp36 are within contact distance of the Ca^{2+} ion. Distances range between 2.08 Å and 2.80 Å. (Obtained courtesy of Dr. D. Ghosh through personal communication.)

The opposite end of the catalytic cleft of STS is bounded by the upper portions of the transmembrane helices 8 and 9. It is thought that the opening to the active site is at the interface of the lipid bilayer and the globular polar domain of STS. Near the proposed opening leading to the active site are a series of residues with hydrophobic side chains that form a “tunnel”: Phe178, Phe230, Phe233, Tyr236, and Phe237. The proposed entrance to the active site is flanked by residues Arg98 and Thr99, the so-called “gate-

keepers” to the “tunnel.” The inside of the active site opposite to the catalytic end is also lined with hydrophobic amino acids such as Phe104, Tyr493, Trp550, Phe553, Leu554, Trp555, and Trp558. These residues are proposed to form the “steroid-binding” pocket as schematically indicated in **Figure 1.9** and as shown in detail in **Figure 1.10**. The contribution of the hydrophobic amino acid side chain residues to substrate binding is visualized by modelling estrone (E1) into the active site (**Figure 1.10**) (Ghosh, 2007). The residues Leu103 and Val486 sandwich the aromatic steroid A-ring and are believed to have importance in preferentially binding estrogen substrate compared to androgens. Further substrate recognition may be aided by a hydrogen bond between Arg98 and the 17-keto functional group of the steroid D-ring.

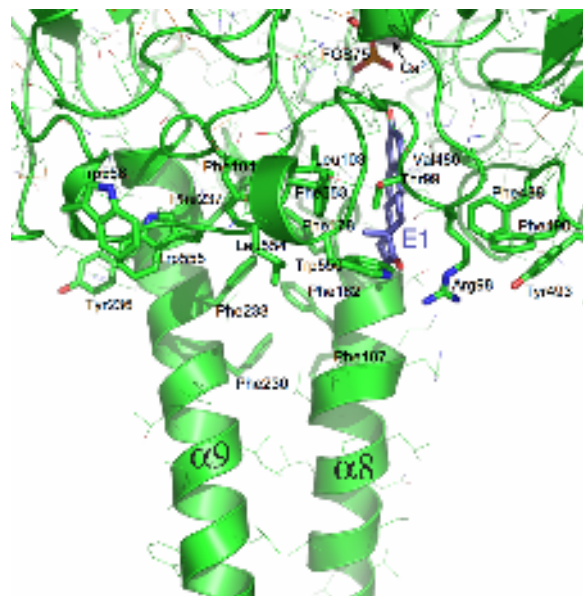


Figure 1.10. STS active site lies at protein-lipid interface. Estrone (E1, blue) is shown modeled into the active site in proximity to catalytic FGly (FGS75). The opposite end of the substrate-binding pocket borders the anti-parallel α helices, $\alpha 8$ and $\alpha 9$. The steroid backbone is shown surrounded by residues in the hydrophobic binding pocket. (Obtained courtesy of Dr. D. Ghosh through personal communication.)

The location of the active site in proximity to the protein-lipid bilayer interface presents several possible explanations for passage of the substrate into the active site (Hernandez-Guzman et al., 2003). One proposed scenario depends on three flexible loops, as implicated by high temperature factors, which might open and close over the active site. These loops are residues Thr470 to Thr495, Glu348 to Fly358 and 94 to 100. The first loop is a proposed “front swing door” directly covering the opening of the active site, while the second loop may constitute the “right swing door,” allowing alternative entry to or from the active site. The third loop is proposed to act as the “left swing door.” Another proposed mechanism for transport to and from the active site makes use of the putative transmembrane helices as a tunnel through the lipid bilayer. This type of substrate entry has been observed for other membrane-associated enzymes such as fatty acid amide hydrolase, squalene cyclase, and prostaglandin H₂ synthase (Bracey et al., 2002; Picot et al., 1994; Wendt et al., 1997).

1.2.9 Comparison of tertiary structures of sulfatases

Sulfatases with known tertiary structures, STS, ARSA, ARSB and PARS, have sequence similarities ranging between 20% and 32% (Ghosh, 2004). With the exception of the putative transmembrane domain, all structures possess a common general tertiary structure with respect to the globular polar domain as depicted by the schematic in **Figure 1.11** comparing the overall folds of ARSA and STS. As shown in **Figure 1.12**, the polar domains containing the catalytic site superimpose on one another very well. The overall fold of the polar domain of STS, the location and composition of the two β -sheets in subdomain 1 and subdomain 2 of STS are the same in ARSA, ARSB and PARS. There are some distinctions between the structures. For example, the central β -

sheet in subdomain 1 of STS has 11 strands, whereas there are 10 in other sulfatases. The missing transmembrane helices $\alpha 8$ and $\alpha 9$ of STS are replaced by a pair of antiparallel β -strands in ARSB. A similar loop region exists in the ARSA structure but with a decreased tendency to form antiparallel β -strands.

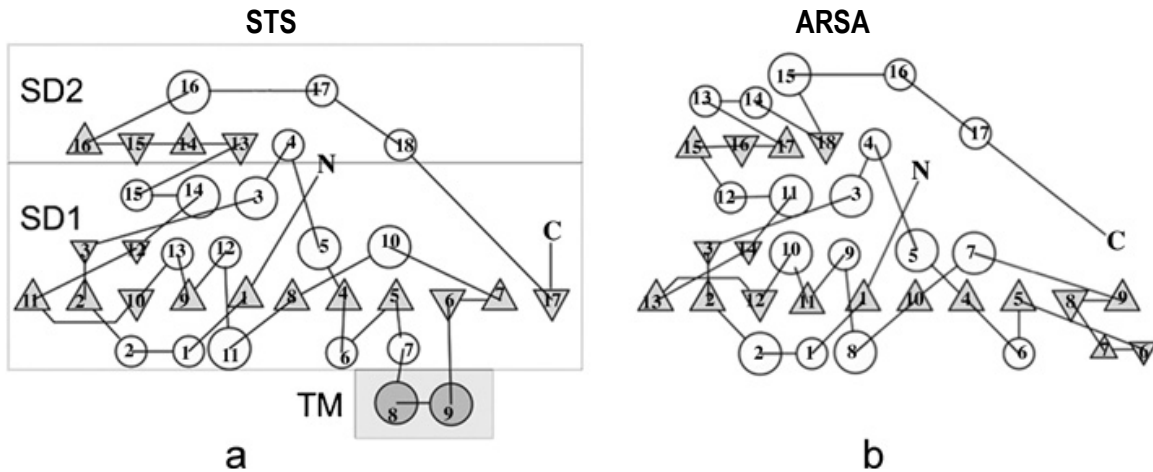


Figure 1.11. Comparison of the overall folds of human STS and ARSA. The similarities between the globular polar domain of STS and ARSA is evident. (a) STS and (b) ARSA. Secondary structure elements are numbered. The circles represent α -helices, and the triangles are β -strands. SD1: subdomain 1, SD2: subdomain 2, TM: transmembrane domain. (Obtained courtesy of Dr. D. Ghosh through personal communication.)



Figure 1.12. Comparison of the tertiary structures of four sulfatases. The structures are superimposed: STS (green), ARSA (blue), ARSB (purple) and arylsulfatase from *Pseudomonas aeruginosa* (PARS) (yellow). The active site Ca^{2+} cation is shown as a sphere. (Obtained courtesy of Dr. D. Ghosh through personal communication.)

1.2.10. Comparison of active site structures of sulfatases

The catalytic portion of the active site in STS is highly homologous to that of ARSA, ARSB and PARS. There is strict conservation of nine of ten catalytically important residues in ARSA, ARSB, STS and PARS: Asp35, Asp36, FGly75, Arg79, Lys134, His136, His290, Asp342, and Lys368. The spatial arrangement of these residues is also identical. Superimposing α -carbon atom positions of these nine residues by least squares minimization results in a root mean square deviation (rmsd) of 0.4 Å, underscoring the theory of a conserved mechanism for sulfatases. The tenth catalytic residue is Gln343 in STS and is an asparagine in ARSA, ARSB and PARS. As shown

in **Figure 1.13**, there is a particularly significant overlap of the four active site residue side chains, Asp35, Asp36, Asp342, and Gln343 in STS with the equivalent residues in ARSA, ARSB and PARS. The oxygen atoms of these residues provide contact to the bivalent cation. When the α -carbon atoms of these residues are superimposed by least squares fitting, a rmsd of 0.2 Å is observed. There is also very close overlap in the position of the bivalent metal cation (rmsd \sim 0.3 Å), whose identity is a Ca^{2+} in the STS (Hernandez-Guzman et al., 2003), ARSB (Bond et al., 1997), and PARS structures (Boltes et al., 2001). However, the metal ion was determined as an Mg^{2+} in the original structure of ARSA (Lukatela et al., 1998), as well as in the structure of a mutant Cys69Ala complexed with *p*-nitrocatechol sulfate (von Bulow et al., 2001).

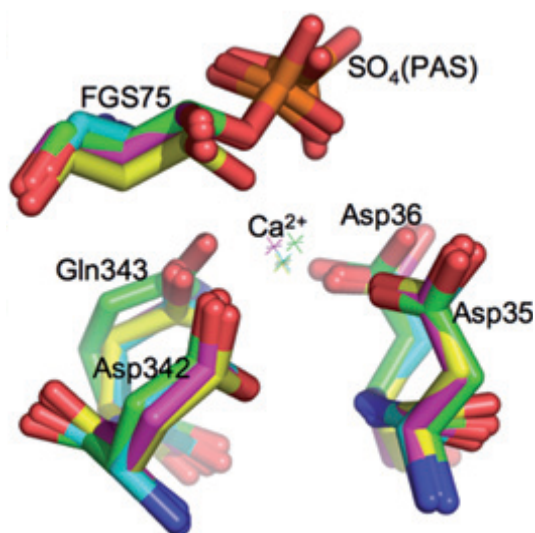


Figure 1.13. Active site residues of sulfatases share a highly similar spatial arrangement. Four active site residues of STS (green) are numbered and are shown superimposed on those of ARSA (blue), ARSB (purple), and PARS (yellow). The sulfated FGly catalytic residue is depicted, as are four active site residues, Gln343, Asp342, Asp35, Asp36 and the Ca^{2+} metal center. In PARS crystal structure the FGly residue is not covalently sulfated. (Obtained courtesy of Dr. D. Ghosh through personal communication.)

However, a recent structure of human placental ARSA depicted the bivalent metal cation as a Ca^{2+} instead of a Mg^{2+} (Chruszcz et al., 2003). The authors suggest that all sulfatases most likely use Ca^{2+} as the bivalent metal ion and that the Mg^{2+} observed in the original structure was due to the high concentrations of magnesium ions during the purification. It is not yet known if sulfate ester catalysis is affected by replacing the Ca^{2+} with another cation (Ghosh, 2007). However, the site-directed mutagenesis studies of residues coordinating the metal ion in ARSA resulted in severe decreases in catalytic activity, highlighting the importance that the metal ion probably plays in substrate binding and sulfate ester bond hydrolysis. Another notable feature of **Figure 1.13** is the overlapping position of the FGly hydrate side chain and its sulfate ester in the structure of STS and ARSB. However, while the FGly hydrate residue of the PARS structure lies in the same position as that of STS and ARSB, a sulfate ester bond is not observed, but rather the sulfate moiety is a 1.0 Å distance away. The FGly residue of ARSA was depicted as a glycine in its original structure, and a chloride ion was modelled in the place where the sulfate ester group would otherwise be observed (Lukatela et al., 1998). However, a subsequent structure of ARSA displayed an FGly hydrate residue covalently attached to a phosphate group (Chruszcz et al., 2003). It was unclear whether the unexpected presence of a phosphate group is an artifact of crystallization, or whether the FGly residue may be phosphorylated at times. Whether true resting state of the FGly residue in all sulfatases is sulfated or not is unknown.

1.2.11 Catalytic mechanism of sulfatases

The mechanism of sulfate ester catalysis by sulfatases is not fully understood, although much progress has been made. The catalytic mechanism for sulfatases was

especially elusive prior to the discovery of the post-translationally installed catalytic FGly residue. The elucidation of the first sulfatase crystal structure, that of ARSB, in 1997 provided the first attempt to explain the mechanism (Bond et al., 1997). This structure depicted an electron density near one of the hydroxyl groups of the FGly hydrate, and it was attributed to a covalent sulfate adduct, formylglycine sulfate (FGlyS). The authors reasoned that the enzyme may be in an equilibrium between the FGly aldehyde and the FGly sulfate, but that the resting state would most likely be that of the aldehyde, as shown in **Figure 1.14**. The mechanism begins with addition of the sulfated substrate to the aldehyde by a nucleophilic attack of one of the oxygen atoms of the sulfate group on the electrophilic carbon atom of the FGly aldehyde. The next step proposes that a nucleophile, such as an activated water molecule, cleaves the sulfur-oxygen bond to allow the phenolic portion of the substrate to leave. The resulting sulfated FGly hydrate might be the resting state of the enzyme, but it could undergo elimination of the sulfate group to the FGly aldehyde.

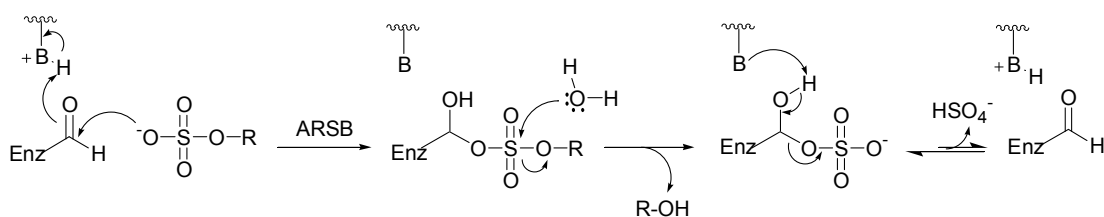


Figure 1.14. Proposed catalytic mechanism for sulfatases based on ARSB crystal structure evidence. Addition-hydrolysis (AH) mechanism proposed by Bond and coworkers (Bond et al., 1997).

Another mechanism for sulfate ester catalysis was proposed after the crystal structure of ARSA was resolved (Lukatela et al., 1997). This mechanism consists of a transesterification-elimination (TE) sequence as shown in **Figure 1.15**.

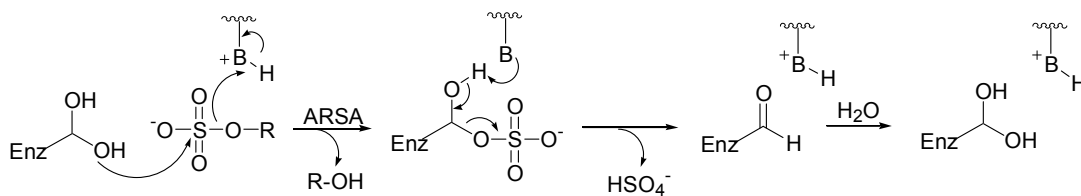


Figure 1.15. Proposed catalytic mechanism for sulfatases based on ARSA crystal structure evidence. Transesterification-elimination (TE) mechanism proposed by Lukatela and coworkers (Lukatela et al., 1998).

Support for the TE mechanism was gained after mutagenesis studies performed on ARSA and ARSB (Recksieck et al., 1998). ARSA and ARSB were expressed with a site-specific mutation to a serine residue in place of the key cysteine that becomes post-translationally modified to FGly. It is known that the formylglycine generating enzyme (FGE) is unable to make the post-translational modification to serine. The mutants were incubated with [³⁵S]-*para*-nitrocatechol sulfate, as were the wild-type enzymes. The wild-type ARSA and ARSB displayed no radioactivity. However, the mutants exhibited a radiolabelled sulfated serine residue, which inactivated both ARSA and ARSB. This meant that the first step of the reaction, transesterification of the substrate to generate sulfated serine and release of the *p*-nitrocatechol was occurring. However, the second “elimination” step involving subsequent release of the sulfate group was not possible due the lack of a second hydroxyl group on serine, as there normally would be on the formylglycine hydrate. These results also disfavour the addition-hydrolysis mechanism proposed for ARSB in which an aldehyde is the resting state of the FGly residue. It is unlikely that one of the oxygen atoms of the sulfated substrate would engage in nucleophilic attack of the serine hydroxyl group to generate a sulfo-serine residue. Further support for the TE mechanism was obtained from a recent co-crystal structure of *para*-nitrocatechol sulfate (pNCS) and an FGly-alanine ARSA mutant (von Bulow et al.,

2001). The mutant co-crystal structure super-imposed with the wild-type ARSA structure and notably displayed the sulfur atom of sulfate moiety of pNCS in an optimal distance (2.85 Å) and orientation from the O γ 1 hydroxyl group. This positioning would appropriately enable the sulfate group for in-line nucleophilic attack by the O γ 1 hydroxyl group.

Further support for the transesterification (TE) mechanism as the most likely one for sulfatase catalysis was based upon recent crystal structural evidence of PARS and mutagenesis studies performed on ARSA (Boltes et al., 2001). As mentioned previously, the 1.3-Å resolution structure of PARS displayed a sulfate group in proximity to the FGly hydrate, but not engaged in a sulfate ester bond (Boltes et al., 2002). The fact that a sulfate moiety was detected in the active site was attributed to the high concentrations of sulfate required to crystallized PARS, and suggests that the resting state of the FGly hydrate is not necessarily sulfated. The crystal structure shows the sulfate group optimally position 2.96 Å away from FGly-O γ 1 and optimally oriented for nucleophilic attack. The detailed sulfatase mechanism proposed by Hanson et al., is depicted in **Figure 1.16** and suggests the resting state is that of a FGly hydrate residue which is stabilized by hydrogen bonds to nearby HisA and AspC residues (Hanson et al., 2004). Surrounding positively charged residues and the metal cation assist in binding and orienting the sulfated substrate so that the sulfur atom is in line for nucleophilic attack by an oxygen atom of one the hydroxyl groups (HO γ 1) from the FGly hydrate. The transesterification is assisted by AspC, which acts as a general base in abstracting a proton from O γ 1. The release of the phenolic portion of the substrate from the active site is promoted by proton transfer from HisB. In an inversion of configuration, the

sulfate moiety is bound to O γ 1 in a sulfate ester bond. Nearby HisA assists in abstracting a proton from O γ 2, which causes cleavage of the sulfate-oxygen bond and elimination of the sulfate group. The FGly aldehyde is regenerated and rehydrated to restore the residue to the resting state.

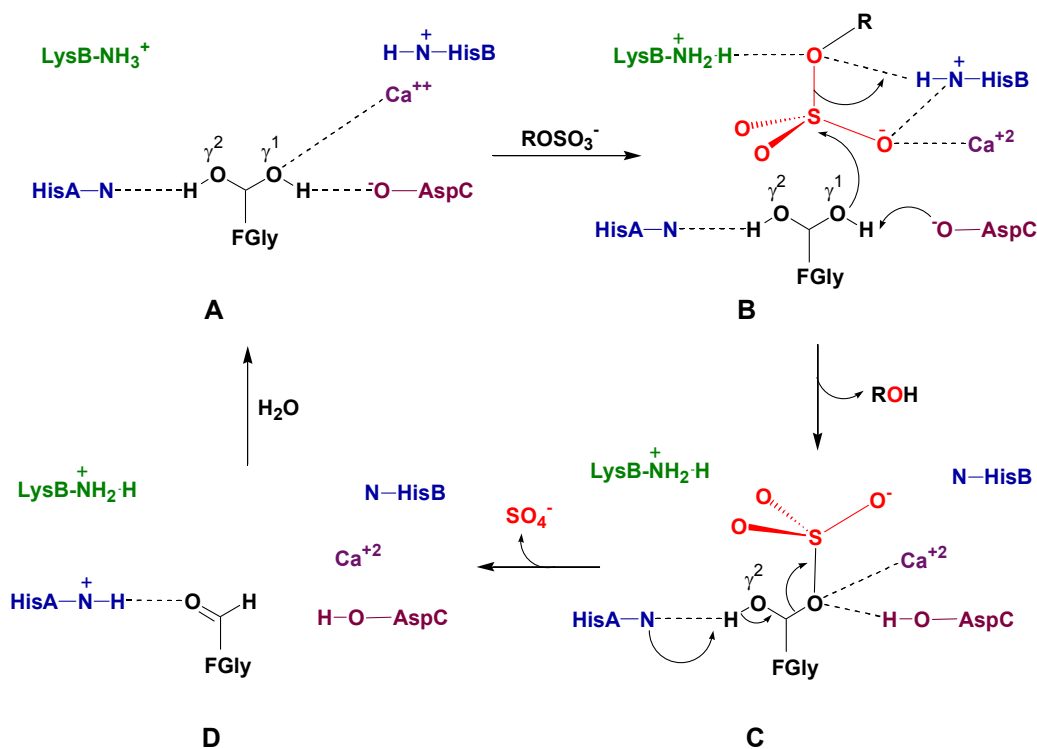


Figure 1.16. Detailed mechanism for sulfatases, including STS, proposed by Hanson and coworkers (Hanson et al., 2004).

1.3 STS Inhibitor development

1.3.1 Reversible inhibitors

In the last fifteen years considerable attention has focused on the design of inhibitors of STS for the purpose of modulating intratumoral levels of estrogen and androgen in hormonal diseases, particularly hormone-dependent breast cancer. There have been recent reviews of STS inhibitors (Purohit et al., 2003; Nussbaumer and Billich, 2004; Reed, et al., 2005; Day et al., 2009). The field of inhibitors can be

divided into two general classes: irreversible arylsulfamate and reversible non-sulfamate inhibitors.

There are relatively few reversible inhibitors of STS reported. Among the first reversible inhibitors were vanadate, **1.1**, and sulfite, **1.2**, whose structures are shown in **Figure 1.17** and which reversibly inhibit STS activity with low micromolar potency (Dibbelt and Kuss, 1991). In contrast, sulfate, **1.3**, was only an inhibitor at very high concentration, which suggests that enzyme-catalyzed hydrolysis of the sulfate ester bond proceeds via a trigonal bipyramidal transition state. This impacts the rational design of STS inhibitors by signifying that this transition state cannot be mimicked through a synthetic compound.

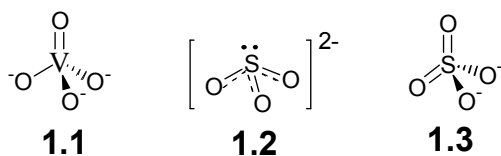
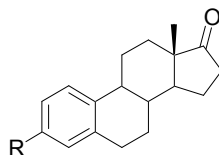


Figure 1.17. Small inorganic inhibitors of STS (**1.1-1.3**).

The first rationally designed reversible inhibitors were substrate analogs of E1S, and were designed with a replacement of the 3-*O*-sulfate ester bridging oxygen atom by S, N, O and C as non-hydrolyzable linker atoms of the head group to the steroidal structure as shown in **Table 1.2**. Overall, the inhibitory potencies of these analogs were weak, with a few examples showing moderate inhibition of placental microsomes and in some cases purified STS in the micromolar range. Introduction of a sulfur atom in compounds **1.4-1.7** as a linker to the steroidal core did not provide a very effective inhibitory strategy (Li et al., 1994; Li et al., 1993). Similarly, introduction of an *N*-linked head group in compounds **1.9-1.10** provided moderate inhibition (Selcer et al., 1995; Selcer et al., 1996). The presence of a *C*-linked sulfate head group, **1.11**, also

provided moderate inhibition of STS with a K_i of 140 μM when assayed with purified placental STS (Li et al., 1995). A more effective E1S analog emerged when a phosphate group was introduced as a sulfate mimic (estrone-3-*O*-phosphate, E1P, **1.12**). E1P displayed a K_i value of 0.3 μM when assayed at pH 7 with purified placental STS (Li et al., 1995). More detailed studies using partially purified STS revealed its potency is pH-dependent with the K_i increasing from 0.1 μM at pH 6.0 to 5.0 μM at pH 8.0 (Anderson et al., 1997). Its higher potency between pH 6 to 7 is attributed to the enzyme display-

Table 1.2. STS inhibitors as estrone-3-*O*-sulfate analogs.



Compound	R	Assay type	% Inhibition or IC_{50}	K_i	Reference
1.4	$-\text{SO}_2\text{Cl}$	Placental microsomes Purified STS	92% at 300 μM 65% at 60 μM	ND 28 μM	Li et al., 1993 Dibbelt et al., 1994
1.5	$-\text{SO}_3^- \text{K}^+$	Placental microsomes	40% at 300 μM	ND	Li et al., 1993
1.6	$-\text{SO}_2\text{NH}_2$	Placental microsomes Purified STS	45% at 300 μM	ND 110 μM	Li et al., 1993 Dibbelt et al., 1994
1.7	$-\text{SO}_2\text{F}$	Placental microsomes Purified STS	44% at 300 μM	ND 35 μM	Li et al., 1993 Dibbelt et al., 1994
1.8	$-\text{SO}_2\text{CH}_3$	Placental microsomes Purified STS	36% at 300 μM	ND 130 μM	Li et al., 1993 Dibbelt et al., 1994
1.9	$-\text{NHSO}_2\text{CF}_3$	Placental microsomes	$\text{IC}_{50} = 10.2 \mu\text{M}$	ND	Selcer et al., 1996
1.10	$-\text{NHCOCF}_3$	Placental microsomes	$\text{IC}_{50} = 8.7 \mu\text{M}$	ND	Selcer et al., 1996
1.11	$-\text{CH}_2\text{SO}_3^-$	Purified STS		140 μM	Li et al., 1995
1.12	$-\text{OPO}_3^{2-}$	Purified STS		0.3 μM	Li et al., 1995
1.13	$-\text{OPS}(\text{CH}_3)\text{OH}$	MCF-7 breast cancer cells	$\text{IC}_{50} = 100 \text{ nM}$	ND	Duncan et al., 1993

ing preference for the monoanionic charge of the phosphate group much over the dianionic form. A variation of the estrone-3-*O*-phosphate derivative inhibitor was found to be the estrone methylthiophosphonate (**1.13**, E1-3-MTP) with an IC₅₀ value of less than 100 nM.

In addition to substrate analogs of STS, certain product analogs such as 17 α -phenyl-or benzyl-substituted estradiol derivatives, **1.14** and **1.15** as illustrated in **Figure 1.18**, have been shown to be reversible inhibitors of STS in homogenates of JEG cells and are the most potent reversible inhibitors to date, with K_i values in the low nanomolar range (Poirier and Boivin, 1998; Boivin et al., 2000). The introduction of long alkyl chains at the 17-position of estradiol had the effect of increasing potency with increasing chain length up to octyl substitution (Boivin et al., 2000). It was reasoned that the high affinity of these compounds may be attributed to the hydrophobic interactions between the alkyl or benzyl moiety at the 17-position and the transmembrane helix of STS.

Recent efforts to design non-hydrolyzable E1S analogs include those of our (Taylor) group. The introduction of difluoromethylene group, **1.16**, as a hydrolytically stable linker of the sulfate group to the steroid core was developed (Lapierre et al., 2004) as a comparison to its non-fluorinated methylene sulfate ester estrone analog, **1.11**, that was earlier described as a weak, mixed-type inhibitor (Li et al., 1995) (**Figure 1.18**). The result was that the presence of the two fluorine atoms provide a 10-fold higher potency compared to the non-fluorinated derivative and the inhibitor switches to a competitive mode of inhibition, with a moderate K_i of 57 μ M. In this series a tetrazole, **1.18**, and difluoromethylene tetrazole moiety, **1.17**, were also examined as a sulfate surrogates, based on reports of tetrazole being an effective sulfate mimic in synthetic

sulfotyrosine-bearing peptides targeting the cholecystinin (CCK) receptor (Tilley et al., 1991). The difluoromethylene tetrazole, **1.17**, was about 4.5 times more potent than

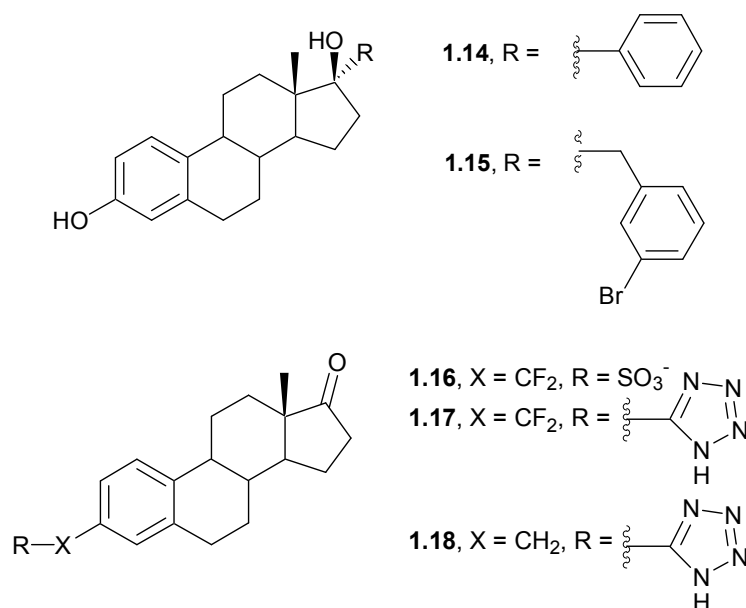


Figure 1.18. 17 α -substituted estradiol derivative, **1.14** and **1.15**, and non-hydrolyzable estrone-3-O-sulfate (E1S) derivatives **1.16-1.18**.

its non-fluorinated analog, **1.18**, which was a non-competitive inhibitor with a K_i of 73 μ M. These studies also revealed the difluoromethylene tetrazole, **1.17**, displayed greater inhibitory potency than the difluoromethylene sulfate ester, **1.16**, with a K_i value of 16 μ M. These structure-activity studies suggested that the enhanced affinity of the difluoromethylene derivatives may be due to favourable interactions between the fluorines and residues in the active site, such as His290.

Apart from rational drug design, high-throughput screening has yielded three new classes of non-steroidal STS inhibitors (**Figure 1.19**): madurahydroxylactone thiosemicarbazones, aryl piperazines and arylsulfonylureas. The thiosemicarbazones are derivatives of the natural product madurahydroxylactone (**1.19**) and were discovered by screening a library of analogs (Jutten et al., 2002). The most potent inhibitor of the

series was **1.20** which showed IC_{50} value of 460 nM and a K_i of 350 nM against placental STS and behave as non-competitive inhibitors. A separate screen conducted by Bayer identified aryl piperazines such as **1.21** as another novel class of STS inhibitors (Hejaz et al., 2004). The most active hits from this screen are compounds **1.21** and **1.22** which displayed IC_{50} values of 48 and 78 nM, respectively, against purified placental STS. The mode of inhibition of these compounds was not investigated, however, it is expected that they would be reversible. The third class of novel STS inhibitors discovered through high-throughput screening are the arylsulfones. Compound **1.23** was shown to behave as a reversible, purely competitive inhibitor of STS with a K_i value of 890 nM against purified STS. Additional studies on derivatives of this compound showed that the hydrazide group was not essential for activity and that the corresponding analog lacking one nitrogen, **1.24**, still resulted in a moderate inhibitor with a K_i of 2.4 μ M.

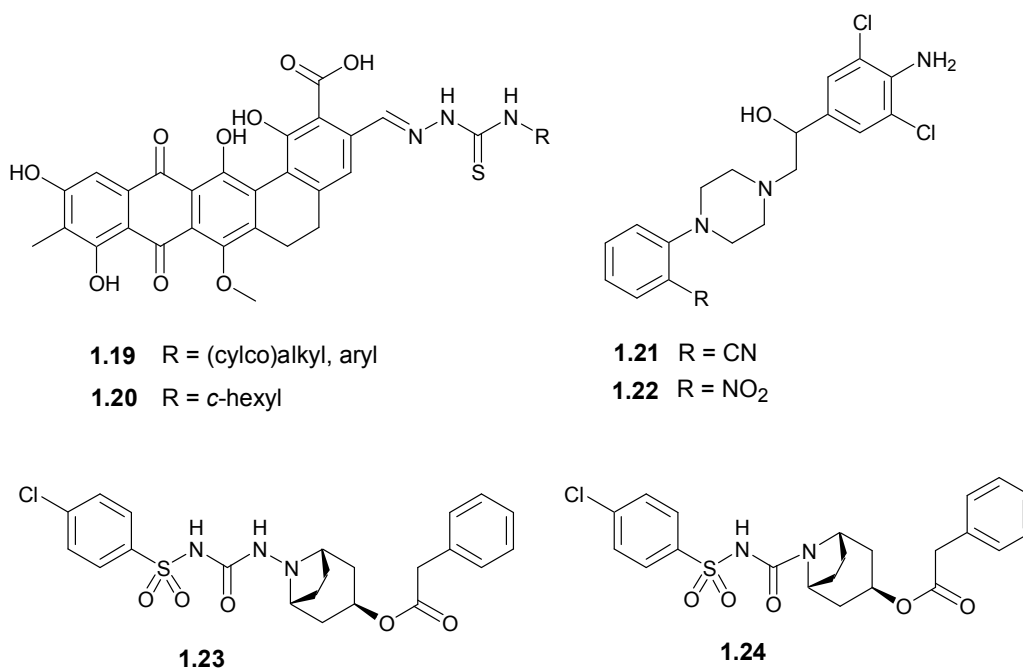
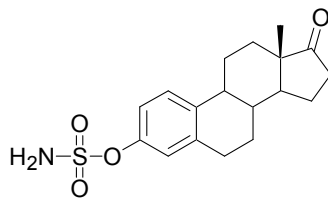


Figure 1.19 STS inhibitors discovered by library screening.

1.3.2 Irreversible inhibitors

A major advance in the field of STS inhibitor design came with the discovery that the sulfamate derivative of estrone-3-*O*-sulfate was a potent, irreversible inhibitor (Howarth et al., 1994). This compound, estrone-3-*O*-sulfamate, became known as EMATE (**1.25**, **Figure 1.20**) and it displayed an IC₅₀ value of 100 nM and a K_i value of 670 nM when assayed against STS in placental microsomes (Purohit et al., 1995). Evaluation of EMATE in intact MCF-7 cells generated an IC₅₀ of 65 pM (Purohit et al., 1995). Although the authors were attempting to design a potent reversible inhibitor, it behaved as a time- and concentration-dependent manner, and STS activity did not return after extensive dialysis. In addition, high concentrations (50 μM) of estrone-3-*O*-sulfate substrate reduced the inhibitory action of EMATE, suggesting that the inhibitor must bind in the active site (Purohit et al., 1995). Taken together, these experiments signify that EMATE was behaving as an irreversible inhibitor, which is often referred to as suicide inhibition or mechanism-based inhibition. Although the data are consistent with an inactivation mechanism involving covalent attachment of the inhibitor to an active site residue, the mode of irreversible inhibition of sulfamate inhibitors of STS is still not fully elucidated. Nevertheless, EMATE was the first representative of a highly potent STS inhibitor class, and a vast array of sulfamate derivatives have since been reported.



1.25 (EMATE)

Figure 1.20. Estrone-3-*O*-sulfamate (EMATE).

Various mechanisms describing the inactivation of STS by aryl sulfamate inhibitors were initially proposed (Woo et al., 1996; Woo et al., 2000). One of the first mechanisms was put forth by Potter and coworkers as shown in **Figure 1.21**. It implicates the catalytic formylglycine in its aldehyde form as the resting state of the enzyme. Addition of the aryl sulfamate to the enzyme yields, (A), the *N*-alkylsulfamate ester hemiaminal. After loss of the corresponding phenol either an *N*-alkyl sulfamic acid hemiaminal (B) results or an iminosulfamic acid (D). The Schiff base represented by (D) would be a dead-end complex and inactivate the enzyme from further catalysis. Similarly, (D) can also be reached by the imine represented by (C), and subsequent loss of the phenolic portion of the inhibitor.

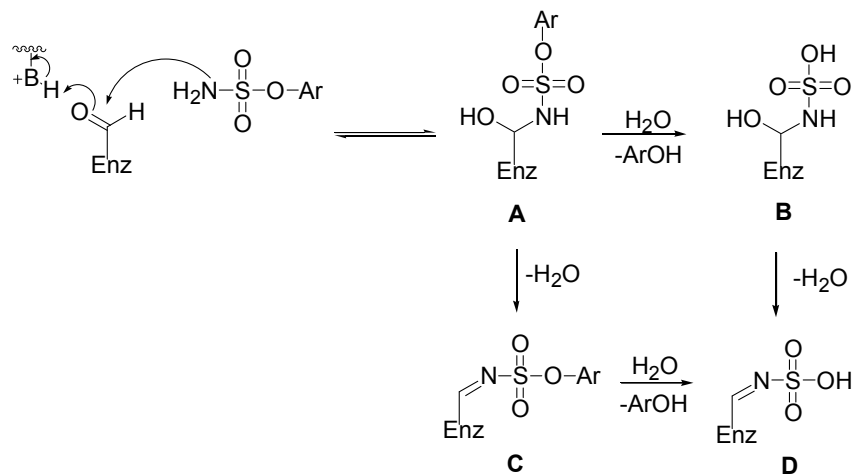


Figure 1.21. Addition of aryl sulfamate to aldehyde FGly residue as proposed by Woo and coworkers (Woo et al., 2000).

However, it was later shown that cleavage of the ArO-S bond of the arylsulfamate is required for irreversible inhibition. For example if the bridging oxygen atom of the sulfamate ester is replaced with a non-hydrolyzable group, irreversible inhibition is not observed (Woo et al., 1997). The corresponding *N*-sulfamate, and *S*-sulfamate analogues are such examples. An amended mechanism proposed by Bojarova et al.,

implicates the FGly residue resting state as that of the formylglycine hydrate as shown in **Figure 1.22** (Bojarova et al., 2008). This mechanism proposes an S_N2 substitution where one of the oxygen atoms of the hydroxyl of the FGly hydrate attacks the sulfur atom of the aryl sulfamate substrate. The ArO-S bond is cleaved and the corresponding phenol is released and an enzyme α -hydroxysulfamate is formed. In step 1 the elimination of sulfamic acid from the sulfamoylated FGly hydrate generates the aldehyde FGly. Free sulfamic acid subsequently reacts with the aldehyde to afford a stable Schiff's base. However, it should be noted that incubation of sulfamic acid to STS does not cause inactivation (Bojarova et al., 2008). The alternative step 2 provides the possibility that the eliminated sulfamic acid can form a reactive amino sulfene that may be subject to attack by any nearby nucleophilic amino acid residue in the enzyme active site or elsewhere.

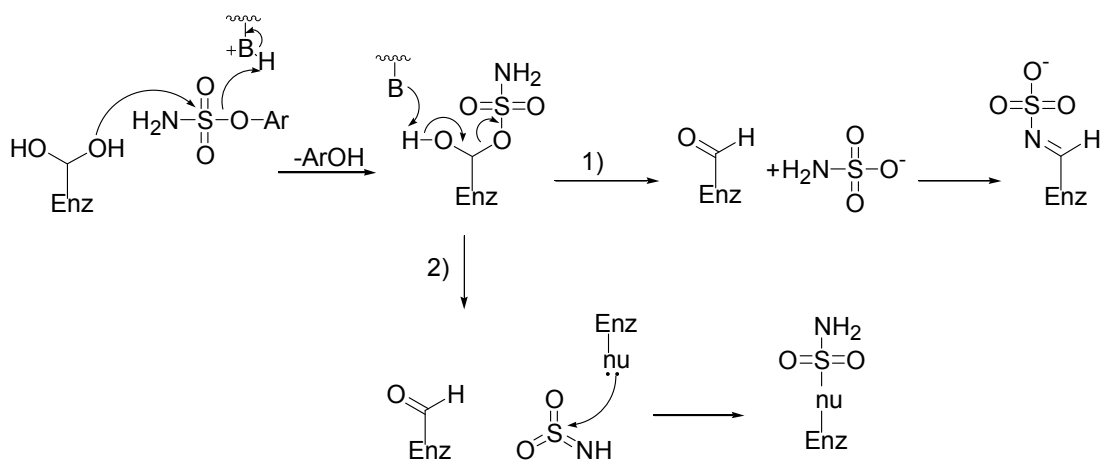


Figure 1.22 Proposed inactivation of STS by aryl sulfamate when FGly hydrate initiates attack on aryl sulfamate (Bojarova et al., 2008).

A third mechanism has been proposed based on studies involving a range of aryl sulfamates with *Pseudomonas aeruginosa* aryl sulfatase (PARS), (Bojarova et al., 2008). The authors examined the differences in efficiency of PARS inactivation by nine

aryl sulfamates with different electron-donating and electron-withdrawing substituents that impart a range of pK_a values to their corresponding parent phenols. A linear free-energy Bronsted plot of the pK_a of the leaving group phenol of a range of aryl sulfamates versus their inactivation efficiency ($\log k_{\text{inact}}/K_I$) has revealed a steep slope with linear character ($\beta_{\text{lg}} = -1.1 \pm 0.2$). This represents that a high degree of charge development in transition state occurs as a result of cleavage of the ArO-S bond of the aryl sulfamate as the first step in the irreversible reaction. The scission of the ArO-S bond has been previously examined by [^3H]-labeled hydroxy group at the 17-position of EMATE (Nussbaumer and Billich, 2004). STS activity was inhibited in a time- and concentration-dependent manner, however no association of the labeled inhibitor with the enzyme preparation was detected. This is expected if the [^3H]-estrone is released after cleavage of the ArO-S bond.

Further evidence of cleavage of the ArO-S was revealed by measuring the stoichiometry of the inactivation process by quantifying the release of the parent phenol after reaction with PARS (Bojarova et al., 2008). The stoichiometry was measured that varied in the range 3–6, with the highest values being observed for the most potent inactivators. This result implies that multiple sulfamoylation events occur during the inactivation process and it was proposed that more than one reaction pathway might occur during inactivation. A reaction mechanism that would result in multiple sulfamoylation events is shown in **Figure 1.23**.

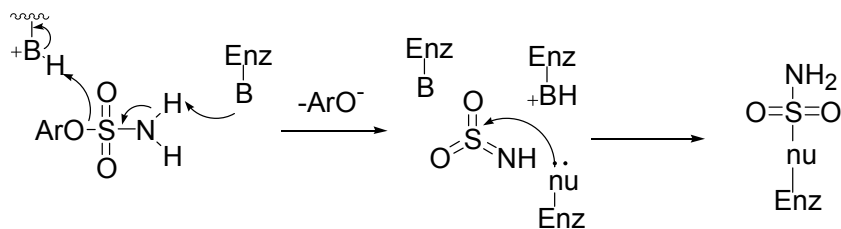


Figure 1.23. Elimination mechanism of the sulfamate moiety from aryl sulfamate resulting in multiple sulfamoylated amino acid residues.

The authors propose that non-specific labelling may occur by elimination of the sulfamate assisted by acid and base residues, breaking the ArO-S bond and releasing the corresponding phenol and the amino sulfene, NH_2SO_2 . The reactive amino sulfene would be subject to non-specific attack by active site nucleophilic residues, forming any number of combinations of covalent attachment. The potential for multiple pathways of inactivation and variable reaction stoichiometry is underscored by kinetic results obtained for aryl sulfamate inhibitors and STS. A plot of log of percent enzyme activity remaining versus time for various concentrations of a number of different arylsulfate inhibitors all reveal biphasic kinetics. Rapid loss of activity initially occurs followed by a slower second phase. If only one inactivation mechanism was followed, a first-order loss of activity would be observed exclusively. Most likely a specific inactivation event is responsible for the initial linear phase observed, such as mechanism 2 depicted in **Figure 1.22**, whereas a combination of inactivation events transpire to change the kinetic behaviour of the second phase.

Further support for the elimination mechanism shown in **Figure 1.23** versus the $\text{S}_{\text{N}}2$ mechanism shown in **Figure 1.22** is that *N,N*-dialkyl-substituted sulfamates such as compound **1.26** are not inactivators of STS (Howarth et al., 1994). In this example the presence of an *N*-dimethyl substituent to EMATE would not allow elimination of the

sulfamate moiety, and no sulfamoylation of any residues would occur. It is also possible that **1.26** cannot react with any active-site residues due to steric factors.

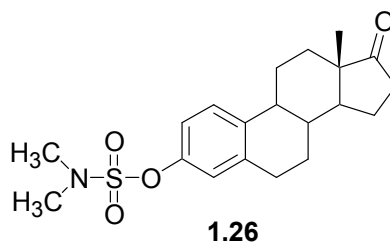


Figure 1.24. *N,N*-dimethyl-substituted EMATE, **1.26**

EMATE can never be pursued as a potential therapeutic because it has the severe drawback of eliciting an estrogenic response *in vivo* (Billich *et al.*, 2000). A 3.5-fold increase in uterine weights was observed when EMATE was administered subcutaneously to ovariectomized rats at a dose of 10 µg/day for 5 days. This observed response is most likely because the phenolic portion released upon cleavage of the ArO-S bond in **Figure 1.21** is estrone (E1)—a product whose metabolite, estradiol (E2), causes growth of breast cancer cells. In fact, the adverse estrogenic effects due to EMATE and other estrogen sulfamates are greater than those observed upon E1 oral administration to rats (Elger *et al.*, 1995). The reason for the enhanced oral activity of estrogen sulfamates is due to their association with red blood cells (RBCs) which enables them to evade first pass metabolism during liver transit, in comparison to E1 which is subject to hepatic metabolism (Howarth *et al.*, 1994; Elger *et al.*, 2001). It was later revealed that estrogen sulfamates bind reversibly to carbonic anhydrase II (CA II) in RBCs (Ho *et al.*, 2003) which is the reason they are protected from first pass metabolism. CA II, which is normally inhibited by sulfonamides, is also inhibited by EMATE (and many other sulfamates) with an IC₅₀ value of 25 nM (Ho *et al.*, 2003).

The finding that EMATE elicits an estrogenic response *in vivo* led to the development of non-estrogenic inhibitors. Many such compounds have been reported however, only the most significant of this class will be discussed here. Coumarins, whose general structure is shown as **1.27** in **Figure 1.25**, were explored as STS inhibitors based on the structure of the known fluorogenic substrate for sulfatases, 4-methylumbelliferyl sulfate (4-MUS, **1.28**). The bicyclic core of the coumarin rings are mimics for the A and B rings of the steroid scaffold. The introduction of a sulfamate to the C-7 position of a coumarin resulted in a potent, irreversible inhibitor without any adverse estrogenic outcome *in vivo* in ovariectomized rats nor did it stimulate the growth of MCF-7 breast cancer cells (Purohit et al., 1996). The compound, 4-methylcoumarin-7-*O*-sulfamate, (**1.29**, **Figure 1.25**), was given the abbreviation COUMATE and displayed an IC₅₀ of 380 nM in MCF-7 cells. A series of COUMATE derivatives were made to examine structure-activity relationships and the three general observations were made (Woo et al., 1998; Woo et al., 2000). First, the sulfamate substitution at only the C-7 position is inhibitory and the conjugation in the coumarin A-ring is vital to inhibitory activity. Lastly, COUMATE derivatives with longer alkyl substitutions to the C-3 and C-4 position are more potent than shorter alkyl substituents. Based on these results, further modifications to the bicyclic coumarin structure determined that a third ring appended to positions C-3 and C-4 improves potency of inhibition. These tricyclic coumarin sulfamates were named 665-COUMATE, 666-COUMATE, 667-COUMATE, etc., based on the number of atoms in the third ring (Woo et al., 2000). 667-COUMATE, (**1.30**, **Figure 1.25**) was the best candidate from this class and exhibited an IC₅₀ value of 8 nM on STS in a placental microsome

preparation. This also represents a three- and 100-fold more potent inhibition value than EMATE and COUMATE, respectively. Similar to EMATE, 667-COUMATE also has an irreversible inhibition profile. No estrogenicity was observed during *in vivo* studies and 667-COUMATE recently completed a phase I clinical trial for the treatment of hormone-dependent breast cancer in post-menopausal women (Stanway et al., 2006). Researchers at Novartis have developed a wide variety of irreversible STS inhibitors based upon the chromenone scaffold. Some of the compounds, such as compound **1.31**, exhibit potencies that are as great or greater than 667-COUMATE though none of these compounds have reached clinical trials.

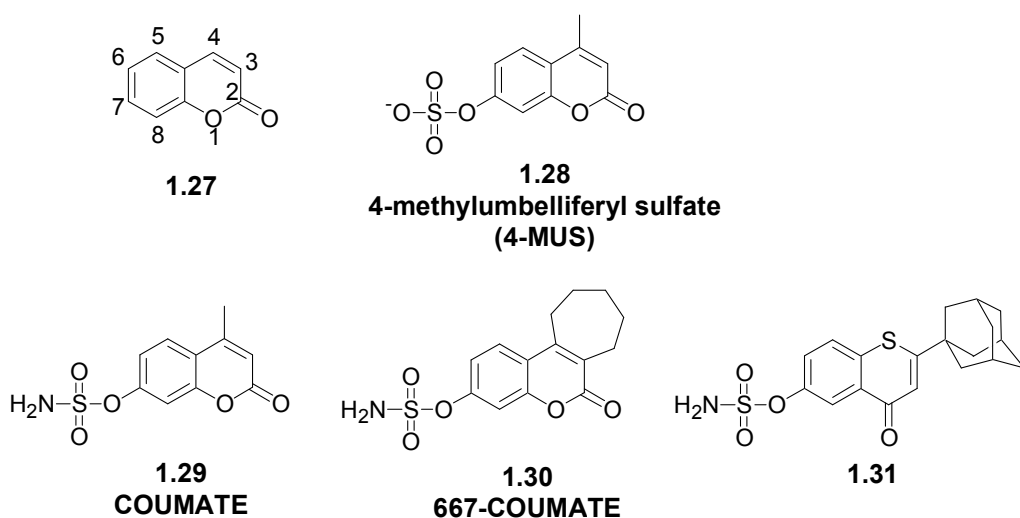


Figure 1.25. The general structure of coumarin, **1.27**, and its numbering scheme. 4-methylumbelliferyl sulfate, 4-MUS, **1.28**, is an artificial fluorogenic substrate for sulfatases. Non-estrogenic aryl sulfamate inhibitors of STS: compound **1.29**, COUMATE, and **1.30**, 667-COUMATE. Compound **1.31** is a chromenone-based inhibitor.

There has been recent effort to concomitantly block the production of estrogen via STS and aromatase through the action of a single inhibitor. These dual aromatase and STS inhibitors (DASI) are based on the structure of a known aromatase inhibitor

and feature a sulfamate substituent (Woo et al., 2003). Two of the best representatives of this new class are **1.32** and **1.33** shown in **Figure 1.26**. Compound **1.32** exhibited an IC_{50} of 2.3 nM against STS, while compound **1.32** had an IC_{50} of 0.82 nM. In terms of aromatase inhibition, the IC_{50} of compound **1.32** was 20 nM and that of compound **1.33** was 39 nM.

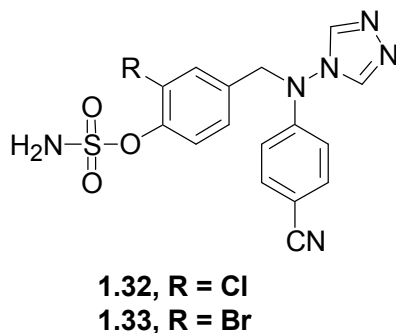


Figure 1.26. Dual aromatase and steroid sulfatase inhibitors (DASIs), **1.32** and **1.33**.

1.4 Research Objectives

STS and PTP1B share a common ancestor in the alkaline phosphatase superfamily but diverged to catalyze the hydrolysis of sulfate and phosphate monoester bonds with great substrate specificity in the cell and with diverse physiological outcome. STS plays a key role in regulating estrogen levels and is seen to have great potential as a therapeutic target for the treatment of hormone-dependent breast cancer, which accounts for 40% of post-menopausal cases. PTP1B is key enzyme in the down regulation of insulin signaling and is a well-established target with tremendous potential for the development of therapeutics for the treatment of type II diabetes mellitus. This doctoral thesis explores the development of reversible and irreversible inhibitors of STS and PTP1B with the goal of improving our understanding of substrate specificity of these enzymes and their mechanisms. Elucidating the mechanism of enzymes is an important

process in the rational design of small molecule inhibitors. One vital aspect to studying the kinetic behaviour of an enzyme's interaction with an inhibitor is a source of purified enzyme. We purified STS to homogeneity from human placenta by adapting a number of literature procedures as described in *Chapter 2*. Boronic acid analogs of coumarins and of the cognate substrate of STS, estrone-3-O-sulfate, were examined as reversible inhibitors of STS and the results are reported in *Chapter 3*. *Chapter 4* explores our efforts to develop quinone methide-generating mechanism-based enzyme inhibitors of STS with the goal of using this strategy to develop proteomic probes for profiling the sulfatase family. The ability to profile the sulfatase family with specific probes should open an avenue for understanding the assignment of sulfatase function and may lead to the identification of potential new therapeutic sulfatase targets. The major challenges facing the development of inhibitors of PTP1B is bioavailability and selectivity against other members of its highly structurally conserved family of protein tyrosine phosphatases. *Chapter 5* discusses our endeavours to understand substrate specificity of PTP1B by examining the difluoromethanesulfonic acid (DFMS) group as a phosphotyrosine (pTyr) mimic in a non-peptidyl platform. The DFMS group is one of the best monoanionic pTyr mimics reported in the literature and is seen to have potential in addressing the bioavailability challenge. *Chapter 5* also presents our results in examining [sulfonamido(difluoromethyl)]-phenylalanine as neutral pTyr mimic in commonly used tripeptide and hexapeptide platforms used to assess the efficacy of a potential pTyr mimic.

Chapter 2 – Purification of Steroid Sulfatase

2.1 Introduction

In order to study inhibitors developed for STS a source of purified enzyme is necessary. To generate accurate kinetic values for an inhibitor designed against an enzyme it is best to conduct these studies using purified enzyme, otherwise, there is a possibility that other enzymes in a mixture may confound the kinetic values obtained. Furthermore, it is sometimes necessary to know the exact concentration of enzyme for data analysis of certain types of inhibitors. In the case of most *reversible* inhibitors the concentration of enzyme does not need to be factored into analysis as the free inhibitor concentration can be assumed to have the same magnitude as the total concentration of inhibitor added to the assay. This assumption is safe to make because the total concentration of enzyme, $[E]_{\text{tot}}$, is much smaller than the dissociation constant for the enzyme-inhibitor complex, K_i (Segel, 1976). The interactions of such inhibitors are treated by Henri-Michaelis-Menten analysis. However, in the case of *tight binding inhibitors*, the steady state assumption does not hold and the concentration of enzyme impacts analysis of its interaction with an inhibitor. As the name suggests, a tight-binding inhibitor binds to its target enzyme with such high affinity that the concentration of free inhibitor in the assay is depleted in comparison to the total concentration of inhibitor added to the assay, due to formation of a strong enzyme-inhibitor interaction. As a general rule, whenever the K_i of an inhibitor is less than 1000 times the concentration of that of the enzyme, these steady state assumptions are not valid (Copeland, 2005; Dixon and Webb, 1979).

However, only a few studies in the literature have reported inhibitor data using purified STS (Li et al., 1995; Dibbelt et al., 1994; Nussbaumer et al., 2002; Selcer et al., 1997). The majority of studies reported use the microsomal fraction from human placenta, or cell lysates from CHO cells expressing STS (Billich et al., 2000; Wolff et al., 2003), lysates from HEK-293 or homogenates from Jeg-3 cells expressing STS or expressing STS (Ciobanu et al., 2001).

STS has been cloned and sequenced (Yen et al., 1987; Stein et al., 1989; GenBank accession numbers M16505 and J04964), however, there has not been much success in expressing STS in bacteria. A report was made on an attempt to express STS in *E. coli* cells using a pGEX-2T system that produces a glutathione S-transferase (GST) fusion protein to facilitate purification (Purohit et al., 1998). The authors obtained a plasmid carrying cDNA of STS and cloned this into a pUC19 vector, from which they eliminated the 5'-untranslated region and cloned the STS gene into a pGEX2T vector. *E. coli* cells were successfully transformed with the recombinant STS-pGEX2T vector and induced, but when subjecting the cell lysate to glutathione affinity beads, the STS fusion protein was not recovered. A protein whose molecular weight corresponded to that of STS (60-65 kDa) was detected only after adding sodium dodecyl sulfate polyacrylamide gel electrophoresis (SDS-PAGE) loading buffer containing bromophenol blue to the affinity beads. After cleaving the recovered protein with thrombin to liberate its glutathione tag the presumed STS had a molecular mass corresponding to about 60 kDa as estimated by PAGE. The recovered enzyme was not catalytically active and it was reasoned that the recombinant fusion STS had such low recovery levels due its

hydrophobic nature and propensity to adhere non-specifically to surfaces during purification.

Attempts to generate recombinant STS expression in *E. coli* in the Taylor and Guillemette labs met with similar challenges (Lapierre, 2003). The STS gene was subcloned into a pET28a vector with an N-terminal histidine tag and was verified by restriction enzyme analysis and sequencing. The vector was used to transform *E. coli* BL21(DE3) cells, however the STS histidine-tagged fusion protein was not isolated after passing the cell lysate through a Ni-charged column. It was thought that translation of this mammalian protein was perhaps hampered because a significant percentage of codons in the STS gene are rare in *E. coli*. The amounts of *tRNA* charged with a specific amino acid in *E. coli* are not available in equal amounts but rather are proportional to the frequency with which the codon appears in expressed genes (Kane, 1995). The major codons appear frequently in the genetic code, while the rare codons appear sparsely. This presents a limitation when attempting to express mammalian proteins whose DNA sequence contains a significant amount codons that are rare in *E. coli*. Translation of such mammalian mRNA in *E. coli* is thought to be problematic because the ribosome pauses at the rare codon and this results in mistranslated protein. The arginine codons AGG and AGA comprise 2.74% of the total STS codons and are designated rare because they are not frequently used within *E. coli*. Their frequency of their use in *E. coli* is 1.4 and 2.1 per 1000 codons respectively (Kane, 1995). There is evidence that these codons can impair the quality and reduce the quantity of the desired protein (Kane *et al.*, 1993; Hua *et al.*, 1994).

A strategy was adopted to address this codon bias where the construct was expressed in a strain of *E. coli* BL21(DE3)-RP that is enriched genes expressing arginine as well as proline *tRNA* to improve the translation of those rare codons. Nevertheless, STS protein was not isolated upon purification efforts. It may have been expressed as insoluble aggregates as evidenced by a smeared band on a SDS-PAGE of cell debris from the crude cell lysate that tenuously corresponded to the molecular mass of STS. Efforts to resolubilize these insoluble cell masses were not successful.

Recently a report appeared in which cDNA of STS was successfully cloned into a pCEP4 vector that was used to transfect 293-EBNA cells (human embryonic kidney cells expressing Epstein Barr virus nuclear antigen-1) from which recombinant STS was purified as a hexa-histidine-tagged fusion protein in the presence of 0.5% Triton X-100 detergent to solubilize the protein (Stengel et al., 2008). Not only was a significant amount of purified active protein recovered (1.5 mg), but this method of transfection was also amenable to expressing mutant STS protein. This was the first report to successfully perform site-directed mutagenesis (SDM) studies on STS. Prior to this the only SDM experiments performed on members of the sulfatase family were those performed using soluble aryl sulfatase A (Waldow et al., 1999) as well as on some lysosomal sulfatases, such as heparan-sulfatase (Villani et al., 2000) and iduronate sulfatases (Di Natale et al., 2000).

It was our desire to obtain purified STS for the evaluation and analysis of our inhibitors. We purified the protein from human placenta, as this tissue is readily available, inexpensive, and no specialized equipment is required as there would be for eukaryotic cell culture in the case of CHO or HEK expression. There are several studies

on the purification of STS from human placenta (van der Loos et al., 1983; Noel et al., 1983; Burns et al., 1983; Dibbelt et al., 1986; Vaccaro et al., 1987; Kawano et al., 1989; Shankaran et al., 1991; Suzuki et al., 1992; Purohit et al., 1998; Hernandez-Guzman et al., 2003). These purified preparations have exhibited great variation in enzymatic properties, including the specific activity.

One of the common procedures of these purification strategies involves an extraction of STS from its membrane environment. STS is localized in the membrane of the endoplasmic reticulum (Conary et al., 1986). When cells are disrupted the endoplasmic reticulum forms vesicles referred to as microsomes (Lodish et al., 1999). The membrane protein is isolated from the microsomal fraction by differential centrifugation at high centrifugal force, $100,000 \times g$.

The extraction also requires a detergent which is an essential reagent in membrane protein biochemistry and is commonly used to disrupt biological membranes and separate desired proteins (Hunter et al., 2003; Prive, 2007). Detergents are also important to maintain a desired membrane protein in a stable, functional, folded state in the absence of a membrane. A good detergent will mimic the original lipid bilayer and allow the protein to exist in a stable and functional state. In the absence of a detergent or if a poor one is employed, most membrane proteins are subject to aggregation and quickly lose functional activity in an irreversible process that may be measured as a time-dependent loss of activity (Bowie, 2001). A distinct physical property of a detergent is its ability to self-assemble into small, defined entities called micelles, unlike the extended structures of lipid bilayers. Detergent micelles may consist of up to a few hundred molecules, and the number of molecules in a single micelle is termed its

aggregation number. Another physical property of detergents is the number of monomers required for the minimal concentration to form a micelle, or the critical micelle concentration (CMC). The CMC is a property that resulting from the amphipathic nature of detergent monomers that cause them to partition into micelles due to their limited solubility in water. A detergent will behave as an effective solubilizing agent at concentrations above its CMC.

Triton X-100 (**2.1**, octylphenolpoly(ethyleneglycoether)_{x, x=10}, **Figure 2.1**) is the detergent used almost exclusively in the literature for solubilizing STS obtained from human placenta. It is a detergent commonly used for solubilization of membrane proteins because its non-anionic charge makes it relatively mild, in comparison to harsher agents that carry a charge (Barbero et al., 1984). The head group of a detergent interacts with a protein while the length of the alkyl chain affects the CMC and aggregation number. Short chain alkyl detergents such as SDS are harsh protein denaturants, while longer chain alkyl maltosides are gentler. Although, as longer chain alkyl detergents are gentler, they become less soluble. The shorter the alkyl length, the higher the CMC, which requires high concentrations of these detergents to solubilize a membrane protein. The CMC of Triton X-100 is 200 μM (Barbero et al., 1984; Schubert et al., 1983).

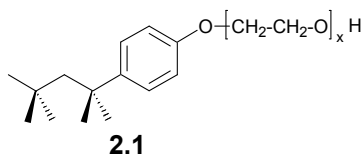


Figure 2.1 Structure of Triton X-100 detergent ($x = 10$).

Once extraction of STS by solubilization from the membrane has been performed the enzyme is isolated by a combination of chromatography steps such as ion

exchange chromatography, affinity chromatography and gel permeation. All methods cited in the literature make use of anion exchange chromatography as the first step to separate STS from other aryl sulfatases (ARSs) also present in placenta. Many methods employ concavallin A sepharose chromatography to take advantage of the glycoprotein nature of STS which binds to this resin with high affinity and is eluted with 10% methylmannoside (Vaccaro et al., 1987; Hernandez-Guzman et al., 2001). Gel permeation chromatography such as Bio-Gel A-1.5m is often used as a final step to yield homogenous STS (Vaccaro et al., 1987; Hernandez-Guzman et al., 2001).

Here a purification of STS from human placenta is presented based on the method of extraction reported by Hernandez-Guzman et al., and using an immunoaffinity chromatography procedure similar to that developed by researchers at Novartis.

2.2 Results and Discussion

The method used by Hernandez-Guzman and coworkers was used to extract STS from human placenta. Cell disruption of the placental tissue was achieved using a lysis buffer of 50 mM tris-HCl, pH 7, 0.25 M sucrose, pH 7.4. To separate the cell debris from the cytosolic portion two successive fractionations were performed at $20,000 \times g$. The cell debris pellet was retained and combined from both fractionations and the desired STS membrane protein was solubilized by resuspension in 20 mM tris-HCl, pH 7.4, 0.3% v/v Triton X-100. Two successive fractionations at $100,000 \times g$ were performed to isolate the microsomal organelles where STS resides in the membrane of the endoplasmic reticulum. At this step the supernatant containing the solubilized STS was retained and combined from both fractionations and the cell pellet discarded.

The first chromatography step employed a diethylaminoethyl (DEAE) anion exchange column. This anion exchange column is used to elute the desired STS whose pI is 6.9 (Shankaran et al., 1991) and exists as an anion at the pH 7.4 of the equilibration buffer and it is eluted by chloride ion from NaCl. Prior to applying the microsomal fraction to the 250 mL bed volume DEAE column, a dialysis step was performed to reduce the concentration of Triton X-100. The microsomal fraction was dialyzed from its 20 mM tris-HCl, pH 7.4 buffer containing 0.3% Triton X-100 to a 20 mM tris, pH 7.4 buffer that contains just 0.1% v/v Triton X-100. The reason is that concentrations of Triton X-100 higher than 0.1% v/v Triton X-100 applied to the DEAE column do not allow the STS protein to adhere and the protein passes through in the void volume. Once the dialysate was applied to the DEAE equilibrated in 20 mM tris, pH 7.4, 0.1% v/v Triton X-100, it was washed with the same buffer for 5 column volumes. Fractions

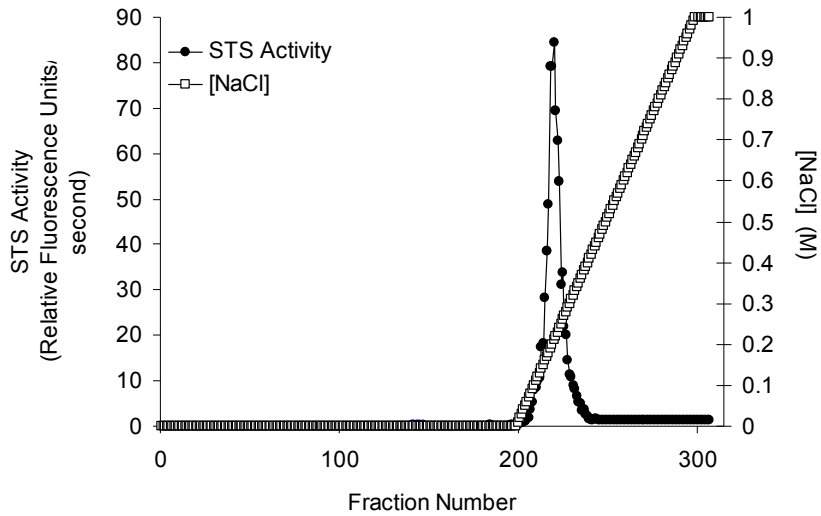


Figure 2.3 Elution profile of STS activity by DEAE chromatography.

The active fractions from the DEAE column were combined and dialyzed into the equilibration buffer for the next chromatographic step, the 2-mL bed volume anti-STS immunoaffinity resin containing covalently linked monoclonal antibodies of STS. Once dialyzed into 50 mM Hepes, pH 7.4, 1% *v/v* Triton X-100, the active STS fraction was applied to the immunoaffinity column pre-equilibrated in the same buffer. The 1% concentration of Triton X-100 does not affect the ability of STS to bind to the immunoaffinity column. The column was washed in 5 column volumes of the same equilibration buffer, followed by a wash with 5 column volumes of 20 mM Hepes, pH 7.4, 100 mM NaCl, 0.1% *v/v* Triton X-100 to wash non-specifically bound proteins, and excess bound STS. STS was eluted from the immunoaffinity column according to a procedure developed by Novartis. This involved subjecting the column to 50 mM citric acid, pH 2.7, 140 mM NaCl, 0.1% *v/v* Triton X-100. All fractions were collected and assayed for STS activity by withdrawing an aliquot from the fractions and diluting them into a solution of 100 mM tris buffer, pH 7.0, containing 200 μ M MUS. As illustrated

in the elution profile in **Figure 2.4**, the STS activity elutes in a distinct peak according to the linear drop in pH over 0.5 column volume from 7.4 to 2.7. The pooled fractions were dialyzed into 20 mM tris, pH 7.4, 0.1% v/v Triton X-100 (storage buffer). The specific activity of STS obtained by this method (method A) is shown in **Table 2.1**.

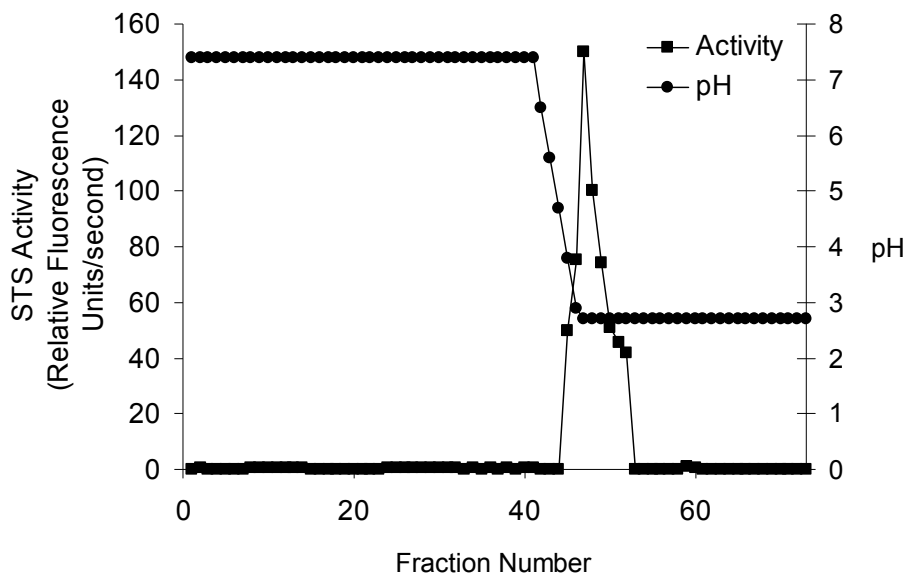


Figure 2.4 Elution profile of STS activity by anti-STS immunoaffinity chromatography.

2.2.1 Study of the effect of neutralization of pH of STS after immunoaffinity purification

Dissociation of a protein ligand from its antibody in immunoaffinity chromatography is commonly performed by an abrupt and steep drop in pH (Sambrook and Russell, 2001). Although we obtained STS with a good specific activity, as shown in **Table 2.1**, we were concerned that eluting STS from the immunoaffinity column using citric acid buffer at pH 2.7 might be harmful to the protein's functional integrity and adversely effect its activity. It has been shown that incubation of rat STS in glycine-HCl buffer at pH 2.5 for 1 h at 4°C completely inactivated the enzyme (Kawano

et al., 1989). Vaccaro and coworkers reported that STS is unstable at acidic pH (Vaccaro et al., 1987). Therefore, we conducted a study on the effect of the citric acid buffer, pH 2.7, on STS stability as measured by activity. STS (40 nM) purified according to Novartis procedure was thawed on ice after removal from storage and incubated in the low pH elution buffer (50 mM citric acid, pH 2.7, 140 mM NaCl, 0.1% v/v Triton X-100) and compared to the same sample of enzyme incubated in enzyme storage buffer (20 mM tris, pH 7.4, 0.1% v/v Triton X-100). Immediately an aliquot (5 μ L) was withdrawn from both enzyme samples and added to a 100 μ L solution of 400 μ M 4-MUS (95 μ L) in 0.10 M tris, pH 7.5 and the rate of production of fluorescent product 4-MU was followed as described in § 2.2.2.1. There was virtually no activity remaining in the sample incubated in the low pH elution buffer compared to that of the control sample incubated in its enzyme storage buffer. This illustrates that STS is very unstable in such acidic buffer. However, since we are clearly able to obtain active enzyme purified using the Novartis procedure then some of the enzyme must have survived the acidic conditions used to elute it for the column. It is possible that the concentration of the enzyme is important. The concentration of the enzyme used (40 nM) for the stability studies was 50-fold lower than that of the stock concentration of enzyme which elutes from the column. Perhaps the enzyme that elutes during the purification procedure is more resilient toward the harsh acidic elution buffer due to the protective benefits from being more concentrated. Nonetheless, it suggests that some portion of the STS activity may be lost during elution for the immunoaffinity column. An alternative to using low pH for removing the enzyme from the column is to go to high pH. Kawano and coworkers have reported a purification of STS using

immunoaffinity chromatography (Kawano et al., 1989). They eluted STS from the column using 10% dioxane containing 0.5 M NaCl, 20 mM tris, 0.3% v/v Triton X-100 at pH 11.0. In order to get pure STS, the material obtained from the immunoaffinity column was subjected to high-pressure anion exchange chromatography. We were hesitant to use this procedure since these workers did not report the purification-fold or even the specific activity of the enzyme. We also did not wish to perform an additional purification step using HPLC.

To see if we could minimize the effects of the acidic buffer during elution from the immunoaffinity column we performed another STS purification except that instead of dialyzing the pooled fractions into storage buffer (20 mM tris, pH 7.4, 0.1% v/v Triton X-100) after the immunoaffinity column (method A, the Novartis procedure), we pooled all of the fractions after the column was complete and then neutralized the pooled fractions using concentrated NaOH (0.5 M) then dialyzed into storage buffer (method B). A relatively high concentration of strong base was used to avoid diluting the purified protein too much. However, the specific activity after this purification was considerably less than before (**Table 2.1**). We performed another STS purification except each fraction from the immunoaffinity column was immediately neutralized with concentrated NaOH as soon as it was collected from the column. The neutralized fractions were then pooled and dialyzed into storage buffer (method C). This gave STS with a specific activity of 1.25 μmol 4-MU produced/mg/min in a buffer of 0.1 M tris, pH 7.0 at 22°C, which is three times and eight times higher than that of the dialysis method (“A”) and the pooled neutralization of (“B”) (Table 2.1). Consequently, all subsequent STS purifications were performed using method C.

Table 2.1. Comparison of Specific Activities of three methods to neutralize STS after immununoaffinity purification.

Sample	Concentration (mg/mL)	Specific Activity (μmol 4-MU produced/mg/min)
Purified STS method A	0.16	0.37
Purified STS method B	0.15	0.16
Purified STS method C	0.39	1.25

2.2.2 Evaluation of specific activity, molecular size, and kinetic parameters of STS and comparison to literature

The literature reports the specific activity of STS purified from placenta in terms of various substrates and assay methods such that a comparison between reports is difficult to make. For example, Hernandez-Guzman and coworkers use the natural substrate, [$7\text{-}^3\text{H}$]dehydroepiandrosterone sulfate (DHEAS), as a tritiated substrate in a radiometric assay to report specific activity in terms of the μmol dehydroepiandrosterone produced/min per mg of enzyme (Hernandez-Guzman et al., 2001). It would be advantageous to compare the specific activity we have determined for STS purified according to “method C” (**Table 2.1**) to that of Hernandez-Guzman, as we employed their method for the preparation of placental microsomes; however, we have used 4-MUS as a fluorogenic substrate in our assays. Of the reports that employ 4-MUS as a substrate, Shankaran et al., report a specific activity of 0.2 nmol 4-MU produced/mg/min in a buffer of 0.25 M tris-HCl, pH 7.3 at 37°C (Shankaran et al., 1991). Vaccaro et al., report a specific activity of 70 nmol 4-MU produced/mg/min in a buffer of 0.02 M tris, pH 6.8, pH 7.0 (Vaccaro et al., 1987). It appears that the specific

activity of the protein purified in our lab (1.25 μmol 4-MU produced/mg/min) is 6250- and 18-fold higher than that of Shankaran et al., and Vaccaro et al., respectively. The method we used employs a fewer number of chromatographic steps than those employed by the authors mentioned here, and the overall decrease the purification time may prevent time-dependent loss of activity of the enzyme. Ultimately, it does not seem that there is any detriment caused by exposure to the acidic elution buffer in the immunoaffinity chromatography step though it appears that neutralization of the individual fractions with NaOH as they elute from the column is best.

All of the purifications (using methods A, B and C) showed high purity by SDS-PAGE. The SDS-PAGE for the material obtained using method C is shown in **Figure 2.4**. It is important to note that the “shadow” bands that are present on our SDS-PAGE have also been reported by others and are attributed to the heterogeneity of the *N*-linked glycosylations present in STS (Dibbelt and Kuss, 1986; Hernandez-Guzman et al., 2001). In addition, Hernandez-Guzman et al., used the preparation of STS that shows faint shadow bands by SDS-PAGE to grow diffraction-quality crystals to elucidate the first X-ray crystal structure of STS (Hernandez-Guzman et al., 2003). The extra shadow bands also appear in a Western blot reported to us by these same authors in a personal communication, suggesting that these indeed correspond to molecular weight heterogeneity and are not contaminant proteins.

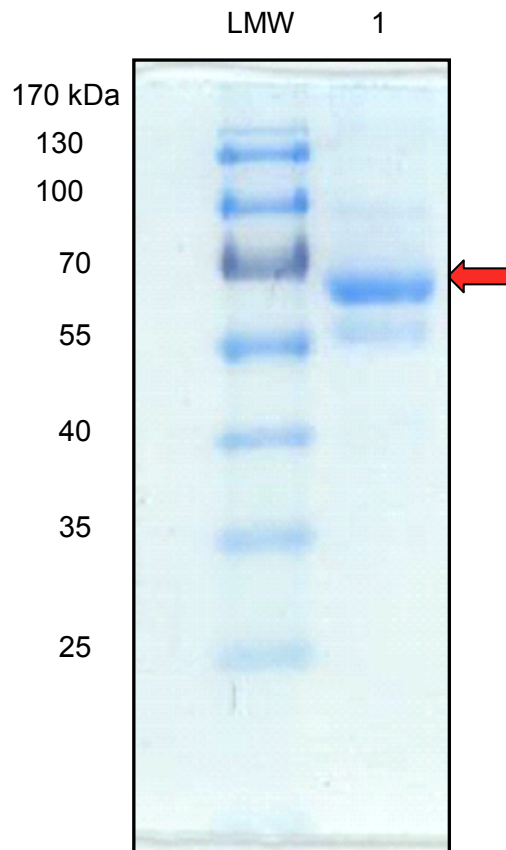


Figure 2.5 10% SDS-PAGE of purified steroid sulfatase. The gel was stained with PageBlue™ Protein Staining Solution according to the manufacturer’s instructions (Fermentas). The low molecular weight (LMW) marker is shown in the leftmost lane. Lane 1 contains a sample obtained after anti-STs immunaffinity chromatography by method “c.” The arrow denotes the major band in this lane at 68 kDa, attributed to STs.

The molecular mass of the major band detected by the SDS-PAGE shown in **Figure 2.5** is approximately 68 kDa which is in good agreement with the results reported by Hernandez-Guzman *et al.*, who reported a molecular mass of 65 kDa based on SDS-PAGE and whose placental extraction method we followed. There used to be conflicting evidence in the literature concerning the functional oligomer of STs, which had been reported as trimeric (Vaccaro *et al.*, 1987), tetrameric (van der Loos *et al.*, 1983), and hexameric (Burns *et al.*, 1983) according to gel filtration. However, with the

publication of the crystal structure (Hernandez-Guzman et al., 2003) there now is agreement that the protein is a monomer, and the previous reports of multimeric forms were caused by variations in detergent solubilization (Vaccaro et al., 1987; Shankaran et al., 1991). There is a wide range of molecular weights for the monomeric protein reported in the literature, 63-78 kDa, as illustrated in **Table 2.2** and this is due to the various glycosylation states of the enzyme (Conary et al., 1986). The sequence of STS predicts a 583 amino acid protein, including 21 residues on N-terminal signal peptide (Stein et al., 1989). The wide distribution of molecular mass is due to the four possible *N*-glycosylation sites on the enzyme (Stein et al., 1989).

Table 2.2 Molecular mass for placental STS reported by SDS-PAGE in literature

Molecular Mass (Da)	Reference
65,000	Hernandez-Guzman et al., 2001
62,000	Kawano et al., 1989
78,000	Vaccaro et al., 1987
74,000	Burns et al., 1983
78,600 ¹	Noel et al., 1983 ¹ ,
72,000 ²	Noel et al., 1983 ²
63,000	Van der Loos et al., 1983

The pH-dependence of k_{cat} , K_m and k_{cat}/K_m using 4-MUS as substrate are shown in **Figures 2.6-2.8**. The dependence of k_{cat} on pH shows a bell-shaped profile with a maximum occurring at pH 8 (**Figure 2.6**). The substrate has K_m values ranging between 100 and 180 μ M pH 6.5 and 7.5, and then the values increase significantly with increasing pH (**Figure 2.7**). k_{cat}/K_m shows a bell-shaped pH profile with a maximum at pH 7.5 (**Figure 2.8**). The pH optima for hydrolysis of 4-MUS substrate for placental STS have been reported between 7.0 and 8.0, however, it is unclear on which parameters these optima are based. For example, Dibbelt and Kuss report a pH optimum for hydrolysis of 4-MUS of 7.0, but the authors do not state whether this value is the

optimal pH for catalytic efficiency, k_{cat}/K_m , or some other kinetic parameter (Dibbelt and Kuss, 1986). Vaccaro et al., and Shankaran et al., report an optimum pH of 6.8 and 7.4, respectively, for the hydrolysis of 4-MUS substrate, but in both cases it is also unclear how this optimum is defined and under which assay conditions it was determined (Shankaran et al., 1991). If we assume that the pH optima for 4-MUS hydrolysis reported in literature is in terms of k_{cat}/K_m , then our value of pH 7.5 falls within the range of values reported.

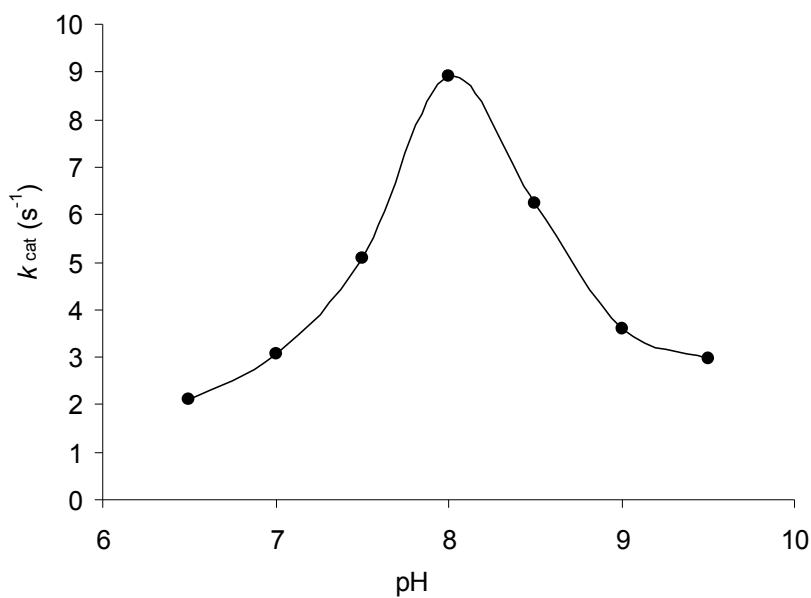


Figure 2.6 pH profile of STS activity in terms of k_{cat} measured with 4-methylumbelliferyl sulfate (4-MUS, **2.2**) as substrate.

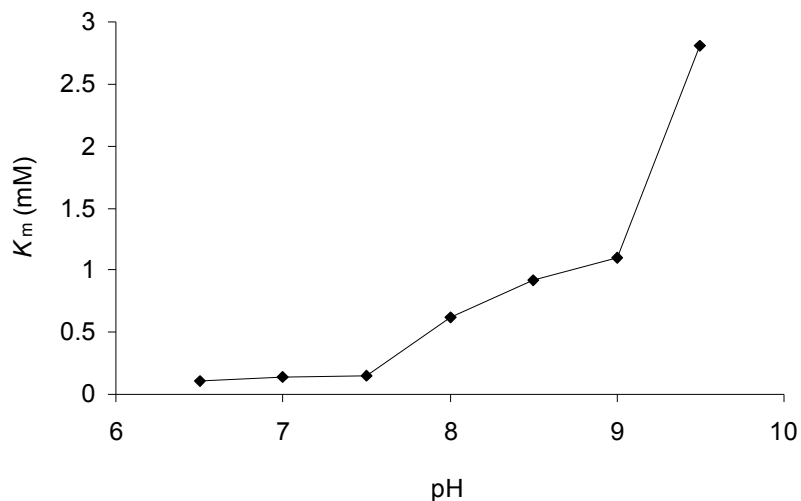


Figure 2.7 pH profile of K_m values of 4-methylumbelliferyl sulfate (4-MUS, **2.2**) for STS as a function of pH.

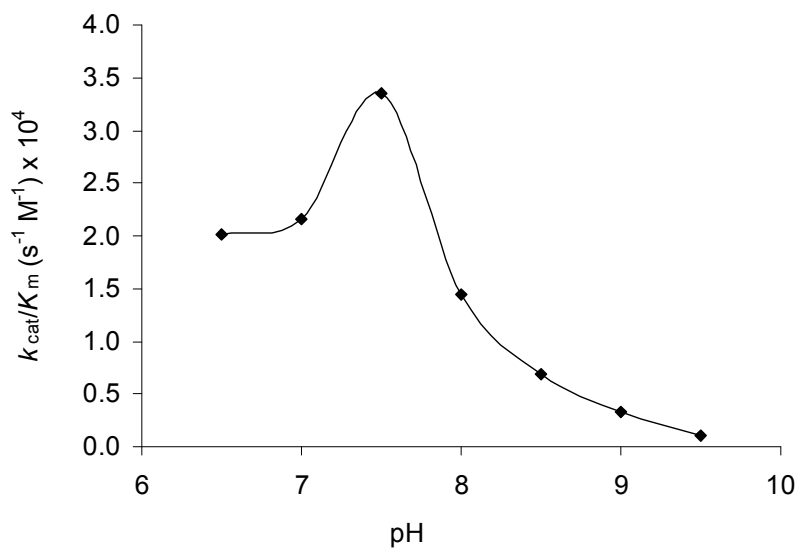


Figure 2.8. pH profile of STS activity in terms of k_{cat}/K_m measured with 4-methylumbelliferyl sulfate (4-MUS, **2.2**) as substrate.

A comparison of our determined K_m value for 4-MUS, 180 μ M, compares well with those reported under similar conditions in literature, as presented in **Table 2.3**. Our value was determined at 22°C using a buffer of 0.1 M bis-tris propane, pH 7.0, 0.01% *v/v* Triton X-100 and the production of the hydrolysis product, 4-MU, **2.3**, was followed

by fluorescence in a continuous mode. Our value compares most closely to that reported by Kawano et al., who report a K_m for 4-MUS of 190 μM at pH 7.0 in a buffer of 0.1 M imidazole-HCl containing 0.3% v/v Triton X-100 at 37°C. Kawano and coworkers also performed their assay for determining K_m in a discontinuous mode where the reaction was stopped by adding 0.5 M glycine-NaOH buffer (pH 10.3). Although the method used by Kawano et al., for determining the K_m of 4-MUS substrate is different from ours in terms of the buffer system, Triton X-100 detergent concentration and the discontinuous mode, our values are very similar. In contrast, the K_m for 4-MUS of 100 μM reported by Vaccaro et al., is approximately 2-fold lower than that reported by our group and Kawano and coworkers. The K_m determined by Vaccaro et al. was determined using a buffer of 0.02 M imidazole HCl, pH 6.8 at 37°C, but similar to the method of Kawano et al., the assay was performed in a discontinuous manner with the addition of 1 M NaOH to basify the assay prior to measurement of fluorescent 4-MU. The differences in assay methods pertaining to buffer system, detergent concentration, temperature, pH and the mode of measurement of the hydrolyzed fluorescent product may account for the differences in K_m values reported in the literature, however, the values that appear in **Table 2.3** fall within a similar range of magnitude.

Table 2.3 Comparison of literature K_m values for 4-MUS substrate.

K_m (μM)	pH	Reference
180	7.0	Present study
190	7.0	Kawano et al., 1989
100	6.8	Vaccaro et al., 1987
270	7.4	Shankaran et al., 1991

2.3 Conclusions

The method we have used for purifying steroid sulfatase from human placenta represents an efficient adaptation of an established ion exchange chromatography method paired with an immunoaffinity method to yield a large quantity of highly purified enzyme, essential for the detailed inhibitor studies we envisage. The manner in which the protein is returned to neutral pH after elution from the immunoaffinity column is an important consideration to ensuring optimally active STS. The purified enzyme's characteristics of molecular size, specific activity, pH optimum and K_m of a commonly used fluorogenic substrate, 4-MUS, compare favorably to those reported in literature.

2.4 Experimental

2.4.1 Materials

Biochemical reagents and buffers were obtained from Sigma Chemical Co. (St. Louis, Missouri) unless stated otherwise. DEAE cellulose (DE-52) was obtained from Whatman (Maidstone, England). Anti-STS monoclonal antibody was a gift from Novartis (Austria) and the procedure for the purification of STS by immunoaffinity chromatography was given to us by Dr. Andreas Billich at Novartis (Austria). Protease inhibitor cocktail was obtained from Sigma. The immunoaffinity column used to purify STS was prepared by coupling the purified anti-STS monoclonal antibody to CNBr-activated Sepharose 4B (Pharmacia) according to the manufacturer instructions at a density of 10 mg/ml resin. DC Protein Assay kit for Bradford protein determination was obtained from BioRad Laboratories (Richmond, California). Gel electrophoresis silver-staining kit was obtained from Invitrogen (Carlsbad, California). Gel electrophoresis PageBlue™ Protein Staining Solution was obtained from Fermentas Life Science (Vilnius, Lithuania). Fluorometric assays were performed using a SpectraMax Gemini XS plate reader equipped with SOFTmax® Pro Version 3.1.1 software from Molecular Devices (Sunnyvale, California). Human placenta was obtained from Credit Valley Hospital, Mississauga, Ontario, shortly after birth and immediately frozen at -80°C until purification, for no longer than two weeks.

2.4.2 Methods

2.4.2.1 Activity Assay

Steroid sulfatase (STS) activity was assayed by the addition of 10 µL of sample to 90 µL of 0.1 M tris, pH 7.0, containing 400 µM 4-methylumbelliferyl sulfate (4-MUS,

2.2, Figure 2.2) in a 96-well black microtiter plate (Corning), similar to the method of Roy, 1971. Production of fluorescent product, 4-methylumbelliferone (4-MU, **2.3**), was monitored for 10 minutes by excitation (360 nm) and emission (460 nm) using a fluorescence platereader (Gemini XS, Molecular Devices, Sunnyvale, CA). Enzyme activity was monitored in terms of relative fluorescence units per second (RFUs/second) using a data acquisition software package, Softmax Pro 3.1.1.

2.4.2.2 Homogenization and Chromatography

200 g of full-term human placenta was homogenized and centrifuged according to the procedure of Hernandez-Guzman and coworkers (Hernandez-Guzman *et al.*, 2003). After membranes were removed and umbilical cord was removed, the placenta was cut into small pieces and homogenized using a Brinkman polytron in 50 mM Tris HCl pH 7.5, 0.25 M sucrose, 1 g protease inhibitor cocktail (Sigma-Aldrich). The homogenate (400 mL) was centrifuged ($20,000 \times g$, 30 minutes, 4°C), and the supernatant was discarded. The pellet was resuspended in the same buffer (300 mL) used in homogenization and subjected to a subsequent centrifugation ($20,000 \times g$, 30 minutes, 4°C). The supernatant was discarded and the pellet was resuspended in an extraction buffer of 20 mM Tris HCl pH 7.4, 0.3% v/v Triton X-100 (300 mL) and subjected to ultracentrifugation ($100,000 \times g$, 70 minutes, 4°C) to obtain the microsomal fraction. After centrifugation the supernatant was saved while the pellet was resuspended in the same extraction buffer (200 mL) and subjected to a second ultracentrifugation ($100,000 \times g$, 70 minutes, 4°C). The resulting supernatant was pooled with that of the first ultracentrifugation and the pellet was discarded. This microsomal fraction (400 mL) was dialyzed into 20 mM tris HCl, pH 7.4, 0.1% v/v Triton X-100 (4

L × 3) and then subjected to a DEAE column (250 mL of DE-52, Whatman) according to the procedure of Hernandez-Guzman *et al.* After the dialysate was applied, the column was washed with 5 column volumes of 20 mM tris HCl, pH 7.4, 0.1% v/v Triton X-100. Pooled fractions containing STS (250 mL) were dialyzed into 20 mM Hepes buffer, pH 7.4, 1% v/v Triton X-100 (2 L × 3). To obtain pure STS, dialyzed fractions from the DEAE column were applied to a monoclonal anti-STS immunoaffinity column (2.5 mL) that had been pre-equilibrated with 10 column volumes of the dialysis buffer based on a method provided to us by Novartis. The immunoaffinity column was prepared by coupling purified monoclonal antibody raised against STS to a CNBr-activated Sepharose 4B at a concentration of 10 mg antibody per mL of resin according to the manufacturer's instructions (Pharmacia). The column was washed with 5 column volumes of the same buffer and then 10 column volumes of 20 mM Hepes, pH 7.4, 100 mM NaCl, 0.1% v/v Triton X-100 and then eluted with 10 column volumes of 50 mM citric acid, pH 2.7, 140 mM NaCl, 0.1% v/v Triton X-100. To neutralize fractions containing STS activity (10 mL), the Novartis procedure recommends basifying each fraction immediately. Because the specific method to basify each fraction was indistinct we adopted three different methods and compared their effects on specific activity of STS as outlined here:

- A) Fractions containing STS activity were immediately pooled and were neutralized by dialysis into 20 mM Tris, pH 7.4, 0.1% v/v Triton X-100 (STS storage buffer).
- B) Fractions containing STS activity were immediately pooled and were neutralized by slow addition of 0.5 M NaOH until approximate neutrality was

reached as measured by litmus paper. Pooled fractions were immediately dialyzed into storage buffer.

C) Fractions containing STS activity were immediately neutralized by slow addition of 0.5 M NaOH until approximate neutrality was reached as measured by litmus paper. Pooled fractions were immediately dialyzed into storage buffer.

After STS from each neutralization method was dialyzed into storage buffer, the dialysate was divided into aliquots of 100 μ L each and flash frozen in $N_2(l)$ and stored at -80°C until use. STS from each neutralization method was purified to $>95\%$ homogeneity as judged by 10% SDS-PAGE (stained with PageBlue™ Protein Staining Solution, Fermentas Life Science).

To further test the stability of STS in low pH, a 40 nM concentration of STS purified by method “C” was incubated in both the immunaffinity elution buffer of 50 mM citric acid, pH 2.7, 140 mM NaCl, 0.1% v/v Triton X-100, and the enzyme storage buffer of 20 mM tris, pH 7.4, 0.1% v/v Triton X-100. Immediately, 5 μ L aliquots were withdrawn in triplicate from both of the incubations and added to wells of a 96-well black microtiter plate containing 95 μ L of 400 μ M 4-MUS (approximately $2 \times K_m$) in 0.1 M tris, pH 7.5. The change in pH of the assay due to the addition of the pH 2.7 buffer was negligible. The production of fluorescent 4-MU product was measured according to the method described in § 2.4.2.1.

2.4.2.4 Protein concentration determination

The protein concentration was determined according to DC Biorad Laboratories (Richmond, CA) protein concentration determination kit instructions using bovine serum albumin (BSA) as a standard. This colorimetric assay is for the determination of

protein concentration following solubilization with a detergent such as Triton X-100. The assay is based on the reaction of protein with an alkaline copper tartrate solution and Folin reagent (Bradford, 1976).

2.4.2.5 Determining kinetic properties

To determine the K_m of STS with 4-MUS a substrate, 90 μL of concentrations of 4-MUS ranging from 83.3 μM – 500 μM in buffer containing 0.1 M tris, pH 7, 0.01% v/v Triton X-100 were in a 96-well black microtiter plate to which 10 μL of purified STS was added to a final concentration of 3 nM. Production of fluorescent 4-MU was followed as described in § 2.2.2.1. The K_m value was determined from a plot of $1/v$ versus $1/[4\text{-MUS}]$ according to the method of Lineweaver-Burk.

2.4.2.6 Determining pH-rate profile

A pH-rate profile was generated by performing assays to generate Lineweaver-Burk plots as described in § 2.4.2.5. A plot was determined for each pH at 6.5, 7, 7.5, 8, 8.5, 9, 9.5 in 0.1 M bis-tris propane buffer whose buffering range is from 6.0 to 9.5 (Eckert and Kunkel, 1991). The K_m and V_{\max} values were determined from the slopes and y -intercepts of $1/v$ versus $1/[4\text{-MUS}]$ Lineweaver-Burk graphs. The catalytic rate constant, k_{cat} , at each pH was calculated by V_{\max}/E_{tot} (Copeland, 2005).

Chapter 3 – Quinone Methide-Generating Active Site-Directed Mechanism-Based Irreversible Inhibitors of Steroid Sulfatase[†]

3.1 Introduction

3.1.1 Mechanism-based enzyme inhibitors

Mechanism-based enzyme inhibitors (MBIs) also referred to as suicide inhibitors (SIs) are compounds that are enzyme substrates yet produce an intermediate or product that reacts covalently with a residue(s) which results in the enzyme's inactivation. A general reaction scheme for SIs is shown in **Figure 3.1**. The SI binds to the enzyme (E) to form an enzyme-SI complex (E—SI). The enzyme becomes inactivated from further catalysis by converting the SI into an activated form (SI[†]) that becomes covalently attached to the enzyme (E—SI[†]). In general, SIs are relatively unreactive in the absence of the enzyme and resemble either the natural product or substrate of an enzyme (Silverman, 1988).

[†] This chapter is based largely on the publication, “Multiple pathways for the irreversible inhibition of steroid sulfatase with quinone methide-generating suicide inhibitors,” which was published in the journal *ChemBioChem* (Ahmed et al., 2009). Express written consent was obtained from the publishers of *ChemBioChem* to reproduce the publication in whole or in part in association with this thesis, as noted in Appendix E. The publication must be cited and the copyright regulation must be stated as follows:

Ahmed, V., Liu, Y., Taylor, S.D. Multiple pathways for the irreversible inhibition of steroid sulfatase with quinone methide-generating suicide inhibitors. *ChemBioChem*, volume 10(9), pages 1457-61, 2009. Copyright © 2009 Wiley-VCH Verlag GmbH & Co., KGaA, Weinheim, Germany.

sensitive technique such that when it is attached to the reporter the proteins to which the reported is attached can be readily detected. The proteins can be digested with a protease and sequenced. This allows one to isolate new members of the target enzyme class and to analyze activity patterns both in normal physiology and in disease pathology.

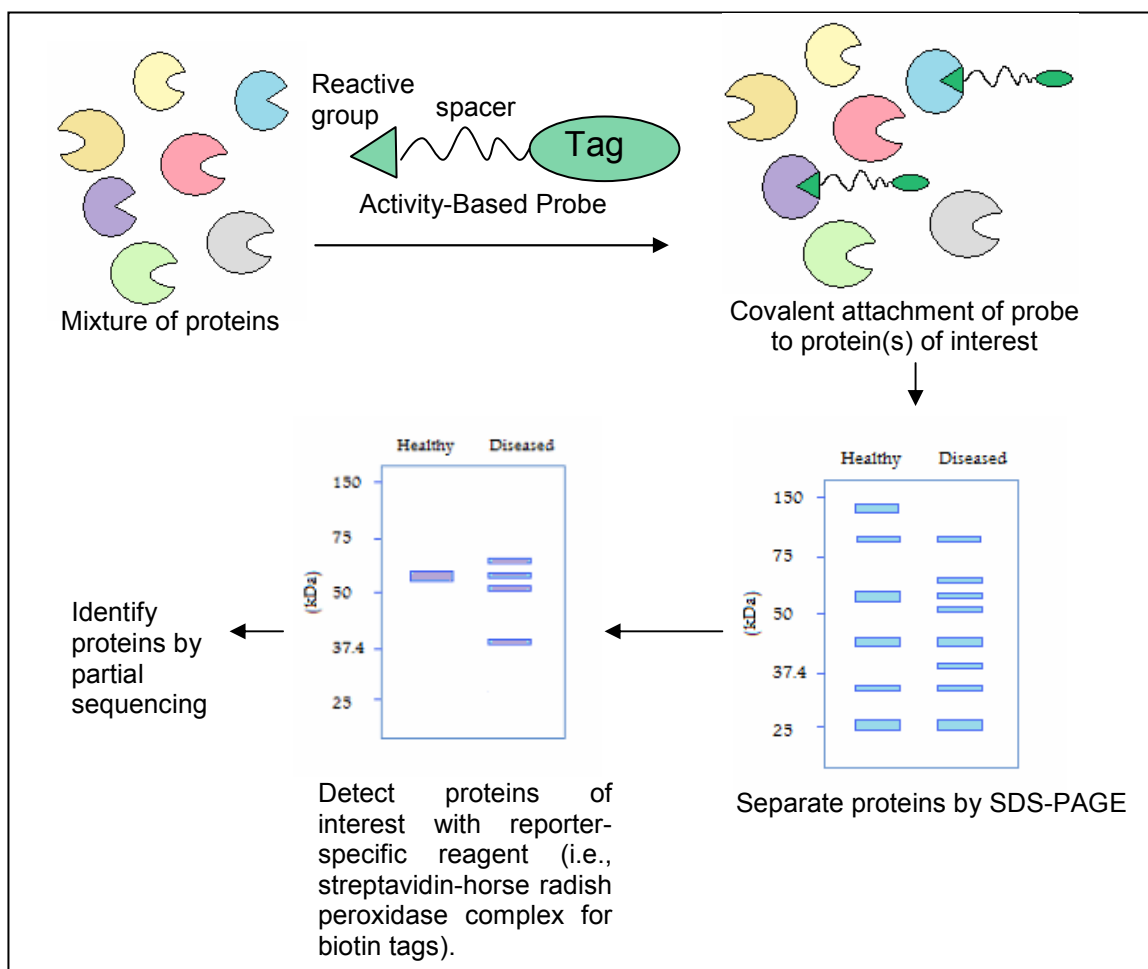


Figure 3.2. General scheme for activity-based proteomic profiling. (Adapted from Cravatt, 2008.)

It is a long-term objective of the Taylor group to develop SIs as activity-based probes for the proteomic profiling of sulfatases. The ability to profile the entire

sulfatase family on the basis of changes in their activity should open an avenue for both the assignment of sulfatase function and the identification of potential new therapeutic sulfatase targets. There is an emerging interest in profiling prokaryotic and eukaryotic sulfatase activity due to their involvement in diverse physiological functions ranging from hormonal regulation, cellular degradation, intracellular communication, and signalling pathways (Hanson and Wong, 2004). Sulfatases are also good candidates for this proteomic profiling strategy because their active sites are highly conserved and they are all believed to catalyze their respective desulfations by a common mechanism (Ghosh, 2007; O'Brien and Herschlag, 1998). The fact that most sulfatases are able to hydrolyze the sulfate ester bond of small molecule aryl sulfates that are non-natural substrates (Roy, 1971) makes this class of enzymes amenable toward proteomic profiling by activity-based probes.

3.1.2 Quinone methide-generating suicide inhibitors

In chapter 1 (§ 1.3.2) a major class of sulfatase suicide inhibitors was discussed, the aryl sulfamates, ($\text{ArOSO}_2\text{NH}_2$) (Nussbaumer and Billich, 2004). Although they are potent irreversible STS inhibitors, it is unlikely that these compounds will ever be used as ABPs for profiling sulfatases since the ArO-S bond must be cleaved by the enzyme and so the phenolic portion of the substrate is released from the active site. The species that ultimately labels the sulfatase is believed to be HN=SO_2 . Thus no reporter group can be covalently attached to the enzyme using this class of SIs.

Numerous SIs have been developed for a wide variety of enzymes (Silverman, 1988). In this thesis we will focus on a specific class of SIs called quinone methide-generating SIs. Quinone methide-generating SIs have previously been developed for a

variety of hydrolytic enzymes. Among the first to use this class of SIs were Halazy and coworkers who demonstrated that di- and monofluoromethylaryl- β -glycosides were SIs of a β -glycosidase (Halazy et al., 1990). An example of one of their inhibitors, compound **3.1**, and its mechanism of action, is shown in **Figure 3.3**. It is believed that the action of a glycosidase on compound **3.1** results in the formation of intermediate **3.2** which spontaneously breaks down to give quinone methide **3.3**. This highly reactive species then reacts with an active site nucleophile(s) and inactivates the glycosidase. Many other SIs based on this strategy have been developed since their report. Some

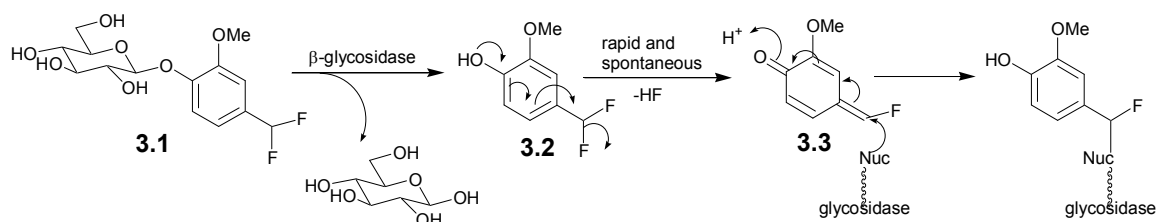


Figure 3.3. Compound **3.1** as a quinone-methide generating SI of a glycosidase.

examples are shown in **Figure 3.4**. For example, Janda and coworkers used the bovine serum albumin (BSA) conjugate of compound **3.4** to screen a phage-Fab library of 9×10^3 members to trap catalytic antibodies with galactosidase activity (Janda et al., 1997). Lo and coworkers designed compound **3.5** as an activity-based probe for glycosidases (Tsai et al., 2002). Myers and Widlanski reported the use of 4-monofluoromethylphenyl phosphate (**3.6**) as a SI of prostatic acid phosphatase (Myers et al., 1993). Shortly thereafter, Withers and coworkers demonstrated that 4-difluoromethylphenylphosphate was also a SI of human prostatic acid phosphatase as well as a phosphotyrosine phosphatase (Wang et al., 1994). Cesaro-Tadic and coworkers screened a phage-display library comprised of 2×10^9 human catalytic antibodies exhibiting phosphatase turnover

by using 2-difluoromethylphenyl phosphate immobilized substrate, **3.7**. (Cesaro-Tadic et al., 2003). Lo and coworkers designed compound **3.8** as an activity-based probe for phosphatases (Lo et al., 2002). All of these compounds inhibit their target enzymes by generating reactive quinone methides in the active site upon activation by their respective enzymes in a manner similar to that described in **Figure 3.3**.

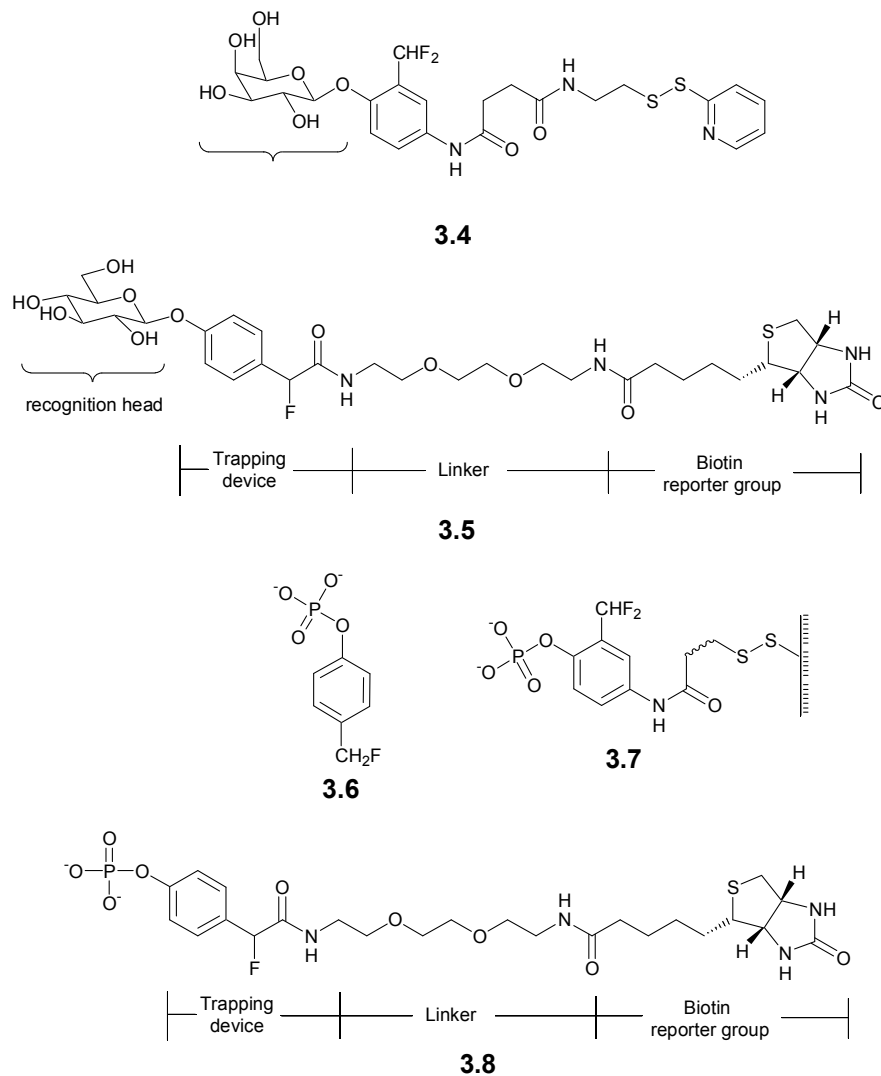


Figure 3.4. Examples of some quinone methide-generating SIs of glycosidases and phosphatases.

3.1.3 Objectives

The objective of the work described in this chapter is to determine if quinone-methide-generating SIs can be developed for sulfatases using STS as a representative sulfatase. If such inhibitors can be developed then an additional objective will be to determine if they exhibit properties that enable them to be used as activity based probes for proteomic studies. These objectives will be achieved by subjecting STS to compounds **3.9-3.16** (**Figure 3.5**) followed by detailed kinetic studies. Hydrolysis of the S–O bonds in **3.9-3.16** would produce quinone methides in the active site which could react with residues required for catalysis thus inactivating STS (as illustrated for compound **3.10** in **Figure 3.6**). Should compounds **3.9-3.16** prove to be SIs of STS and exhibit kinetic properties that are amenable to proteomic studies then it is a long-term goal to use this class of inhibitors as activity-based probes for the proteomic profiling of sulfatases.

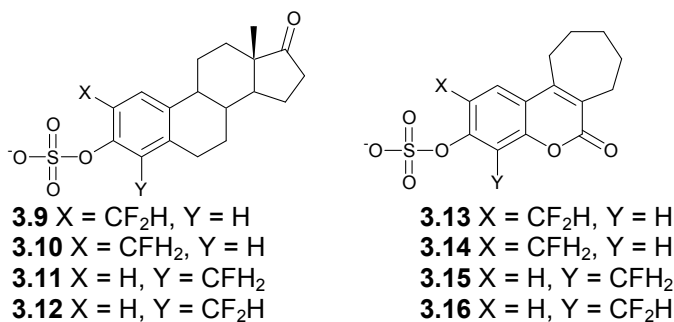


Figure 3.5. Proposed quinone methide-generating inhibitors.

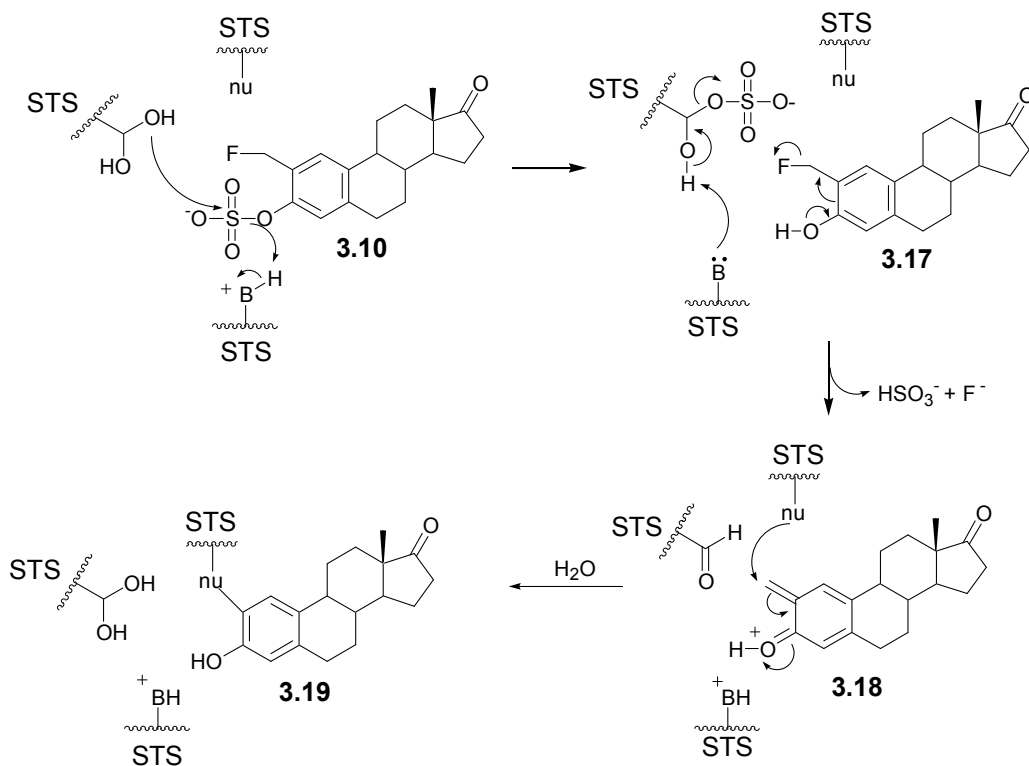


Figure 3.6. Proposed mechanism for the inactivation of STS by compound **3.10**.

3.2 Results and Discussion

3.2.1 General criteria for SIs.

SIs are evaluated experimentally by the following characteristics: (1) time- and concentration-dependent inactivation (ideally, loss of activity should follow pseudo-first order kinetics); (2) saturation inhibition kinetics; (3) substrate protection; and (4) exogenous nucleophiles do not affect rates of inactivation (Silverman, 1988). Evidence for these characteristics indirectly supports modification of the enzyme by covalent attachment of the inhibitor. When possible, it is also desirable to obtain additional evidence for covalent modification by identifying the amino acid residue bearing the covalently attached molecule after enzymatically digesting the putatively covalently modified enzyme and isolating the peptide fragment.

3.2.2 Evaluation of time- and concentration-dependence of compounds **3.10** and **3.11**.

Compounds **3.9-3.12** were prepared by Yong Liu in the Taylor group. I examined for time- and concentration-dependent STS inhibition by incubating the compounds with STS at pH 7.0 in 100 mM tris buffer containing 0.01% Triton X-100 (assay buffer). Aliquots were withdrawn at various time intervals and diluted 50-fold into a solution of a high concentration ($20 \times K_m$) of 4-methylumbelliferyl sulfate (4-MUS) in the same buffer and STS activity was determined by following the production of 4-methylumbelliferone by fluorimetry. The amount of STS activity remaining was compared to that of a control containing no inhibitor (for details see § 3.4.3). The reason that the enzyme-inhibitor incubation is significantly diluted into an excess concentration of substrate is to “quench” any further inactivation events and to allow measurement of the remaining active, free enzyme (Silverman, 1988).

The monofluoromethyl steroid derivatives, **3.10** and **3.11**, were studied first. The 2-monofluoromethyl derivative **3.10** exhibited time- and concentration-dependent inhibition as illustrated in **Figure 3.7A**. At 100 μM of **3.10** almost all STS activity was abolished within 20 minutes. The rate of inactivation did not increase at concentrations above 100 μM and this plateau is indicative of saturation kinetics (Silverman, 1988). At concentrations between 12.5 and 50 μM of inhibitor the inhibition occurred relatively rapidly within the first few minutes but then slowed and eventually reached a plateau. This behaviour has been observed in previous studies of SIs of sulfatases, for example, in members of the aryl sulfamate inhibitor class (Purohit et al., 1995). This suggests that multiple inactivation events are occurring with non-catalytic amino acid residues or

other nucleophiles such as water, and only above a certain concentration of inhibitor is there enough quinone methide generated to react with catalytic amino acids, resulting in irreversible inhibition of the enzyme. Alternatively, this suggests the inhibitor is rapidly consumed and that much of the resulting quinone methide diffuses from the active site and has a high *partition ratio*. The partition ratio is the ratio of the number of times the inhibitors are turned over to the number of enzyme inactivation events (k_3/k_4 in **Figure 3.1**) (Silverman, 1988). In the initial five minutes pseudo-first order reaction rates were observed (**Figure 3.7B**) from which a K_i of 68 μM and a k_{inact} of 0.34 min^{-1} (k_{inact}/K_i of $5000 \text{ M}^{-1} \text{ min}^{-1}$) were derived for **3.10** using the method of Kitz and Wilson (**Figure 3.7B** inset) (Kitz and Wilson, 1962). The K_i for inactivation of an enzyme by a SI is determined experimentally as described in § 3.4.3, by observing the effect on the rate of inactivation due to a change in the inactivator concentration. In contrast, the K_i for reversible inhibitors is defined as the dissociation constant for the enzyme-reversible inhibitor complex, and is experimentally determined by examining the rate of conversion of subsaturable concentrations of substrate to product in the presence of a constant amount of inhibitor (Silverman, 1988). Only if k_2 shown in **Figure 3.1** is rate-determining (when k_1 and k_{-1} are much greater than k_2), the K_i for SIs is analogous to the K_i term for reversible inhibitors, and represents the dissociation of the E-SI complex (Silverman, 1988). However, the rate of inactivation by a SI is determined by the rates of k_2 and k_4 depicted in **Figure 3.1**, so if k_4 becomes even partially rate-determining, then the value of K_i increases and K_i and K_d are no longer equal. Conceptually, K_i is the concentration of the inactivator that produces half the maximum rate of inactivation

(Silverman, 1988). The rate of inactivation, k_{inact} , is a combination of rate constants, k_2 and k_4 , and is experimentally determined as described in § 3.4.3.

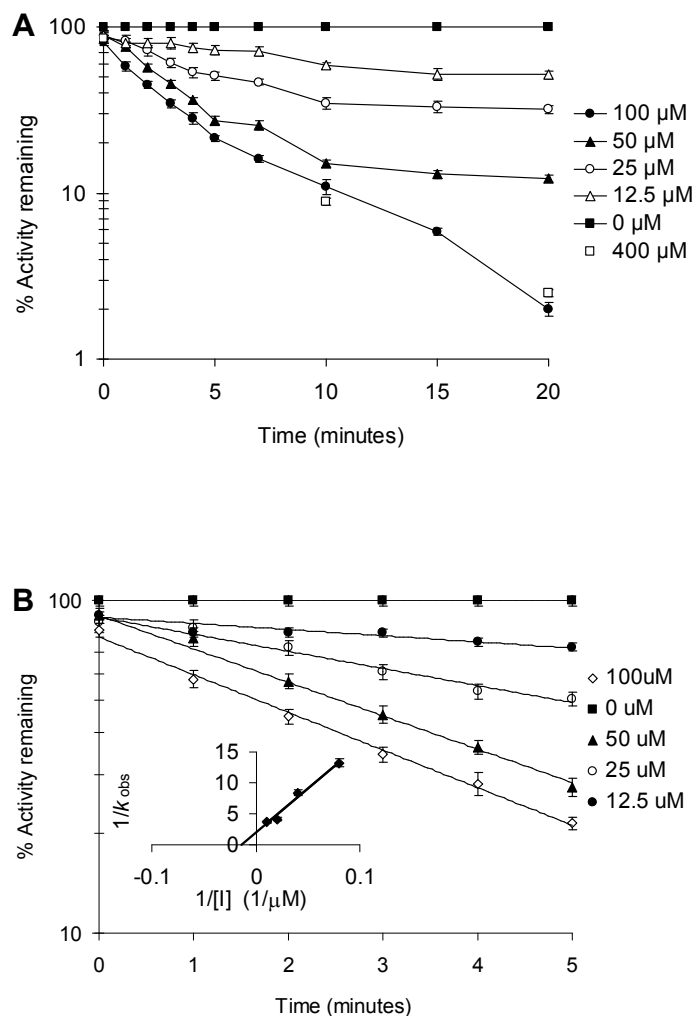


Figure 3.7. Time- and concentration-dependent inhibition of STS with inhibitor **3.10** over 20 minutes (**A**) and 5 minutes (**B**). Inset in **B**: Kitz-Wilson plot. For details see § 3.4.3.

The 4-monofluoromethyl derivative, **3.11**, exhibited behaviour similar to that of the 2-monofluoromethyl derivative, compound **3.10**, as illustrated in **Figure 3.8A**. There is a pseudo-first order loss of activity with respect to time for all concentrations examined, followed by a plateau. As with compound **3.10**, this suggests that multiple inactivation events are required for irreversible inhibition or that the quinone methide is

rapidly consumed and also has a high partition ratio. The initial twenty minutes of the pseudo-first order reaction rates (**Figure 3.8B**) were used to generate a Kitz-Wilson plot and yield a K_I of $3.4 \mu\text{M}$ and a k_{inact} of 0.056 min^{-1} for **3.11** (k_{inact}/K_I of $1.6 \times 10^4 \text{ M}^{-1} \text{ min}^{-1}$).

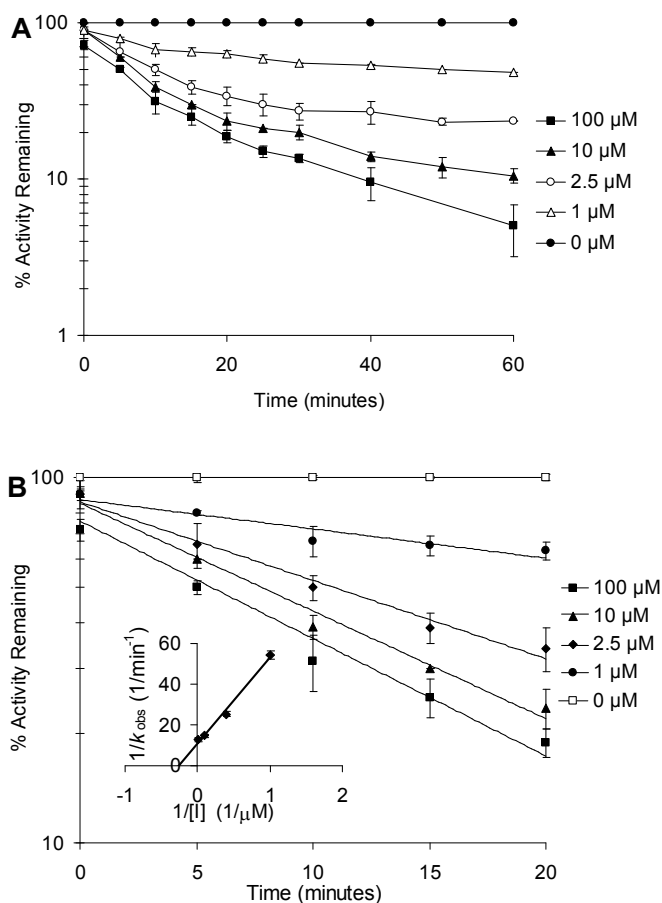


Figure 3.8. Time- and concentration-dependent inhibition of STS with inhibitor **3.11** over 20 minutes (**A**) and 5 minutes (**B**). Inset in **B**: Kitz-Wilson plot. For details see § 3.4.3.

3.2.3 Active site protection and trapping experiments for compounds **3.10** and **3.11**.

To demonstrate that time- and concentration-dependent loss of activity with compounds **3.10** and **3.11** requires activation by STS a protection experiment was

performed. This involves incubating the enzyme with its normal substrate or a known reversible competitive inhibitor concomitant with the proposed inactivator. If the inhibitor requires STS activation for inhibition the competitive inhibitor should compete for binding in the active site and prevent the proposed inactivator from being activated by STS and so a decrease in the rate of inactivation should be seen with increasing concentration of competitive inhibitor. For our studies we used a well-established competitive inhibitor of STS, estrone-3-*O*-phosphate (E1P), which, under our assay conditions (0.1 M tris, pH 7.0, 0.01% Triton X-100) has a K_i of 1 μ M (Anderson et al., 1995). STS could indeed be protected against inactivation by 100 μ M of **3.10** and **3.11** with E1P as illustrated in **Figure 3.9A** and **3.9B**. This indicates that irreversible inhibition by these compounds requires active site binding and enzymatic activation.

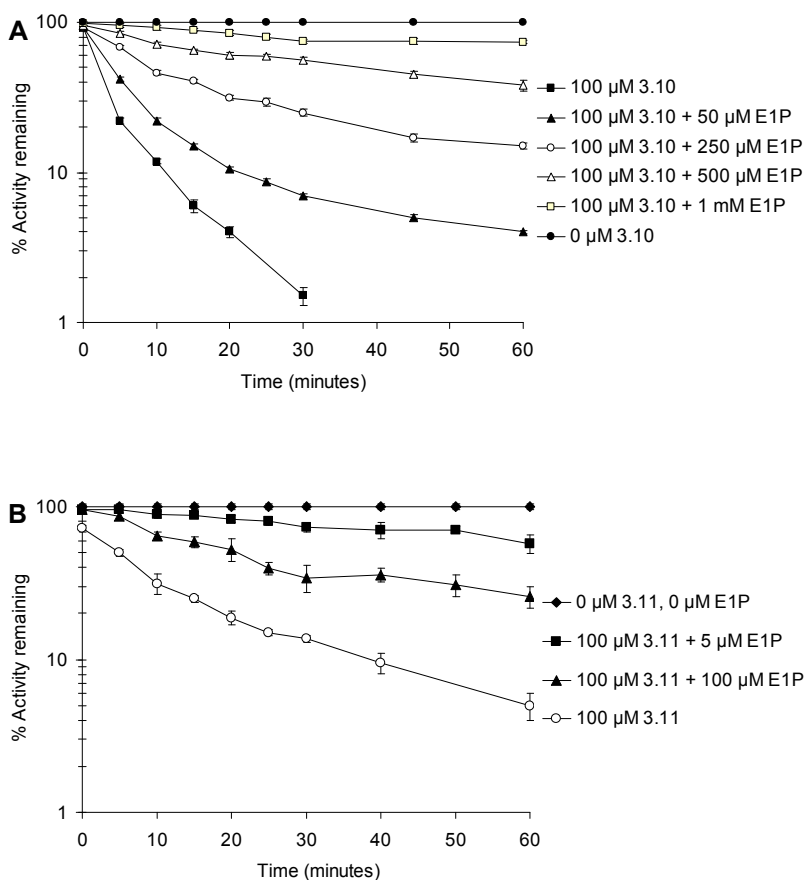


Figure 3.9. Inactivation of STS in the presence of E1P and compound **3.10** (A) and compound **3.11** (B). See §3.4.5 for details.

A mechanism-based inhibitor must be activated in the active site without release into solution and potential re-entry (Silverman, 1988). Otherwise, any inactivation observed may be due to attachment to a residue on the enzyme other than the active site or due to the reactive species leaving the active site and then re-entering the active site after having been modified through reacting with other species in solution. To demonstrate that neither of these situations is responsible for inactivation, the enzyme and inhibitor are incubated with an exogenous nucleophile to “trap” any activated inhibitor that might escape from the active site. Once trapped by the nucleophile the

rate of inactivation observed should decrease. Commonly used nucleophiles for these experiments are thiols such as β -mercaptoethanol (β -ME) or glutathione (Silverman, 1988). It is sometimes preferable to use a bulkier thiol such as glutathione because small thiols such as β -ME can sometimes compete with the inhibitor for the active site, which would defeat the purpose of the experiment. Prior to examining glutathione as an electrophilic trapping agent, its effect on STS activity was examined. A 5 mM concentration of glutathione or β -ME in assay buffer was incubated with STS and the activity was immediately measured using 1 mM of 4-MUS fluorogenic substrate. Only 40% of STS activity remained compared to control and one hour later only 27% of activity remained. In contrast, with β -ME more than 80% of STS activity remained after one hour of incubation of STS. Consequently, β -ME was used for our trapping experiments. Incubation of 100 μ M of each **3.10** or **3.11** with STS in the presence of 5 mM β -ME resulted in little or no decrease in the rate of inactivation as shown in **Figures 3.10A** and **3.10B**. This is consistent with the proposed activated species, the quinone methide, reacting with active site residues. This test demonstrates that the activated species was not released from the active site prior to inactivation and fits the description for a mechanism-based inhibitor.

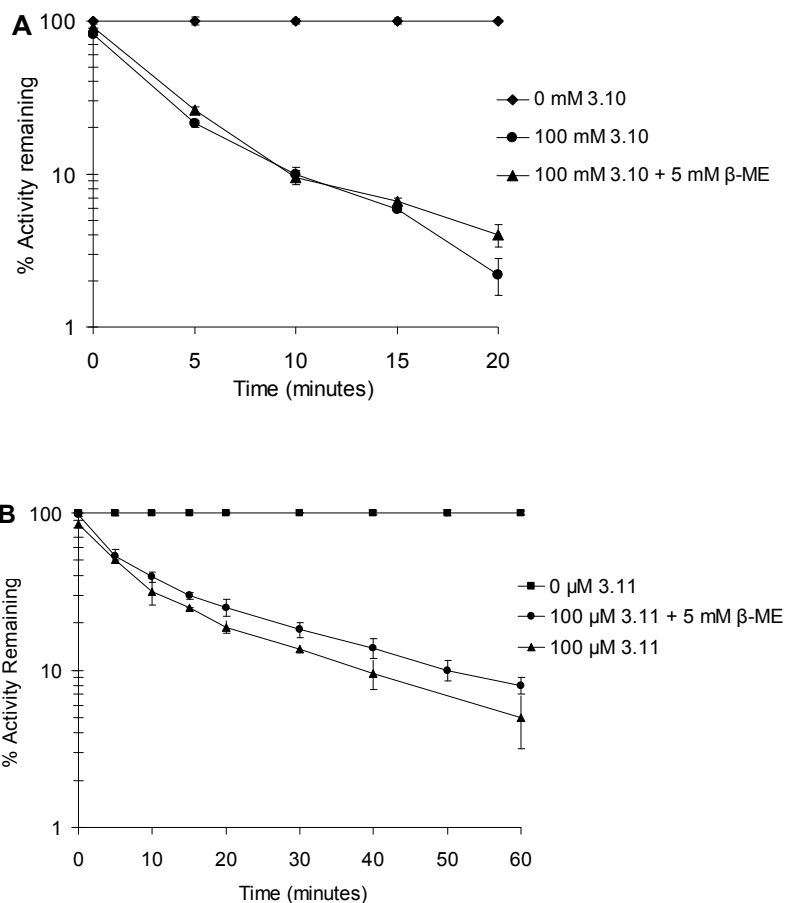


Figure 3.10. Inactivation of STS in the presence of β -ME and compound **3.10** (A) and compound **3.11** (B). For details see § 3.4.6.

3.2.4 Irreversibility of inhibition of STS by compounds 3.10 and 3.11.

In addition to irreversible inhibitors that form a stable covalent bond in the active site of their target enzyme, mechanism-based inhibitors include a category of inhibitors termed *tight binding inhibitors*. It is important to note that tight-binding inhibitors can also exhibit time- and concentration-dependent inhibition, reduced inactivation rates in the presence of a competitive inhibitor and display unaffected inactivation rates in the presence of exogenous nucleophiles. However, because their mode of inhibition is

reversible, extensive dialysis of the inhibited enzyme will restore its activity. In order to distinguish between a tight-binding inhibitor and a irreversible inhibitor, dialysis of the enzyme-inhibitor complex is an essential experiment. Following inactivation of STS by 100 μ M each of compounds **3.10** and **3.11** for 1 hour under our usual conditions, an extensive dialysis amounting to a 10^{12} -fold dilution over a 24-hour period of the enzyme-inhibitor solution was performed in conjunction with a control in the absence of inhibitor. No appreciable STS activity could be recovered after extensive dialysis, emphasizing the irreversibility of the inhibition by these compounds.

3.2.5 Evaluation of time- and concentration-dependence for compound 3.9.

The 2-difluoromethyl derivative, **3.9**, was examined for time-dependent inhibition at 10 μ M, however, no significant inhibition was observed. To determine whether the compound was even a substrate for the enzyme, 10 μ M of **3.9** was incubated with STS and aliquots were withdrawn at $t = 0, 2$ and 5 minutes and analyzed by HPLC. The chromatogram obtained after 2 minutes of incubation shows two peaks (**Figure 3.11**). Peak "A" ($t_R = 12$ min) corresponds to compound **3.9**, according to a control, and peak "B" ($t_R = 34$ min) is reasoned to be a product of the enzyme-catalyzed reaction, as its concentration increases in the chromatogram obtained after 5 minutes, while that of the starting material, peak "A," is abolished.

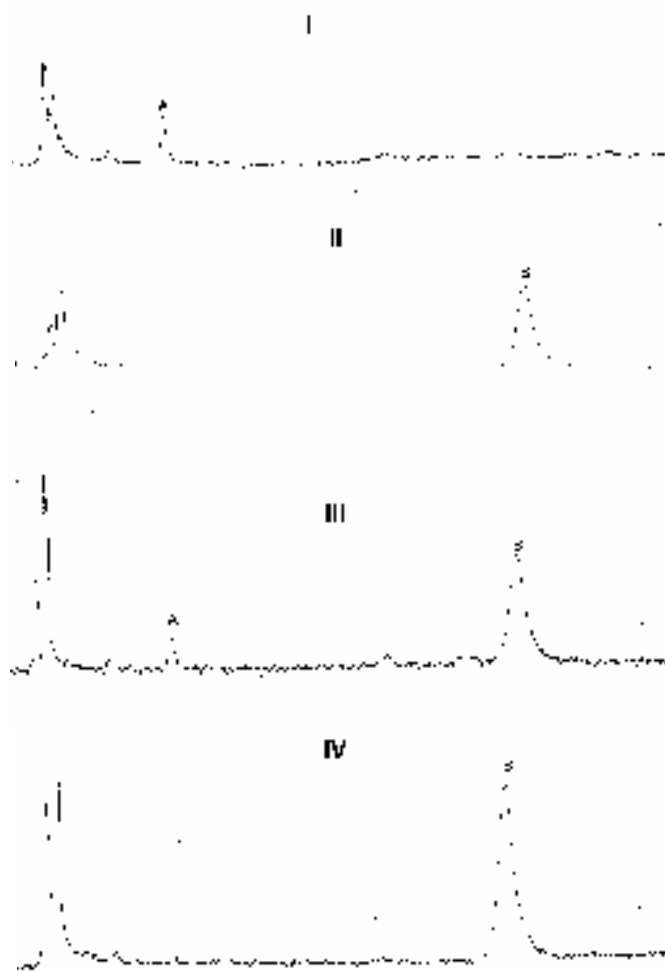


Figure 3.11. RP-HPLC analysis of the reaction of compound **3.9** with STS. **I**: 10 μ M compound **3.9** in assay buffer. Peak A corresponds to compound **3.9** (t_R = 12 min); **II**: 10 μ M 2-FE1 in assay buffer containing 2 % DMSO. Peak B corresponds to 2-FE1 (t_R = 34 min); **III** and **IV**): 10 μ M compound **3.9** with STS in assay buffer after 2 min reaction (**III**) and 5 min reaction (**IV**). See § 3.4.11 for details.

The possible products that may result after STS-catalyzed cleavage of the S-O bond of **3.9** is illustrated in **Figure 3.12**. If the initial hydrolysis product, 2-difluoromethyl estrone (2-diFME1), were to dissociate from the active site prior to formation of the reactive quinone methide, **3.20**, the species would quickly react with water in solution and form 2-formylestrone (2-FE1). To validate whether the identity of

peak “B” could be 2-FE1, the compound was synthesized (Liu et al., 2004) and analyzed by HPLC under the same conditions. Its retention time ($t_R = 34$ min) corresponds to that observed for peak “B.” This evidence suggests that compound **3.9** is a substrate of STS where the S-O bond is cleaved, but instead of following a pathway leading to covalent attachment and inactivation of the enzyme, the reactive quinone methide species is not formed rapidly enough prior to diffusing out of the active site and breaking down in solution to form 2-FE1. The potential of **3.9** as a reversible inhibitor was examined. The Lineweaver-Burk plot for compound **3.9** is shown in **Figure 3.13**. Mixed inhibition is observed and a K_i of $3.7 \pm 0.4 \mu\text{M}$ and αK_i of $1.6 \pm 0.3 \mu\text{M}$ are obtained from the replots shown in insets **A** and **B**, respectively, of **Figure 3.13**.

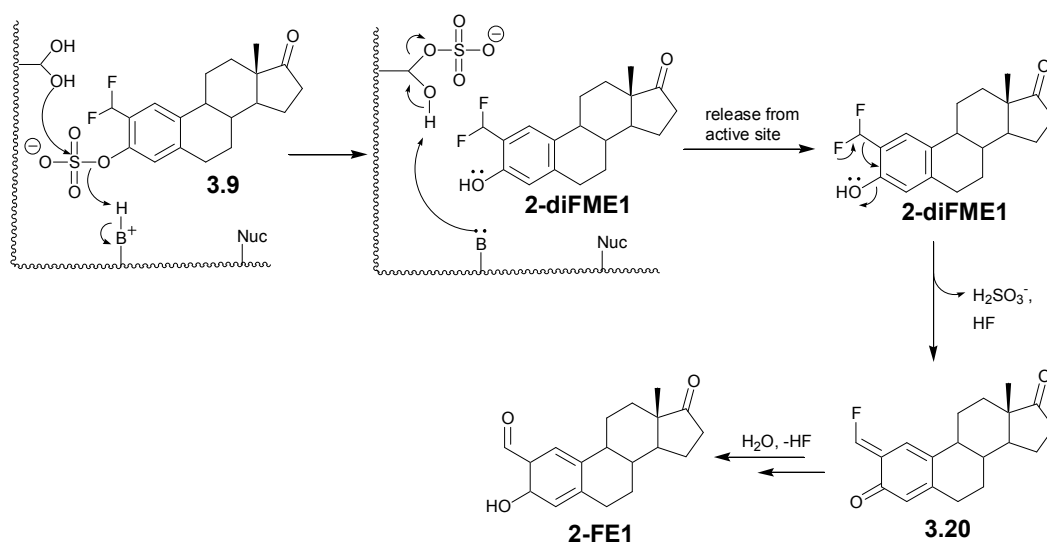


Figure 3.12. Possible products of reaction of **3.9** with STS.

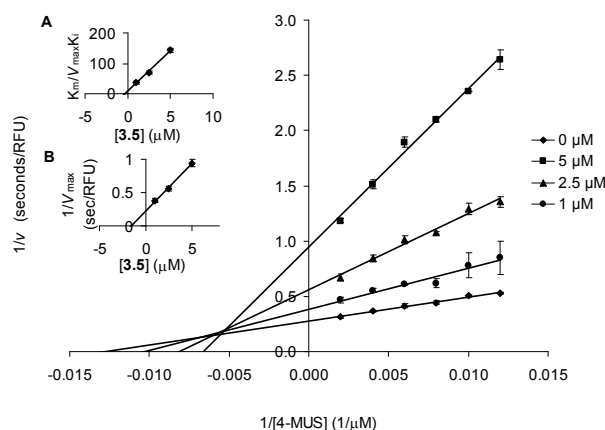


Figure 3.13. Lineweaver-Burk plot for compound **3.9**. **Inset A:** replot of slopes of Lineweaver-Burk plot versus concentration of **3.9**. **Inset B:** replot of y-intercept of Lineweaver-Burk plot versus concentration of **3.9**. See § 3.4.4 for details.

3.2.6 Evaluation of time- and concentration-dependence, effect of exogenous nucleophiles and active site protection for compound **3.12**.

In contrast to the 2-difluoromethyl derivative **3.9**, the 4-difluoromethyl derivative **3.12** displayed time- and concentration-dependent STS inhibition as illustrated in **Figure 3.14A**. However, unlike irreversible inhibitors **3.10** and **3.11**, an initial lag phase was observed followed by loss of activity which did not follow pseudo-first order kinetics. To determine if exogenous nucleophiles had any effect on the rate of inactivation, **3.12** was incubated with STS in the presence of 5 mM β -ME. This resulted in a significant decrease in the rate of deactivation and a change in the inactivation kinetics to pseudo-first order (**Figure 3.15**). The mode of action of **3.12** is most likely active-site directed as EIP protected STS against inactivation (**Figure 3.16**). Only 2-3 % of STS activity could be recovered after extensive dialysis (10^{12} -fold dilution over 24 h) after a 1 hour incubation of STS with **3.12**. Taken together, these results suggest that upon cleavage of the S-O bond, a reactive species was accumulating

in solution and then re-entering the active site and inactivating the enzyme (Silverman, 1988).

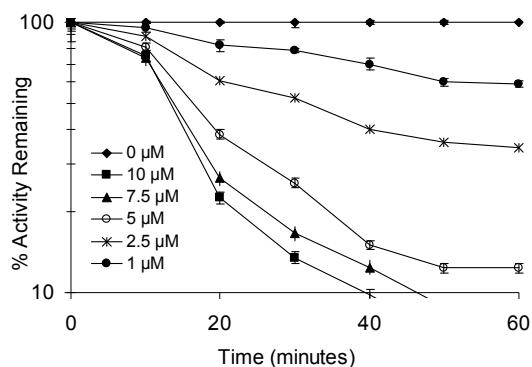


Figure 3.14. Time- and concentration-dependent inhibition of STS with inhibitor **3.12**. See § 3.4.3 for details.

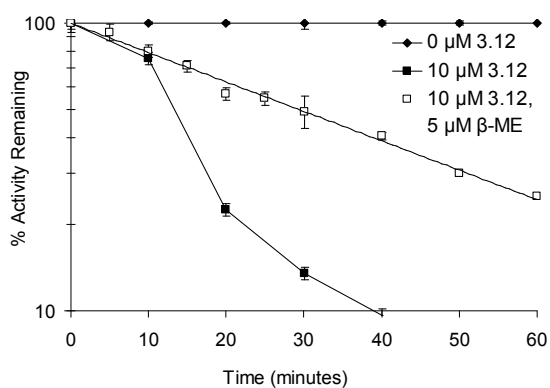


Figure 3.15. Inactivation of STS in the presence of inhibitor **3.12** and β -ME. See § 3.4.6 for details.

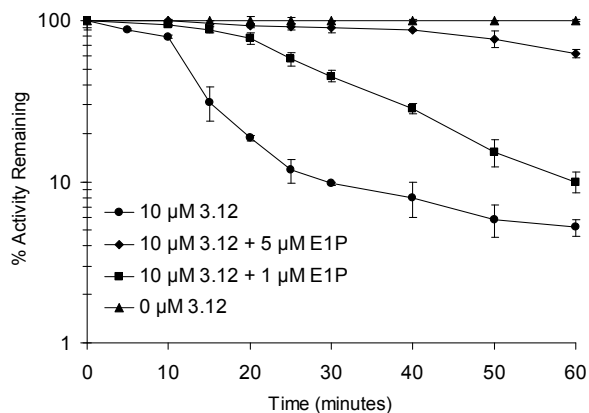


Figure 3.16. Inactivation of STS with inhibitor **3.12** in the presence of E1P. See § 3.4.5 for details.

3.2.7 Monitoring reaction products and intermediates produced by incubation of compound 3.12 and STS by HPLC

To monitor the reaction products of compound **3.12** and determine the identity of possible intermediates, 10 μM of **3.12** was incubated with STS and aliquots were removed at various time points and analyzed by RP-HPLC (**Figure 3.17**). Compound **3.12** elutes as peak “A” ($t_{\text{R}} = 15$ minutes) as shown by a control in chromatogram **I** in **Figure 3.17**. After 5 minutes of incubation of **3.12** with STS, chromatogram **IV** shows a diminished peak “A” corresponding to **3.12**, and two additional peaks (“B” and “C”) that most likely correspond to an intermediate or a product. After 10 minutes of incubation the amount of compound **3.12** corresponding to peak “A,” is significantly diminished as is peak “B,” while peak “C” has increased in area. Finally, after 30 minutes of incubation peaks “A” and “B” are no longer remaining, while peak “C” has grown in area.

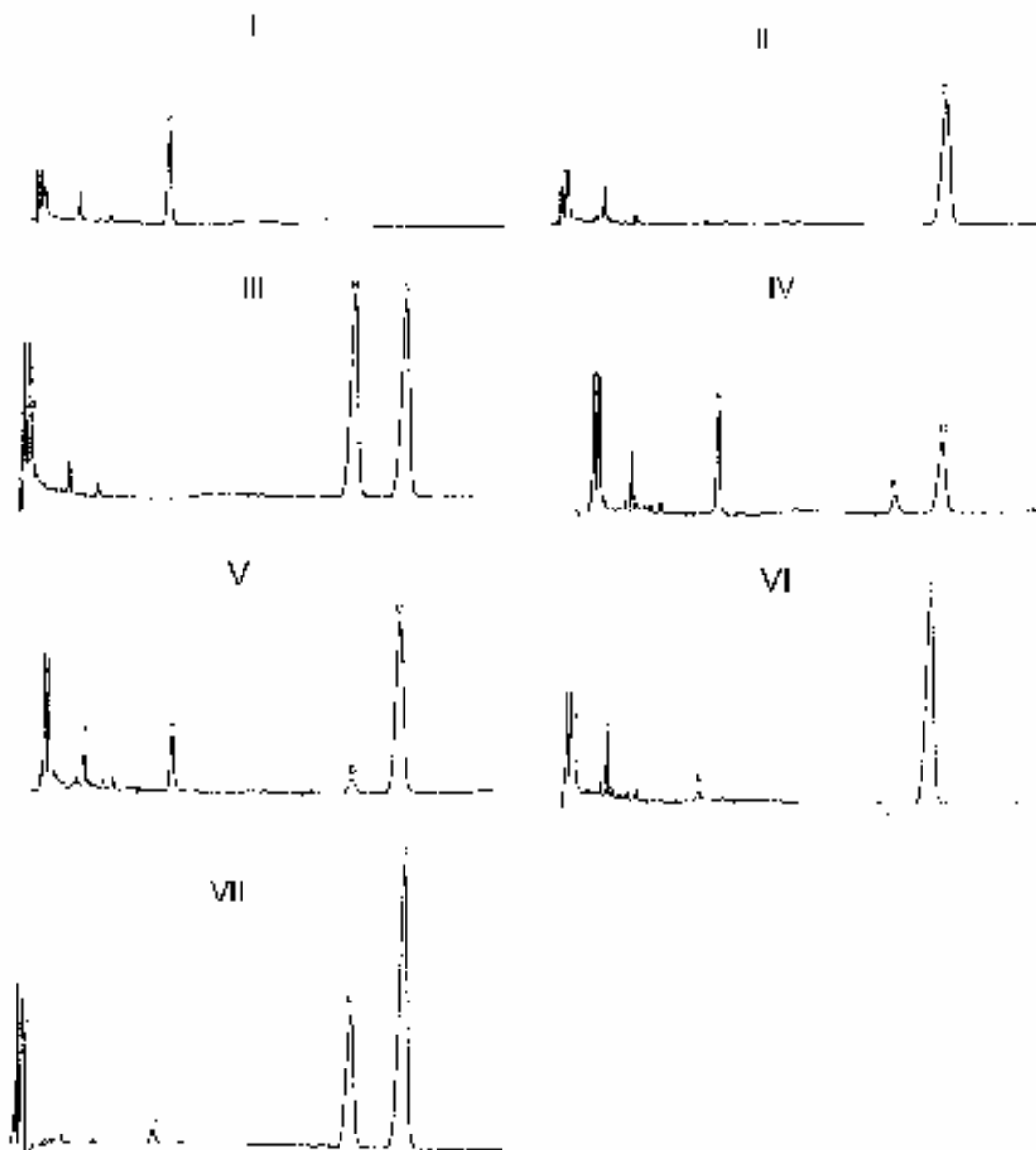


Figure 3.17 RP-HPLC analysis of the reaction of inhibitor **3.12** with STS. **I**: 10 μM Inhibitor **3.12** in assay buffer. Peak A corresponds to inhibitor **3.12** ($t_R = 15$ min); **II**: 10 μM inhibitor 4-FE1 in assay buffer containing 2% DMSO. Peak C corresponds to 4-FE1 ($t_R = 38$ min). **III**: 25 μM 4-diFME1 in assay buffer. Peak B corresponds to 4-diFME1 ($t_R = 33$ min). Although the 4-diFME1 was injected into the HPLC within 15s of dissolving it in the assay buffer, some decomposition to 4-FE1 had occurred in this time interval as evidenced by the presence of peak C. **IV-VI**: 10 μM inhibitor **3.12** with STS in assay buffer after 5 min reaction (**IV**), 10 min reaction (**V**), and 30 minutes reaction (**VI**). **VII**: Reaction of 10 μM inhibitor **3.12** with STS in reaction buffer after 5 min spiked with 25 μM 4-diFME1. See § 3.4.11 for details.

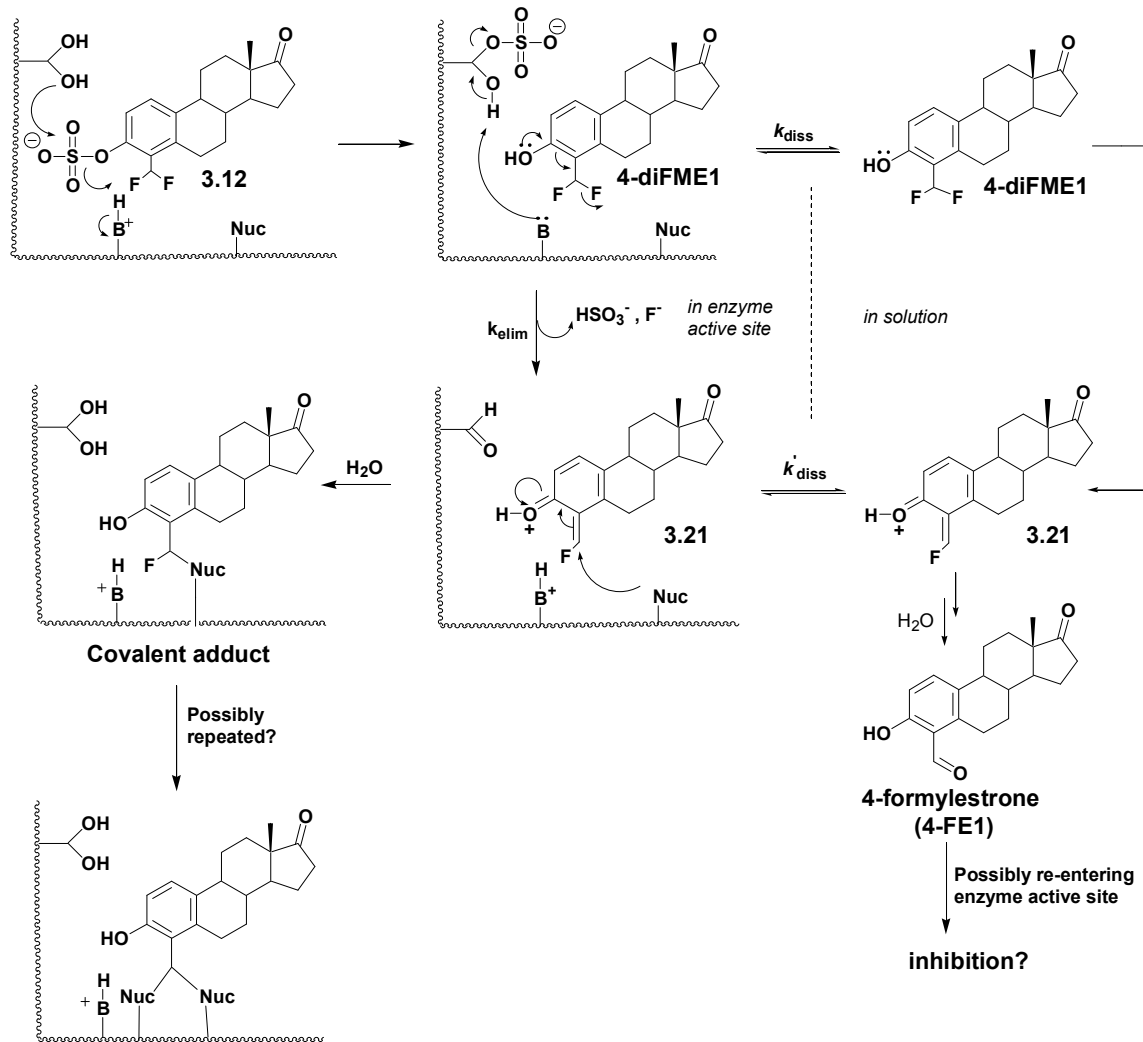


Figure 3.18. Potential modes of inhibition by compound **3.12** and its breakdown product, 4-formylestrone (4-FE1).

STS-catalyzed cleavage of the S-O bond in **3.12** results in the formation of 4-difluoromethyl estrone (4-diFME1) (**Figure 3.18**). If 4-diFME1 remains bound in the active site it undergoes elimination of one of the fluorine atoms and forms the reactive quinone methide, **3.21**, which can be attacked by a nearby nucleophilic active site residue and form the covalent adduct shown in **Figure 3.18**. Alternatively, if 4-diFME1 diffuses out of the active site prior to elimination of one of its fluorine atoms, the

quinone methide, **3.21**, can potentially re-enter the active site. However, **3.21** should be highly reactive and it is more likely that it would react with water in solution and form 4-formylestrone (4-FE1) before it could enter the active site. Similarly, once **3.21** is formed in the active site it is unlikely that it would diffuse out of the active site before reacting with an active site residue and forming a covalent adduct. The intermediate, 4-diFME1 and the breakdown product, 4-FE1, were synthesized in the Taylor lab (Liu et al., 2007) and examined by HPLC (**Figure 3.17**). Chromatogram **III** was obtained for 4-FE1 and its retention time ($t_R = 38$ min) corresponds to that of peak “C” in chromatograms **IV-VI**. Chromatogram **II** was obtained for 4-diFME1 and its retention time ($t_R = 33$ min) is the same as that obtained for peak “B” in chromatograms **IV-VI**, providing evidence this intermediate is formed but that it rapidly breaks down to 4-FE1, peak “C,” in solution. Because 4-diFME1, the initial enzymatic hydrolysis product, could be detected by HPLC this indicates that this species is able to diffuse out of the active site. The identity of 4-diFME1 was further supported by incubating **3.12** and STS for 5 minutes and “spiking” the incubation with 25 μ M of 4-diFME1 prior to HPLC injection. As shown in chromatogram **VI**, peak “B” corresponding to 4-diFME1 becomes larger in concentration in comparison with the 5 minute time point in **V**, as does peak “C” due to the rapid breakdown of 4-diFME1 to 4-FE1.

3.2.8 Examination of 4-FE1 as a time- and concentration-dependent inhibitor of STS

Aldehydes have been known to inhibit enzymes sometimes as very potent tight binding inhibitors (Dax et al., 2005). Therefore it is possible that 4-FE1 is responsible for part of the time-dependent STS inhibition with **3.12**. 4-FE1 was examined for time-

and concentration-dependent STS inhibition. Incubation of STS with 4-FE1 showed that 4-FE1 actually does impart time- and concentration-dependent inhibition as illustrated in **Figure 3.19A**. At low concentrations ($< 1 \mu\text{M}$) of 4-FE1 the inactivation plateaus after about 40 minutes while at higher concentrations ($\geq 1 \mu\text{M}$) pseudo-first order behaviour was observed throughout and almost complete inactivation could be achieved within 60 minutes with just $5 \mu\text{M}$. This behaviour may be due to multiple labelling events that are both productive and unproductive towards inactivation. Extensive dialysis (10^{12} -fold dilution over 24 h) of the 4-FE1-inactivated enzyme resulted in the recovery of only 5% activity indicating that 4-FE1 is essentially an irreversible inhibitor. A Kitz-Wilson analysis using the initial reaction rates (first 30 minutes) yielded a K_I of $1.5 \mu\text{M}$ and a k_{inact} of 0.65 min^{-1} (k_{inact}/K_I of $4.3 \times 10^6 \text{ M}^{-1} \text{ min}^{-1}$) (**Figure 3.19B**). This analysis treats the inactivation process as irreversible which is reasonable since only a small amount of activity was recovered after 24 h of extensive dialysis. However, the slight recovery of activity suggests that a more accurate description of 4-FE1 is that it is a slow tight-binding inhibitor of STS with a very slow off-rate (k_{off}). Ideally, if STS stability permitted (which it does not), the k_{off} rate could be measured as activity completely returned after days or even weeks. EIP protected STS against inhibition by 4-FE1 indicating the 4-FE1 was reacting with an active site residue (**Figure 3.20**). β -ME (5 mM) had no effect on the inhibition with 4-FE1 revealing that the effect of β -ME on the inhibition with compound **3.12** was most likely due to β -ME reacting with quinone methide **3.17** (**Figure 3.21**). Thus, the lag phase seen with inhibitor **3.8** in **Figure 3.14** is most likely due to the time required for sufficient 4-FE1 to accumulate in solution and then enter the active site and inhibit STS.

The fact that some inhibition still occurs in the presence of 5 mM β -ME indicates that some inhibition by the quinone methide **3.21** is occurring though it appears that inhibition by 4-FE1 is the dominant inhibitory pathway.

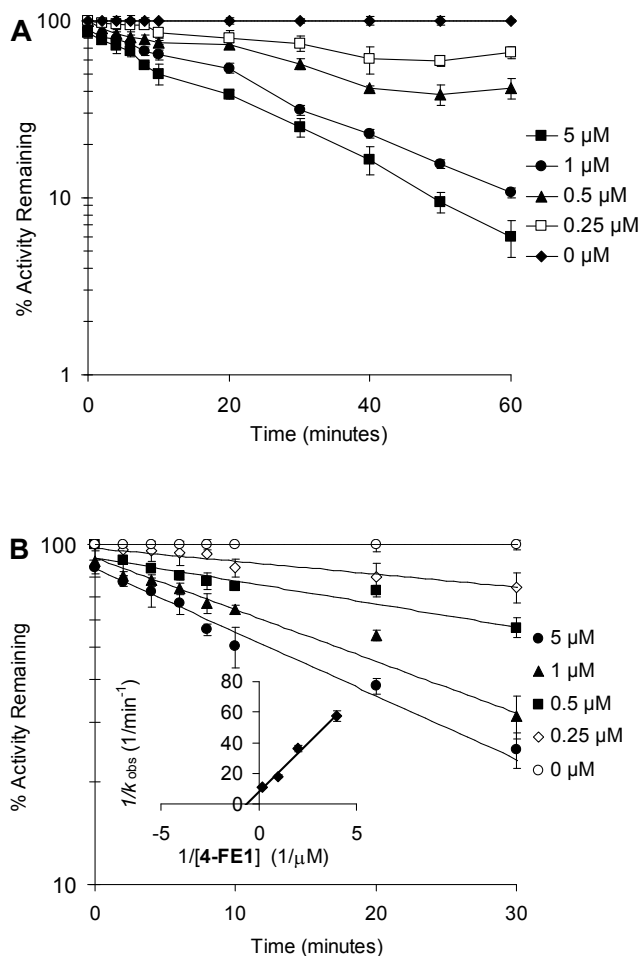


Figure 3.19. Time- and concentration-dependence of STS by 4-FE1 over 60 minutes (**A**), and 30 minutes (**B**). Inset in **B**: Kitz-Wilson plot. See § 3.4.3 for details.

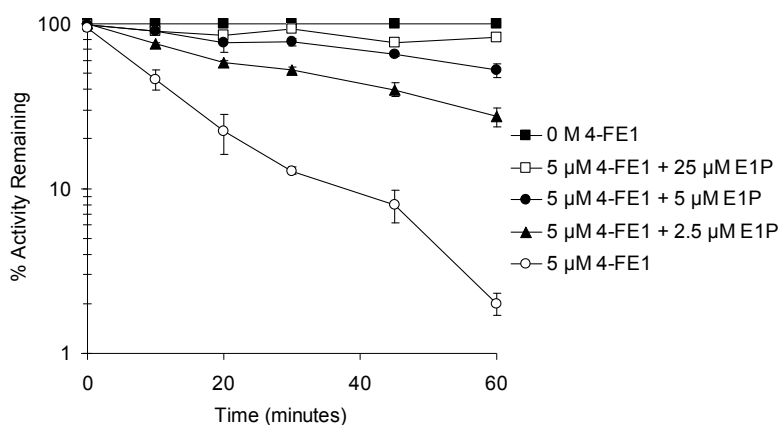


Figure 3.20. Inactivation of STS in the presence of E1P and 4-FE1. See § 3.4.5 for details.

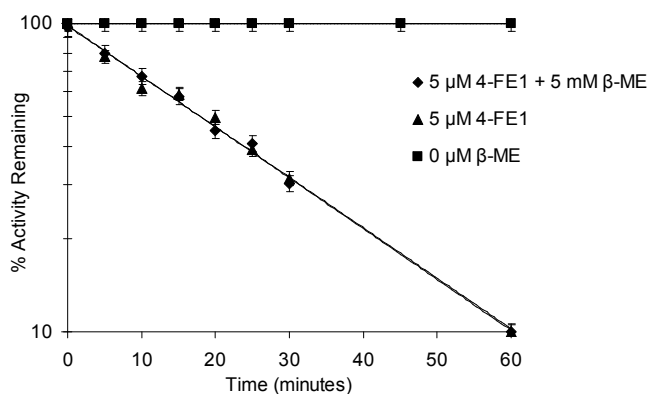


Figure 3.21. Inactivation of STS in the presence of β -ME and compound 4-FE1. See § 3.4.6 for details.

3.2.9 Specificity of inhibition of STS by formylated steroids

As described in § 3.2.4, compound **3.9** is an STS substrate and produces 2-formylestrone (2-FE1) as a product as demonstrated by HPLC experiments. However, no inhibition of STS was found when subjected to 10 μ M **3.9**. This suggests that 2-FE1 is not an STS inhibitor and that inhibition of STS with A-ring-formylated estrones must exhibit some specificity for the formyl group at the 4-position. To confirm this both 2-FE1 and estra-1,3,5(10)-triene-17-one-3-carbaldehyde (**3.22**) (**Figure 3.22**), prepared by

Yong Liu in the Taylor group (Liu, Y., 2007), were examined as time-dependent STS inhibitors. Incubation of STS with 10 μM 2-FE1 and **3.22** did not result in time-dependent inhibition (**Figure 3.23**). We were unable to perform accurate studies with 2-FE1, **3.22**, and 4-FE1 at concentrations greater than 10 μM due to the tendency these compounds to precipitate out at higher concentrations. It is possible that 2-FE1 and **3.22** are inhibitors of STS at concentrations greater than 10 μM .

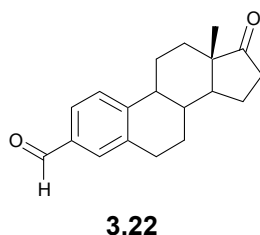


Figure 3.22. Estra-1,3,5(10)-triene-17-one-3-carbaldehyde (**3.22**).

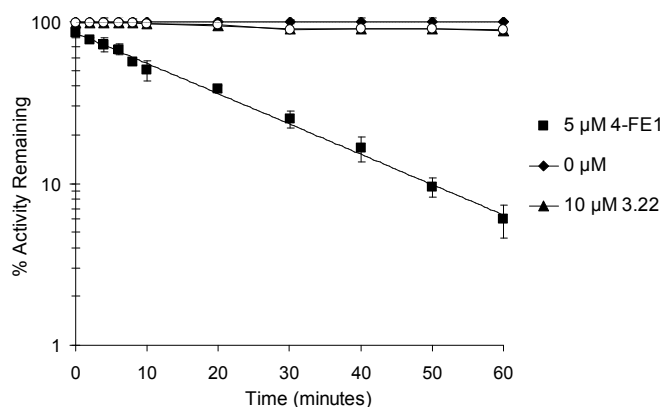


Figure 3.23. A comparison of time-dependent inhibition of STS by formylated estrones. See § 3.4.3 for details.

It is possible that the mechanism for inactivation of STS by 4-FE1 involves formation of a Schiff base with a residue(s) bearing a side chain amine as shown in **Figure 3.24**. The active site in STS contains several amino acids that are capable of Schiff base formation with an aldehyde: Lys134, Lys368 and Arg79 (**Figure 3.25**). There is evidence that certain compounds bearing aldehyde functional groups are

capable of modulating almost irreversible inhibition by forming a stable Schiff base adduct with a nearby amine in the active site (Dax et al., 2005). For example, 1-hydroxy-2-naphthaldehyde 6-phosphate (HNA-P, **3.23**, **Figure 3.26**) inhibits rabbit muscle fructose-1,6-bisphosphate aldolase in a time- and concentration-dependent manner by forming a Schiff base with active site residue Lys107. This mode of inhibition is supported by enzyme kinetics, UV/visible difference spectroscopy, site-directed mutagenesis, and electrospray mass spectrometry. Enzyme activity of the aldolase was only recovered slowly over the course of days by dialysis of the enzyme-inhibitor complex.

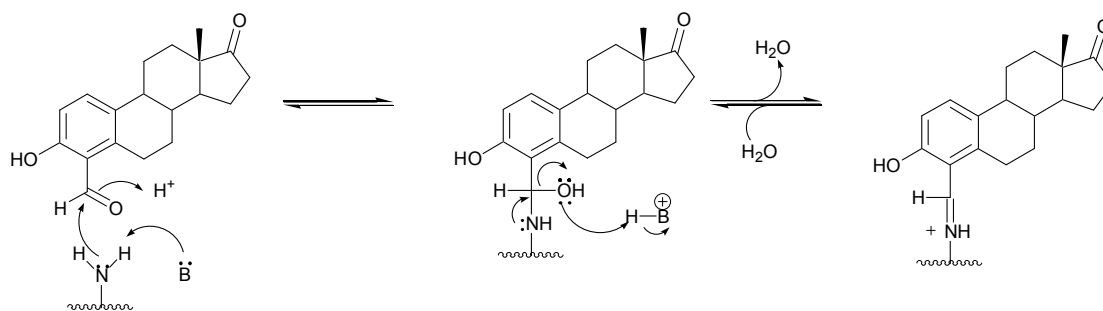


Figure 3.24. Schiff base formation between a residue on STS and 4-FE1.

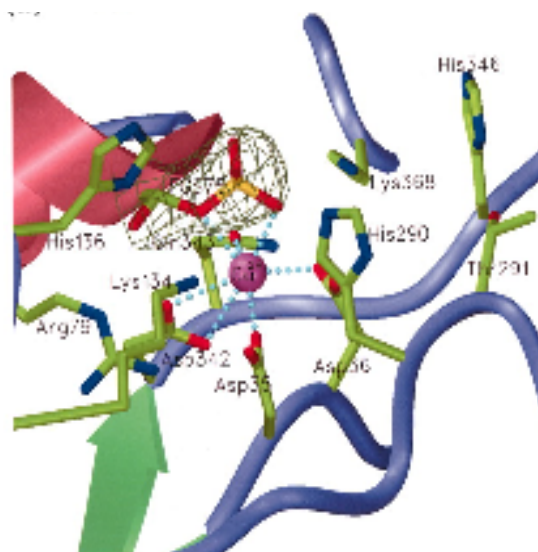


Figure 3.25. Active site of STS (courtesy of Dr. Debashis Ghosh).

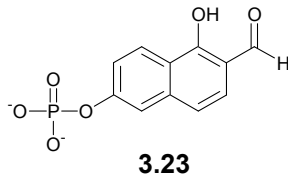


Figure 3.26. 1-hydroxy-2-naphthaldehyde 6-phosphate (HNA-P, **3.23**), a time-dependent inhibitor of fructose-1,6-bisphosphate aldolase (Dax et al., 2005)

A common tactic for determining whether aldehyde-bearing inhibitors form Schiff bases with residues is to subject the inactivated enzyme to NaBH_4 with results in the reduction of the Schiff base to a stable amine. The mixture is then subjected to dialysis and then the activity of the enzyme is determined. If the Schiff base between the enzyme and the inhibitor was reduced by NaBH_4 , it would not be reversibly hydrolyzed by extensive dialysis and activity would not be expected to return. If the interaction between the inhibitor and the enzyme was not due to a Schiff base but rather a reversible tight-binding interaction, some or all activity would be expected to return after dialysis. Although only 5% of STS activity was recoverable upon extensive dialysis of an STS solution that had been subjected to 4-FE1 for 1 h, we reasoned that perhaps no activity at all would be recovered if the STS-4-FE1 complex was subjected to NaBH_4 . First, the effect of 5.0 mM NaBH_4 on STS activity was examined, according to the method described by Blonski et al. for determining Schiff's base formation between rabbit muscle aldolase and **3.23** (Blonski, 1995). However, STS is not stable in the presence of NaBH_4 and so we were unable to undertake this study. It is possible that the formylglycine hydrate is in equilibrium with formylglycine which might be reduced by NaBH_4 . Although we could not do a kinetic analysis in the presence of NaBH_4 , it should be possible to subject the STS-4-FE1 complex to NaBH_4 and then,

after dialysis, subject it to tryptic digest and then sequence the resulting fragments using mass spectrometry. This will enable us to determine if Schiff base formation is indeed occurring and identify the active amino acid that is being modified. Such studies are currently in progress in the Taylor group. In the meantime, we can only speculate as to the site of inactivation. Our collaborator, Dr. Debashis Ghosh at the Hauptman-Woodward Medical Research Institute, Buffalo, NY, whose laboratory elucidated the only crystal structure of STS (Hernandez-Guzman et al., 2003) has attempted to obtain an X-ray crystal structure of the putative 4-FE1 and STS complex. However, no such structure has emerged to date with 4-FE1 or with any other substrate or inhibitor. Modelling studies with STS and 4-FE1 are also in progress in the Taylor group.

3.2.10 2- and 4-Hydroxymethylestrone as STS inhibitors.

The observation that 4-FE1 and 2-FE1 are produced upon STS hydrolysis of **3.12** and **3.9** raises the possibility that a similar process is occurring with the monofluoromethyl estrone derivatives (**3.10** and **3.11**). The possible breakdown products of **3.10** and **3.11** are illustrated in **Figure 3.27**, using **3.10** as an example. Should some of the initial hydrolysis product **3.17** leave the active site it would eventually breakdown in solution, via quinone methide **3.18**, to 2-hydroxymethyl estrone, (**3.24**). The analogous product of **3.11** is 4-hydroxymethyl estrone (**3.25**). HPLC analysis of the reaction of STS with **3.6** and **3.7** reveals that both hydroxymethyl compounds, **3.24** and **3.25**, are produced (**Figures 3.28** and **3.29**) which suggests that that the partition ratio for compounds **3.10** and **3.11** must be significant. However, no lag phase was observed during the inactivation of STS with **3.10** and **3.11** which suggests that neither **3.24** nor **3.25** are time-dependent inhibitors of STS. Nevertheless,

time-dependent loss of activity due to **3.24** and **3.25** was examined and none observed. Both were found to be reversible inhibitors with IC_{50} values of 218 μ M for **3.24** and 158 μ M for **3.25** (see Appendix A for details).

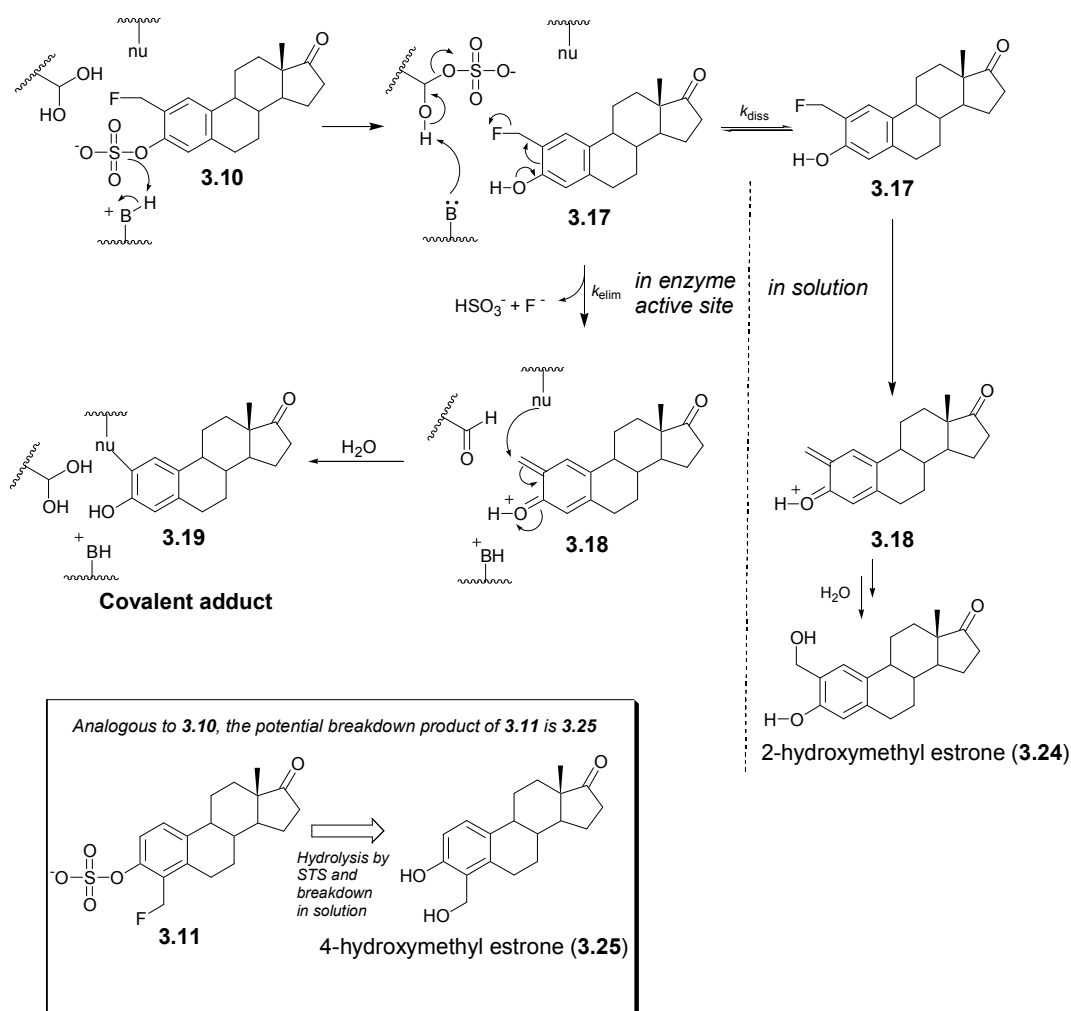


Figure 3.27. 2-Hydroxymethyl estrone (**3.24**), and 4-hydroxymethyl estrone, (**3.25**), are potential products of hydrolysis of compounds **3.10** and **3.11**, respectively.

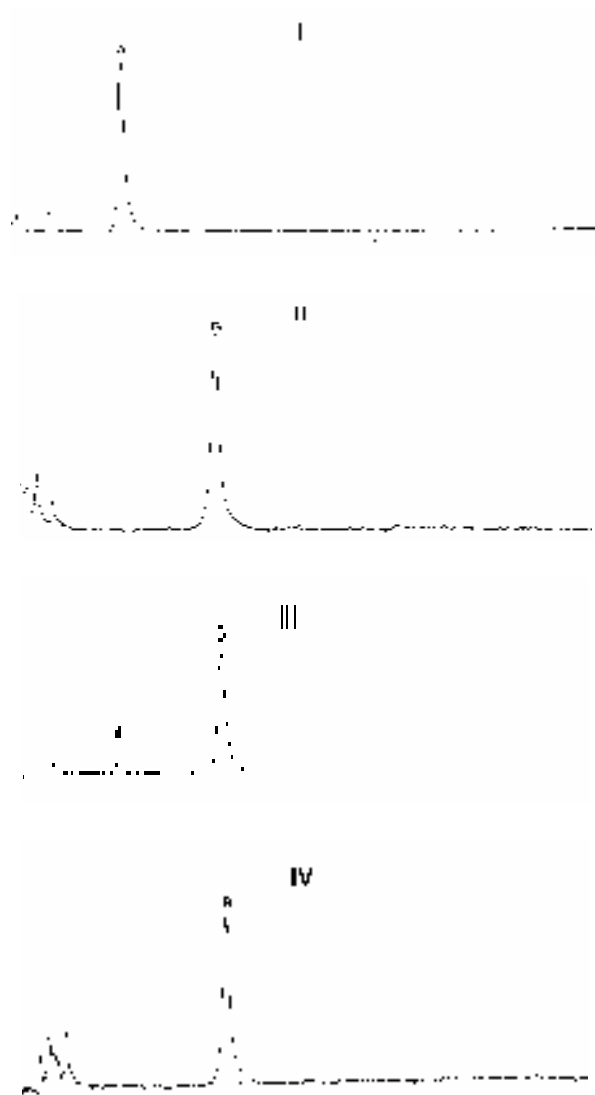


Figure 3.28. RP-HPLC analysis of the reaction of compound **3.10** with STS. **I**: 100 μM **3.10** in assay buffer. Peak A corresponds to compound **3.10** ($t_{\text{R}} = 8$ min); **II**: 100 μM 2-hydroxymethylestrone (**3.24**) in assay buffer. Peak B corresponds to **3.24** ($t_{\text{R}} = 16$ min); **III** and **IV**) : 100 μM compound **3.10** with STS in assay buffer after 2 min (**III**) and 30 min (**IV**) reaction. See § 3.4.11 for details.

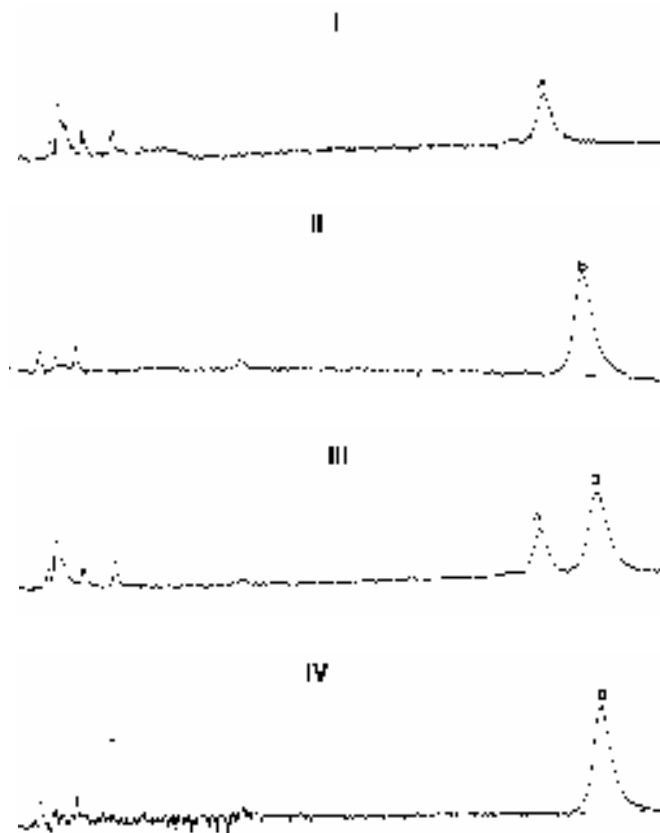


Figure 3.29. RP-HPLC analysis of the reaction of compound **3.11** with STS. **I**: 100 μ M compound **3.11** in assay buffer. Peak A corresponds to compound **3.11** (t_R = 39 min); **II**: 100 μ M 4-hydroxymethylestrone (**3.25**) in assay buffer. Peak B corresponds to **3.25** (t_R = 44 min); **III** and **IV**: 100 μ M compound **3.11** with STS in assay buffer after 15 minutes reaction (**III**) and 60 minutes reaction (**IV**). See § 3.4.11 for details.

The finding that the monofluoro derivatives (**3.10** and **3.11**) function as classic suicide inhibitors while the difluoro derivatives, compound **3.9** and, to a lesser extent compound **3.12**, cannot be explained by the difference in stability between the difluoromethylestrones (2- and 4-diFME1, **Figures 3.12** and **3.18**) compared to the monofluoromethylestrones (such as compound **3.17** in **Figure 3.27**). It is not believed that the enzyme assists in catalyzing elimination of fluoride (Betley et al., 2002; Myers

et al., 1995; Born et al., 1995). *p*-Difluoromethylphenol is known to be more stable than its monofluoro analogue (Wang et al., 1994) and it is likely that 2- and 4-diFME1 are more stable than their monofluoromethyl counterparts in that they break down to form their quinone methide slower than their monofluoromethyl counterparts. This is supported by the fact that we were able to prepare 4-diFME1 but unable to prepare 4-monofluoromethylestrone. Thus, the more stable 2-diFME1 and 4-diFME1 intermediates have more time to diffuse out of the active site (k_{diss}) before decomposition to the corresponding quinone methides (k_{elim}) as illustrated in **Figures 3.12** and **3.18**.

3.2.11 Screening of coumarin derivatives 3.13-3.16 as time-dependent STS inhibitors

Based on successfully demonstrating that some of our quinone methide-generating estrone derivatives function as mechanism-based irreversible inhibitors, we then turned our attention to coumarin derivatives, **3.13-3.16**. Aryl sulfamate STS inhibitors based on the coumarin platform have been shown to be highly potent STS inhibitors (see chapter 1, § 1.3.2 for a discussion on this class of inhibitors). Consequently, it was anticipated that the *ortho*-substituted mono- and difluoromethyl coumarin sulfates **3.13-3.16** would show similar, if not more potent inhibition of STS compared to compounds **3.9-3.12**. In addition, coumarins present the attractive feature of having fluorogenic properties (Musa et al., 2008). This makes them very attractive candidates as activity-based probes for proteomic studies since unlike other activity-based proteomic probes that have been developed, which bear a functional group, linker region and reporter group, the quinone methide-generating coumarins *should act both as*

a chemical tag and reporter. Another attractive feature of using a coumarin scaffold for proteomic studies is that sulfatases in general (not just STS) are capable of hydrolyzing coumarin sulfates (Ahmed et al., 2005).

To begin, compounds **3.13-3.16** were screened for time-dependent inhibition of STS by incubating them (250 μM) with STS in 0.1M tris, pH 7, 0.01% Triton X-100, 5% DMSO. The STS activity remaining after one hour was determined by withdrawing aliquots from the mixtures and diluting them into a solution 4-MUS (4 mM) in the same buffer and following the production of 4-MU. For compounds **3.13**, **3.15** and **3.16**, the percent amount of STS activity remaining compared to that in the absence of inhibitors ranged between 78-86%, while compound **3.14** displayed only 21% of activity remaining.

3.2.12 Kinetic studies with compound 3.14.

As compound **3.14** was the most promising compound of the series, it was selected for detailed kinetic studies. As shown in **Figure 3.30**, incubation of **3.14** with STS imparts a pseudo-first order loss of activity, which is the hallmark behaviour of a true mechanism-based irreversible inhibitor. The inset of **Figure 3.30** represents the Kitz-Wilson analysis of the initial rates of the first 40 minutes, resulting in a $K_I = 219 \mu\text{M}$ and $k_{\text{inact}} = 0.038 \text{ min}^{-1}$ ($k_{\text{inact}}/K_I = \text{M}^{-1} \text{ min}^{-1}$).

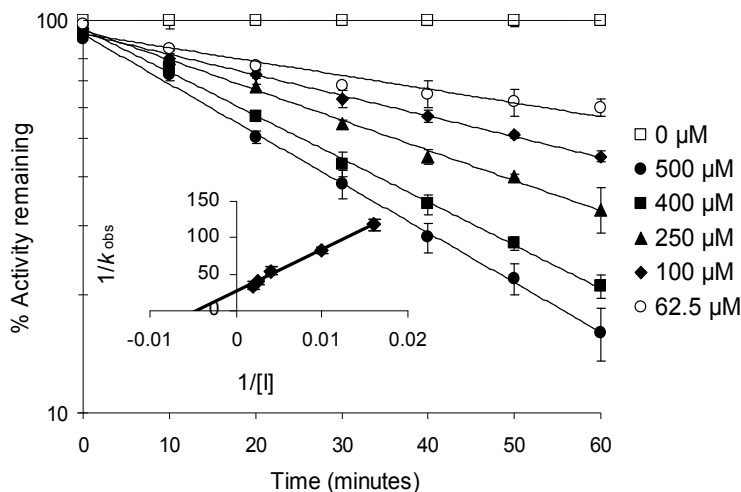


Figure 3.30. Time- and concentration-dependent inhibition of STS by **3.14**. **Inset:** Kitz-Wilson plot. See § 3.4.3 for details.

To demonstrate that **3.14** requires activation by STS, the inactivation rates in the presence of E1P were compared to those in its absence. As illustrated in **Figure 3.31A** increasing concentrations of E1P reduce the observed rate of inactivation of STS incubated with **3.14**. These results indicate that irreversible inhibition by this compound requires active site binding and enzymatic activation. To demonstrate that exogenous nucleophiles do not affect the inactivation rates, STS was incubated in the presence of 5 mM β -ME and **3.14**. As depicted in **Figure 3.31B**, the inactivation rate is not affected. This confirms that inhibition by **3.14** leading to a putative irreversible adduct is due to binding, catalysis, and inactivation solely within the active site and without any electrophilic species diffusing from the active site and subsequently re-entering or due to non-specific labelling on the enzyme surface. Finally, extensive dialysis of STS (10^{12} -fold dilution over 24 h) after being inactivated with 500 μ M of **3.14** revealed no recovery of activity compared to that of a dialyzed sample of untreated STS. Taken

together with the protection and nucleophilic trapping experiments, these results support a mechanism-based irreversible mode of action for **3.14**.

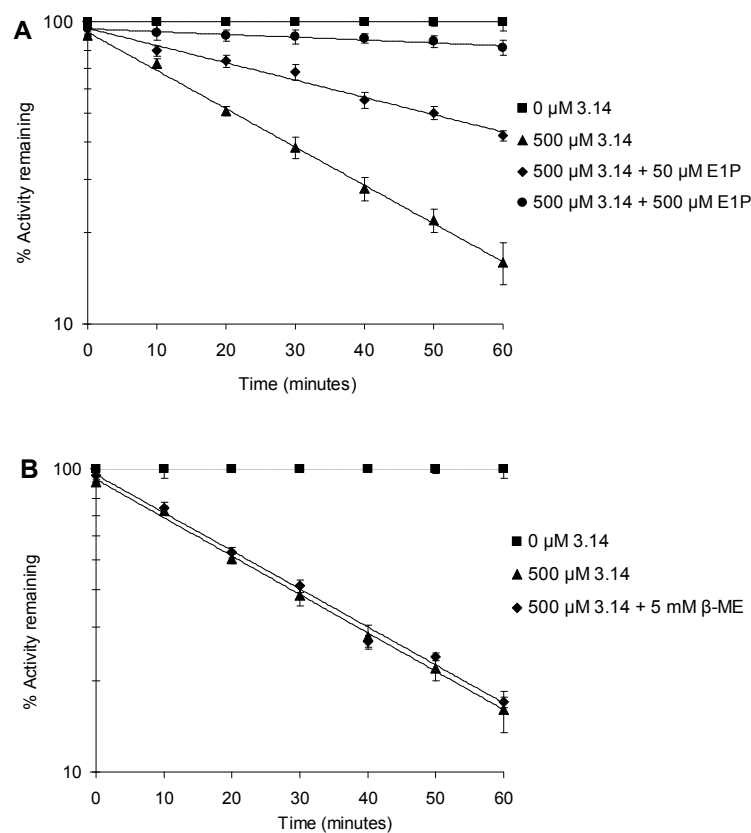


Figure 3.31 (A) Inactivation of STS in the presence of **3.14** and E1P (B) Inactivation of STS in the presence of **3.14** and β -ME. See § 3.4.5 and § 3.4.6 for details.

3.2.13 Determination of the partition ratio for compound **3.14**

As mentioned earlier, the *partition ratio* is a measurement of the number of times turnover of the suicide inhibitor (SI) will lead to a product molecule (P) being released from the active site for each time the enzyme is inactivated (E—I^{''}). In the development of a mechanism-based irreversible inhibitor, an event that results in a species partitioning from the active site is non-productive if a dead-end covalent complex with the enzyme is not the outcome. The partition coefficient is really a

measure of the efficiency of the inactivator. An “ideal” irreversible inhibitor has a partition ratio, k_3/k_4 (**Figure 3.1**) of zero, signifying that every turnover leads to inactivated enzyme. In order for compound **3.14** to be developed into an activity-based probe for proteomic studies, one feature it must exhibit is a very low partition ratio (preferably zero). If it has a high partition ratio then this would mean that a significant quantity of the quinone methide would be generated outside the active site which would result in non-specific labelling of other proteins.

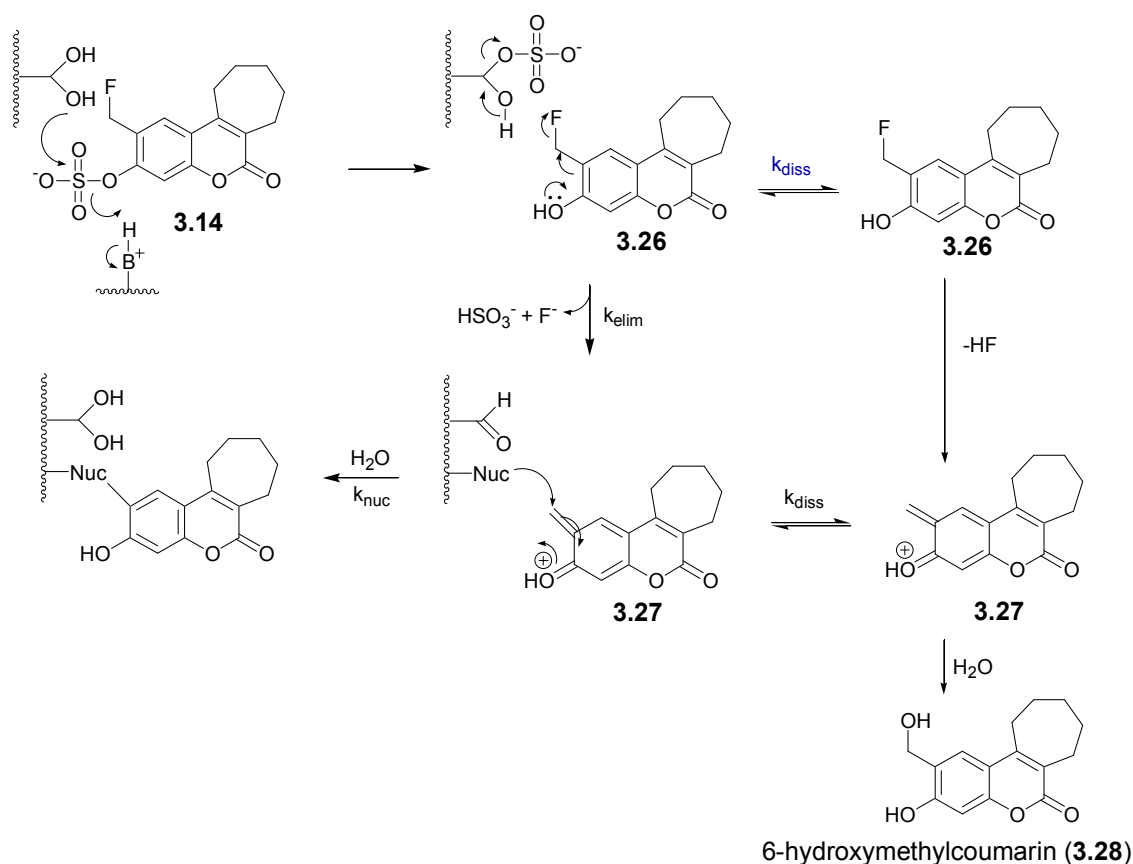


Figure 3.32. Potential hydrolysis products of **3.14**.

Experimentally, the partition coefficient may be determined as the ratio of the amount of product generated (P_{tot}), to the total initial enzyme concentration (E_0), once the enzyme has been completely inactivated, P_{tot}/E_0 , independent of the initial

inactivator concentration. This method allows for direct determination of the partition ratio if the product is readily detected in real time, for example spectrophotometrically. As shown in **Figure 3.32**, hydrolysis of the sulfate ester bond of **3.14** produces an intermediate, **3.26**, that can follow an alternative pathway to covalent inactivation of the enzyme as discussed for compounds **3.9-3.12**. Intermediate **3.26** can dissociate out of the active site and undergo elimination of the fluoride ion, forming quinone methide **3.27**, which reacts with water in solution to form the 6-hydroxymethylcoumarin (**3.28**). Unlike the breakdown products of the estrone derivatives, compound **3.28** has the particular attribute of being highly fluorescent (**Figure 3.33**). When excited at 360 nm (λ_{ex}) compound **3.28** exhibits a maximal emission wavelength (λ_{em}) at 460 nm in 0.100 M tris at pH 7.0. This is in contrast to inhibitor **3.14** which does not exhibit any significant fluorescence under these conditions (**Figure 3.33**). As shown in **Figure 3.34**, a large increase in fluorescence was observed when 500 μM **3.14** is hydrolyzed by 2 nM STS in 0.1 M tris, pH 7, 0.1% Triton X-100. After about 3.8 hours fluorescence production reached a plateau. The addition of an additional 500 μM of **3.14** after 5 h did not result in any further increase in fluorescence indicating that all STS activity was abolished. Non-enzymatic hydrolysis of **3.14** was not observed over the five hour time course of the experiment. The enzyme-inhibitor fluorescence was measured after dialysis of the enzyme-inhibitor solution which removed unhydrolyzed inhibitor and **3.28**. The fluorescence of enzyme-inhibitor complex was low (~131 RFU) in comparison to the large increase in fluorescence observed (5471 RFU) due to the production of **3.28** after 5 hours. The enzyme solution in the absence of inhibitor before

and after dialysis has very little fluorescence ~20 RFUs (the “blank” buffer solution has a fluorescence of ~10 RFUs).

The inset standard curve of **3.28** in **Figure 3.34** was used to calculate the amount of **3.28** produced during the STS reaction. This reveals a partition ratio of 6675 which is very large. This signifies that for each inactivation event there were 6675 molecules of **3.28** being released into solution. This high partition ratio does not bode well for using this coumarin scaffold as a basis for activity-based proteomic profiling of sulfatases since non-specific labeling of other proteins will probably occur.

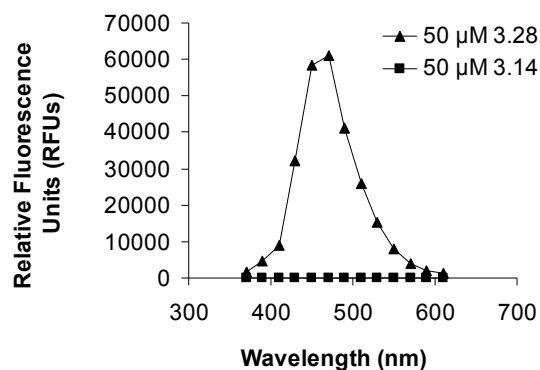


Figure 3.33. Relative fluorescence of 50 μM coumarins **3.28** and **3.14** versus λ_{em} in 0.1 M tris, pH 7.0, 5% DMSO, 0.01% Triton X-100. ($\lambda_{\text{ex}} = 360$ nm). See § 3.4.9 for details.

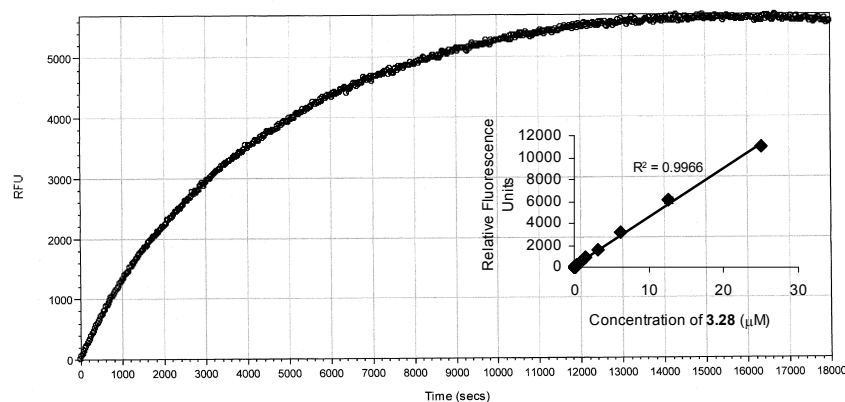


Figure 3.34 Change in fluorescence with time during the reaction of STS with 500 μM **3.14** in 0.1 M tris, pH 7.0, 0.1 % Triton X-100. **Inset:** Standard curve of **3.28**. See § 3.4.9 and § 3.4.10 for details.

3.2.14 Potential for quinone methide-generating SIs as activity-based proteomic profiling probes

While our work was in progress two other research groups examined the potential of quinone methide-generating SIs as probes for proteomic studies on sulfatases. The first of these studies, from the Wong group at Scripps, examined *ortho*- or *para*-difluoromethylphenyl sulfate as time-dependent inhibitors of a sulfatase from *P. aeruginosa* (PARS) (Hanson et al., 2006). However, no irreversible inhibition was observed with these relatively simple compounds. Nevertheless, this same group demonstrated that cyclic sulfamates such as compound **3.29** were SIs of PARS (**Figure 3.35**). They exhibited a much lower affinity for PARS compared to phenylsulfamate (PhOSO₂NH₂) and a slower rate of inactivation of PARS compared to phenylsulfamate. Although their mechanism of action was not elucidated, several mechanisms were proposed including that illustrated in **Figure 3.35** in which the phenolic portion remains attached to the enzyme. Should the phenolic portion remain attached to the enzyme then it raises the possibility that these cyclic sulfamates could be employed as activity-based probes for proteomic studies.

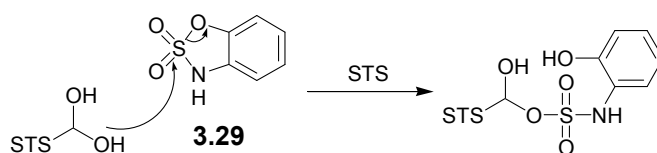
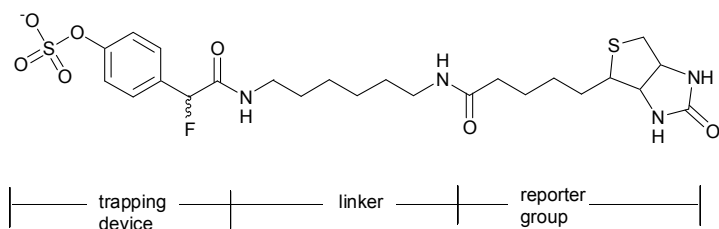


Figure 3.35. Proposed mechanism for the irreversible inhibition of STS by compound **3.29**.

The second report, from Lu et al, involves the development of an activity-based probe, **3.30**, for STS based on *para*-monofluoromethylphenyl sulfate shown in **Figure 3.36** (Lu et al., 2007). This probe has the standard four structural features of an activity

based probe: a sulfate recognition moiety, a latent quinone methide-generating trapping device, a linker region and a biotin reporter group. When the probe is hydrolyzed by a target sulfatase, the released intermediate undergoes a rapid elimination of one of the fluorine atoms to generate a reactive quinone methide. The quinone methide reacts with an active site residue in the target to present a biotinylated enzyme. To test their probe, the authors used CHO cells to express STS. The crude microsomal fraction containing STS was applied to a resin containing the immobilized probe, to which STS and any target sulfatases would become trapped. After incubation and washing to remove unbound proteins, the trapped target biotinylated proteins were cleaved from the resin and subjected to gel electrophoresis. A Western blot using streptavidin-horseradish peroxidase enabled visualization of the biotinylated target proteins. While the desired STS was successfully trapped and biotinylated, unfortunately analysis of the other electrophoretic bands revealed that so were several other non-sulfatase proteins. The quinone methide or its precursor was reasoned to have diffused out of the active site after sulfate ester hydrolysis by STS. The finding that both our steroidal and coumarin based SIs can exhibit high partition ratios raises serious concerns as to the general utility of activity-based probes of this type for proteomic profiling.



3.30

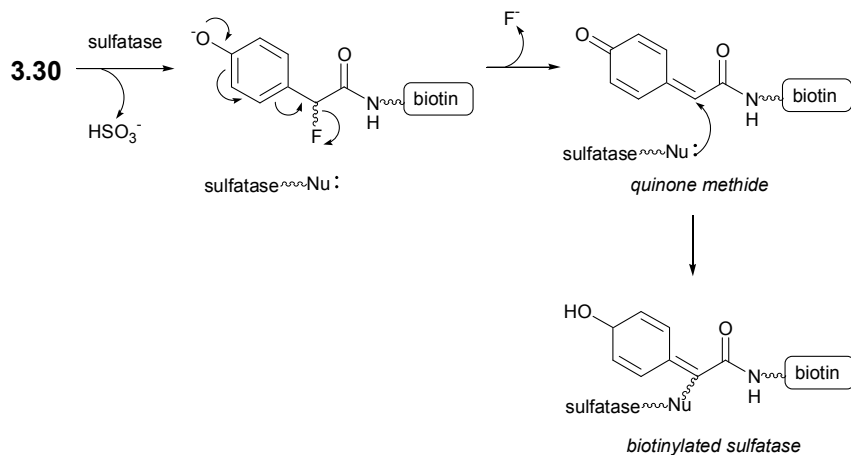


Figure 3.36. The structure of an activity-based probe for steroid sulfatase proposed by Lu and coworkers (Lu et al., 2007).

3.3 Conclusions and Future Work

We have demonstrated that quinone-methide-generating SIs can be developed for STS in that compounds **3.10**, **3.11** and **3.14** exhibited characteristics that are consistent with suicide inhibition. However, we also demonstrated that the partition ratio for these compounds can be very high. Thus, it is unlikely that this class of compounds will ever be used as ABPs for proteomic studies.

Although it is disappointing that quinone-methide-generating SIs are not suitable as ABPs for proteomic profiling of sulfatases, an important discovery did result from our studies in that the inhibition of STS by one of our compounds, **3.12**, involves an unexpected process in which the main inactivation pathway does not entail reaction of a

quinone methide with an active site nucleophile and this has led to the discovery of 4-FE1 as a novel and almost irreversible STS inhibitor. As mentioned in § 3.12, difluoromethyl-based suicide inhibitors operating by generation of quinone methides have been reported for other hydrolytic enzymes and some are currently being examined as activity-based probes for proteomic studies. To our knowledge, this is the first example where this class of inactivator functions by generating an aldehyde which acts as an almost irreversible inhibitor. These studies also underscore the need for a careful kinetic analysis of the inactivation process such that the inhibitory mechanism can be properly addressed.

The finding that 4-FE1 is a potent tight-binding STS inhibitor has prompted further development of this class of compounds as STS inhibitors. For example, aldehydes **3.31-3.33** (**Figure 3.37**) have been prepared in the Taylor lab and I have performed some preliminary inhibition studies with them (See Appendix A for details). At 10 μM compound **3.31** does not exhibit time and concentration-dependent inhibition while compound **3.32** does, albeit much weaker than 4-FE1. Compound **3.31** is a highly potent STS inhibitor with an IC_{50} of approximately 62 nM. Further studies with compound **3.33** are in progress in the Taylor group to determine if the inhibition is time and concentration-dependent and if it is irreversible and active site directed. We are also making other compounds similar to compound **3.33** to further improve potency. We have also examined compound **3.34** as an inhibitor of STS anticipating that if a lysine or arginine is positioned in close proximity to the 4-position then perhaps it would form a salt bridge with the COOH group in **3.34** and so **3.34** would be a potent inhibitor. However, compound **3.34** has an IC_{50} of about 215 μM . Modelling studies to determine

the feasibility of 4-FE1 forming a Schiff's base with active site residues are also in progress.

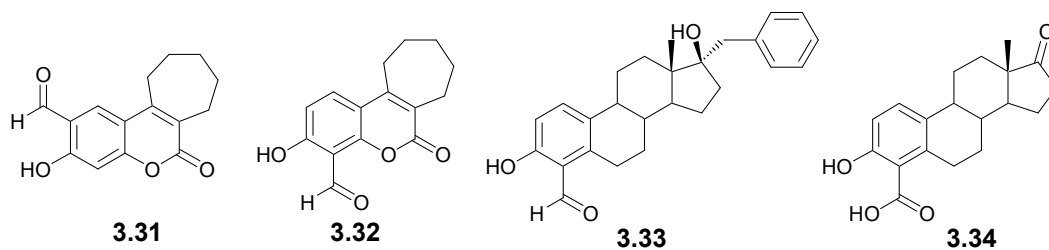


Figure 3.37. Structures of compounds **3.31-3.34**.

Ideally, the Taylor group would like to determine which residues are being modified by each of the inhibitors described here. The modern approach for accomplishing this is to subject the inactivated enzyme to a protease. The resulting peptides are separated and sequenced using liquid chromatograph (LC) in conjunction with MS (LC-MS). In the absence of an LC-MS at the University of Waterloo, one may have to do this the old-fashioned way. This would involve preparing the inhibitors with a radiolabel and then subjecting STS to these radiolabelled inhibitors. The inactivated STS would be digested by a protease and then the radiolabelled peptides would be isolated and sequenced either by Edman degradation or by mass spectrometry (MS). I have attempted to determine how many residues are being modified by some of our inhibitors by determining the molecular weight of inactivated STS (inactivated by our inhibitors) and free (active) STS using MS. However, I was not been able to obtain a mass spectrum of free or inactivated STS using either electrospray ionization (ESI) or MALDI techniques. STS is a membrane associated enzyme and it is well known that

obtaining the mass spectrum of membrane associated enzyme can be problematic. The mass spectrum of STS has never been reported.

3.4 Experimental

3.4.1 General

Compounds **3.9-3.16**, **3.22**, **3.24**, **3.25**, **3.28**, **3.31-3.34**, 4-FE1, 2-FE1 and E1P were prepared by Yong Liu in the Taylor group (Liu et al., 2004; Liu et al., 2007; Liu, Y., Ph.D. thesis, 2007, University of Waterloo). 4-diFME1 was prepared by Dr. Scott Taylor. STS was purified as previously described (Ahmed et al., 2005). All buffers and assay reagents were purchased from Sigma Aldrich (Milwaukee, WI, USA). All fluorescent measurements were carried out on a SpectraMax GeminiXS[®] fluorimeter (Molecular Devices, Sunnyvale, CA, USA) at 22 °C in black microtiter plates from Corning (Corning, MA, USA). Microdialysis units were purchased from Thermo Scientific Inc. (Rockford, IL, USA). HPLC studies were carried out on a Waters (Milford, MA, USA) 600 HPLC system equipped with a Waters 2487 dual wavelength detector set to 270 nm and a Phenomex (Torrance, CA, USA) Jupiter[®] analytical reversed-phase C-18 column. 4-methylumbelliferyl sulfate (4-MUS) was purchased from MP Biomedicals (Solon, Ohio, USA), and 4-MU was prepared by Yong Liu in the Taylor group. All determinations were carried out in triplicate and errors reported as the standard deviation.

3.4.2 Preliminary screening of compounds 3.13-3.16

Compounds **3.13-3.16** were screened for time-dependent inhibition by incubating 250 μ M of each compound with 90 nM STS at 22°C in a 100 μ L solution containing 0.1M tris, pH 7, 0.01% Triton X-100 (assay buffer) containing 5% DMSO.

Controls which did not contain inhibitor were also performed. Immediately upon addition of inhibitor and one hour later a 4 μ L aliquots were removed at various time intervals and added to the wells of a 96-well microtiter plate containing 196 μ L of 4 mM of 4-methylumbelliferyl sulfate (4-MUS), approximately $20 \times K_m$, (Ahmed et al., 2005), in assay buffer. The production of the fluorescent product, 4-methylumbelliferone (4-MU), was followed for 10 minutes ($\lambda_{ex} = 360$ nm, $\lambda_{em} = 460$ nm) at 22 $^{\circ}$ C. The percent activity of STS in the presence of inhibitor after each time interval was calculated as a percentage of activity in the absence of inhibitor.

3.4.3 General procedure for the determination of time and concentration-dependent inhibition of STS

To 90 μ L solutions of various concentrations of compounds **3.9-3.12**, **3.14**, in buffer containing 0.1 M tris, pH 7.0 or the same buffer containing 2% DMSO (for 4-FE1) a 10 μ L solution of 2 μ M STS in 20 mM tris, pH 7.4, 0.1% Triton X-100 was added. Controls which did not contain inhibitor were performed for all experiments. These mixtures were allowed to incubate at 22 $^{\circ}$ C and 4 μ L aliquots were removed at various time intervals and added to the wells of a 96-well microtiter plate containing 196 μ L of 4 mM of 4-MUS sulfate in assay buffer. The production of the fluorescent product, 4-methylumbelliferone (4-MU), was followed as described in § 3.4.2. The percent activity remaining as a function of time was plotted as a semilog graph. For inhibitors **3.10**, **3.11**, **3.14** and 4-FE1, the slopes of the initial linear portions of these plots which represent the pseudo-first order rate constants (k_{obs}) of the early part of the reaction, were used to generate a Kitz-Wilson double reciprocal plot for compounds **3.10**, **3.11**, **3.14** and 4-FE1. Equation 3.1 was used to calculate the inhibition constant, K_I .

$$k_{obs} = \frac{k_{inact}}{1 + \frac{K_I}{[I]}} \quad (3.1)$$

The plot of the reciprocals of the observed inhibition rate constants (k_{obs}) against the reciprocals of the inhibitor concentrations gave a straight line, from which the rate constant for inhibition, K_I , was determined from the intersection on the x -axis at $-1/K_I$ and the rate constant for inhibition, k_{inact} , was determined from the intersection on the y -axis at $1/k_{inact}$.

3.4.4 Lineweaver-Burk analysis of compound 3.9

A 4 mM stock solution of the inhibitor was made in 0.1 M tris, pH 7.0, from which dilutions of 50 μ M, 25 μ M and 10 μ M were made. 10 μ L of each fixed concentration of inhibitor was added to the wells of a 96-well microtiter plate containing 70 μ L of 0.1 M tris, pH 7.0 and 10 μ L of 4-MUS substrate (833 μ M to 5 mM) in the same buffer. A control was made in which inhibitor storage buffer was added instead. The assay was initiated with 10 μ L of 40 nM STS stored in 20 mM tris, pH 7.4, 0.1% Triton X-100. A control was made in which enzyme storage buffer was added instead. Therefore, the final fixed concentration of inhibitor in the assay was 1, 2.5 and 5 μ M for each 4-MUS concentration ranging between 83.3-500 μ M (0.5-3 times the K_m value at pH 7). The final concentration of enzyme in the assay was 4 nM in 0.092 M tris, pH 7.0, 0.01% Triton X-100. The production of the fluorescent product, 4-MU, was followed as described in § 3.4.2. The rates of relative fluorescence at each substrate concentration were subjected to Lineweaver-Burk analysis in Microsoft Excel to determine mode of inhibition and related constants, K_i and αK_i . These data were plotted as Lineweaver-Burk graphs and K_i and αK_i values were calculated from replots of the slopes or

intercepts of the Lineweaver–Burk graphs according to the equations for mixed and competitive inhibition.

3.4.5 Time and concentration-dependent inhibition of STS in the presence of estrone-3-*O*-phosphate (E1P) (protection experiments)

Protection studies with E1P were performed in the same manner as that described above for the time and concentration-dependent inhibition studies (§ 3.4.3) except various amounts of E1P was present in the incubation mixtures. The concentrations of the inhibitors were 100 μ M for inhibitors **3.10** and **3.11**, 10 μ M for inhibitor **3.12**, 5 μ M for 4-FE1 and 500 μ M for **3.14**.

3.4.6 Time and concentration-dependent inhibition of STS in the presence of β -mercaptoethanol (β -ME) (trapping experiments)

Before these studies were performed the effect of 5 mM β -ME on STS activity was determined. This was accomplished by first preparing a solution of STS (200 nM) in assay buffer containing 5 mM β -ME at 22°C. Within 10 seconds of preparing this solution a concentrated stock solution of MUS in assay buffer was added such that the final concentration of 4-MUS was 1 mM and STS activity was immediately determined by measurement of fluorescent 4-MU product in the usual manner. This experiment was then repeated except the STS/ β -ME solution was allowed to incubate at 22°C for 60 minutes before the 4-MUS was added and activity determined. After subjecting STS to 5 mM β -ME for 10 seconds the STS activity was found to be equal to that of a control which did not contain β -ME. After subjecting STS to 5 mM β -ME for one hour STS retained 83% of the activity exhibited by the control reaction indicating that 5 mM β -ME does not seriously affect STS activity within a one hour time frame. We also

examined glutathione as a potential nucleophile for these studies by performing the above experiments except glutathione (GSH) was used in place of β -ME. However, it was found that after subjecting STS to 5 mM glutathione for 10 seconds and one hour only 40% (after 10 seconds) and 27% (after one hour) of the activity remained compared to the control reaction indicating that 5 mM glutathione has a very detrimental affect on STS activity. We also determined the stability of the inhibitors in assay buffer containing β -ME by preparing a 4.8 mM solution of the inhibitors in assay buffer containing 2.4 M of β -ME and then analyzing the mixture by ^{19}F NMR at various time intervals. None of the inhibitors showed any discernable decomposition after 8 hours.

Time- and concentration-dependent inhibition studies of STS by compounds **3.10-3.12**, **3.14** and 4-FE1 in the presence of β -ME were performed in the same manner as that described above for the time and concentration-dependent inhibition studies (§ 3.4.3) except 5 mM β -ME was present in the incubation mixtures. The concentrations of the inhibitors were 100 μM for compounds **3.10** and **3.11**, 10 μM for inhibitor **3.12**, 5 μM for 4-FE1 and 500 μM for **3.14**.

3.4.7 Dialysis experiments

STS (200 nM) was incubated with inhibitor (100 μM of **3.10** and **3.11**, 10 μM of **3.12**, 10 μM of 4-FE1, 500 μM of **3.14**) in assay buffer (200 μL) for inhibitors **3.10-3.12**, **3.14** or assay buffer containing 2% DMSO (200 μL) for 4-FE1. The mixture was allowed to incubate for 1 hour. A control was also performed in an identical manner except that it did not contain inhibitor. 4 μL aliquots were withdrawn and STS activity determined as described in § 3.4.2. Almost no activity remained for all of the mixtures. The remaining incubation mixtures were dialyzed in microdialysis units into 1 L of 0.1

M tris, pH 7, 0.1 % Triton at 4°C. The dialysis proceeded for 24 hours with the dialysis buffer changed after 3, 6 and 9 hours. After 24 h, aliquots (4 µL) were withdrawn from the incubation mixtures and diluted into 196 µL of 4 mM MUS in 0.1 M tris, pH 7 and STS activity followed as described in § 3.4.2. No activity was recovered with inhibitors **3.10** and **3.11** or **3.14**. Only 2% activity was recovered with inhibitor **3.12** and 5% activity was recovered with inhibitor 4-FE1.

3.4.8 Effect of NaBH₄ on STS activity

The effect of 5.0 mM NaBH₄ on enzymatic activity was examined according to a procedure described by Blonski et al., 1995 for trapping Schiff base adducts between an aldehyde inhibitor and rabbit muscle aldolase enzyme. 5 µL of a 0.1 M solution of NaBH₄ in 0.1 NaOH was added to a 95 µL volume of 210 nM STS in 0.1 M tris, pH 7, 0.01% Triton X-100, which gives a final concentration of 5 mM NaBH₄ and 200 nM STS in 0.1 M tris, pH 7, 0.01% Triton X-100. A control was prepared containing no NaBH₄ but with the addition of 5 µL of 0.1 M NaOH, while another control was prepared containing no addition of NaBH₄ nor 0.1 M NaOH. Activity of STS was measured by withdrawing 4 µL from each solution immediately into the wells of a 96-well microtiter plate containing 196 µL of 4 mM MUS in 0.1 M tris, pH 7.4. The production of 4-MU was followed as described in § 3.4.2. The addition of 0.1 M NaOH did not affect the activity of STS, while the addition of 5 mM NaBH₄ reduced STS activity by more than 50% compared to the control.

3.4.9 Generation of standard curve for coumarin 3.28

The emission spectrum of **3.28** was first determined by measuring the fluorescence of a 50 µM solution of **3.28** and **3.10** in 0.1 M tris, pH 7.0, 0.1% Triton X-

100 containing 5% DMSO. The excitation wavelength (λ_{ex}) was held constant at 360 nm and the emission spectrum (λ_{em}) was collected at 20 nm intervals between 370 nm and 700 nm using a 360 nm cutoff wavelength. The maximum emission occurred at 460 nm. Accordingly, a standard curve of **3.28** was generated by measuring the endpoint fluorescence readout ($\lambda_{\text{ex}} = 360$ nm, $\lambda_{\text{em}} = 460$ nm) of 0.024-25 μM solutions in 0.1 M tris, pH 7.0, 0.1% Triton X-100. The equation of the line obtained from a plot of relative fluorescence units (RFUs) versus μmoles **3.28** generated is $y = 4 \times 10^6 x + 131$. See Figure 3.34 inset.

3.4.10 Determination of partition coefficient of compound 3.14

A reaction mixture consisting of STS (2 nM) and 500 μM of inhibitor **3.14** (total volume of 100 μL) in 0.1 M tris, pH 7, 0.1% Triton X-100 was prepared and the production of fluorescent product was followed ($\lambda_{\text{ex}} = 360$ nm, $\lambda_{\text{em}} = 460$ nm). Controls which consisted of STS but no inhibitor (control 1) or inhibitor but no STS (control 2) were also run. After about 3.8 hours fluorescence production reached a plateau. After 5 hours an additional 500 μM of **3.14** was added to the reaction mixture. No further increase in fluorescence was observed indicating that all STS activity was abolished. To ensure that STS activity did not diminish over 5 hours in the absence of the inhibitor, 4-MUS (final concentration 200 μM) was added to the wells of Control 1 and the production of fluorescent 4-MU product was followed in the usual way as described in § 3.2.2 and compared to that of a fresh sample of STS. No significant amount of activity was lost over the 5 hours. Non-enzymatic hydrolysis of **3.14** was not observed over the course of the assay as determined by control 2. After the addition of the second aliquot of **3.10**, the remaining incubation mixtures were dialyzed in microdialysis units into a

1 L buffer of 0.1 M tris, pH 7, 0.1 % Triton at 4°C. The dialysis proceeded for 24 hours with the dialysis buffer changed after 3, 6 and 9 hours to remove unhydrolyzed inhibitor and coumarin **3.28** and the volume and fluorescence of the dialyzed mixture was determined ($\lambda_{\text{ex}} = 360 \text{ nm}$, $\lambda_{\text{em}} = 460 \text{ nm}$). The fluorescence of the dialyzed mixture (131 RFUs) was subtracted from that of the undialyzed mixture (5471 RFU's) to give the RFU's (5347) that are attributable to coumarin **3.28** released into solution during the reaction. From this value and the standard curve the amount of MU released into solution was calculated and from this value the parting coefficient determined.

3.4.11 Monitoring the reactions of compounds 3.9-3.12 with STS by HPLC

Compounds **3.9** (10 μM), **3.10** (100 μM), **3.11** (100 μM) or **3.12** (10 μM) were incubated with STS (200 nM) in assay buffer (100 mM tris, pH 7, 0.01% Triton X-100) at 22 °C. Aliquots were withdrawn after various time intervals and injected into an HPLC equipped with a C-18 reversed phase analytical column and a UV detector set at 270 nm. Compound **3.12** and 2-formyl estrone (2-FE1) were eluted from the column using an isocratic gradient consisting of 55% of 0.1% TFA/H₂O/45% CH₃CN over 45 minutes at 1 mL/minute. The retention times for compounds **3.9** and 2-FE1 are 12 and 34 minutes respectively. Compound **3.10** and 2-hydroxymethylestrone (**3.24**) were eluted from the column using an isocratic gradient consisting of 65% of 0.1% TFA/H₂O/35% CH₃CN over 45 minutes at 1 mL/minute. The retention times for compounds **3.10** and 3.24 are 8 and 16 minutes respectively. Compound **3.11** and 4-hydroxymethylestrone (**3.25**) were eluted from the column using an isocratic gradient consisting of 72 % of 0.1 % TFA/H₂O/28 % CH₃CN over 45 minutes at 1 mL/minute. The retention times for compounds **3.11** and **3.25** are 39 and 44 minutes respectively.

Compound **3.12**, 4-difluoromethylestrone (4-diFME1) and 4-FE1 were eluted from the column using an isocratic gradient consisting of 55% of 0.1% TFA/H₂O/45% CH₃CN over 45 minutes at 1 mL/minute was employed. The retention times for compounds **3.12**, 4-difluoromethylestrone (4-diFME1) and 4-FE1 are 15, 33 and 38 minutes respectively.

Chapter 4 – Boronic acids as Inhibitors of Steroid Sulfatase[†]

4.1 Introduction

4.1.1 Boronic acids as enzyme inhibitors

The past 15 years has seen tremendous research in the development of inhibitors of STS (Purohit et al., 2003; Nussbaumer and Billich, 2004; Winum et al., 2005; Reed, et al., 2005; Day et al., 2009). As discussed in chapter 1, the vast majority of STS inhibitors are aryl sulfamates (Ar-SO₂NH₂) which act as irreversible suicide inhibitors (see chapter 1 § 1.3.2). In comparison to irreversible sulfamate inhibitors, far fewer reversible STS inhibitors have been developed (see chapter 1 § 1.3.1). Many reversible STS inhibitors have been obtained by replacing the sulfate group of estrone or estradiol with *O*-, *N*-, or *S*-linked sulfate surrogates as shown in **Table 1.2** in Chapter 1 (Nussbaumer and Billich, 2004; Winum et al., 2005). However, for the most part, these have not proven to be highly effective inhibitors with the vast majority exhibiting K_i or IC_{50} values in mid-to low μ M range with the better ones being around 10 μ M. In addition, the vast majority of these were never examined with pure enzyme and the

[†] This chapter is based largely on the publication, “Boronic acids as inhibitors of steroid sulfatase,” which was published in the journal *Bioorganic and Medicinal Chemistry* (Ahmed et al., 2006). The publishers of *Bioorganic and Medicinal Chemistry* allow authors to reproduce a journal publication in whole or in part in association with a thesis, as noted in Appendix F. The publication must be cited and the copyright regulation must be stated as follows:

Ahmed, V., Liu, Y., Silvestro, C., Taylor, S.D. Boronic acids as inhibitors of steroid sulfatase. *Bioorganic and Medicinal Chemistry*, volume 14, pages 8564-73, 2006. Copyright © 2006 Elsevier B.V.

modality of inhibition was not determined. Reversible inhibitors that do not bear a sulfate mimic have also been developed. Among the most noteworthy of this class of inhibitors are those developed by Poirier and coworkers who reported that certain 17- α -benzyl-substituted estradiol derivatives, such as **4.1** and **4.2** in **Figure 4.1**, are reversible STS inhibitors (see also chapter 1, § 1.3.1). Some of these compounds, which were tested using homogenates of JEG-3 cells instead of purified enzyme, are the most potent reversible inhibitors reported to date with IC_{50} values in the low nM range (Poirier et al., 1998; Boivin et al., 2000). The modality of inhibition was not reported.

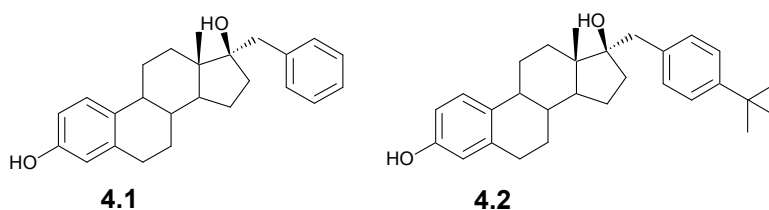


Figure 4.1 Examples of potent 17 α -benzyl estradiol inhibitors of STS reported by Poirier and coworkers (Poirier et al., 1998)

Boronic acids have been used for many years as inhibitors and probes of enzymes and proteins, such as serine proteases. These inhibitors, some of which have K_i values in the subnanomolar range, function by forming reversible covalent adducts with active site residues, such as the crucial serine residue (adduct **4.3**) or an active site histidine residue (adduct **4.4**) as shown in **Figure 4.2**. The inhibition of the boronic acid with a serine protease actually proceeds through a two-step, time-dependent inhibition mechanism (Kettner and Shenvi, 1984). The first step is rapid and involves binding of the inhibitor and formation of a covalent tetrahedral adduct with the active site serine. This is followed by a second slow step in which the enzyme undergoes a conformational change or isomerization to increase the interaction of the inhibitor with the proteolytic active site.

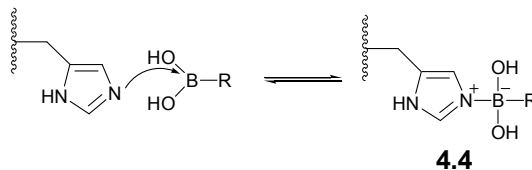
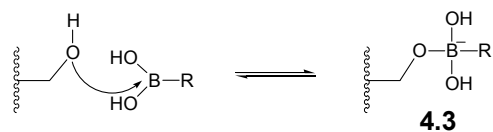


Figure 4.2. Proposed mechanism of inhibition of serine protease enzymes by boronic acids.

Recently, a highly potent and selective protease inhibitor in the form of a peptidyl boronic acid, called Bortezomid (**4.5**, **Figure 4.3**), has been approved by the FDA for treatment of relapsed and refractory multiple myeloma (Yang et al., 2003). Bortezomib binds in the catalytic site of the 26S proteasome which, in normal cells, regulates protein expression and function by degrading of ubiquitylated proteins and cleansing the cell of abnormal or misfolded proteins. Proteasome inhibitors have anti-tumor activity by inducing apoptosis as a result of the regulated degradation of pro-growth cell cycle proteins.

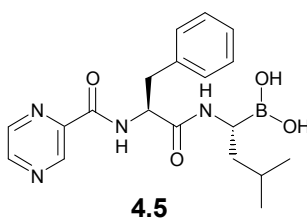


Figure 4.3. Structure of Bortezomid.

Unlike serine proteases, aryl sulfatases (ARSs) do not have an active site serine residue when in their catalytically active form. Instead, all eukaryotic ARSs have an active site formylglycine hydrate which is a result of a post-translational enzymatic modification of a cysteine residue (see chapter 1 § 1.1.2). Addition of water to the

aldehyde yields the formylglycine hydrate which is required for catalysis (Schmidt et al., 1995; von Figura et al., 1998). There is a very high degree of sequence and structural homology at the active site such that their active sites are almost superimposable, hence it is believed that all ARSs function by a common mechanism (Hanson et al., 2004). Several mechanisms have been proposed for ARSs as detailed in chapter 1 (§ 1.2.11). The most widely accepted involves attack of one of the alcohol groups of the hydrate on the sulfur atom of the substrate resulting in displacement of the hydroxyl or phenolic portion of the substrate and formation of a sulfated hydrate (see chapter 1 § 1.2.11, **Figure 1.16**). Elimination of the sulfate from the hydrate yields inorganic sulfate and formylglycine which is then rehydrated.

4.1.2 Objectives

In light of the mechanism proposed for sulfatases, we reasoned that boronic acids might act as potent inhibitors of STS by forming reversible covalent adducts with the active site hydrate and/or histidine residues in a manner similar to serine proteases. For example, a boronic acid might form a covalent adduct with one of the hydroxyl groups of the formylglycine hydrate as shown in reaction 1 in **Figure 4.4**. It is possible that the resulting covalent adduct depicted as “A” could then react with the second hydroxyl group of the formylglycine hydrate to form “B,” or it could react with a nearby histidine residue to form the adduct represented by “D.” Adduct “D” could potentially be reached through reaction 2, where the nucleophilic nitrogen atom of a nearby histidine residue would attack the boron atom of the boronic acid derivative to afford the adduct shown in “C,” which may be able to react with one of the hydroxyl groups of the

formylglycine hydrate. The objective of this work is to evaluate boronic acids as inhibitors of STS using steroidal and non-steroidal boronic acids **4.6-4.9** (Figure 4.5).

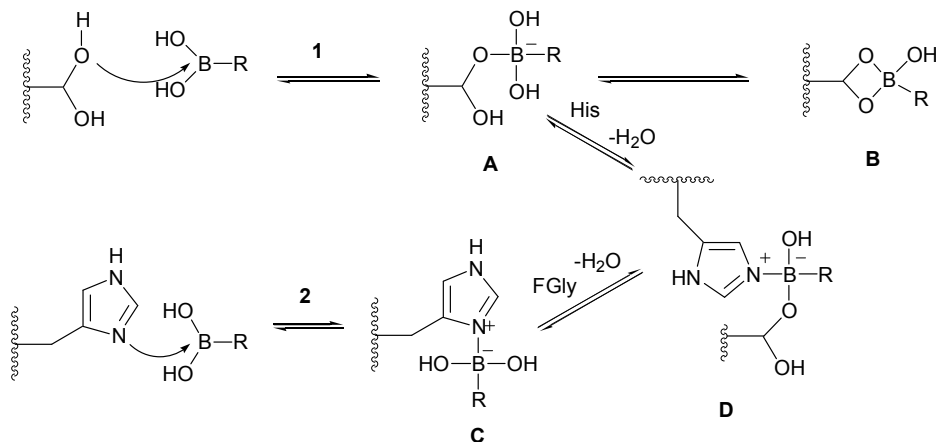


Figure 4.4. Proposed mechanism of inhibition of STS by boronic acids.

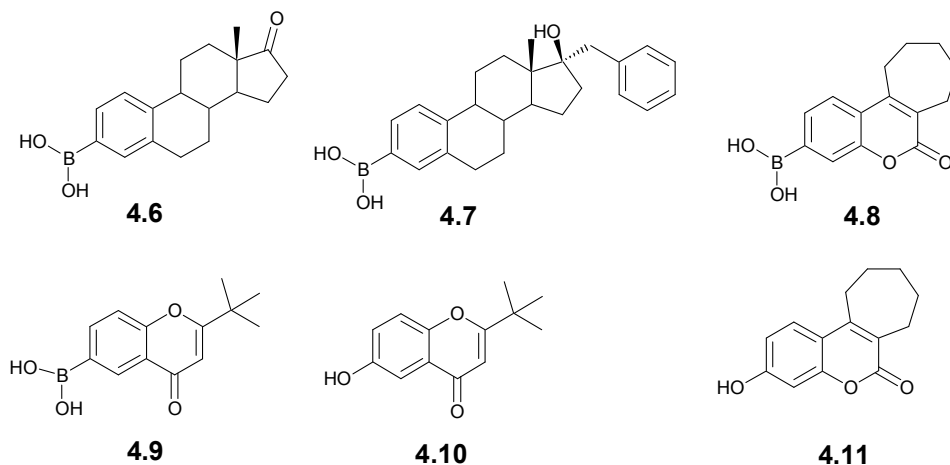


Figure 4.5. Proposed boronic acid inhibitors of STS, **4.6-4.9**. Chromenone **4.10** and coumarin **4.11** were also prepared and examined for comparison of their activities with their boronic acid counterparts.

4.2 Results and Discussion

For these studies boronic acid analogs were examined with the boronic acid group attached to three different scaffolds: a steroid scaffold (compounds **4.6** and **4.7**), a coumarin scaffold (compound **4.8**) and a chromenone scaffold (compound **4.9**). These scaffolds were chosen since aryl sulfamate STS inhibitors based on these scaffolds have proven to be highly potent (see chapter 1 § 1.3). Compound **4.7** was prepared since compound **4.1** is a potent reversible inhibitor of STS.

Inhibition studies were carried out using purified STS in tris buffer containing 5% DMSO with 4-MUS as substrate. K_i or IC_{50} values determined for boronic acids **4.6–4.9** as well as for estrone (E1), steroid derivative **4.1**, and chromenone **4.10** are given in **Table 4.1**.

Table 4.1. K_i or IC_{50} values for compounds **4.1**, **4.6–4.10** and E1.

Inhibitor	pH	K_i or IC_{50} (μ M)	αK_i (μ M)
4.6	7.0	2.8 ± 0.4^a	n/a ^c
4.6	7.5	2.1 ± 0.3^a	n/a ^c
4.6	8.0	3.8 ± 0.5^a	n/a ^c
4.6	8.5	7.0 ± 0.6^a	n/a ^c
4.6	8.8	6.8 ± 0.8^a	n/a ^c
4.7	7.0	0.25 ± 0.2^a	0.30 ± 0.02
4.8	7.0	171 ± 9^b	n.d. ^d
4.9	7.0	86 ± 4^b	n.d. ^d
Estrone (E1)	7.0	63 ± 2^b	111 ± 14
4.1	7.0	0.25 ± 0.02^a	0.42 ± 0.01
4.10	7.0	4.6 ± 0.8^a	40 ± 4

^a K_i

^c n/a, not applicable

^b IC_{50}

^d n.d., not determined

Compound **4.6** can be considered as the boronic acid analog of estrone sulfate (E1S), a natural substrate of STS. Compound **4.6** is a mainly competitive STS inhibitor with a K_i of 2.8 μM at pH 7.0 (**Figures 4.6**). The K_m for E1S in 0.1 M Tris-HCl, 0.1% Triton X-100, at pH 7.5 is 95 μM (Billich et al., 2004). Dibbelt et al. have shown, using [^{35}S]-labeled dehydroepiandrosterone sulfate (DHEAS) as substrate, that E1S is an inhibitor of STS exhibiting mixed inhibition with a K_i of about 1 μM in 0.1 M Tris-acetate at pH 7.0 (Dibbelt et al., 1994). Thus, it appears that compound **4.6** has an affinity for STS that is about equal to E1S. E1 itself is mainly a non-competitive inhibitor with a K_i of 63 μM and αK_i of 110 μM (**Figure 4.7**). Thus, replacing the 3-OH of E1 with a boronic acid moiety resulted in about 23-fold increase in potency and changes the modality of inhibition from noncompetitive to mainly competitive.

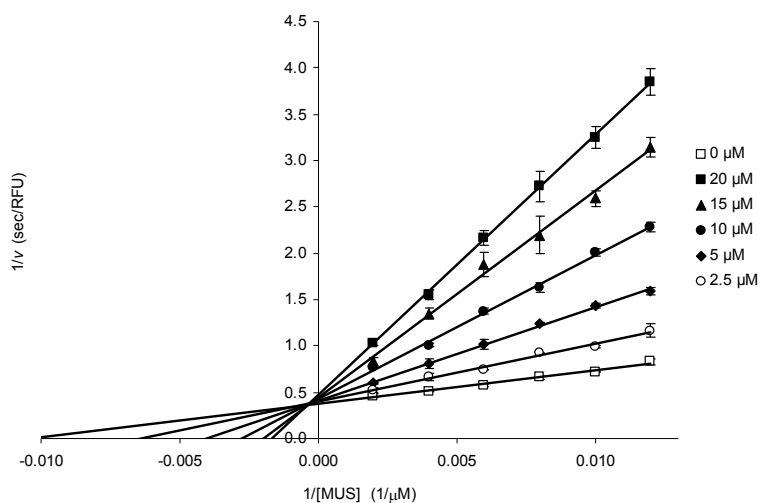


Figure 4.6. Lineweaver-Burk plot for boronic acid **4.6** at pH 7.0 (see Appendix B for the replot of this data that was used to determine the K_i)

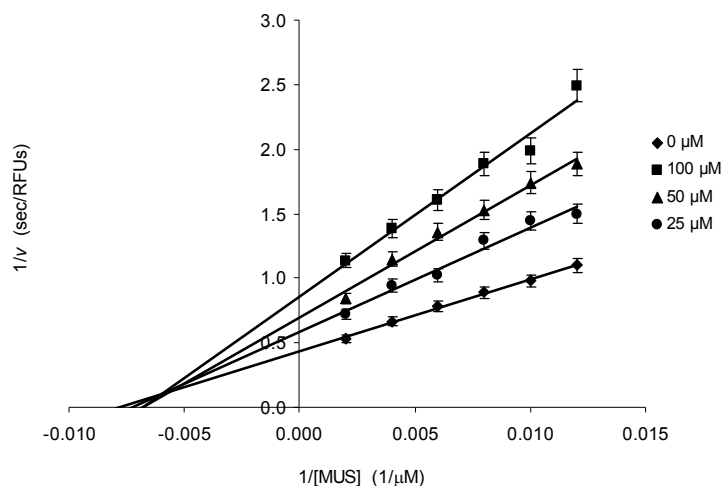


Figure 4.7. Lineweaver-Burk plot for E1 at pH 7.0 (see Appendix B for replots of this data that were used to determine the K_i and αK_i).

Comparing the potency of **4.6** with those of many other estrone derivatives bearing sulfate surrogates that have appeared in the literature is difficult since very few have been examined with pure enzyme and the modality of inhibition was rarely determined. Nevertheless, a comparison of **4.6** with other estrone derivatives bearing sulfate surrogates whose K_i or IC_{50} values have been determined using pure enzyme or placental microsomes reveals that compound **4.6** is one of the most potent inhibitors of this class (see chapter 1, **Table 1.2**). Moreover, compound **4.6** is a mainly competitive inhibitor which is in contrast to many other estrone derivatives bearing sulfate surrogates which often exhibit noncompetitive or mixed inhibition (Liu et al., 2005; Lapierre et al., 2004; Dibbelt et al., 1994; Li et al., 1995). Estrone phosphate (E1P) is one of the better estrone-based STS reversible competitive inhibitors bearing a sulfate surrogate (Li et al., 1995; Anderson et al., 1995). Under our assay conditions, we determined E1P to have an IC_{50} of 5 μ M at pH 7.0 (see Appendix B for details). Thus, compound **4.6** is as potent as E1P at pH 7.0.

In most instances, the inhibition of serine proteases with boronic acids is very pH-dependent. Bender has reported that the inhibition of subtilisin with benzene boronic acid increases significantly between pH 6.0 and 8.0, and then rapidly decreases at pH > 8.0 (Philip et al., 1971). The increase in inhibition from pH 6.0 to 8.0 was attributed to the increase in the concentration of a reactive residue in the active site such as histidine or serine while the decrease was attributed to a decrease in the concentration of the reactive trigonal form of the boronic acid inhibitor. We have observed a modest decrease in inhibitor potency as the pH increases from pH 7.5 to 8.5 then levels off as the pH increases to 8.8 (**Table 4.1**). The inhibition remains mainly competitive throughout this pH range and even at pH 8.8 compound **4.6** is still a good inhibitor with a K_i of 6.8 μM (**Figure 4.8**. See also Appendix B for Lineweaver-Burk plots at pH values 7.5-8.5 and replots). It is unlikely that it is the tetrahedral hydrated form of **4.6** that binds since the concentration of this species should increase with increasing pH and one would expect an increase in inhibition as the

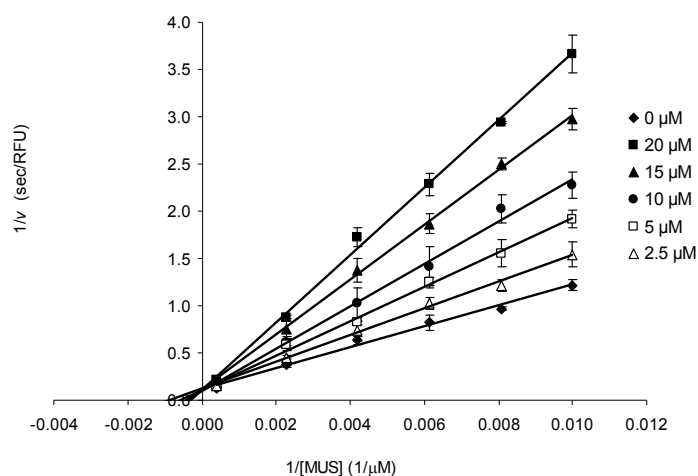


Figure 4.8. Lineweaver-Burk plot for boronic acid **4.6** at pH 8.8 (see Appendix B for the replot of this data that were used to determine the K_i).

pH increases. Moreover, this decrease in inhibition is not due to a decrease in the trigonal form of the inhibitor since its pK_a should be similar to that of 4-methylphenyl boronic acid which is 9.3 (Torsell et al., 1964). The slight increase in K_i with pH found with compound **4.6** is in contrast to the large increase in K_i with pH exhibited by E1P whose K_i increases over 50-fold between pH 7.0 and 8.5 (Anderson et al., 1995). This large increase is a result of the enzyme's preference to bind the monoanionic form of estrone phosphate.

Although our results do not allow us to unambiguously determine whether a reversible covalent adduct is formed between **4.6** and STS, it appears that formation of such an adduct is unlikely for several reasons. First of all, simple aryl boronic acids are generally modest serine protease inhibitors with K_i values ranging from the millimolar to low micromolar depending on the enzyme and the substituents on the boronic acid. However, peptide boronic acids that have the primary specificity requirement for the protease are much more potent inhibitors with K_i values sometimes extending into the subnanomolar range and exhibit an affinity for the protease that is many orders of magnitude greater than the corresponding substrate. Although **4.6** is a good inhibitor, it does not exhibit an affinity for STS that is orders of magnitude greater than that of E1S. Second, peptide boronic acid inhibitors show kinetic properties corresponding to the mechanism for slow-binding inhibitors (Kettner et al., 1984). STS assays performed in the presence of compound **4.6** exhibited a linear increase in product with time during the entire time course of the assays (10 min). Preincubation of **4.6** with STS for up to 60 min did not result in an increase in potency. These results suggest that compound **4.6** is not a slow-binding inhibitor. Moreover, the inhibition was found to be immediately

reversible as demonstrated by experiments in which the activity was recovered by dilution into a solution containing a large excess of substrate (4-MUS). Finally, as pointed out above, the effect of pH on the K_i of inhibitor **4.6** is not typical of a boronic acid inhibitor that forms a covalent adduct with its target enzyme. If **4.6** does form a reversible adduct this adduct is not as stable as that observed with the peptide boronic acid inhibitors of serine proteases. Boronic acid inhibitors of serine proteases are considered to be transition state analog inhibitors in that they mimic the tetrahedral transition state formed during the reaction. The reaction of STS with E1S does not proceed by a tetrahedral transition state. The transition state for the cleavage of the S–O bond of the substrate probably resembles a trigonal bipyramidal intermediate as shown in Chapter 1 in **Figure 1.13**. This may explain why compound **4.6** is not as potent an inhibitor of STS as the peptide boronic acids are of serine proteases. Nevertheless, compound **4.6** is still one of the best estrone-based STS inhibitors bearing a sulfate surrogate ever reported.

Since boronic acid inhibitor **4.6** was considerably more potent than estrone, compound **4.7** was prepared in the anticipation that substitution of the 3-OH moiety in **4.1** with a boronic acid would also result in a significant increase in inhibitory potency. Compound **4.7** is a 10-fold more potent inhibitor than compound **4.6** with a K_i of 252 nM. However, compounds **4.7** and **4.1** exhibited almost identical K_i values and both were mainly non-competitive inhibitors of STS with both inhibitors exhibiting similar affinities for both the free and substrate bound forms of the enzyme (**Figures 4.9** and **4.10**). These results suggest that both **4.7** and **4.4** preferably bind in a region outside the

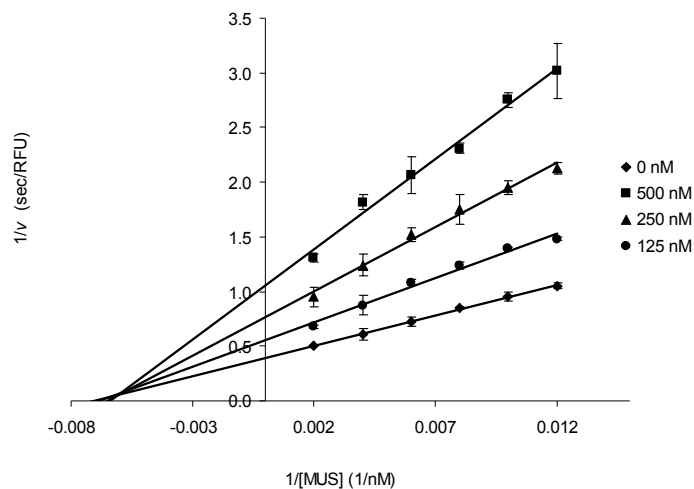


Figure 4.9. Lineweaver-Burk plot for boronic acid **4.7** at pH 7.0 (see Appendix B for replots of this data that were used to determine the K_i and αK_i).

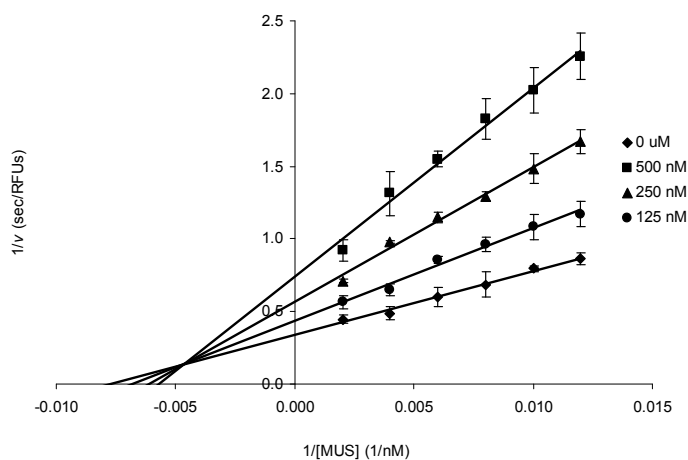


Figure 4.10. Lineweaver-Burk plot for **4.1** at pH 7.0 (see Appendix B for replots of this data that were used to determine the K_i and αK_i).

active site. It has been suggested that the high affinity of estradiol derivatives bearing benzyl groups at the 17-position for STS is a result of the benzyl group extending into a hydrophobic channel between the two antiparallel helices that are believed to insert into the membrane of the endoplasmic reticulum (Nussbaumer et al., 2004). Since our results with compounds **4.1** and **4.7** suggest that these compounds can bind in an area outside the active site, it is possible that they bind in the channel between the helices and

block the entrance to the active which is a small tunnel at the top of the two helices (Hernandez-Guzman et al., 2003).

IC₅₀ values were determined for coumarin and chromenone boronic acids **4.8** and **4.9** at pH 7.0. Both of these compounds were relatively poor STS inhibitors with the coumarin having an IC₅₀ of 171 μM and the chromenone having an IC₅₀ of 86 μM (see appendix B for IC₅₀ plots). We also determined the IC₅₀ of chromenone **4.10** to see if the substitution of the phenolic group in **4.10** with a boronic acid group had any effect on inhibitor potency as found with compound **4.6**. The poor solubility and high fluorescence of coumarin **4.11** prevented us from determining its IC₅₀. Surprisingly, compound **4.10** exhibited an IC₅₀ of 6 μM which is 14 times less than its boronic acid analog **4.9**. A more detailed kinetic analysis revealed that it exhibits mixed inhibition (**Figure 4.11**) with a K_i of 4.6 μM and an αK_i of 40 μM and the inhibition is reversible. Thus, this compound is much more

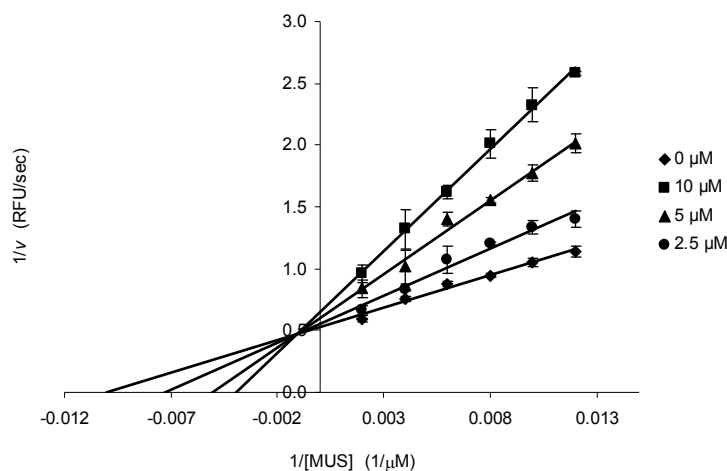
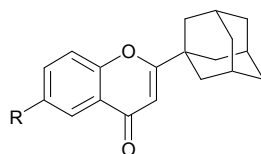


Figure 4.11. Lineweaver-Burk analysis for **4.10** at pH 7.0 (see Appendix B for replots of this data that were used to determine the K_i and αK_i).

potent than its boronic acid analog and almost as potent as steroid boronic acid **4.6**. Like the compounds reported by Poirier and coworkers (such as **4.1** and **4.2**), chromenone **4.10** does not require a sulfate mimic to exhibit good potency. Horvath and coworkers have demonstrated the potential of the chromenone platform for obtaining reversible STS inhibitors (Horvath et al., 2004). These workers examined a series of 6-substituted 2-(1-adamantyl)-4-chromenones as STS inhibitors (Horvath et al., 2004). Those bearing non-ionizable or very weakly acidic moieties at the 6-position, such as **4.11** and **4.12**, were modest reversible inhibitors of STS with K_i values generally greater than 50 μM . The 6-COOH derivative was the most potent of the series having K_i of about 500 nM. The 6-OH derivative was not examined. Although chromenone **4.10** is 20-fold less potent than compound **4.1** it is a smaller, non-steroidal compound and could be used as a lead to the development of yet more potent reversible STS inhibitors.



4.11, R = COOH, K_i = 500 nM

4.12, R = COCH₂OH, K_i = 3.2 μM

Figure 4.12. Structures of compounds **4.11** and **4.12**.

4.3 Conclusions and Future Work

In summary, several novel steroidal and non-steroidal boronic acids were examined as inhibitors of STS. The potency of these compounds and their mode of inhibition varied dramatically. It appears that the boronic acid moiety must be attached to a platform very closely resembling a natural substrate in order for it to impart any beneficial effect on binding affinity. Thus, estrone boronic acid **4.6** is a good

competitive inhibitor of STS even at basic pH. The fact that this compound exhibits a good affinity for STS even at basic pHs may be significant in terms of obtaining the crystal structure of an inhibitor-STS complex. The structure of an STS-inhibitor complex has not yet been reported. Such a structure would be very useful for rational inhibitor design. However, one of the potential difficulties in obtaining the structure of an STS-inhibitor complex is that the enzyme is crystallized at pH 8.5 where its affinity for ligands is often far from optimal (Liu et al., 2005). However, since **4.6** binds to STS with a good affinity at basic pHs, this compound may enable one to obtain the structure of an STS inhibitor complex. Compound **4.7**, an estradiol derivative which, in addition to the boronic acid group at the 3-position also bears a benzyl group at the 17-position, was a potent non-competitive STS inhibitor. However, the fact that compound **4.7** and its phenolic precursor **4.1** have similar affinities and are non-competitive inhibitors suggests that these compounds bind in a region outside the active site, possibly in the hydrophobic channel between the two membrane-spanning helices. The existence of a hydrophobic second binding site has also been suggested by Poirier's group, who initially developed the 17 α -substituted estradiol derivatives such as **4.1** (Boivin et al., 1998). At that time they suggested that a hydrophobic pocket may exist in the enzyme in proximity to the steroid D-ring based upon structure-activity relationships studies of their 17 α -substituted estradiol derivatives with STS in homogenates of JEG cells. The results of the studies reported here have provided the impetus for Poirier and coworkers (Fournier and Poirier, 2009) to design bivalent STS inhibitors that they anticipate will occupy the active site as well as the postulated allosteric site. Crystallographic studies

with compounds **4.6** and **4.7** and STS are in progress in collaboration with Debashis Ghosh, Hauptmann-Woodward Institute, Buffalo, New York.

The coumarin and chromenone boronic acids **4.8** and **4.9** were not good inhibitors. However, the chromenone precursor to **4.8**, compound **4.10**, is a remarkably good STS inhibitor. An obvious direction for future studies entails using compound **4.10** as a lead to the development of yet more potent reversible non-steroidal STS inhibitors that do not bear a sulfate mimic.

4.4 Experimental

4.4.1 General.

Compounds **4.6-4.11** were prepared by Yong Liu in the Taylor group (Liu et al., 2005). STS was purified as previously described (Ahmed et al., 2005). All buffers and assay reagents were purchased from Sigma Aldrich (Milwaukee, WI, USA). All fluorescent measurements were carried out on a SpectraMax GeminiXS[®] fluorimeter (Molecular Devices, Sunnyvale, CA, USA) at 22 °C in black microtiter plates from Corning (Corning, MA, USA). All determinations were carried out in triplicate and errors reported as the standard deviation.

4.4.2 Determination of K_i and αK_i values for compounds 4.1, 4.6, 4.7 and 4.10

An appropriate volume of a MUS stock solution in 0.1 M Tris-HCl of desired pH was added to the wells of a 96-well microtiter plate containing 0.1 M Tris-HCl buffer of the same pH such that the total volume was 80 μ L. To the wells was added 10 μ L of a stock solution of inhibitor in 50% DMSO. For a control, 10 μ L of 50% DMSO was added instead. The assay was initiated by the addition of 10 μ L STS (115 nM stock solution in 20 mM Tris-HCl, pH 7.4, 0.1% Triton X-100). To detect non-enzymatic

hydrolysis of the substrate 10 μL of 20 mM Tris-HCl, pH 7.4, 0.1% Triton X-100 was added instead. The final volume of the assay was 100 μL . The final concentration of buffer was 92 mM TrisHCl, 0.01% Triton X-100, and 5% DMSO. The final enzyme concentration was 11.5 nM. For studies with compound **4.6** at pH 7.0, 7.5, and 8.0, the final concentration of MUS was 83.3–500 μM , or approximately 0.5–3 times the K_m value at pH 7 and 7.5 (145 μM at pH 7.0; 170 μM at pH 7.4) and 0.25–1.5 times the K_m value at pH 8.0 (338 μM). For studies with compound **4.6** at pH 8.5 and 8.8, the final concentration of 4-MUS ranged between 100 and 2500 μM or approximately 0.1–3 times the K_m value (830 μM , pH 8.5; 980 μM , pH 8.8). The final concentration of inhibitor was 0.5–4 times K_i . The reactions were followed by detection of fluorescent product, 4-methylumbelliferone (excitation 360 nm, emission, 460 nm), over 10 min at 30°C. Each reaction was performed in triplicate. Additional controls were performed in an identical manner but did not contain STS. Initial rates (v) were determined by taking the slopes of plots of the change in relative fluorescence units with time. These data were plotted as Lineweaver–Burk graphs and K_i values were calculated from replots of the slopes or intercepts of the Lineweaver–Burk graphs according to the equations for mixed and competitive inhibition.

4.4.3 Determination of IC_{50} s for compounds 4.8, 4.9, and 4.10.

Ten microliters of inhibitor stock solutions in 50% DMSO were added to the wells of a 96-well microtiter plate containing 70 μL of 0.1 M Tris, pH 7.0. 10 μL of a 2.0 mM MUS stock solution in 0.1 M Tris-HCl, pH 7.0, was added. The assay was initiated by adding 10 μL STS (115 nM stock solution in 20 mM Tris-HCl, pH 7.4, 0.1% Triton X-100). The concentration of inhibitor ranged from 7 to 250 μM . The final

concentration of 4-MUS was 200 μ M. The reaction was followed as described above. Eleven concentrations of inhibitor bracketing the IC_{50} value were used for each compound. The initial rates of enzyme activity in relative fluorescence units per second (RFU/s) were used to determine the IC_{50} . The ratio of the initial rate in the presence of inhibitor (V_i) to that in the absence of inhibitor (V_o) was calculated and plotted as a semi-log curve in Grafit (Erithacus Software, Surrey, U.K.), from which the IC_{50} value was calculated based on the following equation: $V_i = V_o/[1 + ([I]/IC_{50})^S] + B$, where: V_i is the initial rate of reaction at an inhibitor concentration concentration of $[I]$; V_o is the velocity in the absence of inhibitor; B is background and s is the slope factor.

Chapter 5 – An assessment of the sulfonic acid and sulphonamide groups as phosphotyrosine mimics for PTP1B Inhibition[†]

5.1 Introduction: Protein Tyrosine Phosphatases

The cellular equilibrium of protein tyrosine phosphorylation is mediated through the opposing chemical reactions of protein tyrosine kinases (PTKs) and protein tyrosine phosphatases (PTPs) (**Figure 5.1A**, Tonks, 2006). PTPs catalyze the hydrolysis of phosphate monoester bonds via a two-step reaction involving formation (k_2) of a covalent phosphocysteine intermediate and its subsequent breakdown (k_3) (**Figure 5.1B**, Guan and Dixon, 1991; Cho et al., 1992). Important insights into protein tyrosine phosphorylation mediated cellular signalling has stemmed from research focussing on PTKs which are commonly accepted as the initiators of signalling pathways and their

[†] The experimental section of this chapter is based largely on the publications, “Enantioselective synthesis of protected L-4-[sulfonamido(difluoromethyl)]-phenylalanine and L-4-[sulfonamido-(methyl)]phenylalanine and an examination of hexa- and tripeptide platforms for evaluating pTyr mimics for PTP1B inhibition,” and “A re-examination of the difluoromethylenesulfonic acid group as a phosphotyrosine mimic for PTP1B inhibition,” which were published in *The Journal of Organic Chemistry* and *Bioorganic and Medicinal Chemistry*, respectively (Hill et al., 2006; Hussain et al., 2008). The publishers of both of these journals allow authors to reproduce a journal publication in whole or in part in association with a thesis, as noted in Appendix G. The publication must be cited and the copyright regulation must be stated as follows:

Hill, B., Ahmed, V., Bates, D., Taylor, S.D. Enantioselective synthesis of protected L-4-[sulfonamido(difluoromethyl)]phenylalanine and L-4-[sulfonamido-(methyl)]phenylalanine and an examination of hexa- and tripeptide platforms for evaluating pTyr mimics for PTP1B inhibition. *Journal of Organic Chemistry*, volume, pages, 2006. Copyright © 2008 American Chemical Society.

Hussain, M., Ahmed, V., Hill, B., Ahmed, Z., Taylor, S.D. A re-examination of the difluoromethylenesulfonic acid group as a phosphotyrosine mimic for PTP1B inhibition. *Bioorganic and Medicinal Chemistry*, volume 16, pages 6764-6777, 2008. Copyright © 2008 Elsevier B.V.

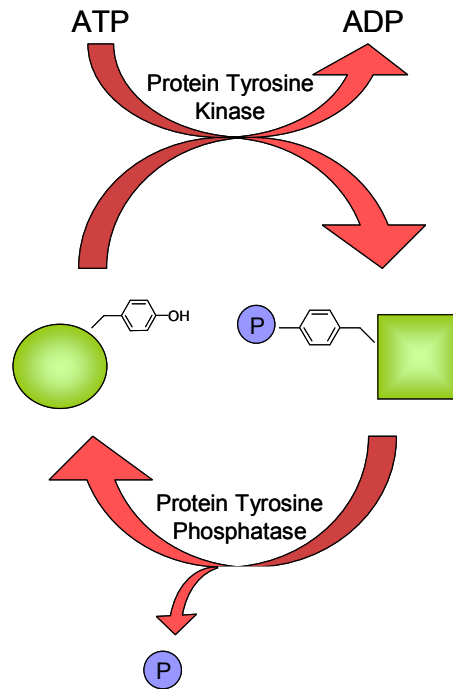
cascades (Hunter, 2000). Aberrant phosphorylation due to an imbalance in PTK and PTP function is linked to human diseases including cancer, diabetes, obesity and inflammation and autoimmunity (Zhang, 2001; Arena, 2005; Begovich et al., 2004). For example, the expression and activation of receptor tyrosine kinases such as the epidermal growth factor (EGFR), and the oncogene non-receptor tyrosine kinases, Src and Abl, are causative factors in cancer (Krause and Van Etten, 2005). As a result, PTPs were initially thought to occupy a small cellular housekeeping role in the reversal of PTK action, and were merely the products of tumor suppressor genes. However, PTPs have come to be regarded as important regulators and effectors of cellular protein tyrosine phosphorylation in collaboration with PTKs (Jiang and Zhang, 2008). It should also be noted that in certain cases PTPs can also potentiate instead of antagonize PTK action (Zheng et al., 1992).

There are 107 members of the PTP family in the human genome and all are characterized by an 11 residue signature sequence, (I/V)HCXAGXXR(S/T/G), which includes the active site catalytic cysteine residue (Alonso et al., 2004). The PTP superfamily can be divided into four subfamilies: (1) classical phosphotyrosine (pTyr)-specific PTPs, (2) dual-specificity phosphatases (DSPs), (3) Cdc25 phosphatases, and (4) low molecular weight (LMW) PTPs (Alonso et al., 2004).

The classical PTPs were discovered due to their ability to desphosphorylate proteins bearing a pTyr residue, and this class can further be divided into subcellular localization of receptor and non-receptor PTPs (RPTPs and NRPTPs, respectively). An important member of the RPTP class includes cluster for differentiation 45 (CD45),

which activates src family PTKs through dephosphorylation with the effect of initiating downstream signalling processes in stimulated T and B cells (Pingel and Thomas, 1989).

A



B

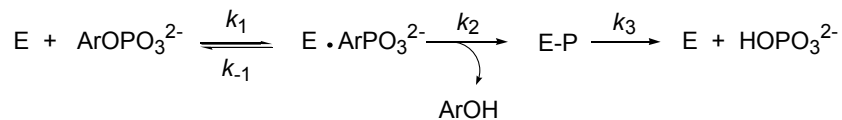


Figure 5.1 (A) Protein phosphorylation is regulated by the dual action of protein tyrosine kinases (PTKs) and protein tyrosine phosphatases (PTPs). (B) General reaction scheme for the PTP reaction that catalyzes phosphate ester hydrolysis via a covalent phosphocysteine intermediate. The reaction proceeds through a two-step mechanism involving formation (k_2) and breakdown (k_3) of the phospho-enzyme intermediate (E–P).

Protein tyrosine phosphatase 1B (PTP1B) is the most prominent member of the class of NRPTPs and plays a critical role in regulating body weight, glucose homeostasis and energy expenditure by acting as a negative regulator in insulin receptor and leptin receptor mediated signaling pathways. Other significant members of the NRPTP

subfamily are the phosphatase of regenerating liver (PRL) phosphatases, which promote cell growth and tumor metastases (Stephens et al., 2005), and SHP2 phosphatase, which is named for its two Src homology domains and a PTP domain (Anderson et al., 1990; Marounet et al., 2000). SHP2 is involved in signaling events downstream of receptors for growth factors, cytokines, hormones that direct the control of cell growth, differentiation, migration and death (Qu, 2000).

Dual-specificity PTPs are able to hydrolyze phosphoserine (pSer) and phosphothreonine (pThr) residues in addition to pTyr residues, such as VH1- and Cdc14-like DSPs. The DSP subfamily also includes phosphatase and tensin homolog (PTEN) and myotubularin, which hydrolyze phosphoinositides.

The Cdc25 phosphatases, which are positive regulators of cell cycle progression, also exhibit dual specificity toward protein substrates, however, they are classified in a separate family because they are more distantly related to other members of the PTP family based on structure and sequence. The LMW PTPs have no significant sequence homology with other members of the PTP superfamily beyond their phosphatase signature sequence.

The cellular pathways regulated by tyrosine phosphorylation offer a rich source of drug targets for treatment of associated diseases. The major phosphatase targets identified to date as therapeutic targets include Cdc25, SHP2, PRL and PTP1B (Jiang and Zhang, 2008). PTP1B is the subject of the studies presented in this Chapter.

5.1.1 PTP1B as a drug target for diabetes and obesity

PTP1B is recognized for its role as a negative regulator in both insulin and leptin signalling (**Figure 5.2**). PTP1B dephosphorylates activated insulin receptor (IR) or

insulin receptor substrates (IRS) and the downstream result is glucose uptake (Bandyopadhyay et al., 1997; Dadke et al., 2000; Goldstein et al., 2000). Support for PTP1B's role as a negative effector of insulin-mediated signalling is derived from studies where overexpression of PTP1B in cell cultures decreases insulin-stimulated phosphorylation of the IR (Ahmad et al., 1995; Kenner et al., 1996; Byon et al., 1998). Conversely, when diabetic mice are treated with PTP1B antisense oligonucleotides, a reduction in the expression of PTP1B is achieved and the effect is a decrease in fat, plasma insulin and blood glucose levels (Zinker et al., 2002). Mice that lack PTP1B through a double-knockout of the PTP1B gene (PTP1B^{-/-}) display an enhanced sensitivity to insulin, and have improved glycemic control, and most interestingly are more resistant to weight gain when fed a high-fat diet compared to wild-type mice (Echelby, M., 1999; Klaman et al., 2000). This resistance to weight gain is unexpected as insulin is also an anabolic factor, and an increased insulin sensitivity can also lead to increased weight gain. It was later shown that PTP1B can also bind to and dephosphorylate Janus kinase 2 (JAK2), which is downstream of the leptin receptor, ObR (Zabolotny et al., 2002; Cheng et al., 2002). Leptin is a peptide hormone that plays a central role in feeding and adiposity (Ahima and Flier, 2000). The leptin receptor (ObR) belongs to the class of type I cytokine receptors that use an associated JAK to transmit signals to downstream molecules (Tartaglia, 1997). Once leptin binds to ObR, the receptor becomes phosphorylated and JAK2 becomes activated, and leads to activation of the transcription factor 3 protein (Stat3). Once activated, Stat3 becomes phosphorylated, allowing it to homodimerize, leading to subsequent translocation to the nucleus where it mediates transcription of target genes that control the negative

feedback loop of leptin signaling. Therefore, the finding that resistance to diet-induced obesity observed in $PTP1B^{-/-}$ mice is likely to be associated with increased energy expenditure because of enhanced leptin sensitivity. Altogether these studies show strong support that inhibition of PTP1B is an effective strategy for treating metabolic diseases such as type 2 diabetes and obesity.

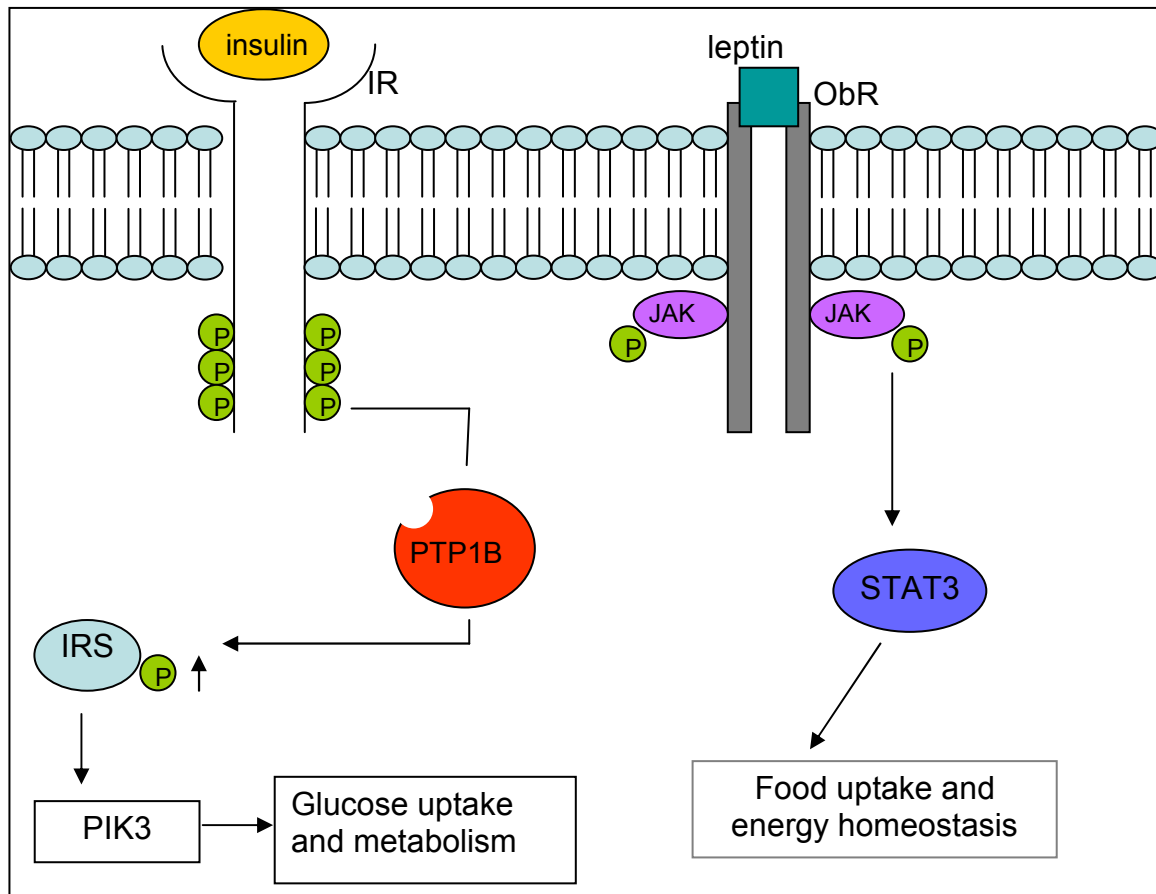


Figure 5.2 The role of PTP1B in insulin and leptin signalling (Adapted from Zhang and Zhang, 2000).

5.1.2 The PTP1B protein: catalytic and regulatory domains

PTP1B (E.C. 3.1.3.48) specifically catalyzes the phosphate ester hydrolysis of phosphotyrosine (pTyr)-containing proteins and peptides (Tonks et al., 1988). Free pTyr is a relatively poor substrate (**5.1**, $K_m = 5$ mM) in comparison to peptides bearing pTyr.

The K_m value for free pTyr is three to four orders of magnitude higher than the best protein/peptide substrates, suggesting that the major determinant of specificity is a pTyr residue in the context of a peptide platform (Tonks et al., 1988; Zhang et al., 1993; Zhang et al., 1994). The sequence surrounding Tyr992 of the epidermal growth factor receptor (Rotin et al., 1992; McNamara et al., 1993), has been established to have high affinity for PTP1B (**Figure 5.3**). As a result the hexapeptide, DADE-pY-L-NH₂, **5.2** ($K_m = 3.6 \mu\text{M}$ for PTP1B), has been one of the most commonly used peptides for probing substrate specificity and inhibition of PTPs (Zhang et al., 1993; Zhang et al., 1994).

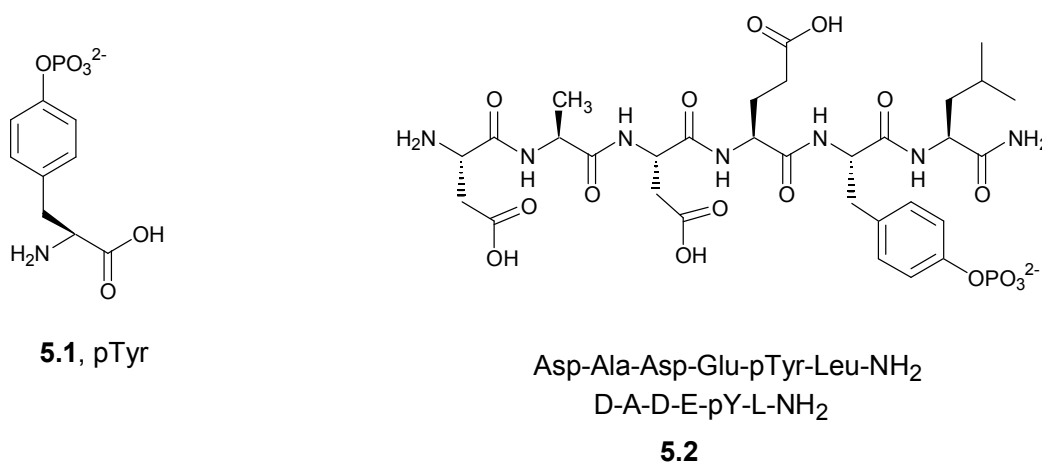


Figure 5.3 Phosphotyrosine and its position in a hexapeptide portion of the epidermal growth factor receptor (EGF).

PTP1B was named for its tyrosine phosphatase activity in a specific fraction resolved by ion-exchange chromatography of a human placenta homogenate (Tonks et al., 1988; Tonks et al., 1988). It was originally purified as a catalytic domain of 37 kDa, however, it was later determined that cDNA-encoded PTP1B consists of a full-length form of the protein that comprises an additional 114 residues on the C-terminal side of the catalytic domain (Brown-Shimer et al., 1990; Chernoff et al., 1990; Guan et al.,

1990). The C-terminal 35 residues are predominantly hydrophobic in nature and act to target the enzyme to the cytoplasmic face of the endoplasmic reticulum (Frangioni et al., 1992). It is thought that targeting PTPs to specific subcellular locations contributes to the regulation of their function by restricting the spectrum of substrates which they can access, and has been referred to as a “zip code” model within the PTP family (Mauro and Dixon, 1994; Tonks, 2003). The C-terminal segment may also have a regulatory role as illustrated by proteolytic cleavage by calpain to generate a soluble 42 kDa form of the enzyme (Frangioni et al., 1993). This truncated PTP1B lacking 75 residues from the C-terminus including the ER-targeting motif is associated with enhanced PTP activity, suggesting that the C-terminus suppresses catalytic function. PTP1B exists as a phosphoprotein *in vivo* with several Ser/Thr phosphorylation sites identified in the regulatory C-terminal segment (Flint et al., 1993). Phosphorylation of Ser378 by protein kinase C (PKC) was observed as well as cell cycle-dependent phosphorylation of Ser352 and Ser386. The mechanism through which PTP1B function is regulated by phosphorylation is unclear, although changes in activity are associated with changes in phosphorylation. The phosphorylation of members of the PTP family is viewed as a regulatory mechanism for activation and inhibition of PTP function (Alonso et al., 2004).

5.1.3 Catalytic mechanism and structure of PTP1B

The three-dimensional crystal structures of PTP catalytic domains share highly conserved features, even though variation exists in the primary structures (Barford et al., 1998; Stuckey et al., 1994; Jia et al., 1995). The PTPs share a common $\alpha + \beta$ tertiary structure of with highly twisted mixed β -sheet flanked by α -helices on both sides (**Figure 5.4**). The PTP active site is located within a $\sim 9\text{-\AA}$ deep crevice on the protein

surface. At the bottom of the active site is the phosphate-binding loop (P-loop) formed by the signature motif. Several loops on the surface of PTP1B surround the active site and influence substrate binding and catalysis (Barford et al, 1994; Jia et al., 1995). For example, a substrate recognition loop contains Arg47 and Tyr46. The Q-loop contains conserved Gln282, which is involved in coordinating and activating an active site water molecule for E-P hydrolysis. A WPD loop is adjacent to the P-loop and contains invariant Asp181 and Trp. Substrate binding triggers a conformational change whereby the WPD loop is brought 10-Å toward the active site, covering it like a flap, and placing Asp181 in close proximity to the scissile oxygen of the substrate. Asp181 acts as a general acid/base in catalysis. The dynamic movement of the WPD-loop to the phosphate-binding site upon substrate binding is supported by resonance Raman and fluorescence spectroscopic studies in addition to deuterium/hydrogen exchange monitored by mass spectrometry (Zhang et al., 1997; Juszczak et al., 1997; Wang et al., 1998).



Figure 5.4 Ribbon diagram of the PTP1B tertiary structure. The image was generated based on the first 2.8-Å resolution crystal structure of human PTP1B (Barford et al., 1994; pdb code: 2HNP), using PyMOL (DeLano, 2002; <http://pymol.org>).

A two-step mechanism for PTP-mediated catalysis has been proposed based on extensive kinetic and crystallographic evidence provided by several research groups. The active site nucleophile is an invariant Cys residue in the PTP signature motif (H/V)C(X₅)R(S/T). The signature sequence forms a semicircular structure about the tyrosyl phosphate group to stabilize the negatively charged phosphoryl group and by an actual ionic bond to the Arg residue in the signature motif (Bradshaw et al., 1998). Site-directed mutagenesis studies reveal that substitution of the Cys residue completely abrogates PTP activity and eliminates the enzyme's ability to form the phosphoenzyme intermediate (Guan and Dixon, 1991). Its unique environment gives the catalytic cysteine a low pK_a, enhancing its role as a nucleophile. The first step of the mechanism

for PTPs involves a nucleophilic attack by the sulfur atom of Cys215, in reference to PTP1B, on the phosphorus atom of the phosphotyrosine substrate (**Figure 5.5**). The invariant Arg221 residue makes bidentate hydrogen bonds with the phosphoryl oxyanions in the substrate through its guanidinium group and plays an important role in both substrate binding and transition state stabilization during hydrolysis. The phosphorus-oxygen bond is cleaved and protonation of the tyrosyl-leaving group is assisted by Asp181 acting as a general acid. This results in formation of a cysteinyl-phosphate catalytic intermediate. The second step involves hydrolysis of the catalytic intermediate to release the phosphate group, which is mediated by a water molecule coordinated to Gln262 and activated by Asp181, functioning as a general base.

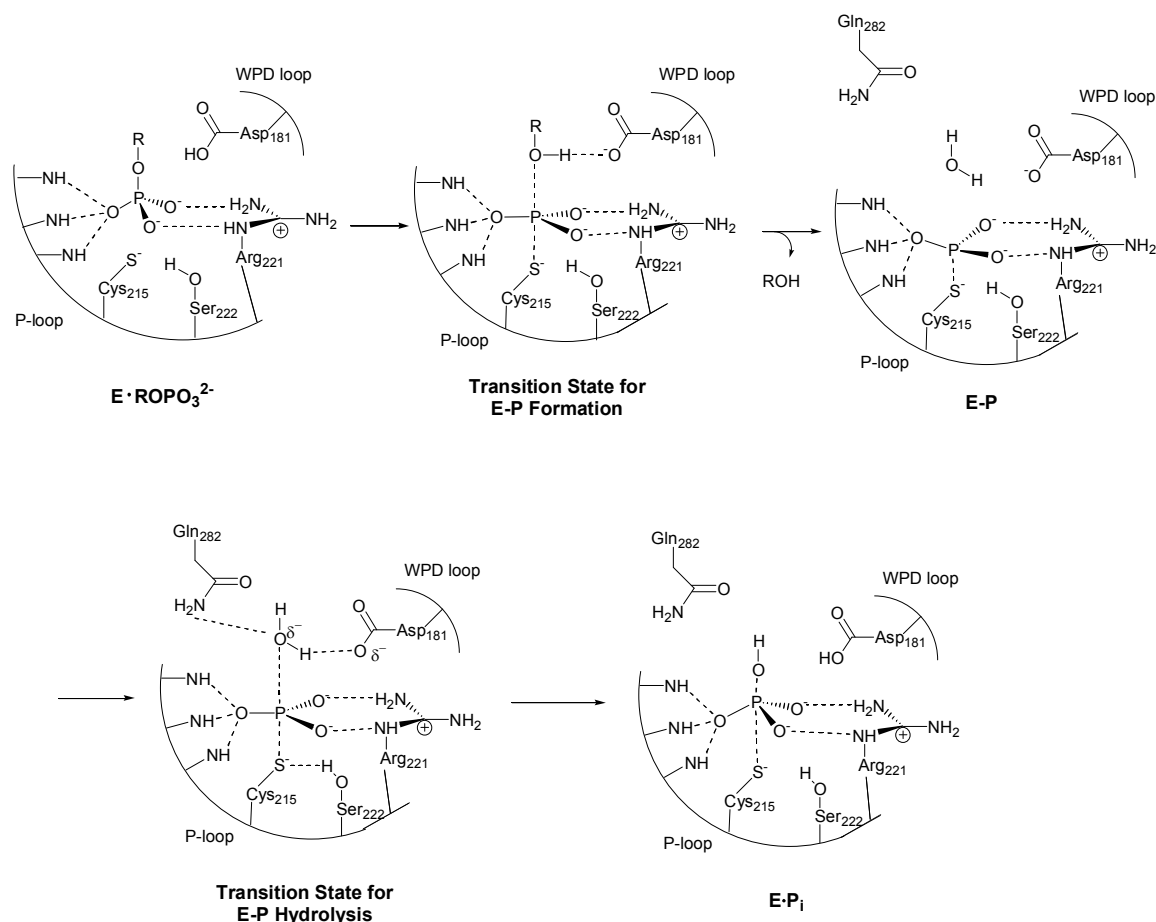
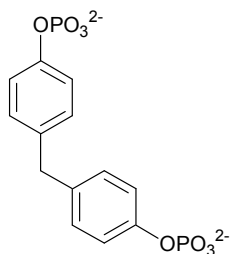


Figure 5.5 Catalytic mechanism and transition state of PTP reaction as proposed by Zhang, Z.-Y. (Zhang, Z.-Y., 2003).

PTP1B also contains a unique second pTyr binding site (Puius et al., 1997). The second site was discovered by co-crystallizing a Cys115Ser mutant PTP1B with bis-(*para*-phosphophenyl) methane (BPPM, **5.1**, **Figure 5.6**). BPPM was one of the highest-affinity low-molecular weight non-peptidic substrates identified for PTP1B at that time. The second site (Arg24 and Arg254) lies within a region that is not conserved among PTPs. As a result, the presence of this second site has been exploited to develop highly specific bidentate inhibitors that are tethered together to bind both the active site and the adjacent noncatalytic site (Zhang et al., 2002).



5.1

Figure 5.6 bis-(*para*-phosphophenyl) methane (BPPM).

5.1.4 PTP1B reversible oxidation

It had been known for a long time that the catalytic cysteine of PTP1B and related classical PTPs are highly susceptible to oxidation *in vitro* and studies require the use of reducing agents such as dithiothreitol (DTT) (Denu et al., 1998). Thus, it had been speculated that oxidation could play a role *in vivo* if PTP1B is exposed to oxidizing agents in the cell. Detailed X-ray crystallographic and kinetic studies provided evidence that such oxidation does indeed occur. The most likely result of oxidation of the catalytic site cysteine would be a stable sulfenic acid derivative (**Figure 5.7**); however, it was most unexpected that the sulfenic acid rapidly transforms into a sulfenyl amide ring involving the adjacent serine residue (Salmeen et al., 2003; van Montfort et al., 2003). This sulfenyl amide is resistant to further oxidation, which would be irreversible, and instead becomes readily reduced back to its catalytically active cysteine form in the presence of a reducing agent such as glutathione (GSH) or DTT.

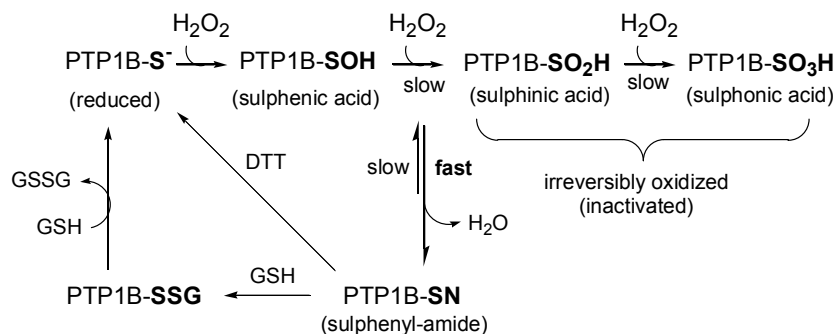
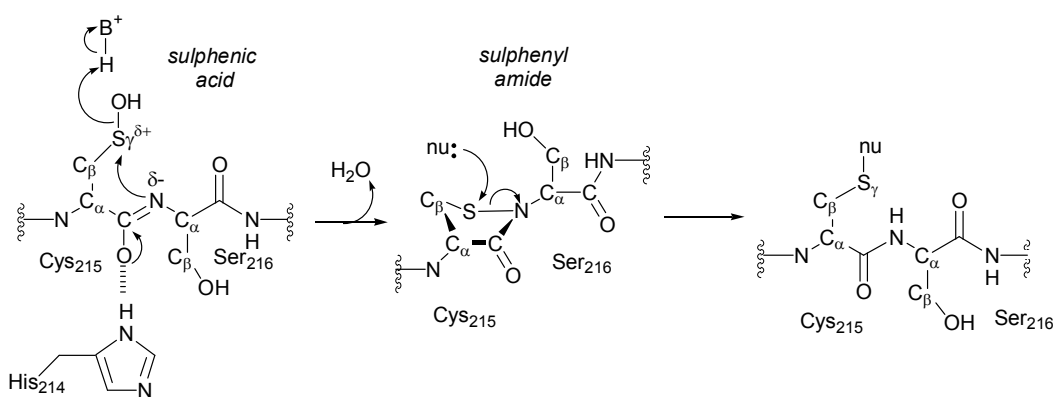
A**B**

Figure 5.7 (A) Schematic illustration of interrelationship of redox states of PTP1B. (B) Proposed mechanism for generating the sulphenyl-amide bond. “Nu” represent a general nucleophilic reducing agent such as glutathione (GSH) or dithiothreitol (DTT).

5.1.5 PTP1B Inhibitor Development

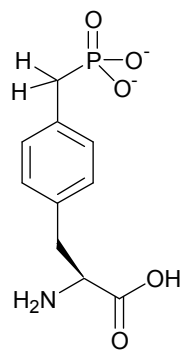
The established role of PTP1B in leptin and insulin signaling has made this enzyme a therapeutic target for the development of inhibitors. One of the challenges in developing PTP1B-based small-molecule therapeutics is selectivity. The conserved nature of the pTyr-binding active site of PTPs has hindered the development of selective inhibitors of PTP1B. However, substrate binding studies have shown that pTyr alone is not sufficient for high-affinity binding and that residues adjacent to the pTyr in a peptide are significant to substrate recognition to PTPs (Zhang, 2002). Another major issue in

developing therapeutics directed at PTP1B is bioavailability. The charged nature of pTyr mimics has reduced their cell permeability and limited their therapeutic application. This has led to an intense search for phosphate mimics that are less highly charged yet still contribute significantly to inhibitor potency when incorporated into a small molecule platform.

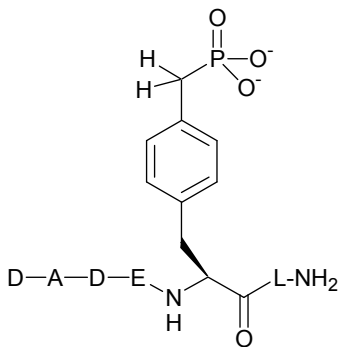
5.1.5.1 Phosphotyrosine mimics

Phosphoryl groups are not suitable for incorporation into potential inhibitors of PTP1B due to the hydrolytic lability of the phosphate ester bond in the presence of other phosphatases in vivo. The design and synthesis of hydrolytically stable phosphotyrosine (pTyr) mimetics has expanded in recent years to the point where it has become almost an entire field of study unto itself and dozens of such mimics have been reported (Burke and Lee, 2003). The most apparent way to overcome phosphoryl hydrolysis is by replacement of the phosphate ester linkage by a stable isostere, or mimic. For example, the phosphonomethyl phenylalanine (Pmp, **5.3**, **Figure 5.8**) has the bridging oxygen atom of a phosphate ester replaced by a methylene group (Marsigne et al., 1988). Incorporation of this group into a peptide **5.4** results in a compound that is stable to enzymatic hydrolysis, however the peptide exhibits a 25-fold lower affinity for PTP1B ($IC_{50} = 200 \mu\text{M}$) compared to its parent compound, **5.2** (Burke et al., 1994). The loss of affinity was suggested to be due to the increase in pK_a and a net reduction in formal charge of the phosphonate whose charge is -1.5 at pH 7, compared to the -2 charge of the phosphate analog. The lower affinity of the phosphonate was also deemed to be due to the loss of hydrogen bonding interactions between the phosphate ester bridging oxygen atom and nearby residues. To overcome the drawbacks of this phosphonate, α -

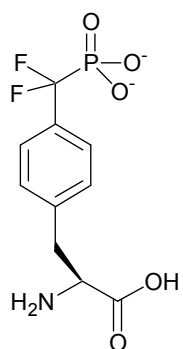
fluorines were introduced onto the bridging methylene group. Incorporating α -fluorines onto aliphatic phosphonates was previously shown to enhance the efficacy of phosphate mimics (Blackburn, 1981; Blackburn, 1983). The development of the α,α -difluoromethylenephosphonic acid (DFMP or F₂Pmp, CF₂PO₃²⁻, **5.5**) group is one of the earliest and still one of the most effective phosphate mimics (Burke et al., 1994; Kole et al., 1995; Chen et al., 1995). A wide variety of potent PTP1B inhibitors, such as peptide **5.6** ($K_i = 24$ nM; Huyer et al., 1998) and small molecule **5.7** ($IC_{50} = 8$ nM; Romsicki et al., 2004), have been prepared bearing this mimic. Overall, the F₂Pmp can exhibit an approximate 1000-fold enhancement in affinity relative to Pmp (Burke et al., 1994). The improvement in affinity of the F₂Pmp-containing peptide over its Pmp analog validated the assumption that pK_a values are important for PTP1B binding. Separate studies on benzylic phosphonates indicated that pK_{a2} values were lowered by one unit for each α -fluorine present (Smyth et al., 1992), such that at pH 7 the F₂Pmp would be completely ionized just as pTyr is at neutral pH. However, subsequent pH studies (Chen et al., 1995), computational studies, and X-ray crystallographic studies (Burke et al., 1996) involving a F₂Pmp-bearing inhibitor complexed to PTP1B strongly suggest that the effect of the fluorines is due to interaction of the fluorines with residues in the active site and is not due to pK_a effects.



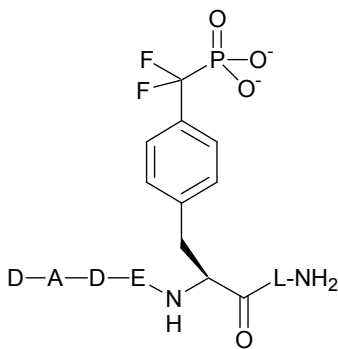
5.3, Pmp



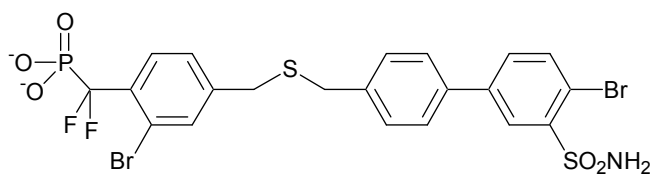
5.4



5.5, F₂Pmp



5.6

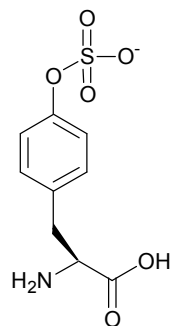


5.7

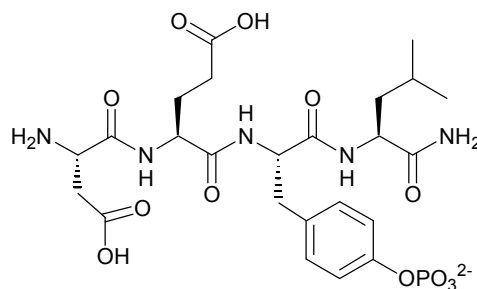
Figure 5.8 Non-hydrolyzable phosphate mimics.

However, the drawback to incorporating the F₂Pmp group into a small molecule or peptidyl platform intended for therapeutic use is the dianionic nature of this mimic, which limits its cell permeability (Burke et al., 2003). An alternative strategy is to develop non-phosphorus-containing pTyr mimics to replicate the phosphate functionality. For example, Desmarais and coworkers examined a series of peptides

bearing sulfotyrosine (**5.8**, sTyr or sY, **Figure 5.9**) as PTP1B inhibitors and found that even relatively simple peptides, such as Ac-DE(sY)L-NH₂, **5.9**, are good reversible competitive inhibitors with IC₅₀ values in the low μM range which indicates that these peptides bind almost as well as the best peptide substrates (Desmarais et al., 1998). These results suggested that the substitution of the phosphorus in pTyr for a sulfur (to sTyr) does not have a serious deleterious effect on ligand binding.



5.8, sTyr



5.9, DE-sY-L-NH₂

Figure 5.9 Sulfotyrosine (sTyr) mimics of phosphotyrosine (pTyr).

Consequently, the Taylor group recently developed difluorosulfonylmethylphenylalanine (F₂Smp, **5.10**, **Figure 5.10**) and demonstrated that is the most effective nonhydrolyzable monoanionic pTyr mimic for PTP1B inhibition when incorporated into the EGF hexapeptide platform, **5.11** (Leung et al., 2002).

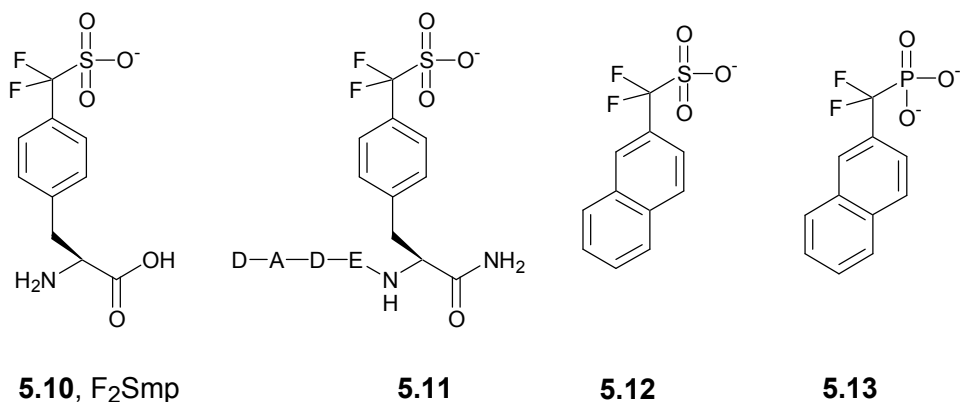


Figure 5.10 Non-hydrolyzable phosphate mimic, difluorosulfonmethylphenylalanine (F₂Smp).

It was reasoned that the F₂Smp group would be an effective monoanionic phosphate mimic for several reasons. For example, it has been shown that peptide **5.6** is almost 1000 times more effective as a pTyr mimic than the corresponding peptide bearing the non-fluorinated analog, **5.4**. Although the F₂Smp-bearing peptide **5.11** was found to be over 100-fold (IC₅₀ = 10 μM) less potent a competitive PTP1B inhibitor than peptide **5.4**, the F₂Smp group is still a much more effective phosphate mimic than other monoanionic mimics that have been evaluated in this hexapeptide platform (Leung et al., 2002; Gao et al., 2000). Interestingly, this 100-fold difference in potency was in stark contrast to the only 6-fold difference in potency between naphthyl sulfonate compound **5.12** (IC₅₀ = 175 μM) and its phosphonate analog **5.13** (IC₅₀ = 35 μM, **Figure 5.10**), two relatively simple non-peptidyl competitive inhibitors (Kotoris et al., 1998). One possible reason for the 100-fold versus 6-fold difference is that the peptide scaffold may be preventing the F₂Smp residue from forming optimal interactions in the active site as suggested by Gao and coworkers for other monoanionic pTyr mimics (Gao et al., 2000). However, neither compound **5.12** nor **5.13** was a highly potent inhibitor and,

consequently, this simple naphthyl platform may not be the most effective platform for assessing the F₂Smp group as a phosphate mimic in a non-peptidyl platform.

Alternative pTyr mimics also include those which bear a carboxylic acid moiety, such as *O*-malonyl tyrosine (OMT, **5.14**, **Figure 5.11**, Kole et al., 1995; Ye et al., 1995) and fluoro-*O*-malonyl tyrosine (FOMT, **5.15**, **Figure 5.11**, Burke et al., 1996), that contain two geminal carboxylic acid groups to replicate the dianionic charge of the phosphate, but which still present challenges to bioavailability. It was proposed that the charged malonyl carboxyl groups could also be synthesized as their ester form, and converted to the free carboxyl groups once inside the cell via the action of cytoplasmic esterases (Ye et al., 1995). However, this did not occur because introducing the OMT-containing peptide to esterase treatment resulted in removal of only one ester (Akamatsu et al., 1995). An improvement in potency of OMT is achieved by translocating one of the carboxylic acid groups from OMT from its geminal position to the aryl 3-position to result in compound **5.16** (**Figure 5.11**, Burke et al., 1998), which has a K_i of 3.6 μM when incorporated into the DADE-X-LNH₂ hexapeptide (Burke et al., 1998; Larsen et al., 2002).

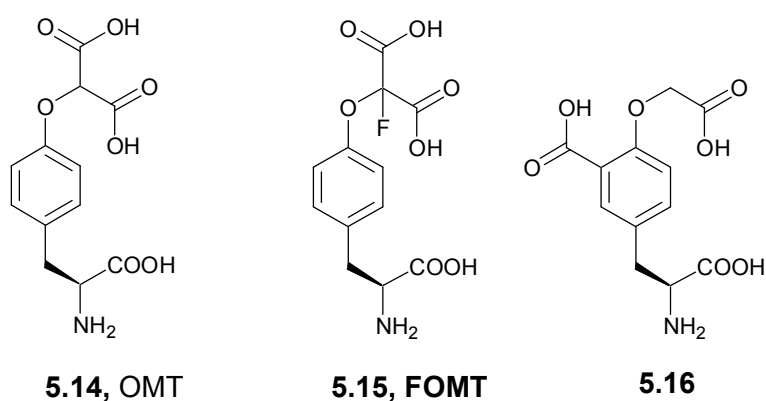
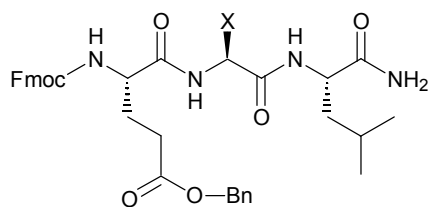


Figure 5.11 Carboxylic acid-containing phosphate mimics.

However, many carboxylic acid-based monoanionic pTyr mimics are not particularly effective in the EGF hexapeptide platform (Gao et al., 2000). Gao and coworkers have provided a possible explanation as to why the D-A-D-E-X-LNH₂ peptides bearing certain pTyr mimics have a poor affinity for PTP1B (Gao et al., 2000). Although the peptide provides beneficial binding contacts with residues outside of the active site, it limits the depth of insertion and freedom of the pTyr mimic within the catalytic pocket. Hence it was suggested that studies using this hexapeptide platform may not allow one to assess the true effectiveness of certain pTyr mimics (Gao et al., 2000). More recently, Lee and coworkers demonstrated that a wide variety of monoanionic and dianionic pTyr mimics exhibiting poor affinity for PTP1B in the hexapeptide platform were considerably more effective in tripeptide platforms such as Fmoc-Glu(OBn)-X-LNH₂ (**5.17**, **Figure 5.12**; Lee et al., 2003; Lee et al., 2005). *Fmoc* and *Bn* are abbreviations for 9*H*-fluoren-9-ylmethoxycarbonyl and benzyl, respectively, and are protecting groups commonly used in solid phase peptide synthesis (SPPS). However, none of the candidates examined in the **5.17** tripeptide platform were as potent as the F₂Pmp-bearing hexapeptide (Lee et al., 2003; Lee et al., 2005). Similar results were also found when these tripeptides were examined as inhibitors of PTP from *Yersinia pestis* (YopH). On the basis of these results, it was suggested that certain monoanionic COOH-based pTyr mimics, which were considered to be of limited utility based on the hexapeptide studies, were indeed good pTyr mimics (Lee et al., 2003). The difference in potency between several of the monoanionic and dianionic mimics studied by Lee et al., when incorporated into the tripeptide mentioned above, was surprisingly small. Indeed, tripeptides bearing monoanionic carboxylic acid-based mimics exhibited

affinities for PTP1B only 2-3-fold greater than the analogous F₂Pmp-bearing tripeptide (Lee et al., 2003; Lee et al., 2005).



5.17, Fmoc-Glu(OBn)-X-L-NH₂

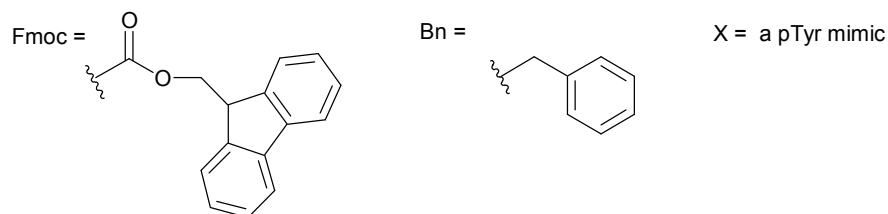


Figure 5.12 Tripeptide display platform examined by Lee and coworkers (Lee et al., 2003; Lee et al., 2005)

5.1.5.2 Bidentate ligands

The design of bidentate ligands that bind in both the PTP catalytic site and the unique adjacent site has enhanced affinity and specificity against other PTPs. Potent bidentate ligands has been discovered through library screening (Shen et al., 2001). One of the first libraries screened was comprised of compounds containing a pTyr group to ensure biased association with the pTyr recognition active site. The pTyr compounds were linked by a set of 23 structurally diverse linkers to a structurally diverse set of eight aryl acids designed to potentially interact with the second subsite. The library was screened against a mutant PTP1B expressing a catalytically inactive Cys215Ser site-directed substitution, as the pTyr-containing compounds are hydrolyzable. The candidate with the greatest affinity for the mutant PTP1B was identified and the non-hydrolyzable F₂Pmp analog, compound **5.18** (**Figure 5.13**) was synthesized and assayed

against wild-type PTP1B. The result was the most potent PTP1B inhibitor identified to date, with a K_i of 2.4 nM. It was also the most selective inhibitor, exhibiting a selectivity of 1000- to 10,000-fold preference for PTP1B in a panel of other PTPs (Shen et al., 2001). One exception in the panel was T-cell PTP (TCPTP), which has a 77% identical sequence homology to PTP1B. Only a 10-fold selectivity was observed for PTP1B over TCPTP. Because compound **5.18** carries five negative charges at neutral pH, it would not be likely to cross a cell membrane. Cell permeability was improved by introducing a highly lipophilic fatty acid group to compound **5.18** to form compound **5.19** (**Figure 5.13**, Xie et al., 2003), and also by introducing the cell penetrating peptide, (D)Arg₈, via disulfide bridge to form **5.20** (**Figure 5.13**; Lee et al., 2005). A pro-drug approach based on **5.18** was also used to address cell permeability (Boutselis et al., 2007). Prodrugs are designed to mask the negative charge enabling the compound to pass through the cell membrane, and once inside the cell, the protecting group is hydrolyzed to regenerate the original intended inhibitor. Compound **5.21** was prepared and studied for cellular delivery of a phosphonate-based compound (**Figure 5.13**). Studies with each of these cell permeable compounds showed that they can increase insulin signaling and result in improved insulin-stimulated glucose uptake (Xie et al., 2003; Lee et al., 2005; Boutselis et al., 2007).

To understand the structural basis for the selectivity of compound **5.18** for PTP1B over other PTPs, a derivative, **5.22** (**Figure 5.13**), was synthesized and studied. Structural analysis of the interactions between PTP1B and **5.22** revealed that the nonhydrolyzable F₂Pmp occupies the pTyr-binding active site while the distal 4-phosphonodifluoromethyl phenylacetyl group participates in van der Waals and ionic

contacts with a proximal non-catalytic site lined by Lys41, Arg47 and Asp48. In comparison to other PTPs, the residues of PTP1B interacting with compound **5.22** are not unique, however, it is reasoned that it is the combination of all contacts which impart selectivity (Sun et al., 2003).

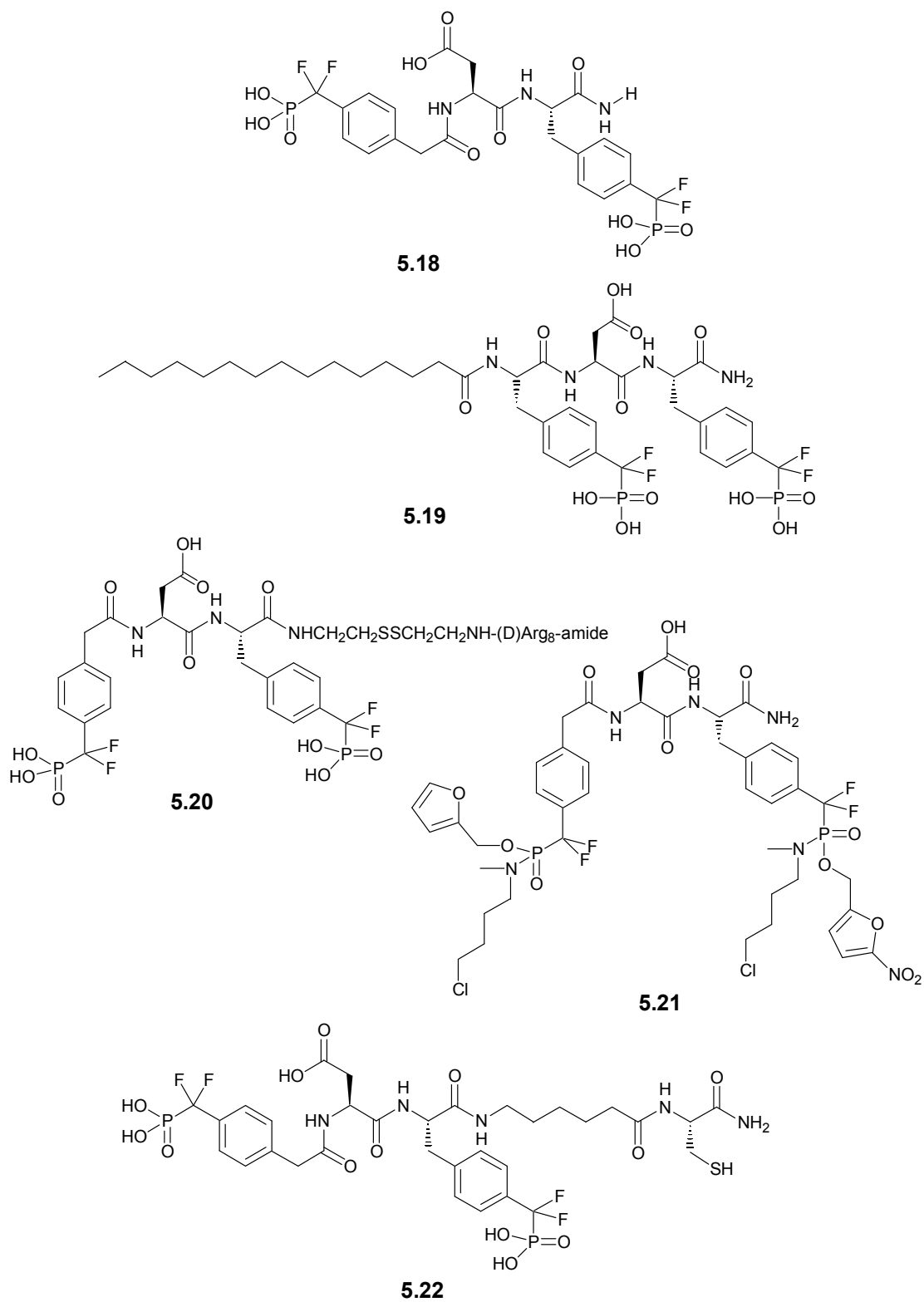


Figure 5.13 Bidentate ligands developed as inhibitors of PTP1B.

More recent development of dual site inhibitors of PTP1B has involved rational design efforts that led to the discovery of the 1,2,5-thiadiazolidin-3-one-1,1-dioxide group as a novel pTyr mimic (Black et al., 2005). The compound was incorporated into a dipeptide structure shown as **5.23** and has a K_i of 0.19 μM (Figure 5.14; Combs et al., 2005). Further development of the isothiazolidinone group as a pTyr mimic led to compound **5.24** which has an IC_{50} of 40 nM (Figure 5.14, Yue et al., 2006). Non-peptidyl inhibitors bearing the isothiazolidinone group were also developed to improve cell permeability and oral bioavailability. One particularly good example of a candidate is compound **5.25** (Figure 5.14), which displayed an IC_{50} of 35 nM. It was also able to cross the cell membrane and increase phosphorylation of the insulin receptor (Combs et al., 2006).

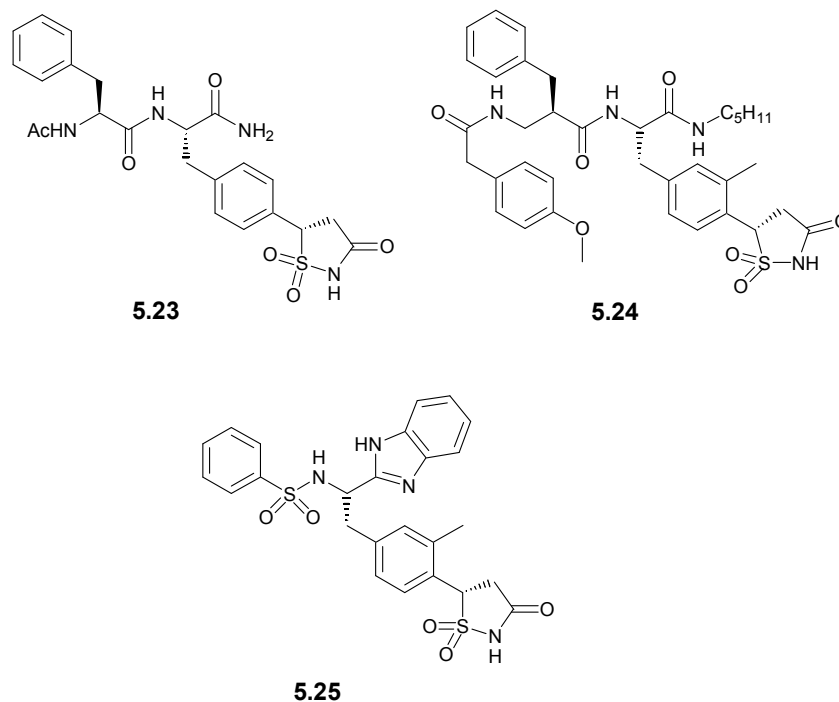
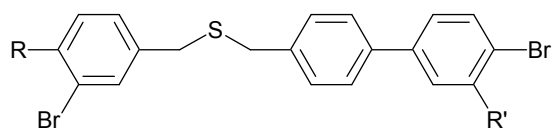


Figure 5.14 Isothiazolidinone-based inhibitors of PTP1B.

5.1.5 Objectives

As discussed in section 5.1.4.1, the Taylor group previously examined the difluoromethyl sulfonic acid (**5.9**, F₂Smp, -CF₂SO₃⁻, **Figure 5.10**) group as a phosphate mimic for PTP1B inhibition (Kotoris et al., 1998; Leung et al., 2002). The first objective of the studies presented in this chapter is to make a more complete assessment of the F₂Smp group as a phosphate mimic for PTP1B inhibition, by replacing the F₂Pmp group in a potent a non-peptidyl competitive inhibitor, such as compound **5.7** (**Figure 5.8**; Romsicki et al., 2004), with a F₂Smp group and then we will compare their inhibitory potencies. Here I describe inhibition studies of inhibitor **5.7**, its F₂Smp analog **5.26**, and its non-fluorinated methylenesulfonyl analog **5.27**. The development of two other derivatives, **5.28** and **5.29**, in which the sulfonamide moiety in compounds **5.7** and **5.26** is replaced with a difluoromethylenesulfonamide group, is also described. Inhibition studies with these compounds and PTP1B reveal surprising results concerning the use of benzylic sulfonates as PTP1B inhibitors.



5.26, R = CF₂SO₃⁻¹, R' = SO₂NH₂

5.27, R = CH₂SO₃⁻¹, R' = SO₂NH₂

5.28, R = CF₂PO₄⁻², R' = CF₂SO₂NH₂

5.29, R = CF₂SO₃⁻¹, R' = CF₂SO₂NH₂

Figure 5.15 Structure of proposed sulfonate and difluorosulfonate inhibitors.

The second set of studies presented here have the objective to examine the inhibition potency of a neutral phosphotyrosine mimic when incorporated into the tripeptide, Fmoc-Glu(OBn)-X-LNH₂ (**5.17**, **Figure 5.12**), in comparison to its

incorporation into the more commonly used peptide for examining phosphate mimics, DADE-X-LNH₂. As mentioned in section 5.1.4.1, Lee and coworkers observed that the potency between several monoanionic and dianionic mimics incorporated into the tripeptide, **5.17**, was surprisingly small (Lee et al., 2003). These results lead one to question whether a neutral pTyr mimic could also be effective in the tripeptide platform. An effective neutral pTyr mimic would be very useful in increasing the bioavailability of PTP inhibitors. Neutral pTyr mimics are rare. Researchers at Sugen have suggested, on the basis of studies with nonpeptidyl PTP1B inhibitors, that the trifluoromethylsulfonamido group is an effective neutral phosphate mimic (Huang et al., 2003). We chose to examine the sulfonamide **5.30** (Figure 5.16) as a potential pTyr mimic. The sulfonamide group has found widespread use as a pharmacophore in medicinal chemistry and numerous bioactive agents bear this functionality (Bowman et al., 1979). It has a geometry similar to that of the phosphate group yet does not bear a negative charge.

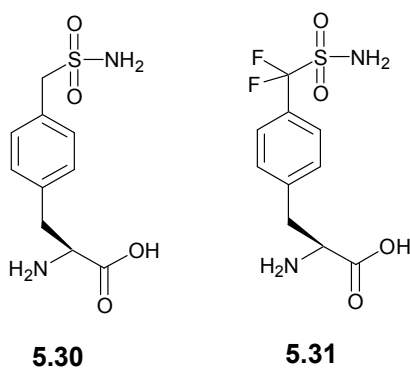


Figure 5.16 Phosphotyrosine mimics.

Recently, Chen and coworkers reported the development of amino acid **5.30** and its incorporation into the D-A-D-E-X-L-NH₂ platform (Chen et al., 2003). Although this peptide was found to be a very poor inhibitor of PTP1B, this amino acid was never

examined as a pTyr mimic in the Fmoc-Glu(OBn)-X-LNH₂ platform (**5.17**, **Figure 5.12**), where the potential constraints of the hexapeptide platform mentioned above may not be as severe. As previously mentioned, Burke and co-workers have shown that peptides bearing F₂Pmp can be up to 1000-fold more potent PTP1B inhibitors than their nonfluorinated analogues (Burke et al., 1994; Kole et al., 1995; Chen et al., 1995). Consequently, the fluorinated analogue of **5.30**, compound **5.31** (**Figure 5.16**), will be examined as a pTyr mimic. Here, I report the evaluation of amino acids **5.30** and **5.31** incorporated into the hexapeptide platform to make peptides **5.32** and **5.33** (**Figure 5.17**). Amino acids **5.30** and **5.31** were also incorporated into the tripeptide platform, **5.17**, described above to yield **5.34** and **5.35** (**Figure 5.17**) and were examined as inhibitors of PTP1B.

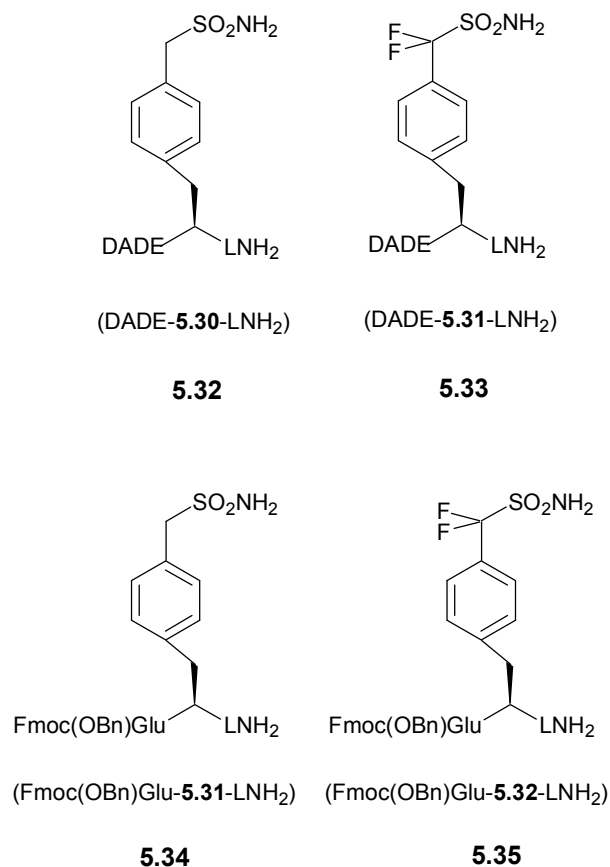


Figure 5.17 Proposed inhibitors of PTP1B.

5.2 Results and Discussion

5.2.1 Inhibition studies with compounds 5.26-5.29

IC₅₀ determinations were carried out under conditions similar to those reported by Merck Frosst for compound **5.7** (50 mM Bis-Tris HCl buffer, pH 6.3 containing 2% glycerol, 0.1% Triton X-100, 4% DMSO, 4.5 mM DTT and 1.8 mM EDTA; Romsicki et al., 2004; Montalibet et al., 2005) with the only significant difference being the presence of 4% DMSO and that 6,8-difluoro-4-methylumbelliferyl phosphate (diFMUP, **5.36**, see § 5.4.3, **Figure 5.23**) was used as substrate at K_m concentration (5 μ M; Montalibet et al., 2005). It should be noted that although only compound **5.29**, a relatively hydrophobic compound, required the presence of 4% DMSO in the assay mix for solubilization, we elected to have 4% DMSO present for assaying all of the compounds so that a direct comparison between the IC₅₀ values could be made. The IC₅₀ for compound **5.7** under our conditions (6 nM) is similar to that reported by Merck Frosst for this compound (8 nM) in the absence of DMSO which indicates that the presence of 4% DMSO in the assay mixture does not significantly affect ligand binding. Moreover, the K_m of the substrate, diFMUP, under our conditions was found to be the same (5 μ M) as that determined by Merck Frosst in the absence of DMSO. Although none of the new compounds (**5.26–5.29**) were as potent as the parent compound **5.7**, some surprising and informative results were obtained (**Table 5.1**). Compound **5.26** is a 1000-fold less potent inhibitor than its phosphonate analog, compound **5.7**. This large difference in potency prompted us to examine whether the modality of inhibition of sulfonate **5.26** was different from that of competitive inhibitors **5.7**, **5.12**, **5.13** and **5.26**. However, sulfonate **5.26** also behaved as a mainly competitive inhibitor with a K_i of

10.6 μM and inhibition was reversible (**Figure 5.18**). Surprisingly, inhibition studies with the nonfluorinated analog of inhibitor **5.26**, compound **5.27**, revealed that it has an IC_{50} that is almost the same as that of compound **5.26**.

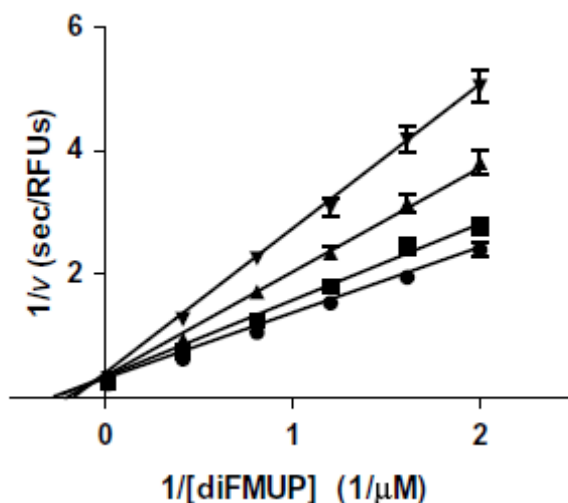


Figure 5.18 Lineweaver-Burk plot for the inhibition of PTP1B with inhibitor **5.26** in 50 mM Bis-Tris HCl, pH 6.3, 20% glycerol, 5 mM DTT, 2 mM EDTA, 0.1% Triton X-100. (●) 0 μM , (■) 5 μM , (▲) 10 μM , (▼) 20 μM . See Appendix C for replot to determine K_i .

Table 5.1 Inhibition of PTP1B with compounds **5.7** and **5.26-5.29**.

Compound	IC_{50} (μM)	K_i (μM)
5.7	0.0060 ± 0.0004	ND
5.26	13 ± 3	10.6 ± 0.4
5.27	19 ± 3	10.3 ± 1.8
5.28	0.030 ± 0.002	0.024 ± 0.003
5.29	6.0 ± 0.4	3.3 ± 0.5

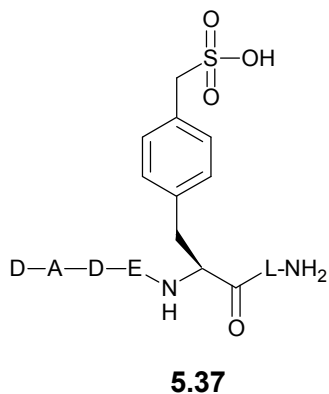


Figure 5.19 Structure of peptide **5.37**.

More detailed studies with inhibitor **5.27** revealed that it too is a competitive inhibitor with a K_i of 10.3 μM which is essentially the same as that of compound **5.26**. The non-fluorinated analog of peptide **5.9**, peptide **5.37** (**Figure 5.19**), was never examined as a PTP1B inhibitor. However, the non-fluorinated analog of inhibitor **5.12** exhibited only 10% inhibition at 500 μM (Kotoris et al., 1998) which indicates that the fluorines in inhibitor **5.12** contribute significantly to the binding of compound **5.12** to PTP1B. Therefore, we had assumed that the fluorines in peptide **5.9** were also making a significant contribution to the potency of this peptide. To determine if this is indeed the case, we prepared peptide **5.37** and examined it, as well as peptide **5.9**, as PTP1B inhibitors under the conditions described above. Under these conditions, peptide **5.9** exhibited an IC_{50} of 24 μM . Most significantly, the IC_{50} of peptide **5.37** was 44 μM , which is less than two-fold higher than that of peptide **5.9**. Thus, our previous assumption that the fluorines in peptide **5.9** contributed significantly to its potency was incorrect. The inability of the fluorines in inhibitors **5.9** and **5.12** to make beneficial contacts with active site residues may partly explain the very large (100- to 1000-fold) difference in potency between these compounds and their F_2Pmp analogs. It is also

possible that this large difference in potency between the S₂Pmp and F₂Pmp inhibitors is because the F₂Pmp group is dianionic at pH 6.5 and PTP1B prefers to bind the dianionic F₂Pmp-based inhibitors as opposed to the monoanionic S₂Pmp-based inhibitors. However, as mentioned earlier, previous studies suggest that PTP1B binds the monoanionic and dianionic forms of F₂Pmp-bearing inhibitors equally well (Chen et al., 1995; Burke et al., 1996). On the other hand, compound **5.12** is much smaller than peptide **5.9** and compound **5.26**, and so compound **5.12** may have greater freedom of motion in the active site. If so, then this may allow the fluorines in inhibitor **5.12** to make some beneficial contacts with active site residues while residues in peptide **5.9** and moieties in compound **5.26** outside the active site may restrict the mobility of the aryl-S₂Pmp group in the active site which could limit the ability of the fluorines to make beneficial contacts. It is worth mentioning that, with the exception of sulfonodifluoromethylphenylalanine (in peptide **5.9**), sulfonomethylphenylalanine (in peptide **5.33**) is a considerably more effective pTyr mimic than other monoanionic pTyr mimics that have been examined in this hexapeptide (DADE-X-LNH₂, X = pTyr mimic) platform (Gao et al., 2000). In compounds **5.28** and **5.29** the sulfonamide moiety in compounds **5.7** and **5.26** is replaced with a difluoromethylenesulfonamide group. This modification was pursued since this allowed us to increase the hydrophobicity of these compounds while at the same time lowering the p*K*_a of the sulfonamide by about three orders of magnitude (from 10.5 to 7.5) by making just a minor structural change (Trepka et al., 1974; Blackburn et al., 2005). Phosphonate inhibitor **5.28** exhibited a 5-fold increase in IC₅₀ compared to compound **5.7** (**Table 5.1**). Further studies revealed that **5.28** is a competitive inhibitor with a *K*_i of 24 nM, still a very potent inhibitor. However,

sulfonate **5.29** exhibited a slight decrease in IC_{50} compared to sulfonate **5.26** (Table 5.1). Moreover, inhibitor **5.29** exhibited reversible mixed inhibition (Figure 5.20) with a K_i of 3.3 μM and an αK_i of 12.5 μM indicating that this more hydrophobic compound is probably binding somewhat differently to PTP1B compared to compound **5.28** and this may account for their different trends in K_i values.

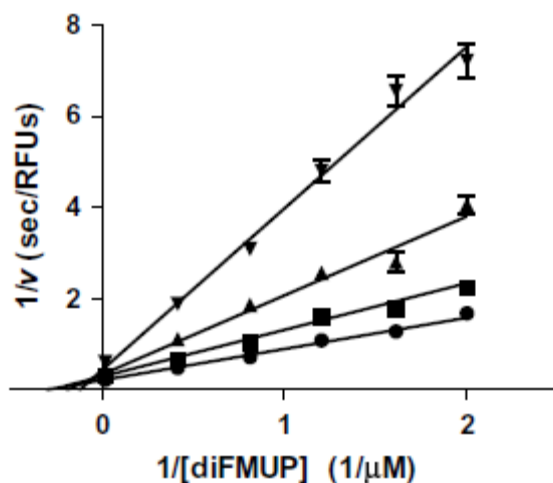


Figure 5.20 Lineweaver-Burk plot for the inhibition of PTP1B with inhibitor **5.29** in 50 mM Bis-Tris HCl, pH 6.3, 20% glycerol, 5 mM DTT, 2 mM EDTA, 0.1% Triton X-100. (●) 0 μM , (■) 2.5 μM , (▲) 5 μM , (▼) 10 μM . Please see Appendix C for replot to determine K_i .

Although monoanionic inhibitors **5.26**, **5.27**, and **5.29** are considerably less potent than their phosphonate counterparts, they compare favorably, in terms of their affinity for PTP1B, to the majority of the best non-peptidyl monoanionic PTP1B inhibitors that have been reported in the literature. Amarasinghe and coworkers reported a monoanionic sulfamide PTP1B inhibitor with an IC_{50} of 2.3 μM though the mode of inhibition was not reported (Figure 5.21, Amarasinghe et al., 2006). Researchers at Abbott have reported monoanionic inhibitors bearing either a 2-(hydroxyphenoxy)phenyl acetic acid moiety or a isoxazole carboxylic acid group with

K_i values of 6–9 μM (**Figure 5.21**, Xin et al., 2006; Liu et al., 2003). Researchers at Sunesis have reported a monoanionic pyrazine carboxylic acid-based PTP1B competitive inhibitor with a K_i of 4 μM (**Figure 5.21**, Erlanson et al., 2003).

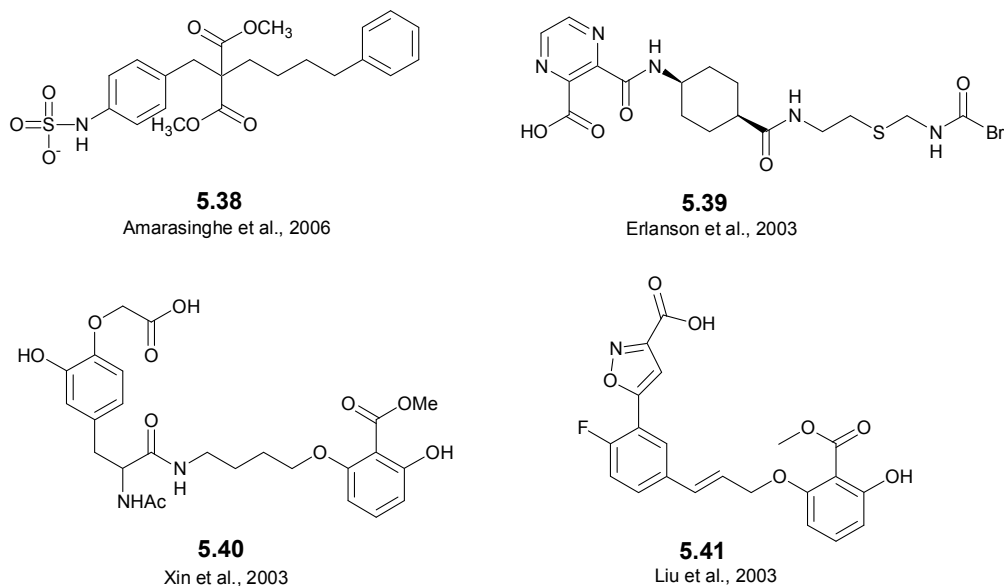


Figure 5.21 Examples of monoanionic inhibitors of PTP1B recently reported in literature.

However, it should be noted that neither our sulfonate inhibitors nor any of the other above mentioned monoanionic inhibitors are as potent as the monoanionic inhibitors bearing the (S)-isothiazolidinone phosphate mimic recently reported by workers at Incyte (**Figure 5.14**, Douty et al., 2008). Although the (S)-isothiazolidinone phosphate mimic has never been examined in the DADE-X-LNH₂ platform, studies with other smaller peptides as well as with non-peptidyl compounds bearing this moiety suggest that it is the most effective monoanionic phosphate reported to date and appears to be even more effective than the F₂Pmp group.

5.2.2 Inhibition studies with compounds 5.32-5.35, 5.11, 5.42, 5.43.

IC₅₀ values of compounds 5.32 to 5.35 and 5.42 to 5.43 with PTP1B were performed in bis-tris buffer at pH 6.5, containing 15 mM NaCl, 2 mM EDTA, 0.001% Triton X-100 and 7.5% DMSO using 6,8-difluoro-4-methylumbelliferyl phosphate (5.36, diFMUP, see § 5.4.3, Figure 5.23) as substrate at *K_m* concentration. IC₅₀ values are given in Table 5.2 (See appendix C for IC₅₀ curves). Hexapeptides 5.32 and 5.33 showed no inhibition even at 1.0 mM. These results are consistent with those of Chen et al. concerning peptide 5.32, which showed that this compound was a very poor inhibitor of PTP1B (Chen et al., 2003).

Table 5.2. Inhibition of PTP1B with peptides 5.32-5.35, 5.42, 5.43, and 5.11.

Compound	Peptide	IC ₅₀ (μM)
5.32	DADE-5.30-LNH ₂	0% inhibition at 1 mM
5.33	DADE-5.31-LNH ₂	0% inhibition at 1 mM
5.34	FmocGlu(OBn)-5.30-LNH ₂	3.4 ± 0.4
5.35	FmocGlu(OBn)-5.31-LNH ₂	6.4 ± 1.0
5.42	FmocGlu(OBn)-5.10-LNH ₂	7.4 ± 1
5.11	DADE-5.10-LNH ₂ ^a	10 ± 1 ^a
5.43	FmocGlu(OBn)-Phe-LNH ₂	4.1 ± 1.0

^a From Leung et al., 2002.

However, tripeptides 5.34 and 5.35 exhibited IC₅₀ values of 3.4 and 6.4 μM, respectively. Clearly, the fluorines in peptides 5.33 and 5.35 had little or no impact on inhibitor potency. We also prepared tripeptide 5.42 bearing F₂Smp (5.10) and found that it exhibited an IC₅₀ similar to 5.34 and 5.35 as well as hexapeptide 5.11 (Leung et al., 2002). Indeed, the IC₅₀ values for tripeptides 5.34, 5.35, 5.42 are, in general, not significantly different from those reported by Lee et al., for a variety of monoanionic carboxylic acid-based pTyr mimics, as well as F₂Pmp (5.5), in the same tripeptide platform (Lee et al., 2003). The similarity of the IC₅₀ values of tripeptides 5.34 and 5.35

to tripeptide **5.42** and to those of Lee et al., prompted us to question if the pTyr mimics were contributing at all to the potency of the tripeptides. An examination of the data reported by Lee et al., revealed that tripeptide FmocGlu(OBn)-Phe-LNH₂ (**5.43**), a control in which no phosphate mimic is present on the phenylalanine side chain, had not been evaluated as a PTP1B inhibitor. Therefore, we synthesized peptide **5.43** and evaluated it as a PTP1B inhibitor. This peptide exhibited an IC₅₀ of 4.1 μM which is similar to the IC₅₀ values for **5.34**, **5.35**, and **5.42** and many of the tripeptides reported by Lee et al., with PTP1B. This result raises the possibility that the phosphate “mimic” portion of the tripeptide inhibitors contributes little or not at all to their inhibitory potency. It is possible that the phosphate-mimicking portion of these tripeptides does not bind or binds very poorly in the active site or elsewhere on the protein and that the majority of the binding energy is a result of the interaction of a hydrophobic group on the inhibitor with a hydrophobic region on the protein. Lee et al. have recently shown that the presence of a hydrophobic aromatic hydrocarbon moiety at the N-terminus was important for obtaining good PTP1B inhibition with their tripeptides (Lee et al., 2005).

Lee et al. examined in some detail the inhibition kinetics of the outer membrane phosphatase derived from *Yersinia pestis* (YopH) with tripeptide **5.44** (**Figure 5.22**) which has an IC₅₀ of 1.8-2.8 μM with PTP1B (Lee et al., 2003; Lee et al., 2005). It did not exhibit a strictly competitive mode of inhibition. It showed a steep IC₅₀ curve with a slope factor of 3-5 depending upon the enzyme concentration suggesting that more than one molecule of inhibitor binds to YopH. IC₅₀ values increased as the concentration of YopH increased. They also observed a time dependency in that preincubation with YopH for 5 minutes decreased the IC₅₀ from 3.2 to 1.5 μM. Treatment of YopH with

200 μM inhibitor **5.44** for 30 minutes followed by dilution into excess substrate resulted in a 40% loss of activity. It is interesting to note that some of these phenomena were also encountered with hydrophobic inhibitor **5.45** (Figure 5.22) and PTP1B in that it too displayed time-dependent inhibition and non-classical inhibition patterns (Johnson et al., 2002; Wrobel et al., 1999). Using **5.42** as a model inhibitor, we have found that some of the above phenomena encountered with **5.44** and **5.45** also occur with PTP1B. A Lineweaver-Burk plot did not exhibit classical inhibition patterns and we were unable to determine a K_i from the plot. The IC_{50} values depended upon PTP1B concentration. At 1.5 nM enzyme, the IC_{50} of **5.42** was 4.3 μM while at 12 nM enzyme the IC_{50} increased to 12 μM , however, the slope factors were 1.2-1.4. We did not observe a significant time dependence upon inhibition. We also examined the reversibility of inhibition by incubating 150 nM PTP1B with 50 μM of **5.42** for either 15 seconds or 60 minutes and then diluting the mixture 50-fold into a solution containing 1.0 mM diFMUP (**5.36**) and assaying enzyme activity. In each case, only 5-10% of the activity was recovered. Moreover, even after extensive dialysis, no activity was recovered. As pointed out by Lee et al., and others, these results are consistent with the properties associated with nonspecific promiscuous inhibitors (McGovern et al., 2002; McGovern et al., 2003). Recent studies have shown that enzyme inhibition can occur due to a process of colloid formation (McGovern et al., 2002; McGovern et al., 2003). Dynamic light scattering measurements by Lee et al., on one of their FmocGlu(OBn)-X-LNH₂ tripeptides bearing a monoanionic pTyr mimic suggested that colloid formation was not occurring. Although inhibition by colloid formation has never been demonstrated to occur with PTP1B inhibitors of any kind, such a phenomenon cannot be ruled out with the

tripeptides examined here or others examined by Lee and coworkers. However, these researchers also point out that some of the observed effects are not as pronounced as previously reported for promiscuous inhibitors (Lee et al., 2003).

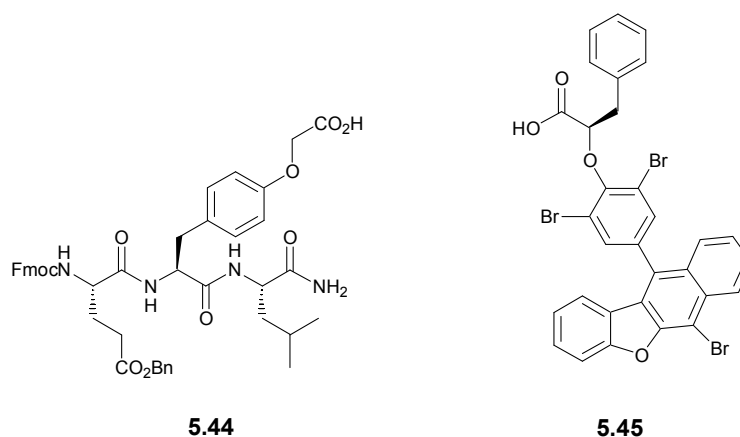


Figure 5.22 Tripeptide inhibitor **5.44** of YopH and PTP1B and a hydrophobic inhibitor **5.45** of PTP1B.

5.3 Conclusions and Future Work

The F₂Smp-bearing inhibitor **5.26** was a much less potent PTP1B inhibitor than phosphonate **5.7**. Replacing the distal sulfonamide moiety with a difluoromethylenesulfonamide group in compound **5.7** did not yield a more potent inhibitor though this substitution in compound **5.26** did yield a slightly better inhibitor. Surprisingly, inhibition studies with the non-fluorinated sulfonates, compound **5.27** and peptide **5.37** bearing sulfonomethylphenylalanine, revealed that the fluorines had little effect on the potency of the F₂Smp-bearing inhibitors which was in contrast to our previously held assumption that the fluorines in F₂Smp-bearing inhibitors contributed significantly to their potency. This may in part explain the large difference in potency between the F₂Smp and F₂Pmp bearing compounds. These results also show that

sulfonodifluoromethylphenylalanine (Liu et al., 2001), is one of the best monoanionic pTyr mimics reported so far when examined in the context of the DADE-X-LNH₂ platform.

Although the tripeptides bearing the pTyr mimics, **5.30** and **5.31**, were relatively good inhibitors, our results suggest that the phosphate mimicking portion of the tripeptides may not be contributing significantly to their potency. Moreover, studies with inhibitor **5.42** reveals that this class of tripeptide inhibitor exhibits nonclassical inhibition patterns with PTP1B. As mentioned above, it has been suggested that the hexapeptide platform may limit the depth of insertion and freedom of the pTyr mimic within the catalytic pocket and this may result in artificially low potencies for certain pTyr mimics (Gao et al., 2000; Lee et al., 2003). These results do not suggest that this hypothesis is incorrect though they do raise serious questions as to the value of the FmocGlu(OBn)-X-LNH₂ peptide as a platform for assessing pTyr mimics for PTP1B inhibition. Indeed, our results emphasize an important point about assessing pTyr mimics in any platform in that it is prudent to compare the platform bearing the pTyr mimic to the analogous structure lacking the phosphate mimicking portion.

Although amino acids **5.30** and **5.31** were not good pTyr mimics for PTP1B, they may also prove to be useful in the development of inhibitors and probes of other enzymes. Chen et al. have shown that peptide **5.32** was a modest inhibitor of *Yersinia* PTP (Chen et al., 2003). The presence of fluorines α to the sulfonamide moiety might enhance its potency with *Yersinia* PTP. It is also worthy of note that tyrosine sulfation has been recognized as an important post-translational modification (Kehoe et al., 2000). The growing list of proteins that bind to sulfotyrosine include viral proteins that

recognize sulfated receptor proteins on cell surfaces (Farzan et al., 1999; Farzan et al., 2000). Hence, a need has also arisen for hydrolytically stable sulfotyrosine mimics. We have recently demonstrated that the difluoromethylenesulfonamide group is a relatively good nonhydrolyzable replacement of the sulfate group in estrone sulfate in that this species is a relatively good reversible inhibitor of steroid sulfatase (Liu et al., 2005). Thus, amino acid **5.31** may prove to be an effective sTyr mimic and useful in the development of inhibitors of protein-protein interactions.

5.4 Experimental

5.4.1 Materials

HiTrapTM Blue and HiTrapTM Q were obtained from Amersham Pharmacia Biotech. A pFLAG plasmid expressing the catalytic domain (residues 1-298) of human PTP1B was a generous gift from Merck Frosst Centre for Therapeutic Research, Pointe-Claire-Dorval, QC. Compounds **5.26-5.29** were synthesized by Munawar Hussain of the Taylor group. Compounds **5.32-5.35** were synthesized by Dr. Bryan Hill of the Taylor group. Centrifugation was performed using a Beckman Avanti J-25I centrifuge (Mississauga, ON) or a Beckman Coulter Avanti JE centrifuge (Fullerton, CA, USA).

5.4.1 Purification of PTP1B

A pFLAG plasmid expressing the catalytic domain (residues 1–298) of human PTP1B was expressed in BL21 (DE3) cells and purified according to a two-step purification protocol (HiTrapTM blue affinity column and HiTrapTM Sepharose Q anion exchange column) previously described by Asante-Appiah (Assante-Appiah et al., 2001). Cells were grown at 37°C and 250 r.p.m. to an optical density (OD) of 0.7 at 600 nm in Luria Bertani (LB) broth supplemented with 100 mg/ml ampicillin (LB-Amp).

The culture was then induced by addition of isopropyl-1-thio- β -D-galactopyranoside (IPTG) to a final concentration of 1 mM. Cells were harvested 3 h post-induction. Bacteria cells were dissolved in lysis buffer containing 20 mM tris, pH 7.5, 0.1 mM EDTA, 5 mM dithiothreitol (DTT), 10 μ M phenylmethansulfonyl fluoride (PMSF) and protease inhibitors (CompleteTM Protease Inhibitor Cocktail, Roche). Lysis was achieved by passage through a high-pressure homogenizer cell. The supernatant was retained following centrifugation of the cell lysate and applied to a HiTrapTM blue affinity column (5 mL volume) equilibrated in 20 mM tris, pH 7.5, 0.1 mM EDTA, 5 mM DTT. Following a five-column volume wash in equilibration buffer, elution was performed in ten column volumes of a linear gradient of 20 mM tris, pH 7.5, 0.1 mM EDTA, 2 M NaCl, 5 mM DTT, the active fractions were pooled and dialyzed into 20 mM tris, pH 7.5, 0.1 mM EDTA, 5 mM DTT, before applying to a HiTrapTM Sepharose Q anion exchange column. Following a wash step of five column volumes of equilibration buffer, the protein was eluted with a ten column volume linear gradient of increasing 20 mM tris, pH 7.5, 0.1 mM EDTA, 2 M NaCl and 5 mM DTT. The resulting homogenous protein was judged to be >95% pure according to a 10% SDS-PAGE and dialyzed for storage into 20 mM Tris-HCl, 0.1 mM EDTA, 5 mM DTT, 150 mM NaCl, 20% (v/v) glycerol at a pH of 7.5. Dialyzed protein was divided into 20 μ L aliquots and flash frozen in for storage at -80°C. All purification steps were carried out at 4°C or on ice.

5.4.3 Kinetic Assays

PTP1B activity was assayed using 6,8-difluoro-4-methylumbelliferyl phosphate (5.36, diFMUP, Invitrogen, **Figure 5.23**) a fluorogenic substrate and following the

production of the fluorescent product, 8-difluoro-4-methylumbelliferoe (diFMU, excitation wavelength of 360 nm and an emission wavelength of 460 nm) (Gee et al., 1999).

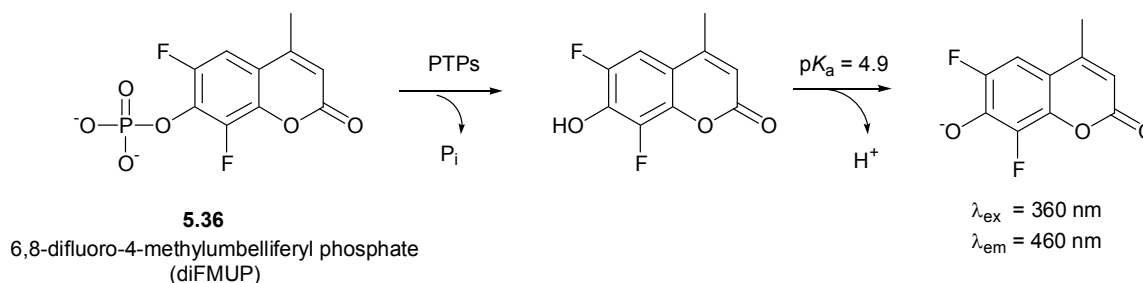


Figure 5.23. Fluorogenic assay for PTP1B.

5.4.2 IC_{50} and K_i determinations of compounds 5.7, 5.26 to 5.29

Stock solutions of the inhibitors were prepared in 40% DMSO/60% buffer containing 50 mM Bis-Tris HCl, pH 6.3. 10 μ L of each inhibitor stock solution was added to the wells of a 96-well microtiter plate containing 90 μ L of 5.5 μ M diFMUP in 50 mM Bis-Tris HCl, pH 6.3, 5 mM DTT, and 2 mM EDTA. The reactions were initiated at 25°C with 10 μ L of a 30 nM solution of PTP1B in a buffer containing 50 mM Bis-Tris HCl, pH 6.3, 20% glycerol, 5 mM DTT, 2 mM EDTA, and 0.1% Triton X-100. The production of fluorescent product diFMU was monitored for 10 min using a spectrofluorimeter plater reader with excitation and emission at 360 nm and 460 nm, respectively. The initial rates of enzyme activity in relative fluorescence units per second (RFU/s) were used to determine the IC_{50} and K_i values. For IC_{50} values, the ratio of the initial rate in the presence of inhibitor (V_i) to that in the absence of inhibitor (V_o) was calculated and plotted as a semi-log curve in Grafit, from which the IC_{50} value was calculated based on the following equation: $V_i = V_o/[1 + ([I]/IC_{50})^S] + B$, where V_i is the

initial rate of reaction at an inhibitor concentration of $[I]$; V_o is the velocity in the absence of inhibitor; B is background and s is the slope factor equal to $V_o - B$. For the K_i values, data were plotted as Lineweaver–Burk graphs and K_i values were calculated from replots of the slopes or intercepts of the Lineweaver–Burk graphs according to the equations for mixed or competitive inhibition.

5.4.3 IC_{50} Determinations for compounds 5.32 to 5.35, and 5.42 and 5.43

Ten microliters of a solution of a stock solution of inhibitor in DMSO-water was added to the wells of a microtiter plate containing 70 μ L of 0.1 M bis-tris, pH 6.3, 2 mM EDTA, 5 mM DTT, 0.001% Triton. A control was prepared by adding 10 μ L of DMSO-water instead of inhibitor. To this, 10 μ L of 200 μ M diFMUP (**5.36**, see § 5.4.3, **Figure 5.17**) stock in 2% DMSO was added to bring the volume up to 90 μ L. The assay was initiated by the addition of 10 μ L of PTP1B stored in 20 mM tris, pH 7.5, 150 mM NaCl, 5 mM DTT, 0.1 mM EDTA, and 20% glycerol. A control was performed by adding 10 μ L of enzyme storage buffer. The final concentration of inhibitor in the assay wells was 100, 80, 60, 40, 20, 15, 10, 5, 2.5, 1, 0.5, and 0 μ M. The final concentration of DMSO was 7.5%. The final concentration of diFMUP substrate in the assay was 20 μ M, the previously determined K_m value under these conditions. The final concentration of PTP1B ranged from 1.5 to 3.0 to 6.0 nM. The production of fluorescent product diFMU was monitored for 10 min at 30°C using a spectrofluorometer platereader with excitation and emission at 360 and 460 nm, respectively. The initial rates of enzyme activity in relative fluorescence units per second (RFU/s) were used to determine the IC_{50} . The ratio of the initial rate in the presence of inhibitor (V_i) to that in the absence of inhibitor (V_o) was calculated and plotted as a semilog curve in Grafit, from which the

IC₅₀ value was calculated based on the following equation: $V_i = V_o/[1 + ([I]/IC_{50})^S] + B$, where V_i is the initial rate of reaction at an inhibitor concentration of $[I]$, V_o is the velocity in the absence of inhibitor, B is background, and s is the slope factor equal to $V_o - B$.

5.4.4 Assay for Time-Dependent Inhibition with Inhibitor 5.42

The IC₅₀ of **5.38** was determined using the procedure described above except the inhibitor solutions were incubated with PTP1B (3 nM) for 30 min at 30°C before initiation of the reaction with DiFMUP (20 μM final concentration).

5.4.5 Assay for Irreversible Inhibition with Inhibitor 5.42

10 μL of a 500 μM stock solution of **5.42** in DMSO-water was added to 80 μL of 0.1 M bis-tris, pH 6.3, 2 mM EDTA, 5 mM DTT, 0.001% Triton, and 10 μL of 1.5 μM PTP1B. A control was similarly made with 10 μL of DMSO-water instead of inhibitor. Upon initiation of the reaction at $t = 0$ and after 20, 40, and 60 min of incubation, a 2 μL aliquot was withdrawn at $t = 15$ s and $t = 60$ minutes and added to a 96-well microtiter plate containing 98 μL of 1.0 mM diFMUP (approximately $50 \times K_m$) in 0.1 M bis-tris, pH 6.3, 2 mM EDTA, 5 mM DTT, 0.001% Triton for a 50-fold dilution of the incubation mixture. The final concentration of the inhibitor in the assay was 1 mM, and the final concentration of enzyme was 150 nM. The production of diFMU was followed for 10 min as described above. The percent of activity remaining in the presence of inhibitor compared to that of the control was determined. After the aliquot was withdrawn from the preincubation mixture after 60 minutes, the remainder was transferred to a dialysis membrane (10 kDa cutoff, SpectraPor) and dialyzed against 500 mL of 0.1 M bis-tris, pH 6.3, 2 mM EDTA, 5 mM DTT, 0.001% Triton X-100,

changed twice over 24 h at 4 °C. At 24 h the amount of activity remaining in the enzyme-inhibitor mixture and its control was measured by withdrawing 2 µL into 98 µL of 1 mM diFMUP (approximately $50 \times K_m$) in 0.1 M bis-tris, pH 6.3, 2 mM EDTA, 5 mM DTT, 0.01% Triton X-100 as described above.

References

- Ahima, R.S., and Flier, J.S. Leptin. *Annu. Rev. Physiol.*, **2000**, 62, 413-437.
- Ahmad, F., Li, P.M., Meyerovitch, J., Goldstein, B.J. Osmotic loading of neutralizing antibodies demonstrates a role for protein-tyrosine phosphatase 1B in negative regulation of the insulin action pathway. *J. Biol. Chem.*, **1995**, 270, 20503-20508.
- Ahmed, S., Owen, C.P., James, K., Sampson, L., Patel, C.K. Review of estrone sulfatase and its inhibitors – an important new target against hormone dependent breast cancer. *Curr. Med. Chem.* **2002**, 9, 263-273.
- Ahmed, V., Ispahany, M., Ruttgaizer, S., Guillemette, G., Taylor, S.D. A fluorogenic substrate for the continuous assaying of aryl sulfatases. *Anal. Biochem.*, **2005**, 340, 80-88.
- Ahmed, V., Liu, Y., Silvestro, C., Taylor, S.D. Boronic acids as inhibitors of steroid sulfatase. *Bioorg. Med. Chem.*, **2006**, 14, 8564-8573.
- Akamatsu, M., Ye, B., Yan, X.J., Kole, H.K., Burke, T.R., Roller, P.P. Characterization of tyrosine-phosphate mimick containing tyrosine phosphatase inhibitory peptides. Japan Peptide Symposium Proceedings, 1995, Osaka, Japan.
- Alperin, E.S., Shapiro, L.J. Characterization of point mutations in patients with X-linked ichthyosis. Effects on the structure and function of the steroid sulfatase protein. *J. Biol. Chem.* **1997**, 272, 20756-20763.
- Alonso, A., Sasin, J., Bottini, N., Friedberg, I., Osterman, A., Mustelin. Protein tyrosine phosphatases in the human genome. *Cell*, **2004**, 117, 699-711.
- Amarasinghe, K.K., Evidokimov, A.G., Xu, K., Clark, C.M., Maier, M.B., Srivastava, A., Colson, A-O., Gerwe, G.S., Stake, G.E., Howard, B.W., Pokross, M.E., Gray, J.L., Peters, K.G. Design and synthesis of potent, non-peptidic inhibitors of HPTPbeta. *Bioorg. Med. Chem. Lett.*, **2006**, 16, 4252.
- Anderson, C., Freeman, J., Lucas, L.H., Farley, M., Dalhoumi, H., Widlanski, T.S. Estrone sulfatase: Probing structural requirements for substrate and inhibitor recognition. *Biochemistry*. **1997**, 36, 2586–2594.
- Anderson, C., Freeman, J., Lucas, L.J.H., Widlanski, T.S. Molecular recognition in biological systems: phosphate esters vs sulfate esters and the mechanism of action of steroid sulfatase. *J. Am. Chem. Soc.*, **1995**, 117, 3889.
- Anderson, D., Koch, C.A., Grey, L., Ellis, C., Moran, M.F., Pawson, T. Binding of SH2 domains of phospholipase C gamma 1, GAP, and Src to activated growth factor receptors. *Science*, **1990**, 250(4983):979–982.

Anson, D.S., Taylor, J.A., Bielicki, J., Harper, G.S., Peters, C., Gibson, G.J., Hopwood, J.J. Correction of human mucopolysaccharidosis type-VI fibroblasts with recombinant N-acetylgalactosamine-4-sulphatase. *Biochem. J.*, **1992**, 284, 789.

Arena, S., Benvenuti, S., Bardelli, A., Genetic analysis of the kinome and phosphatome in cancer. *Cell. Mol. Life Sci.*, **2005**, 2092-2099.

Asante-Appiah, E., Ball, K., Bateman, K., Skorey, K., Friesen, R., Despons, C., Payette, P., Bayly, C., Zamboni, R., Scapin, G., Ramachandran, C., Kennedy, B.P. The YRD motif is a major determinant of substrate and inhibitor specificity in T-cell protein-tyrosine phosphatase. *J. Biol. Chem.*, **2001**, 276, 26036.

Ballabio, A., Shapiro, L.J. Steroid sulfatase deficiency and X-linked ichthyosis, in *The metabolic and molecular bases of inherited disease* (Scriver, C. R., Beaudet, A. L., and Sly, W.S., Eds.), **1995**, pp., 2999-3022, McGraw-Hill, New York.

Bandyopadhyay, D., Kusari, A., Kenner, K.A., Liu, F., Chernoff, J., Gustafson, T.A., Kusari, J. Protein-tyrosine phosphatase 1B complexes with the insulin receptor in vivo and is tyrosine-phosphorylated in the presence of insulin. *J. Biol. Chem.*, **1997**, 272, 1639-1645.

Barbero, M.L., *Arch. Biochem. Biophys.* **1984**, 228, 560-568.

Barford, D., Flint, A.J., Tonks, N.K. Crystal structure of human protein tyrosine phosphatase 1B. *Science*, **1994**, 263, 1397-1404.

Barford, D., Das, A.K., Egloff, M.-P. The structure and mechanism of protein phosphatases: insights into catalysis and regulation. *Annu. Rev. Biophys. Biomol. Struct.* **1998**, 27, 133-164.

Begovich, A.B., Carlton, V.E., Honigberg, L.A., Schrodi, S.J., Chokkalingam, A.P., Alexander, H.C., Ardlie, K.G., Huang, Q., Smith, A.M., Spoerke, J.M. et al. A missense single-nucleotide polymorphism in a gene encoding a protein tyrosine phosphatase (PTPN22) is associated with rheumatoid arthritis. *Am. J. Hum. Genet.*, **2004**, 75, 330-337.

Betley, J.R., Cesaro-Tadic, S., Mekhalfia, A., Rickard, J.H., Denham, H., Partridge, L.J., Pluckthun, A., Blackburn, G.M. Direct screening for phosphatase activity by turnover-based capture of protein catalysts. *Angew. Chem., Int. Edn. Engl.* **2002**, 41, 775-777.

Bielicki, J., Hopwood, J. J., Wilson, P. J., Anson, D. S. Recombinant human iduronate-2-sulphatase: correction of mucopolysaccharidosis-type II fibroblasts and characterization of the purified enzyme. *Biochem. J.*, **1993**, 289, 241.

- Bielicki, J., Hopwood, J. J., Melville, E. L., Anson, D.S. Recombinant human sulphamidase: expression, amplification, purification and characterization. *Biochem. J.*, **1998**, 329, 145.
- Billich, A., Nussbaumer, P., Lehr, P. Stimulation of MCF-7 breast cancer cell proliferation by estrone sulfate and dehydroepiandrosterone sulfate: Inhibition by novel non-steroidal steroid sulfatase inhibitors. *J. Steroid Biochem. Mol. Biol.* **2000**, 73, 225–235.
- Black, E., Breed, J., Breeze, A.L., Embrey, K., Garcia, R., Gero, T.W., Structure-based design of protein tyrosine phosphatase-1B inhibitors. *Bioorg. Med. Chem. Lett.*, **2005**, 15, 2503-2507.
- Blackburn, G.M. Phosphonates as analogues of biological phosphates. *Chem. Ind. (London)* **1981**, 134-138.
- Blackburn, G.M., Parratt, M.J. The synthesis of alpha-fluoroalkylphosphonates. *J. Chem. Soc., Chem. Commun.* **1983**, 886-888.
- Blackburn, G.M., Turkmen, H. Synthesis of alpha-fluoro- and alpha, alpha-difluoro-benzenemethanesulfonamides: new inhibitors of carbonic anhydrase. *Org. Biomol. Chem.*, **2005**, 3, 225.
- Blonski, C., Gefflaut, T., Perie, J. Effects of chirality and substituents at carbon 3 in dihydroxyacetone-phosphate analogues on their binding to rabbit muscle aldolase. *Bioorg. Med. Chem.*, **1995**, 3(9), 1247-1253.
- Boivin, R.P., Luu-The, V., Cachance, R., Labrie, F., Poirier, D., Structure-activity relationships of 17alpha-derivatives of estradiol as inhibitors of steroid sulfatase. *J. Med. Chem.*, **2000**, 43, 4465-4478.
- Boivin, R.P., Poirier, D. 17 alpha-alkyl- or 17 alpha-substituted benzyl-17 beta-estradiols: a new family of estrone-sulfatase inhibitors. *Bioorg. Med. Chem. Lett.*, **1998**, 8, 1891.
- Boivin, R.P., Luu-The, V., Lachance, R., Labrie, F., Poirier, D. Structure-activity relationships of 17alpha-derivatives of estradiol as inhibitors of steroid sulfatase. *J. Med. Chem.* **2000**, 43, 4465–4478.
- Bojarova, P., and Williams, S.J. Sulfotransferases, sulfatases and formylglycine-generating enzymes: a sulfation fascination. *Curr. Opin. Chem. Biol.*, **2008**, 12, 573-581.
- Bojarova, P., Denehy, E., Walker, I., Loft, K., De Souza, D.P., Woo, L.W.L., Potter, B.V.L., McConville, M.J., Williams, S.J. Direct evidence for ArO–S bond cleavage upon inactivation of *Pseudomonas aeruginosa* arylsulfatase by aryl sulfamates. *Chembiochem.*, **2008**, 9, 613-623.

- Bojarová, P., Williams, S.J. Aryl sulfamates are broad spectrum inactivators of sulfatases: effects on sulfatases from various sources. *Bioorg. Med. Chem. Lett.* **2009**, 19(2), 477-80.
- Boltes, I., Czapinska, H., Kahnert, A., von Bulow, R., Dierks, T., Schmidt, B., von Figura, K., Kertesz, M.A., Uson, I. 1.3-Å structure of arylsulfatase from *Pseudomonas aeruginosa* establishes the catalytic mechanism of sulfate ester cleavage in the sulfatase family. *Structure*. **2001**, 9, 483-491.
- Bond, C.S., Clements, P.R., Ashby, S.J., Collyer, C.A., Harrop, S.J., Hopwood, J.J., Guss, J.M. Structure of a human lysosomal sulfatase. *Structure*. **1997**, 5, 277-289.
- Born, T.L., Myers, J.K., Widlanski, J.K., Rusnak, F. 4-(Fluoromethyl)phenyl phosphate acts as a mechanism-based inhibitor of calcineurin. *J. Biol. Chem.* **1995**, 270, 25651-25655.
- Boutselis, I.G., Yu, X., Zhang, Z.Y., Borch, R. Synthesis and cell-based activity of a potent and selective PTP1B inhibitor prodrug. *J. Med. Chem.*, **2007**, 50, 856-864.
- Bowie, J.U. Stabilizing membrane proteins. *Current Opinions in Structural Biology*. **2001**, 11, 397-402.
- Bowman, W.C., Rand, M.J. *Textbook of Pharmacology*, 2nd ed., Blackwell: London, 1979, Chapter 34.
- Bracey, M.H., Hanson, M.A., Masuda, K.R., Stevens, R.C., and Cravatt, B.F. Structural adaptations in a membrane enzyme that terminates endocannabinoid signaling. *Science*. **2002**, 298, 1793–1796.
- Bradford, M.M.. A rapid and sensitive method for the quantitation of microgram quantities of protein utilizing the principle of protein-dye binding. *Anal. Biochem.* **1976**, 72, 248-254.
- Brown-Shimer, S., Johnson, K.A., Lawrence, J.B., Johnson, C. and Bruskin, A. Molecular cloning and chromosome mapping of the human gene encoding protein phosphotyrosyl phosphatase 1B. *Proc. Natl. Acad. Sci. USA.*, **1990**, 87, 5148-5152.
- Burke, T.R., Lee, K. Phosphotyrosyl mimetics in the development of signal transduction inhibitors. *Acc. Chem. Res.*, **2003**, 36, 426.
- Burke, T.R., Kole, H.K., Roller, P.P. Potent inhibition of insulin receptor dephosphorylation by a hexamer peptide containing the phosphotyrosyl mimetic F₂Pmp. *Biochem. Biophys. Res. Commun.*, **1994**, 204, 129-134.

- Burke, T.R., Ye, B., Yan, X., Wang, S., Jia, Z., Chen, L., Zhang, Z.-Y., Barford, D. Small molecule interactions with protein-tyrosine phosphatase PTP1B and their use in inhibitor design. *Biochemistry*, **1996**, 35, 15989-96.
- Burke, T.R., Ye, B., Akamatsu, M., Ford, H., Yan, X.J., Kole, H.K., Wolf, G., Shoelson, S.E., Roller, P.P. 4'-O-[2-(2-fluoromalonyl)]-L-tyrosine: A phosphotyrosyl mimic for the preparation of signal transduction inhibitory peptides. *J. Med. Chem.* **1996**, 39, 1021-1027.
- Burke, T.R., Yao, Z.J., Zhao, H., Milne, G.W.A., Wu, L., Zhang, Z.Y., Voigt, J.H. Enantioselective synthesis of nonphosphoruscontaining phosphotyrosyl mimetics and their use in the preparation of tyrosine phosphatase inhibitory peptides. *Tetrahedron*, **1998**, 54, 9981-9994.
- Burns, G.R.J.. Purification and partial characterization of arylsulfatase C from human placental microsomes. *Biochim. Biophys. Acta.* **1983**, 759, 199-204.
- Byon, J.C.H., Kusari, A.B., Kusari, J. Protein-tyrosine phosphatase 1B acts as a negative regulator of insulin signal transduction. *Mol. Cell. Biochem.*, **1998**, 182, 101-198.
- Campbell, D.A., Szardenings, A.K. Functional profiling of the proteome with affinity labels. *Curr. Opin. Chem. Biol.*, **2003**, 7, 296-303.
- Carrico, I.S., Carlson, B.L., Bertozzi, C.R. Introducing genetically encoded aldehydes into proteins. *Nat. Chem. Biol.*, **2007**, 3, 321-322.
- Cesaro-Tadic, S., Lagos, D., Honegger, A., Rickard, J.H., Partridge, L.J., Blackburn, G.M., Pluckthun, A. Turnover-based in vitro selection and evolution of biocatalysts from a fully synthetic antibody library. Turnover-based in vitro selection and evolution of biocatalysts from a fully synthetic antibody library. *Nat. Biotechnol.* **2003**, 21, 679-685.
- Chen, W.C., Thiboutot, D., Zouboulis, C.C. Cutaneous androgen metabolism: basic research and clinical perspectives. *J. Invest. Dermatol.*, **2002**, 119, 992-1007.
- Chen, L., Wu, L., Otaka, A., Smyth, M.S., Roller, P.R., Burke, T.R., den Hertog, J., Zhang, Z.-Y. Why is phosphonodifluoromethyl phenylalanine a more potent inhibitory moiety than phosphonomethyl phenylalanine toward protein-tyrosine phosphatases? *Biochem. Biophys. Res. Commun.*, **1995**, 216, 976.
- Cheng, A., Uetani, N., Simoncic, P.D., Chaubey, V.P., Lee-Loy, A., McGlade, C.J., Kennedy, B.P., Tremblay, M.L. Attenuation of leptin action and regulation of obesity by protein tyrosine phosphatase 1B. *Dev. Cell*, **2002**, 2, 497-503.

Chernoff, J., Schievella, A.R., Jost, C.A., Erikson, R.L. and Neel, B.G. Cloning of a cDNA for a major human protein-tyrosine-phosphatase. *Proc. Natl. Acad. Sci. USA*, **1990**, 87, 2735-2739.

Cho, H., Krishnaraj, R., Kitas, E., Bannwarth, W., Walsh, C.T., Anderson, K.S. Isolation and structural elucidation of a novel phosphocysteine intermediate in the LAR protein tyrosine phosphatase enzymatic pathway. *J. Am. Chem. Soc.*, **1992**, 114, 7296-7298.

Chruszcz, M., Laidler, P., Monkiewicz, M., Ortlund, E., Lebiody, L., Lewinski, K. Crystal structure of a covalent intermediate of endogenous human arylsulfatase A. *J. Inorg. Biochem.*, **2003**, 96, 386-392.

Ciobanu L.C., Boivin R.P., Luu-The V., Poirier D. Synthesis and steroid sulphatase inhibitory activity of C19-and C21-steroidal derivatives bearing a benzyl-inhibiting group. *Eur. J. Med. Chem.* **2001**, 36, 659-671.

Combs, A.P., Yue, E.W., Bower, M., Ala, P.J., Wayland, B., Douthy, B., Structure-based design and discovery of protein tyrosine phosphatase inhibitors incorporating novel isothiazolidinone heterocyclic phosphotyrosine mimetics. *J. Med. Chem.*, **2005**, 48, 6544-6548.

Combs, A.P., Zhu, W., Crawley, M.L., Glass, B., Polam, P., Sparks, R.B., et al., Potent benzimidazole sulfonamide protein tyrosine phosphatase 1B inhibitors containing the heterocyclic (S)-isothiazolidinone phosphotyrosine mimetic. *J. Med. Chem.*, **2006**, 49, 3774-3789.

Conary, J., Nauerth, A., Burns, G., Hasilik, A., von Figura, K. Steroid sulfatase. Biosynthesis and processing in normal and mutant fibroblasts. *Eur. J. Biochem.* **1986**, 158, 71-76.

Copeland, R. A. *Evaluation of enzyme inhibitors in drug discovery: a guide for medicinal chemists and pharmacologists*. Wiley, Hoboken, N.J., 2005.

Cosma, M.P., Pepe, S., Annunziata, I., Newbold, R.F., Grompe, M., Parenti, G., Ballabio A. The multiple sulfatase deficiency gene encodes an essential and limiting factor for the activity of sulfatases. *Cell*. **2003**, 113, 445-456.

Cravatt, B.F., Wright, A.T., Kozarich, J.W. Activity-based protein profiling: from enzyme chemistry to proteomic chemistry. *Ann. Rev. Biochem.* **2008**, 77, 383-414.

Dadke, S., Kusari, J., Chernoff, J. Down-regulation of insulin signalling by protein-tyrosine phosphatase 1B is mediated by an N-terminal binding region. *J. Biol. Chem.*, **2000**, 275, 23642-23647.

- Dax, C., Coincon, M., Sygusch, J., Blonski, C. Hydroxynaphthaldehyde phosphate derivatives as potent covalent schiff base inhibitors of fructose-1,6-bisphosphate aldolase. *Biochemistry*. **2005**, *44*, 5430.
- Day, J.M., Purohit, A., Tutill, H.J., Foster, P.A., Woo, L.W., Potter, B.V., Reed, M.J. The development of steroid sulfatase inhibitors for hormone-dependent cancer therapy. *Ann. N.Y. Acad. Sci.*, **2009**, 1155, 80-7.
- Daynes, R.A., Dudley, D.J., Araneo, B.A. Regulation of murine lymphokine production in vivo. II. Dehydroepiandrosterone is a natural enhancer of interleukin 2 synthesis by helper T cells. *Eur. J. Immunol.*, **1990**, *20*, 793-803.
- Daynes, R.A., Araneo, B.A., Ershler, W.B., Maloney, C., Li, G-Z., Ryu, S.-Y. Altered regulation of IL-6 production with normal aging. Possible linkage to the age-associated decline in dehydroepiandrosterone and its sulfated derivative. *J. Immunol.*, **1993**, *150*, 5219-5230.
- DeLano, W. L. The PyMOL Molecular Graphics System, 2002. DeLano Scientific, San Carlos, CA, USA. <http://www.pymol.org>.
- Desmarais, S., Jia, Z., Ramachandran, R. Inhibition of protein tyrosine phosphatases PTP1B and CD45 by sulfotyrosyl peptides. *Arch. Biochem. Biophys.*, **1998**, *354*, 225–231.
- Denu, J.M., Tanner, K.G. Specific and reversible inactivation of protein tyrosine phosphatases by hydrogen peroxide: evidence for a sulfenic acid intermediate and implications for redox regulation. *Biochemistry*, **1998**, *37*, 5633–5642.
- De Planque, M.R.R., Kruijtzter, J.A.W., Liskamp, R.M.J., Marsh, D., Greathouse, D.V., Koeppe, R.E., de Kruijff, B., Killan, J.A. Different membrane anchoring positions of tryptophan and lysine in synthetic transmembrane alpha-helical peptides. *J. Biol. Chem.*, **1999**, *274*, 20839-20846.
- Dibbelt, L., Li, P.K., Pillai, R., Knuppen, R. Inhibition of human placental sterylsulfatase by synthetic analogs of estrone sulfate. *J. Steroid Biochem. Mol. Biol.* **1994**, *50*, 261–266.
- Dibbelt, L., Kuss, E. Human placental steryl-sulfatase: enzyme purification, production of antisera, and immunoblotting reactions with normal and sulfatase-deficient placentas. *Biol. Chem. Hoppe-Seyler*. **1986**, *367*, 1223-1229.
- Dibbelt, L., Kuss, E. Human placental sterylsulfatase. Interaction of the isolated enzyme with substrates, products, transition-state analogues, amino-acid modifiers and anion transport inhibitors. *Biol. Chem. Hoppe-Seyler*. **1991**, *372*, 173.

Dibbelt, L., Li, P-K., Pillai, R., Knuppen, R.J. Inhibition of human placental steryl sulfatase by synthetic analogs of estrone sulfate. *Steroid. Biochem. Molec. Biol.*, **1994**, 50, 261–266.

Dierks, T., Schmidt, B., and von Figura, K. Conversion of cysteine to formylglycine: a protein modification in the endoplasmic reticulum. *Proc. Natl. Acad. Sci. USA*. **1997**, 94, 11963-11968.

Dierks, T., Schmidt, B., Borissenko, L.V., Peng, J., Preusser, A., Mariappan, M., von Figura, K. Multiple sulfatase deficiency is caused by mutations in the gene encoding the human C α -formylglycine generating enzyme. *Cell*. **2003**, 113:435-444.

Dierks, T., Dickmanns, A., Preusser-Kunze, A., Schmidt, B., Mariappan, M., von Figura, K., Ricner, R., Rudolph, M.G. Molecular basis for multiple sulfatase deficiency and mechanism for formylglycine generation of the human formylglycine-generating enzyme. *Cell*. **2005**, 541-552.

Di Natale, P., Vanacore, B., Daniele, A., Esposito, S. Heparan N-Sulfatase: In vitro mutagenesis of potential N-glycosylation sites. *Biochemical and Biophysical Research Communications*. **2000**, 280, 1251-1257.

Dixon, M., and Webb, E.C. *Enzymes*, 3rd ed., **1979**, Academic Press, New York.

Douty, B., Wayland, B., Ala, P.J., Bower, M.J., Pruitt, J., Bostrom, L., Wei, M., Klabe, R., Gonville, L., Wynn, R., Burn, T.C., Liu, P.C.C., Combs, A.P., Yue, E.W. Isothiazolidinone inhibitors of PTP1B containing imidazoles and imidazolines. *Bioorg. Med. Chem. Lett.*, **2008**, 18, 66.

Dowsett, M., Cunningham, D.C., Stein, R.C., Evans, S., Dehennin, L., Hedley, A., Coombes, R.C.. Dose-related endocrine effects and pharmacokinetics of oral and intramuscular 4-hydroxyandrostenedione in post-menopausal breast cancer patients. *Cancer Res*. **1989**, 49, 1306-1311.

Drews, J. Drug discovery: a historical perspective. *Science*. **2000**, 287, 1960–1964. 53, 298.

Duncan, L., Purohit, A., Howarth, N.M., Potter, B.V.L., Reed, M.J. Inhibition of estrone sulfatase activity by estrone-3-methylthiophosphonate: a potential therapeutic agent in breast cancer. *Cancer Res.*, **1993**.

Eckert, K.A., and T.A. Kunkel. DNA polymerase fidelity and the polymerase chain reaction. *PCR Methods Appl*. **1991**, 1(1), 17-24.

Elchelby, M., Payette, P., Michaliszyn, E., Cromlish, W., Collins, S., Loy, A.L., Normandin, D., Cheng, A., Himms-Hagen, J., Chan, C.-C., Ramachandran, C., Gresser, M.J., Tremblay, M.L., Kennedy, B.P. Increased insulin sensitivity and obesity resistance

in mice lacking the protein tyrosine phosphatase-1B gene. *Science*, **1999**, 283, 1544-1548.

Eto, Y., Rampini, S., Weisman, U., and Herschkowitz, N. Enzymic studies of sulphatases in tissues of the normal human and in metachromatic leukodystrophy with multiple sulphatase deficiencies: arylsulphatases A, B and C, cerebroside sulphatase, psychosine sulphatase and steroid sulphatases. *J. Neurochemistry*. **1974**, 23, 1161. (method for MUS assay)

Erlanson, D.A., McDowell, R.S., He, M.M., Randal, M., Simmons, R.L., Kung, J., Waight, A., Hansen, S.K. Discovery of a new phosphotyrosine mimetic for PTP1B using breakaway tethering. *J. Am. Chem. Soc.*, **2003**, 125(19):5602-3.

Evers, M., Saftig, P., Schmidt, P., Hafner, A., McLoghlin, D.B., Schmahl, W., Hess, B., von Figura, K., Peters, C. Targeted disruption of the arylsulfatase B gene results in mice resembling the phenotype of mucopolysaccharidosis VI. *Proc. Natl. Acad. Sci. U. S. A.* **1996**, 93, 8214-8219.

Farnsworth, W.E. Human prostatic dehydroepiandrosterone sulfate sulfatase. *Steroids*. **1973**, 21, 647-664.

Farzan, M., Mirzabekov, T., Kolchinsky, P., Wyatt, R., Cayabyab, M., Gerard, N.P., Gerard, C., Sodroski, J., Choe, H. Tyrosine sulfation of the amino terminus of CCR5 facilitates HIV-1 entry. *Cell*, **1999**, 96, 667.

Farzan, M., Vasilieva, N., Schnitzler, C.E., Chung, S., Robinson, J., Gerard, N.P., Gerard, C., Choe, H., Sodroski, J. A tyrosine-sulfated peptide based on the N terminus of CCR5 interacts with a CD4-enhanced epitope of the HIV-1 gp120 envelope glycoprotein and inhibits HIV-1 entry. *J. Biol. Chem.* **2000**, 275, 33516.

Fey, J., Balleininger, M., Borissenko, L.V., Schmidt, B., von Figura, K., Dierks, T. Characterization of posttranslational formylglycine formation by luminal components of the endoplasmic reticulum. *J. Biol. Chem.*, **2001**, 276(50), 47021-8.

Flint, A.J., Gebbink, M.F.B.G., Franza, J.B.R, Hill, D.E, Tonks, N.K. Multi-site phosphorylation of the protein tyrosine phosphatase, PTP1B: identification of cell cycle regulated and phorbol ester stimulated sites of phosphorylation. *E.M.B.O. J.*, **1993**, 12, 1937-1946.

Fonovic, M., Bogoy, M. Activity-based probes as a tool for functional proteomic analysis of proteases. *Expert Rev. Proteomics*. **2008**, 5(5), 721-730.

Foster, P.A., Reed, M.J., Purohit, A. Recent developments of steroid sulfatase inhibitors as anti-cancer agents. *Anticancer Agents Med. Chem.*, **2008**, 7, 732-8.

Fournier, D., Poirier, D. Estradiol dimers as a new class of steroid sulfatase reversible inhibitors. *Bioorg. Med. Chem. Lett.*, **2009**, 19(3), 693-6.

Franco, B., Meroni, G., Parenti, G., Levilliers, J., Bernard, L., Gebbia, M., Cox, L., Maroteaux, P., Sheffield, L., Rappold, G.A., Andria, G., Petit, C., Ballabio, A. A cluster of sulfatase genes on Xp22.3: mutations in chondrodysplasia punctata (CDPX) and implications for warfarin embryopathy. *Cell*, **1995**, 81, 15.

Frangioni, J.V., Beahm, P.H., Shifrin, V., Jost, C.A., Neel, B.G. The nontransmembrane tyrosine phosphatase PTP-1B localizes to the endoplasmic reticulum via its 35 amino acid C-terminal sequence. *Cell*, **1992**, 68, 545-560.

Frangioni, J.V., Oda, A., Smith, M., Salzman, E.W., Neel, B.G. Calpain-catalyzed cleavage and subcellular relocation of protein phosphotyrosine phosphatase 1B (PTP-1B) in human platelets. *E.M.B.O. J.*, **1993**, 12, 4843-4856.

Freeman, C., Hopwood, J.J. Glucuronate-2-sulphatase activity in cultured human skin fibroblast homogenates. *Biochem. J.* **1991**, 279, 399.

Gao, Y., Wu, L., Luo, J.H., Guo, R., Yang, D., Zhang, Z-Y., Burke, T.R. Examination of novel non-phosphorus-containing phosphotyrosyl mimetics against protein-tyrosine phosphatase-1B and demonstration of differential affinities toward Grb2 SH2 domains. *Bioorg. Med. Chem. Lett.*, **2000**, 10, 923.

Gay, B., Suarez, S., Caravatti, G., Furet, P., Meyer, T., Schoepfer, J. Selective Grb2 SH2 inhibitors as anti-Ras therapy. *Int. J. Cancer*. **1999**, 83, 235-241.

Gee, K.R., Sun, W.C., Bhalgat, M.K., Upson, R.H., Klaubert, D.H., Latham, K.A., Haugland, R.P. Fluorogenic substrates based on fluorinated umbelliferones for continuous assays of phosphatases and beta-galactosidases. *Anal. Biochem.*, **1999**, 273, (1) 41-48.

Ghosh, D. Human sulfatases: a structural perspective to catalysis. *Cell. Mol. Life Sci.* **2007**, 64(15), 2013-2022.

Ghosh, D., Mutations in X-linked ichthyosis disrupt the active site structure of estrone/DHEA sulfatase. *Biochimica et Biophysica Acta.*, **2004**, 1739, 1-4.

Ghosh, D. Three-dimensional structures of sulfatases. *Methods Enzymol.*, **2005**, 400, 273-293.

Ghosh, D. Human sulfatases: a structural perspective to catalysis. *Cell. Mol. Life Sci.* **2007**, 64, 2013-2022.

Gieselmann, V., Schmidt, B., Von Figura, K., *In vitro* mutagenesis of potential N-glycosylation sites of arylsulfatase A. *J. Biol. Chem.* **1992**, 267, pp. 13262–13266.

- Goldstein, B.J., Bittner-Kowalczyk, A., White, M.F., Harbeck, M. Tyrosine dephosphorylation and deactivation of insulin receptor substrate-1 by protein-tyrosine phosphatase 1B. Possible facilitation by the formation of a ternary complex with Grb2 adaptor protein. *J. Biol. Chem.*, **2000**, 275, 4283-4289.
- Guan, K.L., Haun, R.S., Watson, S.J., Geahlen, R.L. and Dixon, J.E. Cloning and expression of a protein-tyrosine-phosphatase. *Proc. Natl. Acad. Sci. USA.* **1990**, 87, 1501-1505.
- Halazy, S., Berges, V., Ehrhard, A., Danzin, C. Ortho- and para-(Difluoromethyl)aryl- β -D-glucosides: A new class of enzyme-activated irreversible inhibitors of β -glucosidases. *Bioorg. Chem.* **1990**, 18, 330-344.
- Hanson, S.R., Best, M.D., Wong, C.H. Sulfatases: Structure, Mechanism, Biological Activity, Inhibition, and Synthetic Utility. *Angew. Chem. Int. Ed.*, **2004**, 43, 5736-5763.
- Hanson, S.R., Whalen, L.J., Wong, C-H. Synthesis and evaluation of general mechanism-based inhibitors of sulfatases based on (difluoro)methyl phenyl sulfate and cyclic phenyl sulfamate motifs. *Bioorg. Med. Chem.*, **2006**, 14, 8386-8395.
- Harper, M.E., Pike, A., Peeling, W.B., Griffiths, K. Steroids of adrenal origin metabolized by human prostatic tissue both in vivo and in vitro. *J. Endocrinol.*, **1974**, 60, 117-125.
- Hejaz, H.A., Woo, L.W., Purohit, A., Reed, M.J., Potter, B.V. Synthesis, in vitro and in vivo activity of benzophenone-based inhibitors of steroid sulfatase. *Bioorg. Med. Chem.*, **2004**, 12, 2759.
- Hernandez-Martin, A., Gonzalez-Sarmiento, R., De Unamuno, P. X-linked ichthyosis: an update. *Br. J. Dermatol.* **1999**, 141, 617- 627.
- Hernandez-Guzman, F.G., Higashiyama, T., Osawa, Y., Ghosh, D. Purification, characterization of human placental estrone/dehydroepiandrosterone sulfatase, a membrane-bound enzyme of the endoplasmic reticulum. *J. Steroid Biochemistry & Molecular Biology.* **2001**, 78, 441-450.
- Hernandez-Guzman, F.G., Higashiyama, T., Pangborn, W., Osawa, Y., Ghosh D. Structure of human estrone sulfatase suggests functional roles of membrane association. *J. Biol. Chem.* **2003**, 278, 22989-22997.
- Hobkirk, R.. Steroid sulfation. *Trends Endocrinol. Metab.* **1993**, 4, 69-79.
- Hoffman, R. Enzymology of the hair follicle. *Eur. J. Dermatol.*, **2001**, 11, 296-300.
- Hopwood, J.J., Bate, G., and Kirkpatrick, P. Galsulfatase. *Nat. Rev. Drug Discov.*, **2006**, 5, 101.

- Horvath, A., Nussbaumer, P., Wolff, B., Billich, A. *J. Med. Chem.* **2004**, 47, 4268–4276.
- Howarth, N.M., Purohit, A., Robinson, J.J., Vicker, N., Reed, M.J., Potter, B.V.L. Estrone 3-sulfate mimics, inhibitors of estrone sulfatase activity: homology model construction and docking studies. *Biochemistry*, **2002**, 41, 14801.
- Howarth, N.M., Purohit, A., Reed, M.J., Potter, B.V.L. Estrone sulfamates: Potent inhibitors of estrone sulfatase with therapeutic potential. *J. Med. Chem.*, **1994**, 37, 219–221.
- Hua, Z., Wang, H., Chem, D., Chem, Y., Zhu, D. *Biochemistry and Molecular Biology International*. **1994**, 32, 537-543.
- Huang, P., Ramphal, J., Wei, J., Liang, C., Jallal, B., McMahon, G., Tang, C. Structure-based design and discovery of novel inhibitors of protein tyrosine phosphatases. *Bioorg. Med. Chem.* **2003**, 11, 835.
- Hunter, T. Signaling—2000 and beyond. *Cell*, **2000**, 113-127.
- Hunter, T. The phosphorylation of proteins on tyrosine: its role in cell growth and disease. *Philosophical transactions of the Royal Society of London. Series B, Biological sciences*. **1998**, 353, 583-605.
- Hunte, C., Von Jagow, G., Schagger, H.. *Membrane Protein Purification and Crystallization: A Practical Guide*, Academic Press, London, 2003.
- Huyer, G., Kelly, J., Moffat, J., Zamboni, R., Jia, Z., Gresser, M.J., Ramachandran, C. Affinity selection from peptide libraries to determine substrate specificity of protein tyrosine phosphatases. *Anal. Biochem.*, **1998**, 258, 19-30.
- James, V.H.T., McNeill, J.M., Lai, L.C., Newton, C.J., Ghilchik, M.W., Reed, M.J. Aromatase activity in normal breast and breast tumour tissue: in vivo and in vitro studies. *Steroids*. **1987**, 50, 269-279.
- Janda, K.D., Lo, L.-C., Lo, L.-H., Sim, M.-M., Wang, R., Wong, C.-H., Lerner, R.A. Chemical selection for catalysis in combinatorial antibody libraries. *Science*, **1997**, 275, 945-948.
- Jeffery, D.A., Bogoyo, M. Chemical proteomics and its application to drug discovery *Curr. Opin. Biotechnol.* **2003**, 14, 87-95.
- Jia, Z., Barford, D., Flint, A.J., Tonks, N.K. Structural basis for phosphotyrosine peptide recognition by protein tyrosine phosphatase 1B. *Science*, **1995**, 268, 1754-1758.

Jiang, Z.-X., Zhang, Z.-Y. Targeting PTPs with small molecule inhibitors in cancer treatment. *Cancer Metastasis Rev.*, **2008**, 27, 263-272.

Johnson, T. O., Ermolieff, J., Jirousek, M.R. Protein tyrosine phosphatase 1B inhibitors for diabetes. *Nature Rev.* **2002**, 1, 696.

Jonat, W., Howell, A., Blomquist, C. A randomised trial comparing two doses of the new selective aromatases anastrozole (Arimidex) with megestrol acetate in post-menopausal patients with advanced breast cancer. *Eur. J. Cancer.* **1996**, 32A, 404-412.

Jonas, S., van Loo, B., Hyvonen, M., Hollfelder, F. A new member of the alkaline phosphatase superfamily with a formylglycine nucleophile: structural and kinetic characterisation of a phosphonate monoester hydrolase/phosphodiesterase from *Rhizobium leguminosarum*. *J. Mol. Biol.* **2008**, 384(1), 120-136.

Juszczak, L. J., Zhang, Z.-Y., Wu, L., Gottfried, D.S., Eads, D.D. Rapid loop dynamics of Yersinia protein tyrosine phosphatases. *Biochemistry*, **1997**, 36, 2227-2236.

Jutten, P., Schumann, W., Har`tl, A., Heinisch, L., Grafe, U., Werner, W., Ulbricht, H. A novel type of nonsteroidal estrone sulfatase inhibitor. *Bioorg. Med. Chem. Lett.* **2002**, 12, 1339-1342.

Kane, J.F. Effects of rare codon clusters on high-level expression of heterologous proteins in Escherichia coli. *Current Opinion in Biotechnology.* **1995**, 6, 494-500.

Kane, J.F., Violand B.N., Curran, D.F., Staten, N.R., Duffin, K.L., Bogosian, G. Contacts between mammalian RNA polymerase II and the template DNA in a ternary elongation complex. *Nucleic Acids Research.* **1993**, 20, 6707-6712.

Kawano, J., Kotani, T., Ohtake, S., Minamino, N., Matsuo, H., Oinumu, T., Aikawa, E. Characterization of rat and human steroid sulfatases. *Biochim. Biophys. Acta*, **1989**, 997, 199-205.

Kehoe, J.W., Bertozzi, C.R. Tyrosine sulfation: a modulator of extracellular protein-protein interactions. *Chem. Biol.* **2000**, 7, 57-61.

Kenner, K.A., Anyanwu, E., Olefsky, J.M., Kusari, J. Protein-tyrosine phosphatase 1B is a negative regulator of insulin- and insulin-like growth factor-I-stimulated signalling. *J. Biol. Chem.*, **1996**, 271, 19810-19816.

Kettner, C. A., and Shenvi, A.B. Inhibition of the serine proteases leukocyte elastase, pancreatic elastase, cathepsin G, and chymotrypsin by peptide boronic acids, *J. Biol. Chem.* **1984**, 259, 15106-15114.

Klaman, L.D., Boss, O., Peroni, O.D., Kim, J.K., Marino, J.L., Zabolotny, J.M., Moghal, N., Lubkin, M., Kim, Y.B., Sharpe, A.H., Stricker-Krongrad, A., Shulman, G.I., Neel, B.G., Kahn, B.B. Increased energy expenditure, decreased adiposity, and tissue-specific insulin sensitivity in protein-tyrosine phosphatase 1B-deficient mice. *Mol. Cell. Biol.*, **2000**, 20, 5479-5489.

Kole, H.K., Akamatsu, M., Ye, B., Yan, X., Barford, D., Roller, P.P., Burke, T.R. Protein-tyrosine phosphatase inhibition by a peptide containing the phosphotyrosyl mimetic, L-O-malonyltyrosine. *Biochem. Biophys. Res. Commun.*, **1995**, 209, 817-822.

Kolodny, E.H., Fluharty, A.L. (Scriber CR, Beaudet AL, & Sly WS, Eds.), *Metachromatic Leukodystrophy and Multiple Sulfatase Deficiency: Sulfatide Lipidosis*, In *The Metabolic and Molecular Bases of Inherited Disease*, pp. 2693–2739, **1997**, McGraw-Hill, New York,.

Kríz, L., Bicíková, M., Mohapl, M., Hill, M., Cerný, I., Hampl, R. Roles of Steroid Sulfatase in Brain and Other Tissues. *Physiol. Res.*, **2008**, 57(5), 657-68.

Kitz, R., and Wilson, I.B. Esters of methanesulfonic acid as irreversible inhibitors of acetylcholinesterase. *J. Biol. Chem.* **1962**, 237(10), 3245-3249.

Krause, D.S., Van Etten, R.A. Tyrosine kinases as targets for cancer therapy. *New England Journal of Medicine*, **2005**, 353, 172-187.

Kuroguchi, M., Nishamura, S-I., Lee, Y.C. Mechanism-based fluorescent labeling of beta-galactosidases. An efficient method in proteomics for glycoside hydrolases. *J. Biol. Chem.* **2004**, 279, 44704.

Labrie, F., Belanger, A., Cusan, L., Labrie, C., Simard, J., Luu-The, V., Diamond, P., Gomez, J.L., Candas, B. *Endocrine Rel. Canc.*, **1996**, 3, 243-278.

Laemmli, U.K. *Nature*. **1970**, 227, 680-685.

Lapierre, Jennifer. Ph.D thesis. University of Waterloo, Waterloo, 2003.

Lapierre, J., Ahmed, V., Chen, M.-J., Ispahany, I., Guillemette, J.G., Taylor, S.D. The difluoromethylene group as a replacement for the labile oxygen in steroid sulfates: A new approach to steroid sulfatase inhibitors. *Bioorg. Med. Chem. Lett.*, **2004**, 14, 151-155.

Larsen, S.D., Barf, T., Liljebris, C., May, P.D., Ogg, D., O'Sullivan, T.J., Palazuk, B.J., Schostarez, H.J., Stevens, F.C., Bleasdale, J.E. Synthesis and biological activity of a novel class of small molecular weight peptidomimetic competitive inhibitors of protein tyrosine phosphatase 1B. *J. Med. Chem.* **2002**, 45, 598-622.

Lee, W., DeRome, M., DeBear, J., Noell, S., Epsatein, D., Mahle, C., DeCarr, L., Woodruff, K., Huang, Z., Dumas, J., Aryl piperazines: A new class of steroid sulfatase inhibitors for the treatment of hormone-dependent breast cancer. Abstract of Papers, 226th ACS National Meeting, New York, NY, USA, Sept. 7–11, 2003.

Lee, K., Gao, Y., Yao, Z.-J., Phan, J., Wu, L., Liang, J., Waugh, D.S., Zhang, Z.-Y., Burke, T.R. Tripeptide inhibitors of Yersinia protein-tyrosine phosphatase *Bioorg. Med. Chem. Lett.*, **2003**, *13*, 2577.

Lee, K., Boovanahalli, S.K., Nam, K.-Y., Kang, S.-U., Lee, M., Phan, J., Wu, L., Waugh, D.S., Zhang, Z.-Y., No, K.T., Lee, J.J., Burke, T.R. Synthesis of tripeptides as potent Yersinia protein tyrosine phosphatase inhibitors. *Bioorg. Med. Chem. Lett.*, **2005**, *15*, 4037.

Lee, S.-Y., Liang, F., Guo, X.-L., Xie, L., Cahill, S.M., Blumenstein, M., Design, construction, and intracellular activation of an intramolecularly self-silenced signal transduction inhibitor. *Angewandte Chemie. International Edition*, **2005**, *44*, 4242-4244.

Leder, I.G. A novel 3-O sulfatase from human urine acting on methyl-2-deoxy-2-sulfamino-alpha-D-glucopyranoside 3-sulfate. *Biochem. Biophys. Res. Commun.*, **1980**, *94*, 1183.

Le Roy, I., Mortand, S., Tordjman, S., Donez-Darcel, E., Carlier, M., Degrelle, H., Roubertoux, P.L. Genetic correlation between steroid sulfatase concentration and initiation of attack behavior in mice. *Behav. Genetics.*, **1999**, *29*, 131-136.

Leung, C., Lee, J., Meyer, N., Jia, C., Grzyb, J., Liu, S., Hum G., Taylor, S.D. The difluoromethylenesulfonic acid group as a monoanionic phosphate surrogate for obtaining PTP1B inhibitors. *Bioorg. Med. Chem.*, **2002**, *10*, 2309-2323.

Li, J., Kleeff, J., Abiatari, I., Kayed, H., Giese, N.A., Felix, K., Giese, T., Büchler, M.W., Friess, H. Enhanced levels of Hsulf-1 interfere with heparin-binding growth factor signaling in pancreatic cancer. *Mol. Cancer*, **2005**, *4*:14.

Li, P.K., Pillai, R., Young, B.L., Bender, W.H., Martino, D.M., Lin, F.T. Synthesis and biochemical studies of estrone sulfatase inhibitors. *Steroids*, **1993**, *58*, 106–111.

Li, P.K., Pillai, R., Dibbelt, L. Estrone sulfate analogs as estrone sulfatase inhibitors. *Steroids*, **1995**, *60*, 299–306.

Li, P.-K., Rhodes, M.E., Burke, A.M., Johnson, D.A. Memory enhancement mediated by the steroid sulfatase inhibitor (p-O-sulfamoyl)-N-tetradecanoyl tyramine. *Life Sciences including Pharmacology Letters*, **1996**, *60*, 45-51.

Lindahl, U., Backstrom, G., Thunberg, L., Leder, I.G. Evidence for a 3-*O*-sulfated D-glucosamine residue in the antithrombin-binding sequence of heparin. *Proc. Natl. Acad. Sci. USA*, **1980**, 77, 6551.

Liu, Y., Ph.D. Thesis, 2007, University of Waterloo.

Liu, Y., Lien, I-F., Ruttgaizer, S., Dove, P., Taylor, S.D. Synthesis and protection of aryl sulfates using the 2,2,2-trichloroethyl moiety. *Org. Lett.* **2004**, 6, 209.

Liu, Y., Kim, B., Taylor, S.D. Synthesis of 4-formyl estrone using a positional protecting group and its conversion to other C-4 substituted estrogens. *J. Org. Chem.* **2007**, 72(23), 8824-30.

Liu, Y., Ahmed, V., Hill, B., Taylor, S.D. Synthesis of a non-hydrolyzable estrone sulfate analogue bearing the difluoromethanesulfonamide group and its evaluation as a steroid sulfatase inhibitor. *Org. Biomol. Chem.*, **2005**, 3, 3329-3335.

Liu, G., Xin, Z., Pei, Z., Hajduk, P.J., Abad-Zapatero, C., Hutchins, C.W., Zhao, H., Lubben, T.H., Ballron, S.J., Haasch, D.L., Kaszubska, W., Rondinone, C.M., Trevillyan, J.M., Jirousek, M.R. Fragment screening and assembly: a highly efficient approach to a selective and cell active protein tyrosine phosphatase 1B inhibitor. *J. Med. Chem.* **2003**, 46, 4232-4235.

Lo, L.-C., Pang, T.-L., Kuo, C.-H., Chiang, Y.-L., Wang, H.-Y., Lin, J.-J. Design and synthesis of class-selective activity probes for protein tyrosine phosphatases. *J. Proteome Res.* **2002**, 1, 35-40.

Lodish, H., Berk, A., Zipursky, Lawrence, S., Matsudaira, P., Baltimore, D., Darnell, J.E. *Molecular Cell Biology*. **1999**, New York, W. H. Freeman & Co.

Loubinoux, B., Miazimbakana, J., Gerardin, P. Reactivity of new precursors of quinone methides. *Tetrahedron Lett.*, **1989**, 30, 1939-1942.

Lu, C-P., Ren, C-T., Wu, S-H., Chu, C-Y., Lo, L-C. Development of an Activity-based Probe for Steroid Sulfatases. *ChembioChem.* **2007**, 8, 2187-2190.

Lukatela, G., Krauss, N., Theis, K., Selmer, T., Gieselmann, V., von Figura, K., Saenger, W. Crystal structure of human arylsulfatase A: the aldehyde function and the metal ion at the active site suggest a novel mechanism for sulfate ester hydrolysis. *Biochemistry.* **1998**, 37, 3654-3664.

Maroun, C.R., Naujokas, M.A., Holgado-Madruga, M., Wong, A.J., Park, M. The Tyrosine Phosphatase SHP-2 Is Required for Sustained Activation of Extracellular Signal-Regulated Kinase and Epithelial Morphogenesis Downstream from the Met Receptor Tyrosine Kinase. *Mol. Cell Biol.*, **2000**, 20, 8513-25.

- Marseigne, I., Roques, B.P. Synthesis of new amino acids mimicking sulfated and phosphorylated tyrosine residues. *J. Org. Chem.*, **1988**, 53, 3621-3624.
- Martel, C., Melner, M.H., Gagne, D., Simard, J., Labrie, F. Widespread tissue distribution of steroid sulfatase, 3 beta-hydroxysteroid dehydrogenase/delta 5-delta 4 isomerase (3 beta-HSD), 17 beta-HSD 5 alpha-reductase and aromatase activities in the rhesus monkey. *Mol. Cell Endocrinol.*, **1994**, 104, 103-111.
- Masamura, S., Santner, S.J., Santen, R.J. Evidence of in situ estrogen synthesis in nitrosomethylurea-induced rat mammary tumors via the enzyme estrone sulfatase. *J. Steroid Biochem. Mol. Biol.* **1996**, 58, 425-430.
- Mauro, L.J., Dixon, J.E. 'Zip codes' direct intracellular protein tyrosine phosphatases to the correct cellular 'address'. *Trends Biochem. Sci.*, **1994**, 19, 151-155.
- McGovern, S.L., Caselli, E., Grigorieff, N., Shoichet, B.K. A common mechanism underlying promiscuous inhibitors from virtual and high-throughput screening. *J. Med. Chem.*, **2002**, 45, 1712-22.
- McGovern, S.L., Shoichet, B.K. Kinase inhibitors: not just for kinases anymore. *J. Med. Chem.* **2003**, 47, 1478.
- McNamara, D.J., Dobrosin, E.M., Zhu, G., Decker, S.J., Saltiel, A.R. Inhibition of binding of phospholipase C gamma 1 SH2 domains to phosphorylated epidermal growth factor receptor by phosphorylated peptides. *Int. J. Pept. Protein Res.*, **1993**, 42, 240-248.
- Meroni, G., Franco, B., Archidiacono, N., Messali, S., Andolfi, G., Rocchi, M. and Ballabio, A. Characterization of a cluster of sulfatase genes on Xp22.3 suggests gene duplications in an ancestral pseudoautosomal region. *Hum. Mol. Genet.*, **1996**, 5, 423-431.
- Miki, Y., Nakata, T., Suzuki, T., Darnel, A.D., Moriya, T., Kaneko, C., Hidaka, K., Shiotsu, Y., Kusaka, H., Sasano, H. Systemic distribution of steroid sulfatase and estrogen sulfotransferase in human adult and fetal tissues. *J. Clin. Endocrinol. Metab.*, **2002**, 87, 5760-5768.
- Miyoshi, Y., Ando, A., Hasegawa, S., Ishitobi, M., Taguchi, T., Tamaki, Y., Noguchi, S. High expression of steroid sulfatase mRNA predicts poor prognosis in patients with estrogen receptor-positive breast cancer. *Clin. Cancer Res.* **2003**, 9, 2288.
- Montalibet, J., Skorey, K.I., Kennedy, B.P. Protein tyrosine phosphatase: enzymatic assays. *Methods*, **2005**, 35, 2.
- Morimoto-Tomita, M., Uchimura, K., Werb, Z., Hemmerich, S., Rosen, S.D. Cloning and characterization of two extracellular heparin-degrading endosulfatases in mice and humans. *J. Biol. Chem.* **2002**, 277, 49175.

- Morrison, J.F. Kinetics of the reversible inhibition of enzyme-catalysed reactions by tight-binding inhibitors. *Biochim. Biophys. Acta.* **1969**, 185, 269.
- Musa, M.A., Cooperwood, J.S., Khan, M.O. A review of coumarin derivatives in pharmacotherapy of breast cancer. *Curr. Med. Chem.* **2008**, 15(26), 2664-79.
- Myers, J.K., Widlanski T.S. Mechanism-based inactivation of human prostatic phosphatase. *Science.* **1993**, 262, 1451-1453.
- Myers, J.K., Cohen, J.D., Widlanski, T.S. Substituent effects on the mechanism-based inactivation of prostatic acid phosphatase. *J. Am. Chem. Soc.* **1995**, 117, 11049-11054.
- Newman, S.P., Purohit, A., Ghilchik, M.W., Potter, B.V.L, Reed, M.J. *J. Steroid Biochem. Mol. Biol.*, **2000**, 75, 259-264.
- Noel, C.T., Reed, M.J., Jacobs, H.S., James, V.H.T.. The plasma concentration of oestrone sulphate in post-menopausal women: lack of diurnal variation, effect of ovariectomy, age and weight. *J. Steroid Biochem.* **1981**, 14, 1101-1105.
- Noel, H., Beauregard, G., Potier, M., Bleau, G., Chapdelaine, A., Roberts, K.D. The target sizes of the in situ and solubilized forms of human placental steroid sulfatase as measured by radiation inactivation. *Biochim. Biophys. Acta.* **1983**, 758, 88-90.
- Noel, H., Plante, L., Bleau, G., Chapdelaine, A., Roberts, K.D.. Human placental steroid sulfatase: purification and properties. *J. Steroid Biochem.* **1983**, 19, 1591-1598.
- Nussbaumer, A., Lehr, P., Billich, A. 2-Substituted 4-(thio)chromenone 6-O-sulfamates: potent inhibitors of human steroid sulfatase *J. Med. Chem.*, **2002**, 45, 4310.
- Nussbaumer, P., Bilban, M., Billich, A. 4,4 O-Benzophenone-O,O'-disulfamate, a potent inhibitor of steroid sulfatase. *Bioorg. Med. Chem. Lett.* **2002**, 12, 2093-2095.
- Nussbaumer, A., and Billich, A. Steroid sulfatase inhibitors. *Med. Res. Rev.*, **2004**, 24(4), 529-576.
- Nussbaumer, P., Horvath, A., Lehr, P., Wolff, B., Geyl, D., Billich, A. *Bioorg. Med. Chem. Lett.* **2003**, 13, 3673-3677.
- O'Brien, P.J., Herschlag, D. Sulfatase Activity of *E. coli* Alkaline Phosphatase Demonstrates a Functional Link to Arylsulfatases, an Evolutionarily Related Enzyme Family. *J. Am. Chem. Soc.* 1998, 120, 12369-12370.
- Obaya, A.J. Molecular cloning and initial characterization of three novel human sulfatases. *Gene*, **2006**, 372, 110-117.

- Pannifer, A.D., Flint, A.J., Tonks, N.K., Barford, D. Visualization of the cysteinyl-phosphate intermediate of a protein-tyrosine phosphatase by X-ray crystallography. *J. Biol. Chem.* **1998**, 273, 10454–10462.
- Parenti, G., Meroni, G. and Ballabio, A. The sulfatase gene family. *Curr. Opin. Genet. Dev.*, **1997**, 7, 386–391.
- Park, J., Fu, H., Pei, D. Peptidyl Aldehydes as Reversible Covalent Inhibitors of Src Homology 2 Domains. *Biochemistry*, **2003**, 42, 5159–5167.
- Park-Chung, M., Malayev, A., Purdy, R.H., Gibbs, T.T., Farb, D.H. Sulfated and unsulfated steroids modulate gamma-aminobutyric acid_A receptor function through distinct sites. *Brain Res.*, **1999**, 830, 72-87.
- Peters, C., Schmidt, B., Rommerskirch, W., Rupp, K., Zuhlsdorf, M., Vingron, M., Meyer, H., Pohlmann, R., von Figura, K. Phylogenetic conservation of arylsulfatases: cDNA cloning and expression of human arylsulfatase B. *J. Biol. Chem.* **1990**, 265, 3374-81.
- Philipp, M., Bender, M.L. Inhibition of serine proteases by arylboronic acids. *Proc. Natl. Acad. Sci. U.S.A.* **1971**, 68, 478–480.
- Picot D., Loll P.J., Garavito, R.M. The X-ray crystal structure of the membrane protein prostaglandin H2 synthase-1. *Nature*, **1994**, 367, 243–249.
- Pingel, J.T., Thomas, M.L. Evidence that leukocyte-common antigen is required for antigen-induced T lymphocyte proliferation. *Cell*, **1989**, 58, 1055-1065.
- Pitts, R.L. Serum elevation of dehydroepiandrosterone sulfate associated with male pattern baldness in young men. *J. Am. Acad. Dermatol.*, **1987**, 16, 571-573.
- Poirier, D., Boivin, R.P. 17-alpha-alkyl- or 17alpha-substituted-17beta-estradiols. A new family of estrone-sulfatase inhibitors. *Bioorg. Med. Chem. Lett.*, **1998**, 8, 1891-1896.
- Ponniah, S., Wang, D., Lim, D.L., Pallen, C.J. Targeted disruption of the tyrosine phosphatase PTPalpha leads to constitutive downregulation of the kinases Src and Fyn. *Current Biology*, **1999**, 9, 535-538.
- Poortman, J., Andriessse, R., Agema, A., Donker, G.H., Schwartz, F., Thijssen, J.H.H.. Adrenal androgen secretion and metabolism in post-menopausal women, in: A.R. Genazzani, J.H.H. Thijssen, P.K. Siiteri (Eds). *Adrenal Androgens*, Raven Press, New York. 1980. pp. 219-240.
- Poulin, R., Labrie, F. Stimulation of cell proliferation and estrogenic response by adrenal C19-delta 5-steroids in ZR-75-1 human breast cancer cell line. *Cancer. Res.*, **1986**, 46, 4933-4937.

- Preusser-Kunze, A., Mariappan, M., Schmidt, B., Gande, S.L., Mutenda, K., Wenzel, D., von Figura, K., Dierks, T. Molecular characterization of the human Calpha-formylglycine-generating enzyme. *J. Biol. Chem.* **2005**, 280(15), 14900-10.
- Puca, A. A., Zollo, M., Repetto, M., Andolfi, G., Guffanti, A., Simon, G., Ballabio, A., Franco, B. Identification by shotgun sequencing, genomic organization, and functional analysis of a fourth arylsulfatase gene (ARSF) from the Xp22.3 region. *Genomics.* **1997**, 42, 192.
- Puius, Y.A., Zhao, Y., Sullivan, M., Lawrence, D.S., Almo, S.C., Zhang, Z.-Y. Identification of a second aryl phosphate-binding site in protein-tyrosine phosphatase 1B: A paradigm for inhibitor design. *Proc. Natl. Acad. Sci. U.S.A.*, **1997**, 94, 13420-13425.
- Purohit, A., Potter, B.V.L., Parker, M.G., Reed, M.J. Steroid sulphatase: expression, isolation and inhibition for active-site identification studies *Chem.-Biol. Interact.* **1998**, 109, 183-193.
- Purohit, A., Williams, G.J., Howarth, N.M., Potter, B.V.L., Reed, M.J. Inactivation of steroid sulfatase by an active site-directed inhibitor, estrone-3-O-sulfamate. *Biochemistry*, **1995**, 34, 11508-11514.
- Purohit, A., Woo, L.W.L., Singh, A., Winterborn, C.J., Potter, B.V.L., Reed, M.J. In vivo activity of 4-methylcoumarin-7-O-sulfamate, a nonsteroidal, nonestrogenic steroid sulfatase inhibitor. *Cancer Res.* **1996**, 56, 4950.
- Purohit, A., Woo, L.W.L., Chander, S.K., Newman, S.P., Ireson, C., Ho, Y., Grasso, A., Leese, M.P., Potter, B.V.L., Reed, M.J. Steroid sulfatase inhibitors for breast cancer therapy. *J. Steroid Biochem. Mol. Biol.*, **2003**, 86, 423-432.
- Prive, G.G. Detergents for the stabilization and crystallization of membrane proteins. *Methods.* **2007**, 41, 388-397
- Qu, C.K. The SHP-2 tyrosine phosphatase: signaling mechanisms and biological functions. *Cell Res.*, **2000**, 10, 279-88.
- Recksiek, M., Selmer, T., Dierks, T., Schmidt, B., von Figura, K. Sulfatases, trapping of the sulfated enzyme intermediate by substituting the active site formylglycine. *J. Biol. Chem.* **1998**, 273(11), 6096-103.
- Ree, M.J., Purohit, A., Woo, L.W., Newman, S.P. and Potter, B.V. Steroid sulfatase: molecular biology, regulation and inhibition. *Endocr. Rev.*, **2005**, 26, 171-202.
- Reed, M.J., Purohit, A. Sulphatase inhibitors: the rationale for the development of a new endocrine therapy. *Rev. Endocrine-Related Cancer.* **1993**, 45, 51-62.

- Reed, M.J., Purohit, A., Howarth, N.M., Potter, B.V.L. Steroid sulphatase inhibitors: a new endocrine therapy. *Drugs Future*. **1994**, 19, 673-680.
- Reed, M.J., Owen, A.M., Lai, L.C., Coldham, N.G., Ghilchik, M.W., Shaikh N.A., James, V.H.T.. In situ oestrone synthesis in normal breast and breast tumour tissues: effect of treatment with 4-hydroxyandrostenedione. *Int. J. Cancer*. **1989**, 44:233-237.
- Reed, M.J., Purohit, A., Howarth, N.M., Potter, B.V.L. Steroid sulphatase inhibitors. A new endocrine therapy. *Drugs Future*. **1994**, 19, 673-680.
- Reed, M.J., Purohit, A., Woo, L.W., Newman, S.P., Potter, B.V. Steroid sulfatase: molecular biology, regulation, and inhibition. *Endocr Rev*. **2005**, 26(2), 171-202.
- Roeser, D., Preusser-Kunze, A., Schmidt, B., Gasow, K., Wittmann, J.G., Dierks, T., von Figura, K, Rudolph, M.G. A general binding mechanism for all human sulfatases by the formylglycinegenerating enzyme. *Proc Natl Acad Sci U.S.A.* **2006**, 103, 1-86.
- Romsicki, Y., Reece, M., Gauthier, J.-Y., Asante-Appiah, E., Kennedy, B.P. Protein tyrosine phosphatase-1B dephosphorylation of the insulin receptor occurs in a perinuclear endosome compartment in human embryonic kidney 293 cells. *J. Biol. Chem.*, **2004**, 279, 12868.
- Rook, G.A.W., Hernandez-Pando, R., Lightman, S. Hormones, peripherally activated prohormones and regulation of the Th1/Th2 balance. *Immunol. Today*. **1994**, 15:301-303.
- Rotin, D., Margolis, B., Mohammadi, M., Daly, R. J., Daum, G., Li, N., Fischer, E.H., Burgess, W.E., Ullrich, A., Schlessinger, J. SH2 domains prevent tyrosine dephosphorylation of the EGF receptor: identification of Tyr992 as the high-affinity binding site for SH2 domains of phospholipase C gamma. *EMBO J*. **1992**, 11, 559-567.
- Roy, A.B., in *The Enzymes*, Vol. V (Ed. P.D. Boyer), Academic Press, New York, 1971.
- Ruder, H.J., Loriaux, D.L., Lipsett, M.B.. Estrone sulphate: production rate and metabolism in man. *J. Clin. Invest.* **1972**, 51, 1020-1023.
- Salmeen, A., Anderson, J.N., Myers, M.P., Meng, T.-C., Hinks, J.A., Tonks, N.K., Barford, D. Redox regulation of protein tyrosine phosphatase 1B involves a sulphenylamide intermediate. *Nature*, **2003**, 423, 769-773.
- Sambrook, J., and Russell, D. *Molecular Cloning: A Laboratory Manual*. 3rd Ed. Cold Spring Harbor Laboratory Press, 2001.
- Santen, R.J., Santner, S.J., Davis, B., Veldhuis, J., Samojilik, E., Ruby, E.. Aminoglutethimide inhibits extraglandular estrogen production in post-menopausal women with breast carcinoma. *J. Clin Endocrinol. Metab.* **1978**, 47, 1257-1265.

Santner, J., Feil, P.D., Santen, R.J. In situ estrogen production via estrone sulfatase pathway in breast tumors: relative importance versus aromatase pathway. *J. Clin. Endocrinol. Metab.* **1984**, 59, 24-33.

Sardiello, M., Annunziata, I., Roma, G., Ballabio, A. Sulfatases and sulfatase modifying factors: an exclusive and promiscuous relationship. *Hum. Mol. Genet.*, **2005**, 14, 3203-3217.

Sasano, H., Nagasaki, S., Miki, Y., Suzuki, T. New developments in intracrinology of human breast cancer: estrogen sulfatase and sulfotransferase. *Ann. N. Y. Acad. Sci.*, **2009**, 1155:76-9.

Scott, H.S., Blanch, L., Guo, X.H., Freeman, C., Orsborn, A., Baker, E., Sutherland, G.R., Morris, C.P. and Hopwood, J.J. Cloning of the sulphamidase gene and identification of mutations in Sanfilippo A syndrome. *Nat. Genet.*, **1995**, 11, 465-467.

Schmidt, B., Selmer, T., Ingendoh, A., von Figura, K. A novel amino acid modification in sulfatases that is defective in multiple sulfatase deficiency. *Cell*. **1995**, 82, 271-278.

Schubert, D., Boss, K., Dorst, H.J., Flossdorf, J., Pappert, G. The nature of the stable noncovalent dimers of band 3 protein from erythrocyte membranes in solutions of Triton X-100. *FEBS Letters*, **1983**, 163, 81-84.

Segel, I.H. *Enzyme Kinetics*, **1975**, Wiley, New York.

Selcer, K.W., Li, P.K. Estrogenicity, antiestrogenicity and estrone sulfatase inhibition of estrone-3-amine and estrone-3-thiol. *J. Steroid Biochem. Mol. Biol.* **1995**, (5)2, 281-286.

Selcer, K.W., Jagannathan, S., Rhodes, M.E., Li, P.K. Inhibition of placental estrone sulfatase activity and MCF-7 breast cancer cell proliferation by estrone-3-amino derivatives. *J Steroid Biochem. Mol. Biol.*, **1996**, 59, 83-91.

Selcer, K.W., Kabler, H., Sarap, J., Xiao, Z., Li, P.K. Inhibition of steryl sulfatase activity in LNCaP human prostate cancer cells. *Steroids*, **2002**, 67, 821-826.

Selcer K.W., Hedge P.V., Li P.K. Inhibition of estrone sulfatase and proliferation of human breast cancer cells by nonsteroidal (p-O-sulfamoyl)-N-alkanoyl tyramines. *Cancer Res.* **1997**, 57, 702-707.

Selmer, T., Hallmann, A., Schmidt, B., Sumper, M., von Figura, K. The evolutionary conservation of a novel protein modification, the conversion of cysteine to serinesemialdehyde in arylsulfatase from *Volvox carteri*. *Eur. J. Biochem.*, **1996**, 238, 341-345.

Shankaran, R., Ameen, M., Daniel, W., Davidson, R.G., Chang, P.L. Characterization of arylsulfatase C isozymes from human liver and placenta. *Biochemica et Biophysica Acta.* **1991**, 1078, 251-257.

Shen, K., Keng, Y.F., Wu, L., Guo, X.L., Lawrence, D.S., Zhang, Z.-Y. Acquisition of a specific and potent PTP1B inhibitor from a novel combinatorial library and screening procedure. *J. Biol. Chem.*, **2001**, 276, 47311-47319.

Silverman, R.B. CRC Mechanism-based enzyme inactivation: Chemistry and Enzymology, Volume 1. **1998**, CRC Press, Boca Raton, USA.

Smyth, M.S., Ford, H., Jr., Burke, T.R., Jr. A general method for the preparation of benzylic alpha, alpha-difluorophosphonic acids; non-hydrolyzable mimetics of phosphotyrosine. *Tetrahedron Lett.*, **1992**, 33, 4137-4140.

Speers, A.E., Cravatt, B.F. Chemical strategies for activity-based proteomics. *ChemBioChem*. **2004**, 5, 41-47.

Stankovic, C.J., Surendran, N., Lunney, E.A., Plummer, M.S., Para, K.S., Shahripour, A., Fergus, J.H., Marks, J.S., Herrera, R., Hubbell, S.E., Humblet, C., Saltiel, A.R., Stewart, B.H., Sawyer, T.K. The role of 4-phosphonodifluoromethyl- and 4-phosphonophenylalanine in the selectivity and cellular uptake of SH2 domain ligands. *Bioorg. Med. Chem. Lett.*, **1997**, 7, 1909-1914.

Stanway, S.J., Purohit, A., Woo, L.W., Sufi, S., Vigushin, D., Ward, R., Wilson, R.H., Stanczyk, F.Z., Dobbs, N., Kulinskaya, E., Elliott, M., Potter, B.V., Reed, M.J., Coombes, R.C. Phase I study of STX 64 (667 Coumate) in breast cancer patients: the first study of a steroid sulfatase inhibitor. *Clin. Cancer Res.* **2006**, 12, 1585-1592.

Steckelbroeck, S., Nassen, A., Ugele, B., Ludwig, M., Watzka, M., Reissinger, A., Clusmann, H., Lutjohann, D., Siekmann, L., Klingmuller, D., Hans, V.H. Steroid sulfatase (STS) expression in the human temporal lobe: enzyme activity, mRNA expression and immunohistochemistry study. *J Neurochem.*, **2004**, 89(2), 403-17.

Stuckey, J.A., Schubert, H.L., Fauman, E., Zhang, Z.-Y., Dixon, J.E., Saper, M.A. Crystal structure of Yersinia protein tyrosine phosphatase at 2.5 Å and the complex with tungstate. *Nature*, **1994**, 370, 571-575.

Stein, C., Hille, A., Seidel, J., Rijnbout, S., Waheed, A., Schmidt, B., Geuze, H., von Figura, K. Cloning and Expression of Human Steroid-sulfatase: Membrane topology, glycosylation, and subcellular distribution in BHK-21 cells. *J. Biol. Chem.* **1989**, 264 (23), 13865-13872.

Stengel, C., Simon, P., Newman, J., Day, M., Tutill, H.J., Reed, M.J., Purohit, A. Effects of mutations and glycosylations on STS activity: A site-directed mutagenesis study. *Molecular and Cellular Endocrinology*, **2008**, 283, 76-82.

Stephens, B.J., Han, H., Gokhale, V., and Von Hoff, D.D. PRL phosphatases as potential molecular targets in cancer. *Mol. Cancer Ther.*, **2005**, 4, 1653-1661.

- Stevens, R.L., Fluharty, A.L., Skokut, M.H., Kihara, H. Purification and properties of arylsulfatase A from human urine. *J. Biol. Chem.*, **1975**, 250, 2495-2501.
- Sugawara, T., Shimizu, H., Hoshi, N., Fujimoto, Y., Nakajima, A., Fujimoto, S. PCR diagnosis of X-linked ichthyosis: identification of a novel mutation (E560P) of the steroid sulfatase gene. *Human Mutat.*, **2000**, 15, 296.
- Sun, J.-P., Federov, A.A., Lee, S.-Y., Guo, X.-L., Shen, K., Lawrence, D.S. Crystal structure of PTP1B in complex with a potent and selective bidentate inhibitor. *J. Biol. Chem.*, **2003**, 278, 12406-12414.
- Supuran, C.T. Carbonic anhydrases as drug targets—an overview. *Curr. Top. Med. Chem.*, **2007**, 7(9), 825-833.
- Suzuki, T., Hirato, K., Yanaihara, T., Kodofuku, T., Sato, T., Hoshino, M., Yanaihara, N.. Purification and properties of steroid sulfatase from human placenta. *Endocrinol. Jpn.* **1992**, 39 (1), 93-101.
- Suzuki, T., Nakata, T., Miki, Y., Kaneko, C., Moriya, T., Ishida, T., Akinaga, S., Hirakawa, H., Kimura, M., Sasano, H. Estrogen sulfotransferase and steroid sulfatase in human breast carcinoma. *Cancer Res.* **2003**, 63(11), 2762-2770.
- Szameit, C., Miech, C., Balleininger, M., Schmidt, B., von Figura, K., and Dierks, T. The iron sulfur protein AtsB is required for posttranslational formation of formylglycine in the *Klebsiella sulfatase*. *J. Biol. Chem.* **1999**, 274, 15375-15381.
- Tartaglia, L.A. The leptin receptor. *J. Biol. Chem.* **1997**, 272, 6093-6096.
- Tilley, J.W., Danho, W., Lovey, K., Wagner, R., Swistok, J., Makofske, R., Michalewsky, J., Triscari, J., Nelson, D., Weatherford, S. Carboxylic acids and tetrazoles as isosteric replacements for sulfate in cholecystokinin analogues. *J. Med. Chem.*, **1991**, 34(3), 1125-36.
- Tobacman, J. Does deficiency of arylsulfatase B have a role in cystic fibrosis? *Chest.* **2003**, 123(6), 2130-9.
- Tonks, N.K., Diltz, C.D., and Fischer, E.H. Purification of the major protein-tyrosine-phosphatases of human placenta. *J. Biol. Chem.* **1988**, 263, 6722-6730.
- Tonks, N.K., Diltz, C.D., and Fischer, E.H. Characterization of the major protein-tyrosine-phosphatases of human placenta. *J. Biol. Chem.* **1988**, 263, 6731-6737.
- Tonks, N.K. PTP1B: From the sidelines to the front lines! *F.E.B.S. Letters*, **2003**, 546, 140-148.

- Tonks, N.K. Protein tyrosine phosphatases: from genes, to function, to disease. *Nat. Rev. Mol. Cell Biol.*, **2006**, 7, 833-846.
- Tomatsu, S., Fukuda, S., Masue, M., Sukegawa, K., Fukao, T., Yamagishi, A., Hori, T., Iwata, H., Ogawa, T., Nakashima, Y. Morquio disease: isolation, characterization and expression of full-length cDNA for human N-acetylgalactosamine-6-sulfate sulfatase. *Biochem. Biophys. Res. Commun.* **1991**, 181, 677.
- Torsell, K. In *Progress in Boron Chemistry*; Steinberg, H., McCloskey, A.L. Eds., Pergamon: New York, 1964; Vol. 1, pp 369–415.
- Trepka, R.D., Harrington, J.K., Belisle, J.W. Synthesis and herbicidal activity of fluorinated N-phenylalkanesulfonamides. *J. Org. Chem.* **1974**, 39, 1094.
- Tsai, C.S., Li, Y.K., Lo, L.C. Design and synthesis of activity probes for glycosidases. *Org. Lett.* **2002**, 4, 3607–10.
- Uchimura, K., Morimoto-Tomita, M., Bistrup, A., Li, J., Lyon, M., Gallagher, J., Werb, Z., Rosen, SD. HSulf-2, an extracellular endoglycosaminase-6-sulfatase, selectively mobilizes heparinbound growth factors and chemokines: effects on VEGF, FGF-1, and SDF-1. *BMC Biochemistry*, **2006**, 7, 2.
- Vaccaro, A.M., Salvioli, R., Muscillo, M., Renola, L. Purification and properties of arylsulfatase C from human placenta. *Enzyme.* **1987**, 37, 115-126.
- van der Loos, C.M., Van Breda, A.J., Van den Berg, F.M., Walboomers J.M.M., Jobsis A.C. Human placental steroid sulfatase purification and monospecific antibody production in rabbits. *J. Inher. Metab.* **1983**, 7, 97-103.
- von Bulow, R., Schmidt, B., Dierks, T., von Figura, K., Uson, I. Crystal structure of an enzyme-substrate complex provides insight into the interaction between human arylsulfatase A and its substrates during catalysis. *J. Mol. Biol.* **2001**, 305, 269.
- von Figura, K., Schmidt, B., Selmer, T., Dierks, T. A novel protein modification generating an aldehyde group in sulfatases: its role in catalysis and disease. *BioEssays*, **1998**, 20, 505–510.
- Villani, G.R.D., Daniele, A., Balzano, N., di Natale, P. Expression of five iduronate-2-sulfatase site-directed mutations. *Biochimica et Biophysica Acta.* **2000**, 1501, 71-80.
- Wakselman, M. *Nouv. J. Chimie.* **1983**, 7, 439-447.
- Waldow, A., Schmidt, B., Dierks, T., von Bulow, R., von Figura, K. Amino acid residues forming the active site of arylsulfatase A. Role in catalytic activity and substrate binding. *J. Biol. Chem.* **1999**, 274, 12 284.

- Watanabe, T., Harada, N., Sasaki, H. Quantitative analysis of mRNA expression of estrone sulfatase in endometrial carcinoma and benign endometrium. *Jikeikai Med. J.* **2000**, 47, 121–127.
- Warren, J.C., and French, A.P. Distribution of steroid sulfatase in human tissues. *J. Clin. Endocrinol. Metab.* **1965**, 25, 278-282.
- Wang, Q., Dechert, U., Jirik, F., Withers, S.G. Suicide inactivation of human prostatic acid phosphatase and a phosphotyrosine phosphatase. *Biochem. Biophys. Res. Comm.* **1994**, 200, 577-583.
- Wang, F., Li, W., Emmett, M.R., Hendrickson, C.L., Marshall, A.G., Zhang, Y.-L., Wu, L., Zhang, Z.-Y. Conformational and dynamic changes of Yersinia protein tyrosine phosphatase induced by ligand binding and active site mutation and revealed by H/D exchange and electrospray ionization Fourier transform ion cyclotron resonance mass spectrometry. *Biochemistry*, **1998**, 37, 15289-15299.
- Welte, S., Baringhaus, K.H., Schmider, W., Muller, G., Petr, S., Tennagels, N. 6,8-Difluoro-4-methylumbiliferyl phosphate: a fluorogenic substrate for protein tyrosine phosphatases. *Anal. Biochem.*, **2005**, 38, 32-38.
- Wendt, K.U., Poralla, K., Schultz, G.E. Structure and function of a squalene cyclase. *Science*, **1997**, 277, 1811–1815.
- Winum, J.Y., Scozzafava, A., Montero, J.L., Supuran, C.T. Sulfamates and their therapeutic potential. *Med Res. Rev.* **2005**, 25(2): 186-228.
- Wolff B., Billich A., Brunowsky W., Herzig G., Lindley I., Nussbaumer P., Pursch E., Rabeck C., Winkler G. Microtiter plate cellular assay for human steroid sulfatase with fluorescence readout. *Anal. Biochem.* **2003**, 318, 276–284.
- Woo, L.W.L., Purohit, A., Reed, M.J., Potter, B.V.L. In vivo activity of 4-methylcoumarin-7-O-sulfamate, a nonsteroidal, nonestrogenic steroid sulfatase inhibitor. *Bioorg. Med. Chem. Lett.*, **1997**, 7, 3075.
- Woo L.W.L., Howarth, N.M., Purohit, A., Jejaz, H.A.M., Reed, M.J., Potter, B.V.L. Steroidal and nonsteroidal sulfamates as potent inhibitors of steroid sulfatase. *J. Med. Chem.*, **1998**, 41, 1068.
- Woo, L.W.L., Purohit, A., Malini, B., Reed, M.J., Potter, B.V.L. Potent active site-directed inhibition of steroid sulphatase by tricyclic coumarin-based sulphamates. *Chem. Biol.* **2000**, 7:773-791.
- Woo, L.W., Sutcliffe, O.B., Bubert, C., Grasso, A., Chander S.K., Purohit A., Reed, M. J., Potter, B.V. First dual aromatase-steroid sulfatase inhibitors. *J. Med. Chem.*, **2003**, 46, 3193.

Wrobel, J., Sredy, J., Moxham, C., Dietrich, A., Li, Z., Sawicki, D.R., Seestaller, L., Wu, L., Katz, A., Sullivan, D., Tio, C., Zhang, Z.-Y. PTP1B inhibition and antihyperglycemic activity in the ob/ob mouse model of novel 11-arylbenzo[b]naphtho[2,3-d]furans and 11-arylbenzo[b]naphtho[2,3-d]thiophenes. *J. Med. Chem.* **1999**, *42*, 3199-3202.

Xie, L., Lee, S.-Y., Andersen, J.N., Waters, S., Shen, K., Guo, X.-L., Cellular effects of small molecule PTP1B inhibitors on insulin signalling. *Biochemistry*, **2003**, *42*, 12792-12804.

Xin, Z., Liu, G., Abad-Zapatero, C., Pei, Z., Szczepankiewicz, B.G., Li, X., Zhang, T., Hutchins, C.W., Hajduk, P.J., Ballron, S.J., Stashko, M.A., Lubben, T.H., Trevillyan, J. M., Jirousek, M.R. *Bioorg. Med. Chem. Lett.*, **2003**, *13*(22), 3947-50.

Yamamoto, T., Kitawaki, J., Urabe, M., Honjo, H., Tamura, T., Noguchi, T., Okada, H., Sasaki, H., Tada, A., Terashima, Y. Estrogen productivity of endometrium and endometrial cancer tissue; influence of aromatase on proliferation of endometrial cancer cells. *J. Steroid Biochem. Mol. Biol.* **1993**, *44*, 463-468.

Yang, W., Gao, X., Wang, B. *Med. Res. Rev.*, **2003**, *23*, 346-368.

Ye, B., Akamatsu, M., Shoelson, S.E., Wolf, G., Giorgetti-Peraldi, S., Yan, X.J., Roller, P.P., Burke, T.R. L-O-(2-malonyl)-tyrosine: A new phosphotyrosyl mimetic for the preparation of Src homology 2 domain inhibitory peptides. *J. Med. Chem.* **1995**, *38*, 4270-4275.

Yen, P.H., Allen, E., Marsh, B., Mohandas, T., Wang, N., Taggart, Shapiro, L.J. Cloning and expression of steroid sulfatase cDNA and the frequent occurrence of deletions in STS deficiency: implications for X-Y interchange. *Cell*, **1987**, *49*, 443-454.

Yen, P.H., Marsh, B., Allen, E., Tsai, S.P., Ellison, J., Connolly, L., Neiswanger, K., Shapiro, L.J. The human X-linked steroid sulfatase gene and a Y-encoded pseudogene: evidence for an inversion of the Y chromosome during primate evolution. *Cell*, **1988**, *55*, 1123-1135.

Yue, E.W., Wayland, B., Douty, B., Crawley, M.L., McLaughlin, E., Takvorian, A., et al., Isothiazolidinone heterocycles as inhibitors of protein tyrosine phosphatases: synthesis and structure-activity relationships of a peptide scaffold. *Bioorg. Med. Chem.*, **2006**, *14*, 5833-5849.

Zabolotny, J.M., Bence-Hanulec, K.K., Stricker-Krongrad, A., Haj, F., Wang, Y., Minokoshi, Y., Kim, Y.B., Elmquist, J.K., Tartaglia, L.A., Kahn, B.B., Neel, B.G. PTP1B regulates leptin signal transduction in vivo. *Dev. Cell*, **2002**, *2*, 489-495.

Zhang, Z.-Y. Chemical and Mechanistic Approaches to the Study of Protein Tyrosine Phosphatases. *Acc. Chem. Res.*, **2003**, 36, 385-392.

Zhang, Z.-Y., Thieme-Seffler, A.M., Maclean, D., McNamara, D.J., Dobrusin, E.M., Sawyer, T.K., Dixon, J.E. A continuous spectrophotometric and fluorimetric assay for protein tyrosine phosphatase using phosphotyrosine-containing peptides. *Proc. Natl. Acad. Sci. U.S.A.*, **1993**, 90, 4446.

Zhang, Z.-Y., Maclean, D.J., McNamara, J., Sawyer, T.K., Dixon, J.E. Protein tyrosine phosphatase substrate specificity: size and phosphotyrosine positioning requirements in peptide substrates. *Biochemistry*, **1994**, 33, 2285-2290.

Zhang, Z.-Y., Wu, L. The single sulfur to oxygen substitution in the active site nucleophile of the Yersinia protein-tyrosine phosphatase leads to substantial structural and functional perturbations. *Biochemistry*, **1997**, 36, 1362-1369.

Zhang, S., Zhang, Z.-Y. PTP1B as a drug target: recent developments in PTP1B inhibitor discovery. *Drug Discovery Today*, **2007**, 12(9), 373-381.

Zhang, Z.-Y. Protein tyrosine phosphatases: prospects for therapeutics. *Curr. Opin. Chem. Biol.*, **2001**, 5, 416-423.

Zhang, Z.-Y., Protein tyrosine phosphatases: structure and function, substrate specificity, and inhibitor development. *Ann. Rev. Pharmacol. Toxicol.* **2002**, 42, 209-234.

Zheng, X.M., Wang, Y., Pallen, C.J. Cell transformation and activation of pp60c-src by overexpression of a protein tyrosine phosphatase. *Nature*, **1992**, 359, 336-339.

Zinker, B.A., Rondinone, C.M., Trevillyan, J.M., Gum, R.J., Clampit, J.E., Waring, J.F., Xie, N., Wilcox, D., Jacobson, P., Frost, L., Kroeger, P.E., Reilly, R.M., Koterski, S., Opgenorth, T.J., Ulrich, R.G., Crosby, S., Butler, M., Murray, S.F., McKay, R.A., Bhanot, S., Monia, B.P., Jirousek, M.R. PTP1B antisense oligonucleotide lowers PTP1B protein, normalizes blood glucose, and improves insulin sensitivity in diabetic mice. *Proc. Natl. Acad. Sci. U.S.A.*, **2002**, 99, 11357-11362.

Appendix A – Preliminary kinetic studies for compounds 3.24, 3.25 and 3.32-3.34

A.1. General procedure for IC₅₀ determinations of compounds 3.24, 3.25, 3.33 and 3.34.

10 µL of solutions of various concentrations of the inhibitors in DMSO/0.1 M tris, pH 7.0 (1:1) (for compounds 3.24, 3.25 and 3.33) or 0.1 M tris, pH 7.0 (for compound 3.34) were added to the wells of a microtiter plate containing 80 µL of 250 µM 4-MUS in 0.1 M tris, pH 7.0. The reaction was initiated by the addition of 10 µL of 40 nM STS stored in 20 mM tris, pH 7.4, 0.1% Triton X-100 to a final concentration of 4 nM STS and 200 µM 4-MUS (K_m concentration) in 0.1 M tris, pH 7.0, 0.01% Triton X-100, 5% DMSO. The production of 4-MU was followed for 10 minutes ($\lambda_{ex} = 360$ nm, $\lambda_{em} = 460$ nm) at 22°C. The percent activity of STS in the presence of inhibitor after each time interval was calculated as a percentage of activity in the absence of inhibitor. IC₅₀ plots of % activity versus log concentration of the inhibitor are shown **Figures A1-A4** below. The initial rates of enzyme activity in relative fluorescence units per second (RFUs/sec) were used to determine the IC₅₀. The ratio of the initial rate in the presence of inhibitor (V_i) to that in the absence of inhibitor (V_o) was calculated and plotted as a semi-log curve in Grafit (Erithacus Software, Surrey, U.K.), from which the IC₅₀ value was calculated based on the following equation: $V_i = V_o/[1 + ([I]/IC_{50})^s] + B$, where: V_i is the initial rate of reaction at an inhibitor concentration concentration of $[I]$; V_o is the velocity in the absence of inhibitor; B is background and s is the slope factor.

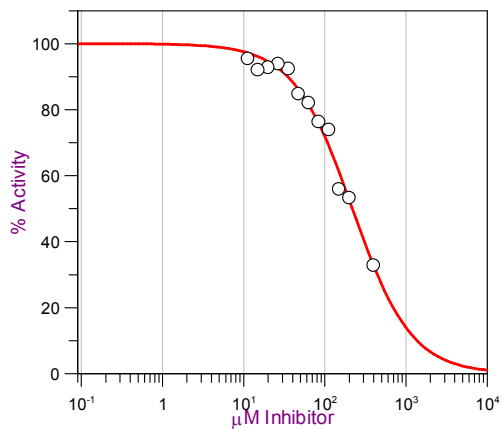


Figure A.1. IC₅₀ plot for compound **3.24**. Inhibitor concentrations range from 11-400 μM. IC₅₀ = 218 ± 12 μM.

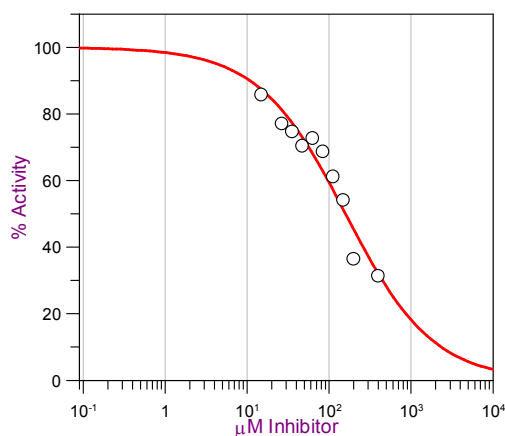


Figure A.2. IC₅₀ plot for compound **3.25**. Inhibitor concentrations range from 15-400 μM. IC₅₀ = 158 ± 17 μM.

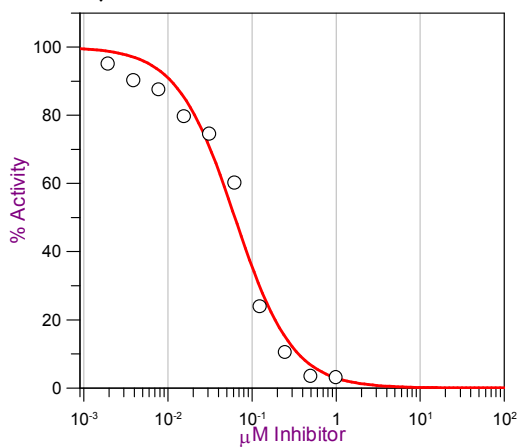


Figure A.3. IC₅₀ plot for compound **3.33**. Inhibitor concentrations range from 2-1000 μM. IC₅₀ = 62 ± 7 nM.

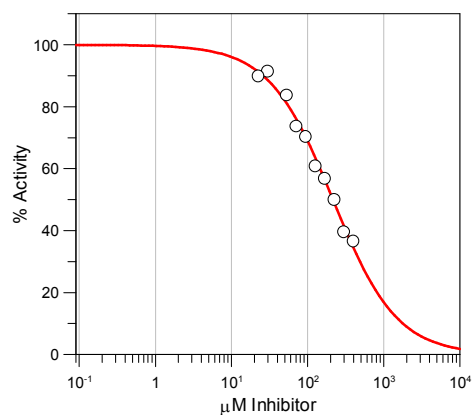


Figure A.4. IC_{50} plot for compound **3.33**. Inhibitor concentrations range from 22-400 μM . $IC_{50} = 215 \pm 8 \mu\text{M}$.

A.2 Preliminary studies on the time- and concentration-dependent inhibition of STS with compound 3.32.

This was determined using the same procedure as that used for 4-FE1 (§ 3.4.3).

The results are shown in **Figure A.5** below.

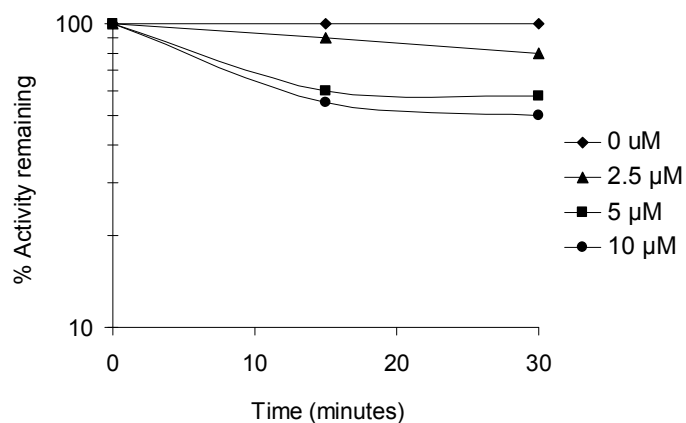


Figure A.5. Time- and concentration-dependent inhibition of STS with inhibitor **3.32** over 30 minutes.

Appendix B – Supplementary Figures for Compounds 4.6, 4.7, 4.10, 4.11

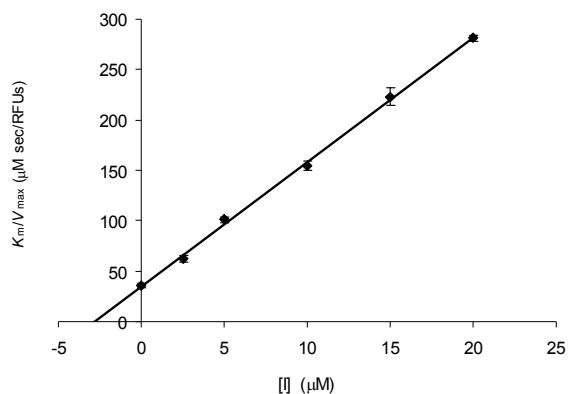


Figure B.1. Replot of the data from **Figure 4.6** to determine the K_i of inhibitor **4.6** at pH 7.0.

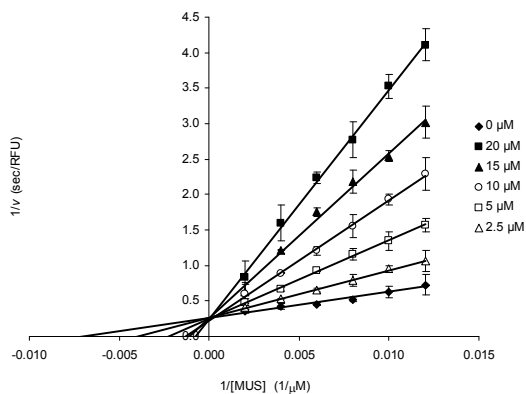


Figure B.2. Lineweaver-Burk plot of inhibitor **4.6** at pH 7.5.

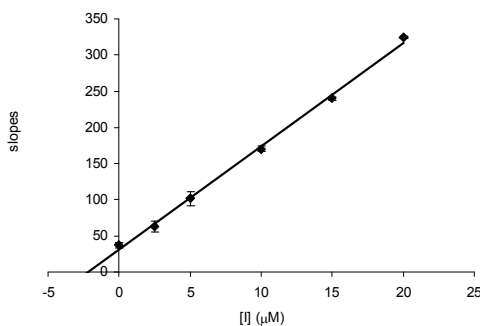


Figure B.3. Replot of the data from **Figure B.2** to determine the K_i of inhibitor **4.6** at pH 7.5.

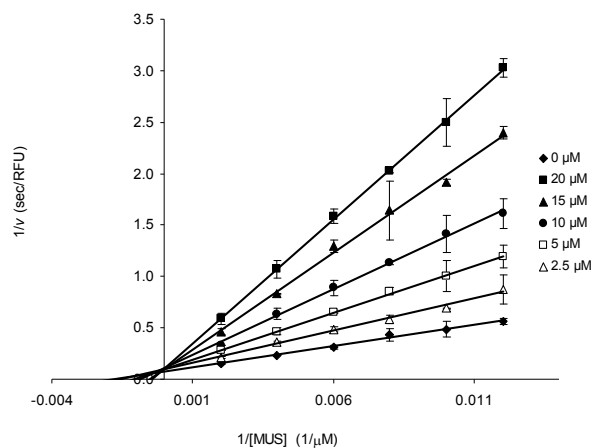


Figure B.4. Lineweaver-Burk plot of inhibitor **4.6** at pH 8.0.

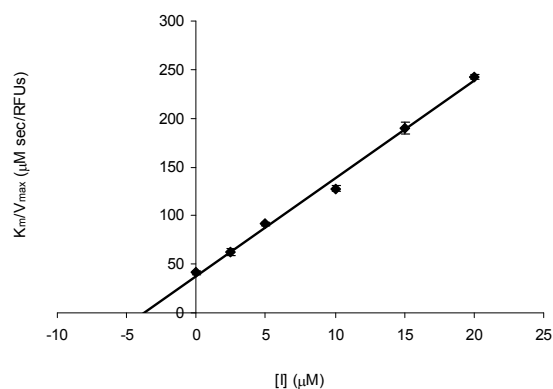


Figure B.5. Replot of the data from **Figure B.4** to determine the K_i of inhibitor **4.6** at pH 8.0.

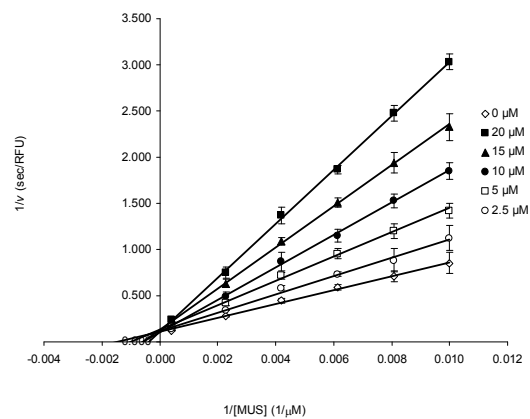


Figure B.6. Lineweaver-Burk plot of inhibitor **4.6** at pH 8.5.

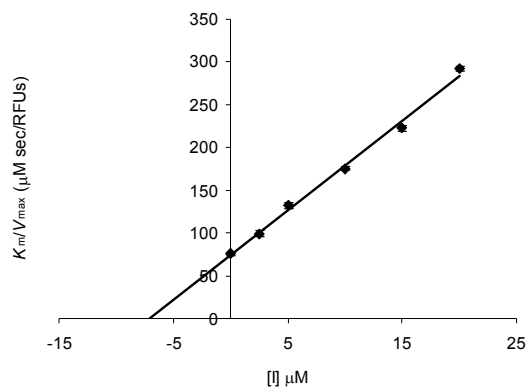


Figure B.7. Replot of the data from **Figure B.6** to determine the K_i of inhibitor **4.6** at pH 8.5.

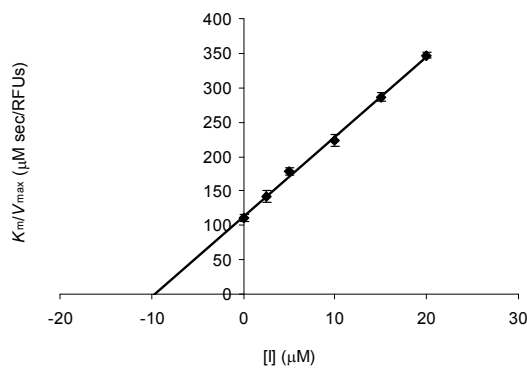


Figure B.8. Replot of the data from **Figure 4.8** to determine the K_i of inhibitor **4.6** at pH 8.8.

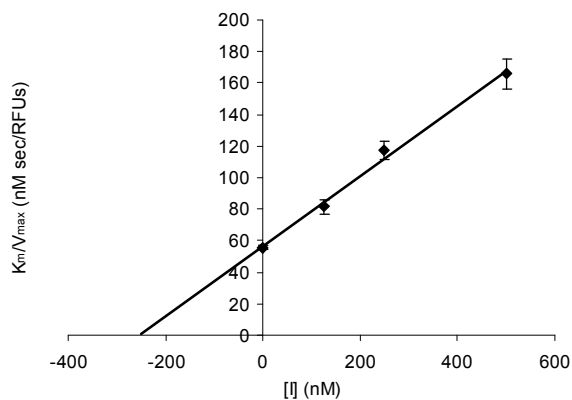


Figure B.9. Replot of the data from **Figure 4.9** to determine the K_i of inhibitor **4.7** at pH 7.0.

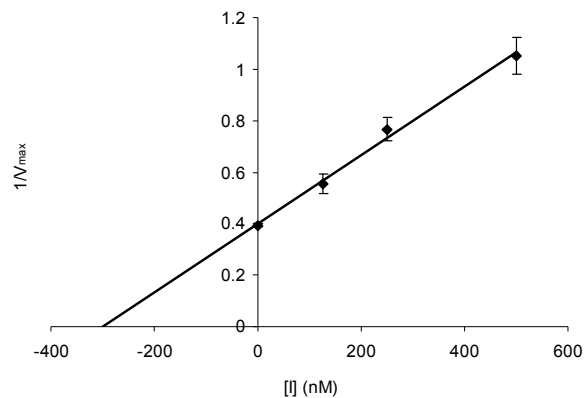


Figure B.10. Replot of the data from **Figure 4.9** to determine the αK_i of inhibitor **4.7** at pH 7.0.

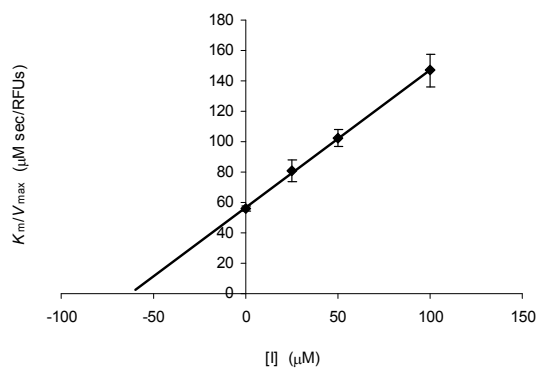


Figure B.11. Replot of the data from **Figure 4.7** to determine the K_i of inhibitor estrone (E1) at pH 7.0.

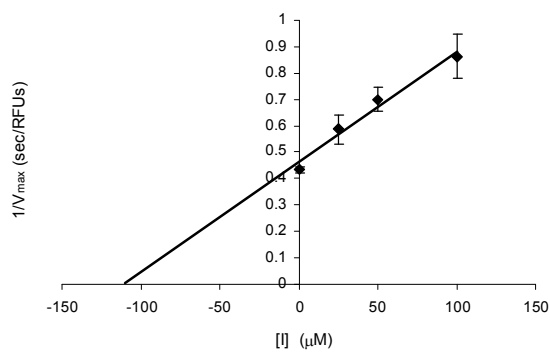


Figure B.12. Replot of the data from **Figure 4.7** to determine the αK_i of inhibitor estrone (E1) at pH 7.0.

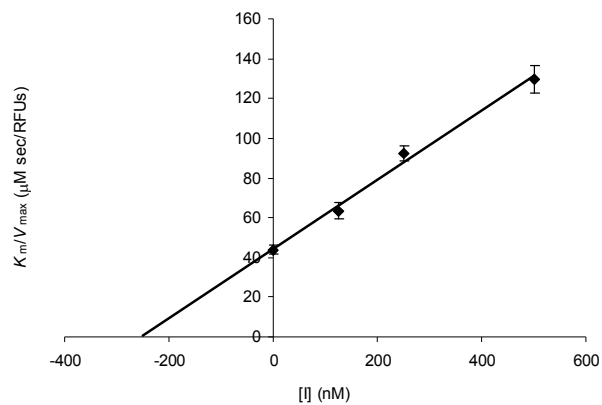


Figure B.13. Replot of the data from **Figure 4.10** to determine the K_i of inhibitor **4.1** at pH 7.0.

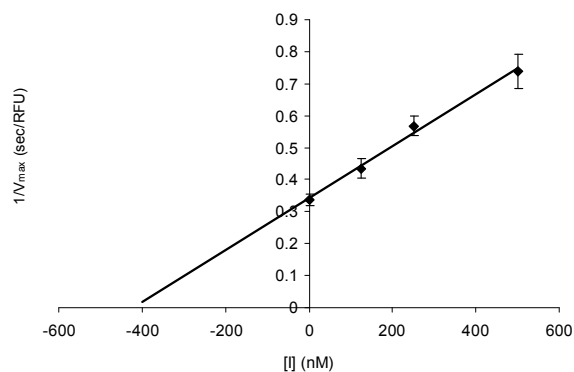


Figure B.14. Replot of the data from **Figure 4.10** to determine the αK_i of inhibitor **4.1** at pH 7.0.

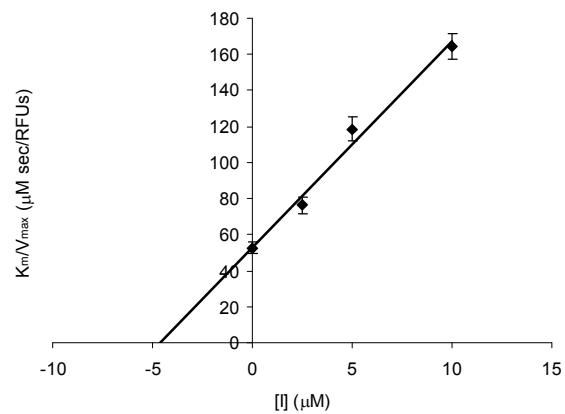


Figure B.15. Replot of the data from **Figure 4.11** to determine the K_i of inhibitor **4.10** at pH 7.0.

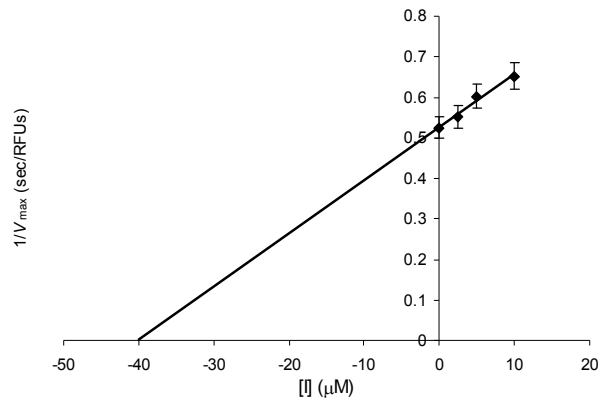


Figure B.16. Replot of the data from **Figure 4.11** to determine the αK_i of inhibitor **4.10** at pH 7.0.

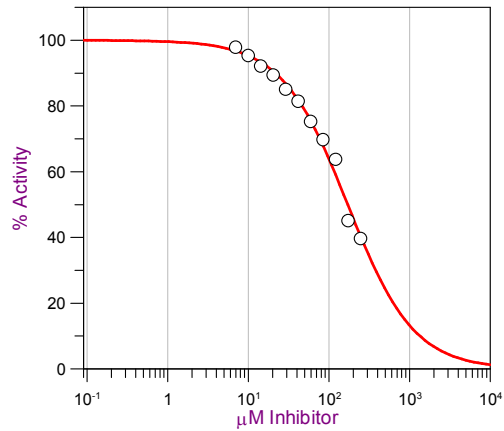


Figure B.17. IC_{50} plot for inhibitor **4.8** at pH 7.0.

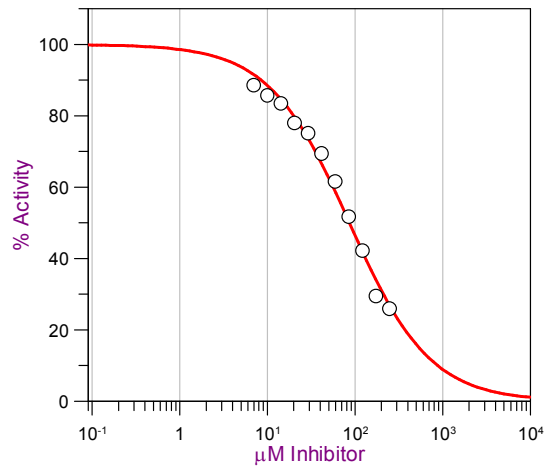


Figure B.18. IC_{50} plot for inhibitor **4.9** at pH 7.0.

Appendix C – Supplementary Figures for Compounds 5.26, 5.27, 5.28, 5.29, 5.34, and 5.42

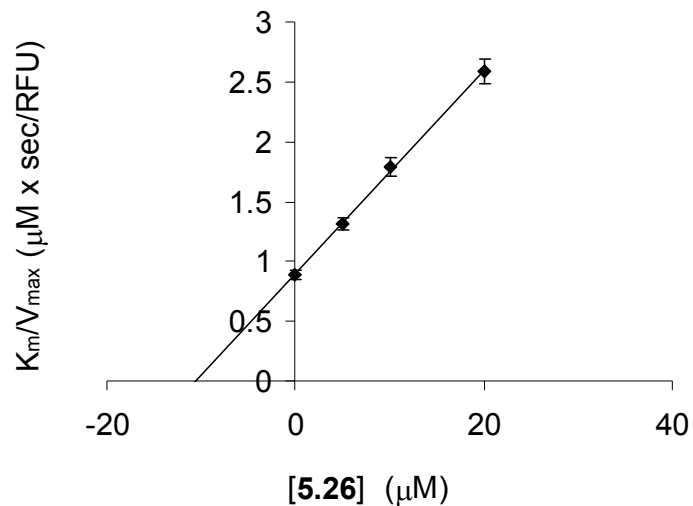


Figure C.1. Replot of the data from Figure 5.19 to determine the K_i of inhibitor 5.26.

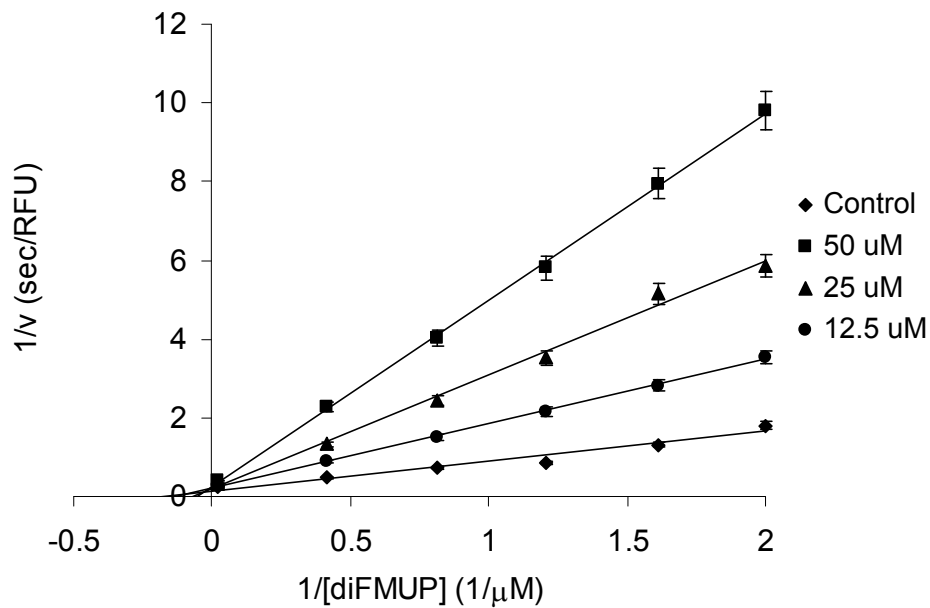


Figure C.2. Lineweaver-Burk plot of compound 5.27.

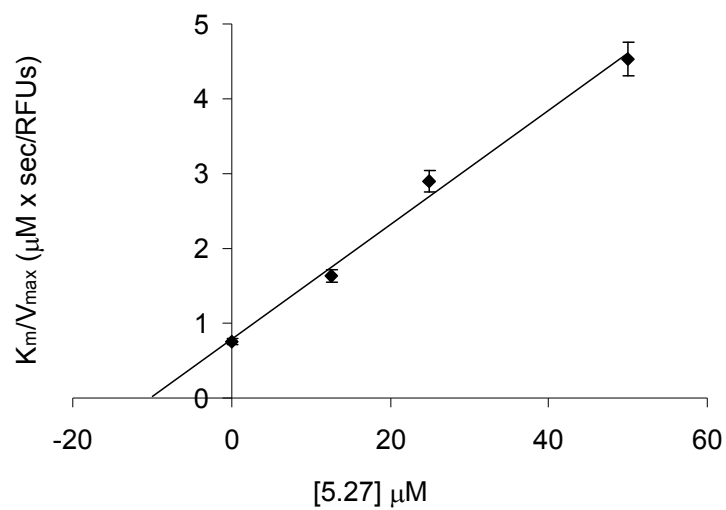


Figure C.3. Replot of the data from **Figure C.2** to determine the K_i of inhibitor **5.27**.

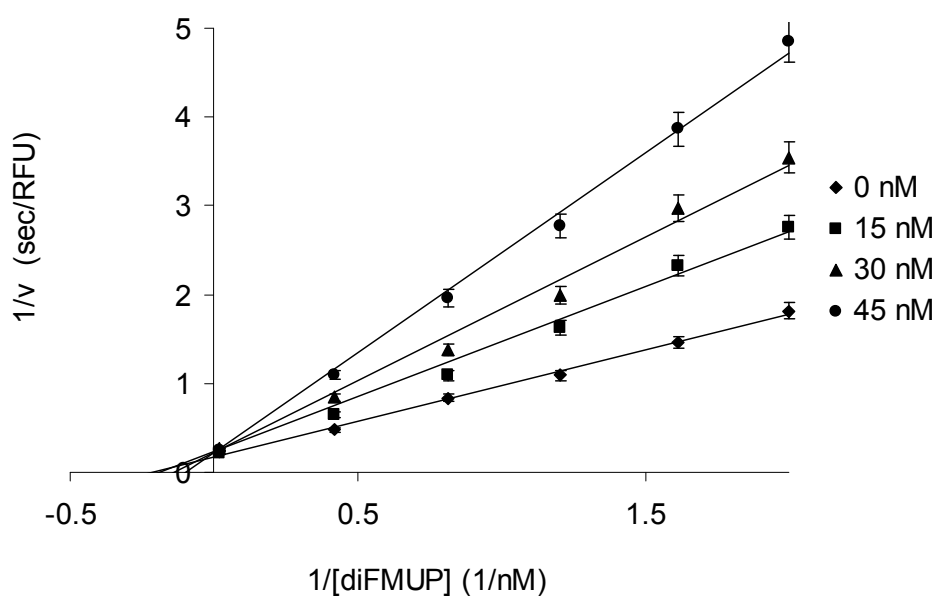


Figure C.4. Lineweaver-Burk plot of compound **5.28**.

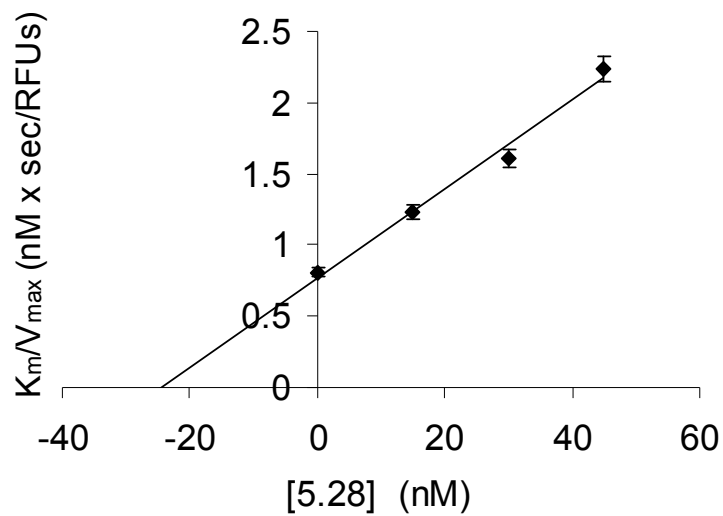


Figure C.5. Replot of the data from **Figure C.4** to determine the K_i of inhibitor **5.28**.

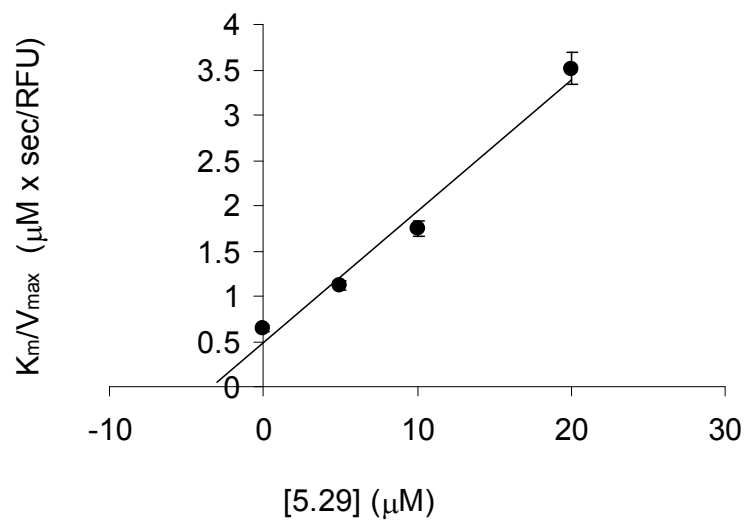


Figure C.6. Replot of the data from **Figure 5.21** to determine the K_i of inhibitor **5.29**.

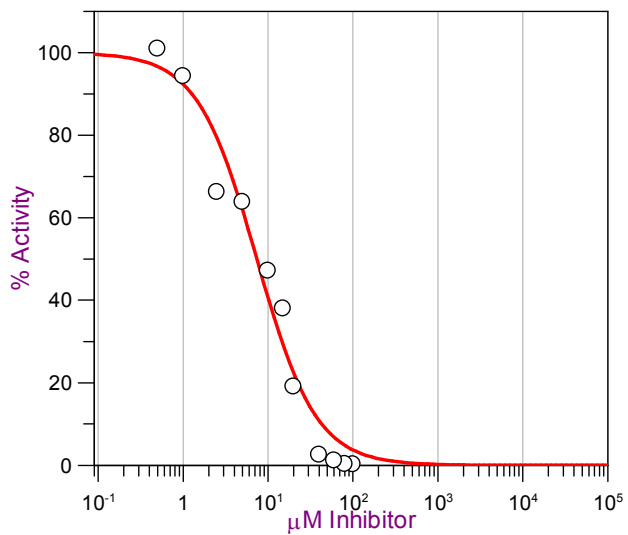


Figure C.7. IC₅₀ of compound **5.42** using 3 nM PTP1B.

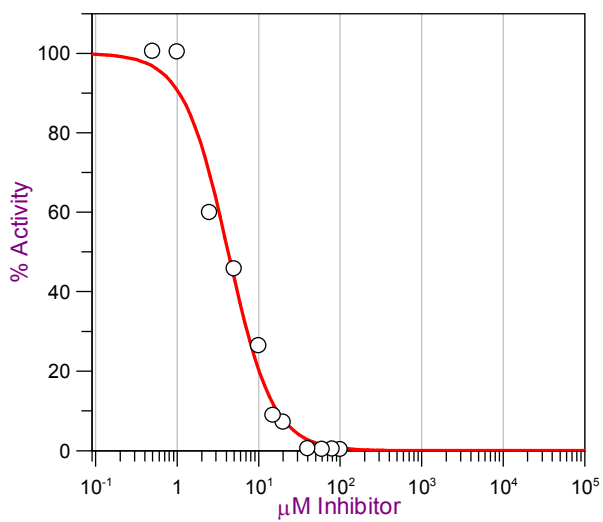


Figure C.8. IC₅₀ of compound **5.42** using 1.5 nM PTP1B.

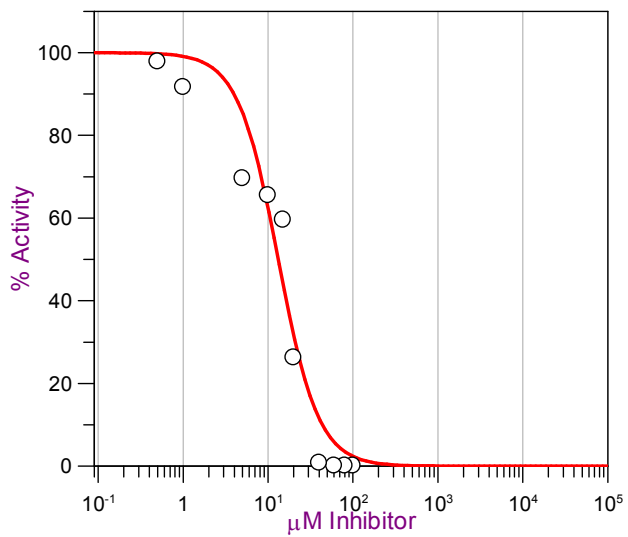


Figure C.9. IC₅₀ of compound **5.42** using 6.0 nM PTP1B.

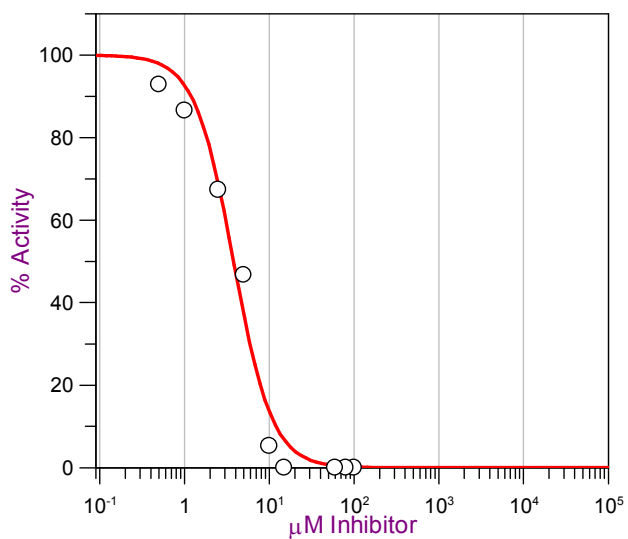


Figure C.10. IC₅₀ of compound **5.34**.

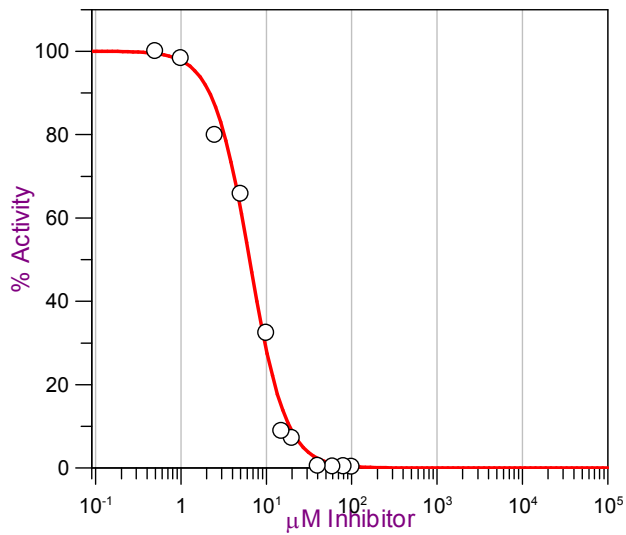


Figure C.11. IC₅₀ of compound **5.35**.

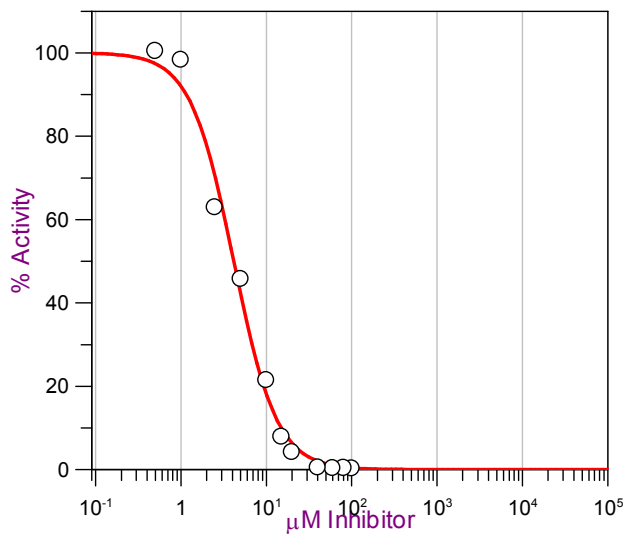


Figure C.12. IC₅₀ of compound **5.43**.

Appendix D — Permission to reproduce Figures 1.7 to 1.13 obtained by personal communication with a collaborator

The following is correspondence I received from Dr. Debashis Ghosh, a collaborator, regarding my request to use the material appearing in Figures 1.7 to 1.13 in association with this thesis:

September 2, 2009

Hi Vanessa,

You certainly have my permission to use any of those figures as you please. I can send you the originals. These .tif files are large (~1-5MB each) and cannot be sent by email. I'll burn a CD/DVD and mail to you, let's say by next week. Please send me your mailing address.

Best wishes,

Debashis Ghosh, Ph.D.
Associate Member/Professor of Oncology, Pharmacology & Therapeutics
Roswell Park Cancer Institute
Senior Scientist, Hauptman-Woodward Institute

Appendix E — Permission to reproduce copyright material in Chapter 3 in association with this thesis

The following is correspondence I received from Ms. Bettina Loycke, the copyright and licensing manager of Wiley-VCH, regarding my request to use material appearing in Chapter 3 of this thesis:

August 24, 2009

Dear Customer

Thank you for your request.

We hereby grant permission for the requested use expected that due credit is given to the original source.

For material published before 2007 additionally: Please note that the author's permission is also required.

If material appears within our work with credit to another source, authorisation from that source must be obtained.

Credit must include the following components:

- Books: Author(s)/ Editor(s) Name(s): Title of the Book. Page(s). Publication year. Copyright Wiley-VCH Verlag GmbH & Co. KGaA. Reproduced with permission.

- Journals: Author(s) Name(s): Title of the Article. Name of the Journal. Publication year. Volume. Page(s). Copyright Wiley-VCH Verlag GmbH & Co. KGaA. Reproduced with permission.

With kind regards

Bettina Loycke
Copyright & Licensing Manager
Wiley-VCH Verlag GmbH & Co. KGaA
Boschstr. 12
69469 Weinheim
Germany

Appendix F — Permission to reproduce copyright material in Chapter 4 in association with this thesis

The following statement appears on the Elsevier website, www.elsevier.com, regarding journal author rights and permissions:

“As a journal author, you retain rights for large number of author uses, including use by your employing institute or company. These rights are retained and permitted without the need to obtain specific permission from Elsevier. These include:

- the right to include the journal article, in full or in part, in a thesis or dissertation”

Elsevier Global Rights Department

Appendix G — Permission to reproduce copyright material in Chapter 5 in association with this thesis

The following statement appears on the Elsevier website, www.elsevier.com, regarding journal author rights and permissions:

“As a journal author, you retain rights for large number of author uses, including use by your employing institute or company. These rights are retained and permitted without the need to obtain specific permission from Elsevier. These include:

- the right to include the journal article, in full or in part, in a thesis or dissertation”

Elsevier Global Rights Department

The following statement appears on the American Chemical Society (ACS) website, www.pubs.acs.org, regarding author rights and permissions:

“Thank you for your request for permission to include **your** paper(s) or portions of text from **your** paper(s) in your thesis. Permission is now automatically granted; please pay special attention to the implications paragraph below. The Copyright Subcommittee of the Joint Board/Council Committees on Publications approved the following:

Copyright permission for published and submitted material from theses and dissertations

ACS extends blanket permission to students to include in their theses and dissertations their own articles, or portions thereof, that have been published in ACS journals or submitted to ACS journals for publication, provided that the ACS copyright credit line is noted on the appropriate page(s).”

American Chemical Society